WEAR AND DEGRADATION OF UHMWPE TOTAL HIP REPLACEMENT COMPONENTS

Michael Kipping, BEng(Hons.), MSc.

The University of Nottingham

Thesis submitted to the University of Nottingham for the degree of Doctor of Philosophy
December 2006

ABSTRACT

Long term (>2 years) failure of UHMWPE components in-vivo is predominantly caused by wear of the UHMWPE component. The surface properties of UHMWPE greatly influence the adhesive and abrasive mechanisms of wear that occur in the hip. However, there is not a clear understanding of how in-vivo wear mechanisms influence surface mechanical properties of UHMWPE. In addition, previous researchers have reported wear rates for Charnley UHMWPE acetabular components that vary considerably between patients. It is conceivable that these variations in wear are a result of variations in the surface mechanical properties of UHMWPE.

This study used a combination of instrumented indentation testing and FT-IR imaging to assess the depth dependent micromechanical and chemical properties of 32 retrieved UHMWPE acetabular components.

Significant variations in the mechanical and chemical properties of samples taken from worn and unworn regions of retrieved UHMWPE acetabular components were found. In unworn regions, these variations were principally caused by post-irradiation ageing. However, in worn regions, the variation in properties was primarily caused by the wear process.

DEDICATION

This thesis is dedicated to my family. To my wife, Rebecca Kipping and our children for their unwavering support and encouragement that enabled me to pursue my goal of completing this research and embarking on a new career in the field of medical devices. To my parents, Graham and Christine Kipping, who engendered in me a thirst for knowledge and encouraged me to pursue higher education in order to fulfil my own ambitions in life.

"Too often we give our children answers to remember rather than problems to solve." (Rogen Lewin)

ACKNOWLEDGEMENTS

I would like to express my appreciation to my supervisor, Dr. Nicola Everitt for her guidance and support that enabled me to pursue and develop a research project based on my own technical interests.

I would also like to acknowledge and thank the many technical staff members in the Department of Mechanical Materials and Manufacturing at the University of Nottingham who assisted me during my research. Most notable amongst these were Mark Parry (Biomechanics Laboratory Manager) who helped with the fabrication of mechanical test equipment and test samples and Keith Dinsdale (Chief Experimental Officer) who advised me on UHWMPE sample preparation.

I'd like to thank my examiners, Prof. David Grant (internal) and Dr. Sarah Green (external) for their helpful insights and comments regarding my thesis.
It is my pleasure to thank David Brooks at Orthoplastics Ltd. (formerly Perplas) for supplying me with samples of UHMWPE that enabled me to carry out initial benchmarking tests.

An important part of my research was the FT-IR mapping of retrieved UHMWPE components and I want to thank Dr. Trevor Emmett at Anglia Ruskin University for allowing me to use their FT-IR mapping equipment and the discussions we had on the subject.

It is with great fondness that I acknowledge the role of family in enabling me to complete my research. My parents, Graham and Christine Kipping and siblings, Catherine, Richard and Christopher Kipping provided my with advise and practical support during my research. I would also like to acknowledge the support of my wife's parents, Jackie and John Taylor who supported my family and me, whilst I wrote up this thesis and was searching for a job.

CONTENTS

LIST OF FIGURES

LIST OF TABLES

1 INTRODUCTION

Total hip replacement (THR) is an invasive technique used to treat patients suffering from severe musculoskeletal disorders or trauma to the hip. The bearing surfaces of the femur (thigh bone) and hip are replaced by prostheses that restore the function of the hip.

Total hip replacements are predominantly carried out on patients who have debilitating musculoskeletal disorders with arthritic conditions accounting for -90% of referrals [1]. In recognition of the negative impact of musculoskeletal disorders on the quality of life of people, the World Health Organization (WHO) has designated the first decade of the new millennium (2001-2010) as the 'Bone and Joint Decade'. A number of organisations in the UK, such as the British Orthopaedic Research Society and British Orthopaedic Association along with organisations from 25 other countries are supporting the Bone and Joint Decade. The aim of the WHO initiative is to raise awareness of musculoskeletal conditions and encourage research in this area. Incidence of certain diseases is closely linked to the age of the person. For example, the average age of patients undergoing primary THR in Sweden is 70.1 years old (68.8 years old for men and 71.0 for women)[2]. The WHO has predicted that the number of people older than 65 will double between 1990 and 2020 and therefore the number of people requiring treatment for musculoskeletal disorders will also increase. Around half of all chronic musculoskeletal conditions are caused by joint disease [3].

In the year 2000, the National Institute for Clinical Excellence (NICE) estimated that around 35,000 THR's are carried out in the National Health Service (NHS) in England and 2,800 in Wales each year [1]. These figures were part of a document providing guidance on the selection of THR components. It is likely that current figure of people undergoing THR would be in excess of those listed. NICE have recently announced (13/11/2003) a second technology appraisal of THR components in order to update their guidance on prosthesis selection. In the United States, the number of THR's carried out each year far exceeds the number carried out in the United Kingdom. The American Academy of Orthopaedic Surgeons (AAOS) states that the number of primary THR's carried out has risen from 117,000 to 152,000 per annum and that a total of 1,389,000 primary THR's were carried out between 1991 and 2000. The number of revision THR's currently stands at approximately 30,000 with the total number of revision THR operations being -292,000 between 1991 and 2000.

Since the 1960's, ultra high molecular weight polyethylene (UHMWPE) has been extensively used to fabricate acetabular hip replacement components. Despite having been used for over 40 years, there is a poor understanding of component wear and its relationship with surface properties of UHMWPE.

1.1 Justification for Research Study

Long term (>2 years) failure of UHMWPE components in-vivo is predominantly caused by wear of the UHMWPE component. The surface properties of UHMWPE greatly influence the adhesive and abrasive mechanisms of wear that occur in the hip. However, there is not a clear understanding of how in-vivo wear mechanisms influence surface mechanical properties of UHMWPE. In addition, previous researchers have reported wear rates for Charnley UHMWPE acetabular components that vary considerably between patients [4, 5]. It is conceivable that these variations in wear are a result of variations in the surface mechanical properties of UHMWPE.

Wear of UHMWPE components generates debris from the bearing surface which is released into the surrounding biological tissue. It is the subsequent biological reactions to this wear debris that are the primary failure mechanism of joint replacements, rather than bulk failure or wear-through of the UHMWPE component. Therefore, it is important to investigate the surface and subsurface mechanical properties of retrieved UHMWPE components on the scale of size as the wear debris in order to develop an understanding of its generation in-vivo.

1.2 Objectives

The primary objective of this research was to accurately assess the through thickness micro-mechanical properties of retrieved UHMWPE acetabular components in unworn and worn regions in order to investigate the material's response to in-vivo service.

Additional objectives of this study included assessing the amount of component wear and its correlation with patient factors and whether in-vivo service had

resulted in through thickness variations in chemical properties or morphological features.

Specific objectives for comparison included:

- The collection of patient information, including activity levels using modified Baecke Physical Activity questionnaire.
- Accurate assessment of linear and volumetric wear using a co-ordinate measuring machine.
- Investigation of the distribution of through thickness hardness and elastic modulus values in worn and unworn regions using instrumented indentation testing.
- Assessment as to whether relationships between instrumented indentation test data existed, using SPSS statistical software:
    - Variations between worn and unworn regions of the same component.
    - Variations between unworn regions and worn regions of the same component where linear wear has been accounted for.
    - Variations between worn regions of different components.
    - Variations between unworn regions of different components.
- Accurate measurement of the degree of crystallinity, oxidation and fluid ingress as a function of distance from the bearing surface using Fourier transform infrared (FT-IR) imaging.
- Examination of acetabular component bearing surfaces to investigate surface features generated in-vivo.

- Examination of the through thickness microstructure of different regions of retrieved UHMWPE using environmental scanning electron microscopy (ESEM) and optical microscopy.

1.3 Hypotheses

- Wear rates would be influenced by the size of the acetabular cup with large internal diameters (32mm) resulting in high wear rates and small internal diameters (22.25mm) leading to reduced wear rates.
- Indentation behaviour would be different between through thickness areas of worn and unworn regions.
    - Worn regions would have higher hardness and elastic modulus values as a result of wear process induced plastic deformation at the surface.
    - Unworn regions would exhibit subsurface increases in hardness and elastic modulus as a result of post-irradiation ageing.
    - Values of hardness and elastic modulus in bulk regions of worn and unworn regions would be comparable due to minimal post-irradiation ageing and absence of wear.
    - Changes in elastic modulus correlated with regions of plastic deformation due to wear process.
- Distribution of chemical properties in through thickness areas of unworn and worn regions would differ because:
    - Fluid absorption would occur on all external surfaces but with increased absorption at the worn surface due to mechanical loading

and associated localised increases in fluid pressure.

  - Post-irradiation oxidation and increased crystallinity in subsurface areas of worn and unworn components.

- Polymer morphology would reflect chemical changes that had occurred in the material as a result of post-irradiation aging i.e. subsurface 'white band' associated with severe oxidation of UHMWPE.

1.4 Outline of Thesis

The next two chapters detail the theoretical background information for this work. Chapter Two discusses various aspects of total hip replacement and the use of ultra-high molecular weight polyethylene (UHMWPE) along with various issues surrounding its wear performance in-vivo. The theory behind instrumented indented testing and a discussion of the analytical techniques used in this study are presented in Chapter Three. Chapter Four details the specific experimental methodology that was used during this study to evaluate retrieved UHMWPE acetabular components. Chapter Five contains the results and statistical data from the testing carried out on components. A discussion of the work is presented in Chapter Six. Conclusions from this study and directions for future work are discussed in Chapter Seven.

2 BACKGROUND

2.1 Human Hip Joint

2.1.1 Healthy Hip Joint

The hip joint is a synovial ball-in-socket articulation formed where the head of the thighbone (femur) meets the socket of the hipbone (acetabulum) (Figure 2-1). The bones of a healthy hip joint are covered by hyaline cartilage that protects the bones whilst allowing easy motion. A fibro-cartilage rim called the acetabular labrum is attached to the margin of the acetabulum and enhances the depth of the acetabulum. As the diameter of the acetabular rim is smaller than the head of the femur, dislocation of the femur is rare.

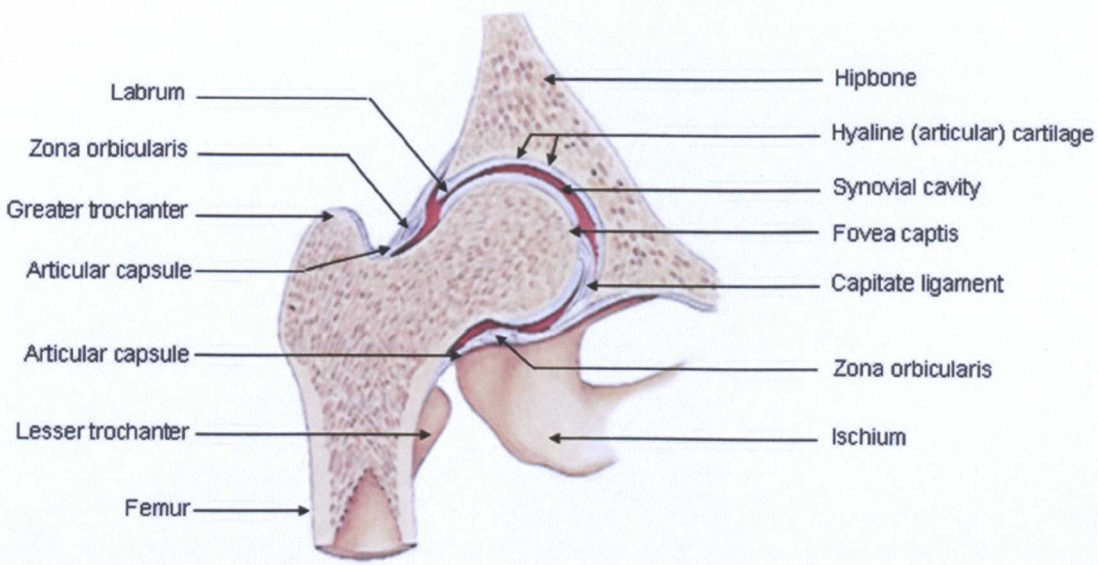

Figure 2-1 Frontal section of a healthy hip joint

Surrounding the hip joint is an articular capsule (Figure 2-2) that encloses the synovial cavity. The capsule extends from the rim of the acetabulum to the

neck of the femur and consists of circular and longitudinal fibres. Circular fibres are called zona orbicularis and form a collar around the neck of the femur. Longitudinal fibres are reinforced by accessory ligaments: iliofemoral, pubofemoral and ishiofemoral ligaments (pubofemoral ligament hidden from view on Figure 2-2). [1]

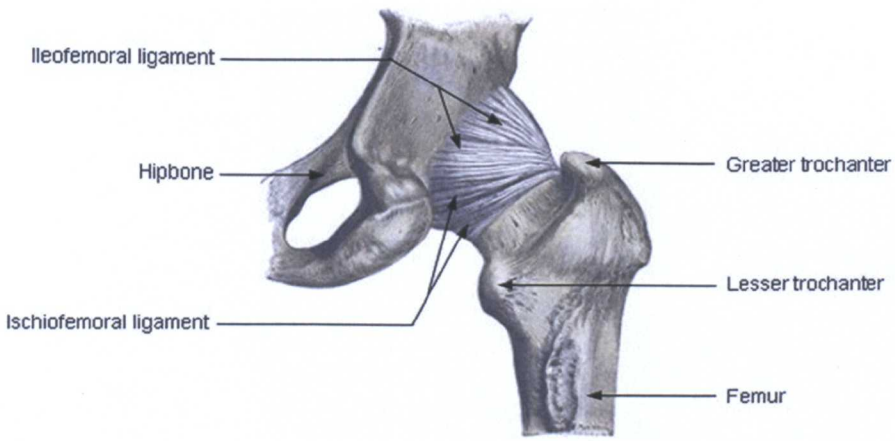

Figure 2-2 View of a healthy hip joint (posterior view) showing articular capsule

The inner layer of the articular capsule is formed by a synovial membrane. The synovial membrane secretes synovial fluid that lubricates and reduces friction in the joint. It also supplies nutrients to and removes metabolic wastes from, the chondrocytes (cells of mature cartilage) of the articular cartilage. A further function of the synovial fluid is to remove microbes and debris resulting from wear and tear of the joint. [6]

In addition to bone, the hip joint comprises of a number of different facets including ligaments, blood vessels, muscles and nerves.

2.1.2 Degeneration of the Human Hip

Degeneration of the hip can occur in numerous ways and with different levels of severity. Arthritic conditions account for -90% of Total Hip Replacement (THR) operations each year[1]. THR may also be recommended for other conditions such as severe hip trauma, osteonecrosis, Paget's disease and congenital dysplastic or dislocated hips [7].

Arthritis is a general term for over 100 diseases that cause pain, stiffness and swelling from the inflammation of a joint or the area around a joint. The exact causes of Arthritis are unknown and as there are so many different forms, the causes are likely to vary. Scientists are currently examining how the major factors including genetics and lifestyles affect the development of Arthritis. Of the different forms of Arthritis, Osteoarthritis and Rheumatoid Arthritis are the most common forms that are cited as reasons for THR [1].

Osteoarthritis is a non-inflammatory form of Arthritis and the most common cause of disability in the western world. It usually affects middle-aged and elderly people. As ageing occurs, degeneration of the hyaline cartilage covering the bones of the hip joint takes place. In Osteoarthritis, the cartilage cushioning the bone surfaces wears away, causing the bones to rub against each other causing pain.

2.1.2.1 Osteoarthritis

Osteoarthritis of the hip starts with fibrillation of the articular surface and formation of wear particles. Wear particles are swept to the side of the joint where they irritate the synovium and are responsible for some of the patients pain and formation of osteophytes.

As the disease progresses, articular cartilage is lost, subchondral bone is exposed and

the bone surfaces become roughened. Grooves form in the joint surfaces and the hip is gradually converted from a ball and socket into a roller bearing. Later, cysts form in the bone and the femoral head may collapse. If the hip is not treated, it can become fixed in flexion, adduction and external rotation, seriously interfering with mobility. Characteristic symptoms of osteoarthritis are pain, loss of movement and abnormal gait [7-9].

Figure 2-3 Healthy femoral head

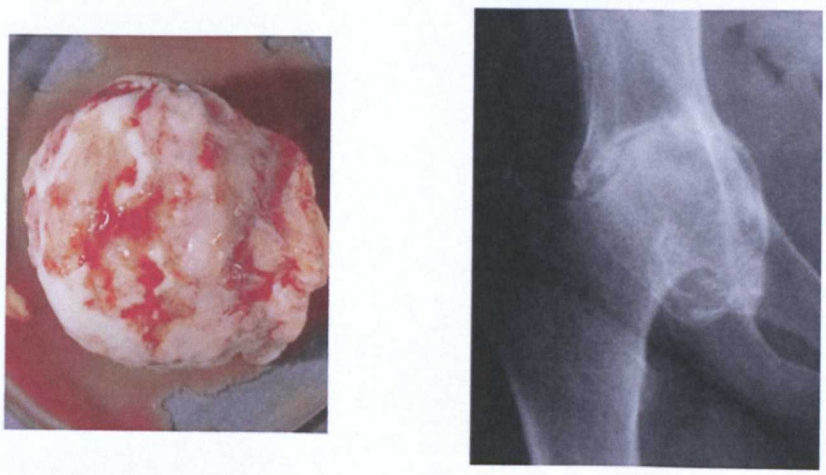

Figure 2-4 Osteoarthritis of the femoral head

2.1.2.2 Rheumatoid Arthritis

Rheumatoid Arthritis is the most common form of inflammatory Arthritis and usually first occurs between the ages of 25 and 50. However, it can also occur in children and in senior citizens. Three quarters of all people with this disease are women. Rheumatoid Arthritis is a symmetric disease, meaning that it will usually involve the same joints on both sides of the body. Unlike Osteoarthritis, Rheumatoid Arthritis may also affect the heart, lungs and eyes of some patients and can cause an overall feeling of sickness and fatigue as well as weight loss and fever. Rheumatoid Arthritis is caused by the body's own immune system attacking the synovial lining of the hip joint causing it to become inflamed. Inflammation of the synovium causes chemicals to be released by the body which thicken the synovium and damage the cartilage and bone of the affected joint. Over time, the femoral head is gradually eroded and may collapse suddenly resulting in true shortening of the leg. Symptoms of Rheumatoid Arthritis are joint pain, swelling and the skin over the joint may appear swollen and red, and feel hot when touched [7-9].

2.2 Patient Parameters

2.2.1 Age & Pathological Diagnosis

The average age of patients undergoing primary THR is in the range 67 [10] to 69 years[11]. Of the -35,000 total hip replacements carried out in the UK, 2/3 are for patients >65 years old with women outnumbering men by nearly two to one [12]. However, primary THR have been carried out on patients at opposite ends of the age spectrum from adolescents [13] to patients aged 100 years [14].

In Sweden, a survey of 44,124 patients of all ages showed an implant survival rate at 18 years of 83% [15]. The implant survival rate in younger patients (<40 years) however, has been shown to be significantly less [16-21]. The increased rate of revision in younger patients is partially related to the pathological diagnosis for primarily THR. Sochart et al [22] carried out a study containing 226 cemented Charnley THR's in 161 patients aged between 17 and 39 years of age (mean 31.7yrs). They found that the average implant survival rate at 25 years was 68%. However, patients with congenital dislocation (n=44) had an associated implant survival rate of 58%, osteoarthritis (n=54) 59% and Rheumatoid Arthritis (n=63) had a higher implant survival rate of 79%. The link between pathological diagnosis and risk of revision was also highlighted by Joshi et al [17]. In a study involving 218 Charnley prostheses in 141 patients aged <40 years they found that the probability of implant survival for the acetabular component was 84% at 20 years. However, Rheumatoid Arthritis patients had an acetabular component survival rate of 96% compared to 51% for Osteoarthritis patients.

Along with pathological diagnosis, several other factors were identified by Torchia et al [23] as risk factors for revision for <20 year old patients. These included history of

more than one procedure, previous trauma involving the hip, high postoperative level of activity and a pre-operative weight of more than 60kg.

2.2.2 Gender

In a review of 1198 Charnley THR's, Fender et al [24] found that male patients had a significantly higher risk of failure than women at 5 years. The increased risk of revision for men has also been shown in a number of other studies [25-27] where women were also shown to have better functional outcomes. A possible stereotypical explanation for this difference may be that men are more able to deal with the pain associated with their pathological diagnosis. However, in a functional assessment study of patients about to undergo primary hip replacement Holtzman et al [28] found that in fact women were more disabled at the time of THR than men and do not do as well at 1 year. The researchers postulated that this difference arises from the patient's own preference or bias in the health care system.

The cause of the difference in revision rate between men and women is in all likelihood due to the interaction of multiple variables such as age, co-morbidity, and physical activity.

2.2.3 Weight & Body Mass Index (BMI)

Previous researchers have found links between patient weight and BMI and an increased risk of joint replacement along with an increased risk of revision.

In two recent studies, an increased risk of primary THR was identified and linked to the increased risk of primary Osteoarthritis due to higher patient weights and body mass

indices [29, 30]. A BMI of >32 was shown to increase the relative risk of hip replacement by a minimum of 2.3 times in women and 3.4 times in men. The risk factor associated with BMI decreased with increasing age e.g. someone who became obese in later years (55-59 years) carried a lower risk of hip replacement than someone that had been obese at a younger age (< 25years).

An increased risk of revision for cemented acetabular components has also been identified in a number of previous studies [26, 30-32]. Surin and Sundholm [32] found that patients weighing more than 80 kg were at significantly greater risk of prosthetic failure requiring revision. A logical assumption is that for patients with a pathological diagnosis of osteoarthritis, an increased risk of revision may be due to the increased risk of progression of osteoarthritis due to increased patient mass and BMI.

2.2.4 Physical Activity

Little previous research into the link between physical activity level of patients and component failure has been carried out. From a research perspective, this issue would ideally be approached by continuously monitoring the physical activity of patients over the entire service life of the joint replacement. No such study has been conducted and it is extremely unlikely that patients would agree to this level of intrusion into their daily lives over an extended period of time.

Researchers have approached the issue of assessing patient physical activity in two main ways, continuous monitoring of patients over limited periods of time or by using self report methods such as diaries and retrospective physical activity questionnaires.

Continuous monitoring of patients was a technique employed by Goldsmith et al [33].

They monitored 54 people who had undergone THR with each person being fitted with a pedometer for a 2-4 week period. In addition to activity levels, they measured the linear wear rate that had occurred in each joint replacement via a radiographic method [34, 35] and sought to correlate wear and activity level. No correlation was found between activity level and linear wear rate. Activity levels of patients in this study may have been influenced by the time of year in which the measurements were taken and whether patients were all assessed at the same time of year.

In the current study, continuous monitoring of patient activity was not viable because patients were only approached to take part in the study on admission to hospital. Therefore, an assessment of patient's physical activity level at the time of revision would be distorted by the diminished functionality of their hip replacement. In addition, assessing a patient's current physical activity status wouldn't give any insight into how their joint had been used over the earlier service period of the joint replacement components. The only available option for assessing the physical activity of patients was to use a physical activity questionnaire.

There are many different standardised questionnaires which can be used to assess physical activity including the Baecke habitual activity questionnaire [3 6], PASE [37], Godin leisure-time exercise questionnaire [38] and Minnesota leisure-time physical activity questionnaire [39]. They vary in complexity, target demographic and period of time considered.

The Modified Baecke Questionnaire for Older Adults (MBQOA) [40] was chosen for the current study for a number of reasons. The questionnaire is simple in nature with the questions being tailored to older people making it as easy as possible for the patient to

understand and also straightforward to administer. Information about sports and other leisure-time activities are elicited as type of activity, duration (hours per week), frequency (number of months per year), and intensity that the activity was normally performed. Intensity of activity is coded based on the work of Bink et al [41]. These intensity codes are unit-less codes that were originally based on energy costs.

A number of studies validating the use of the questionnaire have been carried out. Good repeatability of the questionnaire was demonstrated by Pols et al [42] who administered it to 134 individuals at 0, 5 and 11 months. The researchers also assessed the validity of the questionnaire by comparing its results to a three-day diary that was repeated four times. Results from the tests were correlated and in line with similar comparative studies carried out with other questionnaires. In a separate study, Pols et al [43] investigated the validity and repeatability of the questionnaire specifically in women aged 55-71 years old. Questionnaires were compared with a physical activity diary (12 d) as the main reference method, a single 24-h Caltrac accelerometer score, and energy intake estimated from a 24-h dietary recall repeated 12 times. The researchers found that the questionnaires were able to rank the women in order of physical activity level. In a separate study by Florindo et al [44], the researchers found that the questionnaire was able to accurately assess habitual physical activities in adult males.

There are of course limiting factors and sources of error in the use of questionnaires [45]. For instance, because of the limitations in human memory, the reliability of information generally decreases with the length of the period surveyed. When reporting information, people tend to overestimate physical activity and underestimate sedentary pursuits such as watching television [46].

2.3 History of Total Hip Replacement

Surgeons have been trying for over a century to successfully treat the debilitating effects of Arthritis resulting in the use of total hip arthroplasty (also referred to as total hip replacement). The term arthroplasty can be defined as "surgery to relieve pain and restore range of motion by realigning or reconstructing a joint" [7]. The concept of arthroplasty originally arose from the presence of joints that had stiffened following pyrogenic or tuberculosis infection or by serious injury. Before the advent of joint replacement, attempts to treat arthritic hips included arthrodesis (fusion of femur and acetabulum), osteotomy (re-alignment of femoral head or hip bone), nerve division, and joint debridements (removal of arthritic spurs, calcium deposits, and irregular cartilage in an attempt to smooth the surfaces of the joint) [7,47].

Hip replacements were first attempted at the end of the 1800s when a technique termed 'interpostional hip arthroplasty' was introduced [48]. This technique consisted of a spacer being placed between the femoral and acetabular bearing surfaces of the hip. A range of different materials were evaluated that included zinc, tin, rubber, celluloid and gold leaf [7, 48]. Biological materials such as muscle, ivory, fascia and chromatised pig's bladder were also tested with little success [48,49].

Boston surgeon, Dr. Marius Smith-Peterson developed the idea of hip interposition and in 1926 introduced the 'mould arthroplasty' [50]. The articular surface of the femoral head was removed using a reamer and a glass hollow hemisphere used to cover the femoral head. Unfortunately, the glass wasn't able to withstand the stresses placed upon it and fractured after short implantation times. In 1937, he adopted cobalt-chrome alloy named Vitallium (60% Co / 20% Cr / 5% Mo and traces of other substances [51]) for his mould arthroplasties [7]. The introduction of cobalt-chrome

proved sufficiently successful to allow the widespread use of mould arthroplasties [52]. However, pain relief following cup arthroplasty wasn't very predictable and hip movement was limited. In addition, the technique didn't allow surgeons to treat a range of arthritic deformities of the hip [47].

In the late 1930's, Philip Wiles developed a total hip arthroplasty at the Middlesex Hospital in London. The all-metal prosthesis consisted of a cup that screwed into the acetabulum and a femoral stem bolted to the outside of the femur (Figure 2-5). In 1938, Wiles carried out the first total hip replacement. The technique was offered to patients who predominantly had juvenile chronic Arthritis and were bedridden or just able to walk. Results were stated as being 'only tolerable' in 25% of cases although a full explanation of the outcomes was not given [47].

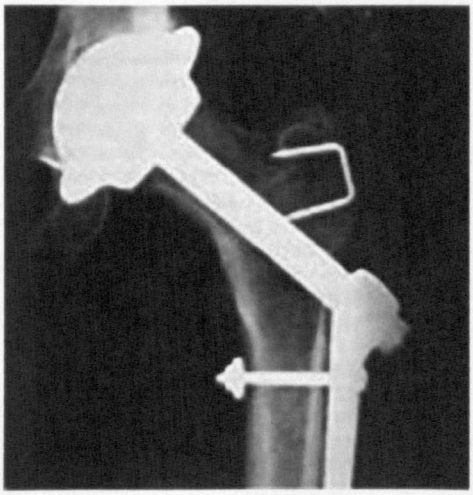

Figure 2-5 Wiles total hip replacement

In 1946, the Judet brothers carried out a 'resection-reconstruction' using a poly-methyl methacrylate (PMMA) femoral stem that passed axially down the neck of the femur [48, 53]. Although the prosthesis quickly proved too weak, the work led to the acceptance of the intermedullary shaft as a means of locating femoral prostheses.

Acrylic may have proved to be unsuccessful as a bearing material, but in the 1950's, Dr. Haboush successfully used an acrylic fast-setting dental cement to anchor hip prostheses. In the 1960's Charnley used a pink dental acrylic cement called 'Nu-Fix' to anchor THR components in position (Figure 2-6).

Figure 2-6 Section of a Charnley PTFE acetabular cup showing pink dental cement

The application of acrylic as a bone cement brought with it a new era in orthopaedic fixation techniques with acrylic still being used today.

During the 1950's a number of surgeons began regularly installing stainless steel THR. Charnley had noted the 'squeaking' noise emanating from these early metal-metal arthroplasties [53]. He performed experiments [54, 55] to show that metal-metal joints had high frictional torque and postulated that this might lead to loosening of the implant. As a result, in 1958 he developed a low friction arthroplasty consisting of a polytetrafluoroethylene (PTFE, Teflon™) acetabular cup and a Moore stainless-steel

prosthesis (Figure 2-7) [53].

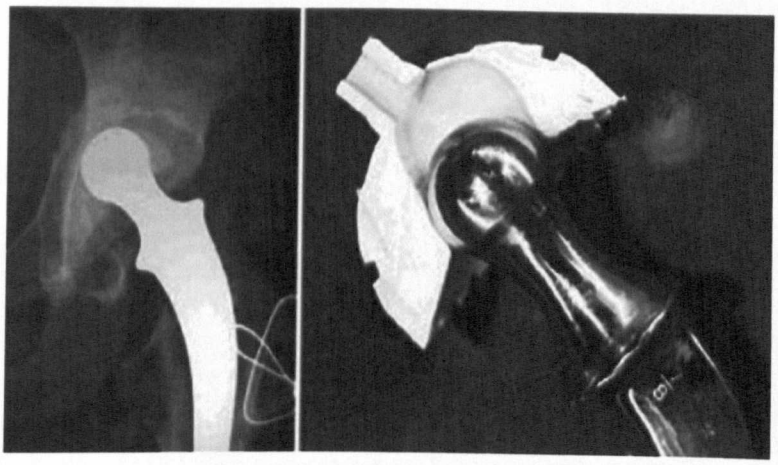

Figure 2-7 Photo and x-ray of an early Charnley THR

Charnley used this combination up until 1963 when the use of Teflon was halted. Although the joint articulation was successful in the first one to two years after surgery, over 99% had to be revised within two to three years of implantation due to severe wear and the inflammatory response provoked by the PTFE wear debris.

Undeterred, Charnley experimented with a glass filled PTFE called 'Fluorosint' [56]. Wear testing on acetabular components made from this material were encouraging as wear predictions indicated a 10 times improvement in wear rate over PTFE. Components fabricated from Fluorosint were implanted but displayed severe wear rates. Following the clinical failure of filled PTFE Charnley briefly abandoned the development of his THR system. In May 1962, Charnley was introduced to a new polymer called Ultra-High Molecular Weight Polyethylene (UHMWPE). Charnley was initially sceptical about this new material and it was his technician Mr Craven who took it upon himself to fabricate some acetabular components from UHMWPE and conduct wear testing on the devices. After three weeks of wear testing, the UHMWPE

had displayed an equivalent degree of wear as was seen for PTFE components after only 24 hours of testing. These results convinced Charnley to pursue the use of UHMWPE for acetabular components [53]. The material used by Charnley was compression moulded RCH-1000 UHMWPE manufactured by Ruhrchemie (later merged into Hoechst) [57]. In November 1962, he carried out the first THR using an UHWMPE cemented acetabular cup in conjunction with a stainless steel 316L femoral head 22.25mm diameter [57]. The combination of UHMWPE cup and stainless steel femoral component was termed the 'low friction arthroplasty' (LFA) and proved to be a great success in terms of component function and longevity. Since the 1960s, numerous designs have been developed based on Charnley's LFA concept but the LFA is still regarded as the 'gold standard' worldwide. Charnley's selection of a 22.25mm diameter articulation was based on preliminary testing that demonstrated that the use of smaller diameter femoral heads resulted in reduced wear rates compared to larger diameter heads. The use of 22.25mm diameter femoral heads compared to 28mm or 32mm minimises torque and sliding distance resulting lower rates of wear. Creep of the liner can occur quickly and increase the contact area by up to 56% leading to a reduction of contact pressure by up to 41% [58]. The use of smaller femoral heads can result in greater creep penetration but leading to higher linear wear penetration but reduced volumetric wear. An additional issue relating to femoral component diameter is the prevalence of posterior joint dislocation [59] with 22.25mm joints. When researchers increased the femoral head size from 22.25 to 28mm the range of flexion prior to impingement 5.6 degrees and by an average of 7.6 degrees prior to posterior dislocation. However, when the head size was increased from 28mm to 32mm, no significant improvement occurred in the patient's range of motion.

2.4 Total Hip Replacement Design

There is considerable variation in prosthesis design, but THR can be placed into three broad categories based on the fixation technique used; cemented, un-cemented and hybrid (cemented stem with an un-cemented acetabular cup). Of the three, cemented prostheses make up about 90% to 95% of the current total UK THR market [1]. It is estimated that in total there are 60 different THR prostheses currently available. In addition to the introduction of new designs, current prostheses may undergo developmental iterations by the manufacturer. There have been numerous instances where the introduction of new prostheses or changes to existing prostheses, have resulted in early failure rates of THR in some patients [1].

The National Institute for Clinical Excellence (NICE), state that the best prostheses (using long term viability as the determinant) demonstrate a revision rate of 10% or less at 10 years. This should be regarded as the current 'benchmark' in the selection of prostheses for primary THR [1].

Along with the mechanical design of THR components, materials selection is also an important part of the design process. As mentioned earlier, Charnley's LFA concept consisting of a UHMWPE acetabular cup and metal (CoCr of stainless steel) femoral stem is the gold standard. There are THR systems that utilize acetabular components with ceramic or metal bearing surfaces and femoral heads with ceramic bearing surfaces. However only cemented DePuy UHMWPE acetabular THR components were assessed during this study due to the widespread use of this joint type and manufacturer in Nottinghamshire.

Extraction of hip replacement components can involve the use of a range of equipment including osteotomes, gouges, drills and high-speed burrs. In order to remove the acetabular component it is first disrupted from the cement mantle. The cement should be carefully removed using gouges and osteotomes to disrupt the cement bone interface with the minimum of bone loss. Specialist tools such as the Explant (Zimmer, Warsaw, Indiana) (Figure 2-8) are also available to simplify the extraction process. The device functions by the use of short and then long blades to break the bone-prosthesis interface with minimal bone resection. Any residual soft tissue is debrided to allow visualisation of the rim of the acetabulum circumferentially to enable an estimation of bone defect to be made [60].

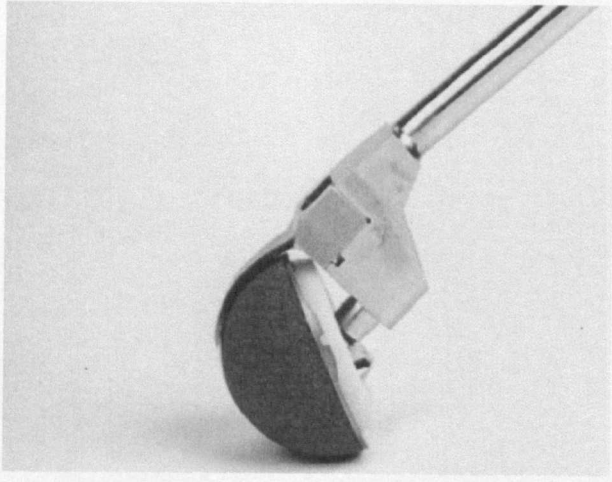

Figure 2-8 Zimmer Explant tool

2.5 UHMWPE

2.5.1 History

German organic chemist Karl Ziegler and Giulio Natta shared the Nobel Prize for Chemistry in 1963. Ziegler and Natta discovered in 1953 a family of stereo-specific catalysts capable of introducing an exact and regular structure to various polymers. This discovery formed the basis of nearly all later developments in synthetic plastics, fibres, rubbers, and films derived from such olefins as ethylene (ethene) and butadiene (but-1,2:3,4-diene).

Between 1932 and 1935, a research program was initiated by ICI to develop new high pressure reaction materials. Around 50 different reactions were tried, all without success but one failure resulted in the accidental discovery of polyethylene. One of the mixtures included ethylene, a very light gas prepared from petroleum and the high pressure reaction left a white waxy solid on the walls of the reaction vessel that was later found to be polyethylene. However, unknown to researchers, the synthesis of polyethylene had occurred due to an air leak in the apparatus that led to oxygen being present during the polymer synthesis. A major development programme was then initiated by ICI to attempt to produce polyethylene but this failed as it was only later that the role of oxygen in the process was identified.

In 1953 in Germany, Karl Ziegler made the crucial discovery, by which one could make the molecules of ethylene join up in a more disciplined manner on the surface of particles of "Ziegler catalyst", and without the high pressures and temperatures previously required, which also entailed a lot of expensive engineering. This produced polyethylene with the linear chains everyone was hoping for. It was much more rigid, and could handle boiling water. Meanwhile, Robert L. Banks and J. Paul

Hogan were developing the Phillips process which used a cheaper and easier to handle catalyst, but required medium pressure and therefore more engineering. Both processes are widely used to this day.

Ziegler shared the Nobel Prize for his discovery with Giulio Natta, who simultaneously discovered how to discipline other monomers in order to produce other plastics, of which polypropylene is by far the most important. That is why, in general, these are referred to as Ziegler-Natta catalysts).

2.5.2 UHMWPE Structure

Polyethylene is a generic term for polymeric materials based on the ethylene monomer unit (Figure 2-9).

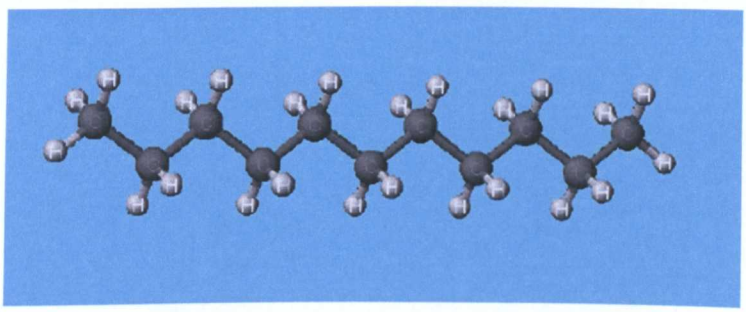

Figure 2-9 Polyethylene -(CH_2CH_2)~

Ultra-high molecular weight polyethylene (UHMWPE) is a member of the polyethylene family along with low density polyethylene (LDPE) (linear or branched) and high density (HDPE) polyethylene. Differentiation between the various forms of polyethylene is primarily based on molecular weight, itself dependant on the chain length and structure.

UHMWPE consists of long, linear chains more than a kilometre long giving the material a very high molecular weight [61] in the region 2-6 million g/mol. As the molecular weight of UHMWPE is so high, it cannot be measured directly using conventional techniques and is instead inferred by its intrinsic viscosity [62].

UHMWPE is a semi crystalline polymer and as such, contains crystalline lamellae embedded in amorphous regions. Crystalline lamellae can be formed when UHMWPE is cooled below its melt temperature. This is due to rotation of the polymer chain about C-C bonds that causes chain folding and the creation of localized ordered areas. Tie molecules are parts of the polymer chain that link amorphous and crystalline areas. Figure 2-10 depicts the structure of UHMWPE [61, 63]. The degree and orientation of crystalline regions within UHMWPE depends on a number of such as molecular weight, processing conditions, and environmental conditions (i.e. loading). The percentage of crystallization in bulk UHMWPE material is typically between 50-55% [62]. The mechanical properties of UHMWPE are determined by the ratio and distribution of crystalline and amorphous regions (crystallinity), the number of connections between the crystalline regions (number of tie molecules, which is inversely proportional to the thickness of the crystallite), the number and nature of connections within the amorphous regions (the degree of mechanical entanglements and crosslinks) and the presence or absence of orientation of the crystallites [64].

The elastic modulus of UHMWPE is sensitive to changes in crystallinity and crystalline orientation increasing almost linearly with increasing crystallinity. If the elastic modulus increases without a proportional increase in yield strength the probability of plastic contact in the UHMWPE may increase leading to an increase in the wear rate [65]

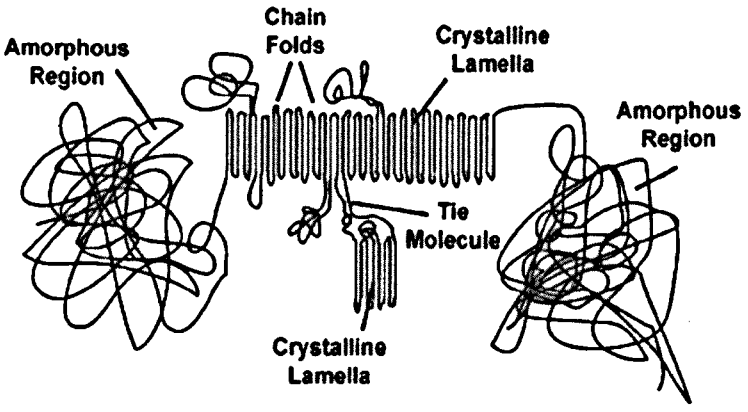

Figure 2-10 Structure of UHMWPE

2.5.3 UHMWPE Polymerisation

Commercial polymerization of UHMWPE first began in 1955 by Ruhrchemie (now known as Ticona) using the Ziegler-Natta catalyst process. UHMWPE is polymerised from ethylene gas using hydrogen and titanium tetra chloride (catalyst) to form resin powder. Polymerisation is carried out in a solvent used to aid mass and heat transfer. Chemical formula's for ethylene (C_2H_4) and polyethylene $-(C_2H_4)_n-$ are depicted in Figure 2-11 and Figure 2-12 respectively [66].

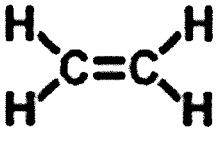

Figure 2-11 Chemical structure of ethylene

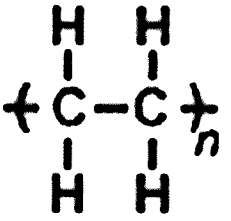

Figure 2-12 Chemical structure of polyethylene

Until recently, there were two companies that produced UHMWPE resins for orthopaedic applications, Ticona and Basell Polyolefms. Basell Polyolefins produced 1900H type 3 resin but production ceased in January 2002. This left Ticona as the sole supplier of UHMWPE resins for orthopaedic applications. Ticona uses the designation GUR for its UHMWPE grades worldwide; the acronym GUR is derived from (G)ranular (U)HMWPE (R)uhrchemie [67]. They currently produce two grades of UHMWPE, GUR 1050 and GUR 1020 having recently stopped production of GUR 1 150 and GUR 1 120 resins. GUR 1 150 and GUR 1 120 contained added calcium stearate [66].

In addition to the resins mentioned, there are numerous references in the literature to different trade names for UHMWPE, many of which are no longer used.

The requirements for medical grade UHMWPE powder are specified in ASTM standard F648 and ISO standard 5834-1. Medical grade resins are categorised as being Type 1, 2, or 3 depending on the molecular weight and producer. The catalyst is responsible for the trace impurities of Ti, Al and Cl whilst the storage and handling of the powder after polymerization influence the trace levels of Ca and Ash content (Table 1) [66, 68].

Property	Requirements	
Resin Type	Types 1 & 2	Type 3
Trade Name	GUR 1020 & 1050	1900H
Producer	Ticona Inc.	Basell Polyolefins (discontinued)
Ash (mg/kg)*	150	300
Ti (ppm)*	40	150
Al (ppm)*	40	100
Ca (ppm)*	50	50
Cl (ppm)*	20	90

* Maximum allowable

Table 1 Table outlining the requirements for medical grade UHMWPE powder

Calcium stearate was used as an additive in the production of UHMWPE resin up until 2002. It was added to UHMWPE resin as it acts as a scavenger for residual catalyst components and it also acts as a lubricant and release agent [63]. When calcium stearate is added to UHMWPE resin, the surface of polymer particles are coated by the calcium stearate. In the early 1980's, calcium stearate was implicated as a cause of fusion defects and oxidation of UHMWPE [63, 69, 70].

Fusion defects can have a deleterious effect on the fatigue and fracture behaviour of UHMWPE whilst oxidation has been shown to affect the wear behaviour of UHMWPE. However, when fusion defects are not present, the effect of trace levels of calcium stearate is unclear. In the 1990's, improvements in polymerisation and processing technology meant that calcium stearate was no longer necessary. In 2002 Ticona discontinued production of their calcium stearate containing resins (GUR 1120 and 1150) due to lack of demand from orthopaedic manufacturers [66].

2.5.4 UHMWPE Consolidation

The high melt viscosity of UHMWPE means that it has to be consolidated under elevated temperatures and pressures. Thermoplastic polymers can generally be processed using a range of techniques including injection moulding, blow moulding and screw extrusion. However, the high melt viscosity precludes the use of these processing methods so compression moulding and ram extrusion are the main techniques used.

Manufacturers are very guarded on the process conditions used to produce UHMWPE however the fundamental scientific basis for the consolidation of UHMWPE powder has been discussed in some detail. [71, 72]. The primary mechanism involved in the consolidation of UHMWPE is diffusion. Adjacent resin particles interact at a molecular level with the processing conditions (temperature and pressure) controlling the rate of diffusion. High temperatures and pressures are used to improve the mobility of polymer chains and reduce the distance between interfaces. Because the process is diffusion-dependant, the material has to be kept at the processing temperature and pressure for the specified amount of time. This is to give the molecular chains time to migrate across grain boundaries.

Compression moulding has been used to produce UHMWPE since the 1950s and the material was initially sold under the trade name RCH1000/ Hostalen GUR 412.

The process involves heating the UHMWPE powder in a press with heated platens in order to produce sheet material. Processing can take up to 24 hours in the case of large sheets of material (2m x 4m x 80mm). RCH1000 was the material used by Sir John Charnley to fabricate acetabular components in the 1960s. The material was also distributed under the name CHIRULEN and is very similar to contemporary GUR 1020. It should be noted that GUR412 contained calcium stearate whilst GUR1020

does not. There are currently two companies that produce compression moulded GUR1020 and GUR1050 UHMWPE, Perplas Medical and Poly Hi Solidur Meditech.

Ram extrusion was developed in the 1970s in the United States. The process starts with UHMWPE powder being continuously fed into a heating chamber where the powder becomes molten. Heated UHMWPE is then forced through a heated die and the formed rod exits the extruder through an outlet. The rod then gradually passes through a series of heated mantles to slowly cool it. Rod diameters ranging from 20 to 80 mm are produced for medical applications. As with compression moulding, the production rate can be extremely slow depending on the dimensions of the consolidated form and production rates of the order mm/minute are not uncommon. Only a small number of companies that currently supply ram extruded GUR1020 and GUR 1050 UHMWPE, Poly Hi Solidur, Westlake Plastics and Perplas Medical.

Despite the differences in processing routes, the properties of GUR 1020 and GUR1050 produced via extrusion and compression moulding are very similar. Kurtz et al (2001) investigated the properties of these resins and found that the material density was sensitive to the type of resin but not the conversion method. However, the impact strength and the tensile mechanical properties were sensitive to the type of resin and conversion method [73].

A summary of properties of UHMWPE along with other polymeric materials and metals used for femoral heads is given in Table 2.

	Material	Molecular weight ($gmor^{1}$)	Coefficient of friction	Crystallinity (%)	Density (kg/m^{3})	Elastic Modulus (GPa)	Yield Strength (MPa)	Ultimate Tensile Strength (MPa)	Elongation to Failure (%)
Metal	Co-Cr	n/a	0.4	n/a	8.5	230	410	896	12
	Stainless steel316L	n/a	0.8	n/a	8	200	290	560	40
	Ti 6Al-4V	n/a	0.5	n/a	4.5	100-120	760	1170	10-15
Polymers	UHMWPE GUR 1020	3.3 million	0.1-0.2	45-55	0.93	0.8-1.5	22	54	450
	UHMWPE GUR 1050	5.0 million	0.1-0.2	45-55	0.93	0.8-1.5	21	51	400
	HDPE	0.5 million	0.29	33	0.94	0.5-1.2	15-40	40	6.6-800
	LDPE	0.001 million	0.4	50	0.91-0.94	0.1-0.3	5-25	21	400
	PTFE	0.01 million	0.05-0.2	20	2.2	0.3-0.8	10-40	140	400
	PEEK	0.0lmillion	0.18	30	1.3	3.7-1.0	70	110	240

Table 2 Physical and mechanical properties of extruded and moulded UHMWPE

2.5.5 Fabrication of UHMWPE Implants

Components are machined in two steps, an initial rough machining followed by a finishing stage. Since UHMWPE can be damaged by excessive heat, the machining variables such as feed rate, tool cutting force, and spindle speed have to be carefully controlled. However, details of machining variables are proprietary and therefore little information is available about the effect of machining parameters on the properties of UHMWPE. [74]. The machining process has been shown to produce a modified surface layer with polymer molecules oriented in the direction of machining. Preferential orientation of this surface layer results in an increase in crystallinity in this layer.

2.6 Anti-microbial Processing of UHMWPE

2.6.1 Introduction

Anti-microbial is a generic term that refers to both sterilization and disinfection techniques. This chapter discusses various sterilisation/disinfection techniques that are used to process new components prior to implantation and also following their retrieval.

2.6.2 Sterilisation versus Disinfection

The term sterile generally refers to the inability of living organisms to reproduce however sterile can also be defined as "free from living micro-organisms" [75]. In the case of anti-microbial processing, the latter definition is applicable. Technically, the presence of a single micro-organism would render the article un-sterile; therefore terms such as 'partially sterile' or 'almost sterile' shouldn't be used. That said it is impossible to guarantee that every micro-organism subjected to a particular treatment will be killed or that every implant has been 100% sterilised. Therefore a sterility assurance level (SAL) is used. The SAL is defined in EN556 as "...the theoretical level of not more than one microorganism is present in 1 xlO^6 sterilized units of the final product" [76].

Disinfection techniques are processes that reduce the number of viable microorganisms in a load but which may not necessarily inactivate some viruses and bacterial spores. In addition, disinfection techniques don't guarantee a specific minimum level of micro-organisms [76].

2.6.3 Sterilisation of New Components.

NHS guidelines on sterilization (HTM 2010) state that all materials, devices, equipment etc. must be sterilised prior to use in invasive surgical procedures. Sterilisation of medical devices is carried out in accordance with ENS52 and EN556 standards. There are many sterilisation techniques in existence but the majority are unsuitable for processing UHMWPE. The decision to adopt a particular sterilisation route is a balance between the risk of damage to material, the potential hazard of residues of toxic sterilization agents, and the risk of lack of efficacy of the sterilization process.

High temperature techniques such as steam sterilisation use temperatures of 120°C or above so are unsuitable for processing UHMWPE that has a melting temperature of approximately 135°C. In addition, researchers investigating retrieved UHMWPE components found that chemical analysis of steam sterilised components gave erroneous results with increased oxidation index values [77]. Gaseous compounds such as ethylene oxide have been used (Wright Medical) but long process times and concerns over the presence of potentially harmful residues have limited its use. Ionising radiation is the prevalent approach to the sterilization of UHMWPE components with gamma irradiation being the most widely used technique. Gamma irradiation (also referred to as gamma ray) has been used to sterilise UHMWPE implants since the 1960's and is the current industry standard today [78].

Gamma irradiation was routinely carried out in air until the mid 1990's. At this time it was realised that processing UHMWPE in this manner made the material prone to oxidation leading to a significant reduction in service-lives of THR UHMWPE joint replacement components. Between 1995 and 1998 orthopaedic UHMWPE component manufacturers began packaging components using reduced oxygen atmosphere or

nitrogenous atmospheres to minimize oxidation. The use of barrier packaging that stops the diffusion of gases into or out of the packaging is also now used. Total elimination of oxidation is not possible though as there will always be small amounts of oxygen present within the structure of UHMWPE.

2.6.4 Gamma-irradiation Process

Gamma sterilization involves the irradiation of components with gamma rays (high-energy photons). The technique uses the radioisotope Cobalt 60 as an energy source and the irradiation process takes place in a specially designed cell. Gamma radiation consists of photons that are emitted from the nucleus of an atom with energies of 1.17MeV or 1.33MeV. Their negligible mass and no charge mean that gamma rays have very high penetrating power with a small percentage of the original gamma 'stream' able to pass through several feet of concrete.

Energy from the photons causes electronic excitations within single atoms of the UHMWPE resulting in highly active electrons and highly reactive free radicals. Sterilization occurs due to these highly active species inducing breaks in the DNA double helix, preventing replication. The unit of absorbed dose is termed the Gray, expressed as kGy or Mrad and typical doses range from 25 to 40kGy (2.5 to 4Mrad) [79].

2.6.5 Primary Electronic Excitations

Photons interact with UHMWPE during the gamma irradiation process causing the electronic excitation of electrons in the material that can then lead to chemical changes in the material. There are three physical mechanisms by which photons interact with electrons of individual atoms: photoelectric effect, Compton scattering and pair production. The photoelectric effect occurs when photons have low energy (<0.5MeV) and all of their energy is transferred to an electron that is then ejected from orbit, and results in the annihilation of the photon. Ejected electrons have energies equal to the difference between the photon's energy and the initial binding energy in the atom. If the photon has more energy than is required to eject an electron the excess energy results in an increase of kinetic energy for the electron.

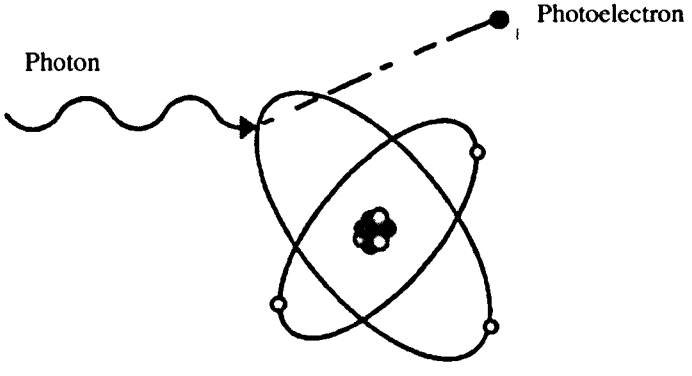

Figure 2-13 Diagram depicting Photoelectric effect

Compton scattering occurs when a photon with increased energy (0.5MeV to 3.5MeV) transfers part of its energy to an electron causing it to be ejected but in addition, a photon containing the remaining energy is emitted in a different direction to the original photon.

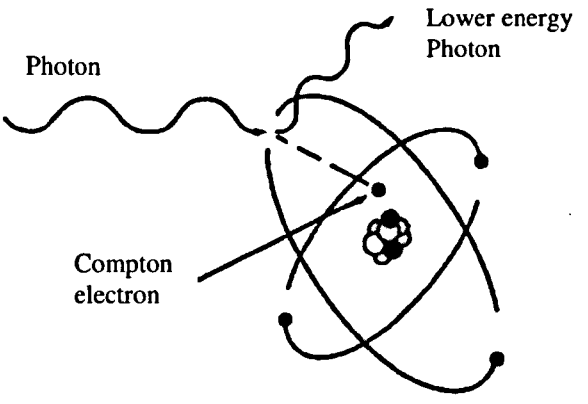

Figure 2-14 Diagram depicting Compton scattering

Pair production occurs when photons with energies >1.02MeV interact with the nucleus of an atom to form an electron-positron pair. 1.02MeV is just sufficient to provide the rest masses of the electron and positron. Any excess energy is divided equally between these two particles producing ionisation as they travel through the material. Positrons are eventually captured by electrons leading to the annihilation of both particles. This annihilation results in the release of two photons each with 0.51MeV. These photons are known as annihilation radiation and lose their energy by Compton scattering or the photoelectric effect.

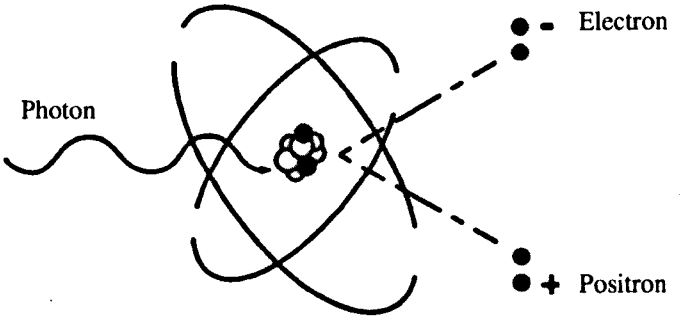

Figure 2-15 Diagram depicting pair production

The dominant mechanism of electronic excitation in organic polymers is Compton scattering. Ejected electrons and scattered photons have sufficient energy to interact with other molecules resulting in the ejection of further electrons. Electrons rapidly recombine with polymer ions but the additional energy provided by the gamma photons during irradiation produces molecules with excited electronic states. In order for molecules to restore their original ground state of electronic excitation, the excess energy has to be transferred. Excess energy is released in the form of heat and emission of light but also chain scission of C-C or C-H bonds causing the formation of primary free radicals as a by-product. The population of primary free radicals is proportional to the total radiation dose.

2.6.6 Secondary Chemical Reactions

Production of primary free radicals leads to secondary chemical reactions within UHMWPE. The chemical reactions that take place are dependant on the environment in which irradiation is carried out under, rate of formation (dose rate), and their mobility (molecular size, crystalline vs. amorphous phase and temperature.). The presence and level of oxygen in the atmosphere in particular has a strong influence over the secondary chemical reactions. This is because free radicals have a high affinity for oxygen and oxidation of the polymer will preferentially occur if oxygen is present in sufficient quantities in the atmosphere. Oxidation of UHMWPE has been shown to cause degradation in the structural and hence mechanical properties of the material. However, when irradiation is carried out in the absence of atmospheric oxygen e.g. under vacuum or inert gas, a different set of chemical reactions will dominate leading to crosslinking of polymer chains.

The effect that secondary chemical reactions have on the structure and hence mechanical properties of UHMWPE are different and exert a great deal of influence on the in-vivo service life of UHMWPE joint replacement components.

Changes in the chemical nature of gamma irradiated UHMWPE have been observed in components that have been stored for long periods of time with oxidation particularly prevalent [80-83]. When radicals initiate within crystalline regions of UHMWPE they are unable to react with oxygen or crosslink due to the tight packing within the lamellae [84, 85]. Migration of these radicals occurs instead over long time periods in order to reach boundaries with the amorphous phase where radical propagation reactions can proceed [86]. Propagation of radical reactions within the amorphous phase continues until all radicals have been terminated which may occur long after gamma irradiation.

It should be noted that as a norm, a limited amount of oxygen will be present in the material itself irrespective of the atmosphere, but it is the absence or presence of atmospheric oxygen that has the major influence on secondary and tertiary chemical reactions.

2.6.7 Post-irradiation Oxidation

Oxidation and chain scission of UHMWPE causes a reduction in the molecular weight of the material and an increase in crystallinity and density which affect the mechanical properties of the material.

The mechanism by which oxidation occurs following gamma irradiation is a complex one and has been previously described by Costa et al [87]. The initial interaction between photons and individual molecules leads to chain scission of C-C and C-H bonds and

generation of primary alkyl free radicals. Numerous secondary and tertiary chemical interactions then occur but there are two key interactions that will be discussed further. The first is formation of new CH_3 end groups that result in a reduction in molecular weight. Alkyl radicals first cause scission of a C-C bond breaking the polymer chain and resulting in two reactive chain ends. Reformation of the C-C bond can occur at this point but if there are free H atoms present (that have been released from CH_2 molecules by radicals) these can react with the C atoms of the broken C-C bond to form stable CH_3 end groups.

The second reaction of note is the formation of hydroperoxides and additional free radicals that leads to the propagation of the oxidation cycle through the material. This occurs when oxygen reacts with secondary radicals leading to the formation of secondary peroxide radicals. The secondary peroxide radicals extract H atoms from additional CH_2 molecules leading the formation of secondary hydroperoxides and tertiary radicals. Hydroperoxide group effects are also significant because they add a time-temperature dependence to the degradation mechanism that results in long-term post-irradiation effects via autoxidation [88, 89].

2.6.8 Sub-surface White Band

Post-irradiation aging of UHMWPE is a time-dependant process that can result in severe degradation of the mechanical properties of sub-surface regions of UHMWPE as a result of increased levels of oxidation and associated increases in crystallinity.

The formation of this brittle subsurface layer commonly referred to as 'white band' [90-92] is essentially governed by the availability of oxygen to free radicals generated during gamma irradiation. At the surface of components, there is an abundance of atmospheric oxygen and high surface area. Free radicals are consumed in this region as they rapidly react with the atmospheric oxygen. As the distance from the bearing surface increases, the availability of oxygen decreases but the presence of free radicals increases enabling oxidation of the material. In the bulk of the material, there are available free radicals but oxygen levels are not sufficient to promote oxidation of the material. The presence of 'white band' (Figure 2-16) has been reported in a number of UHMWPE component retrieval studies [91, 93, 94].

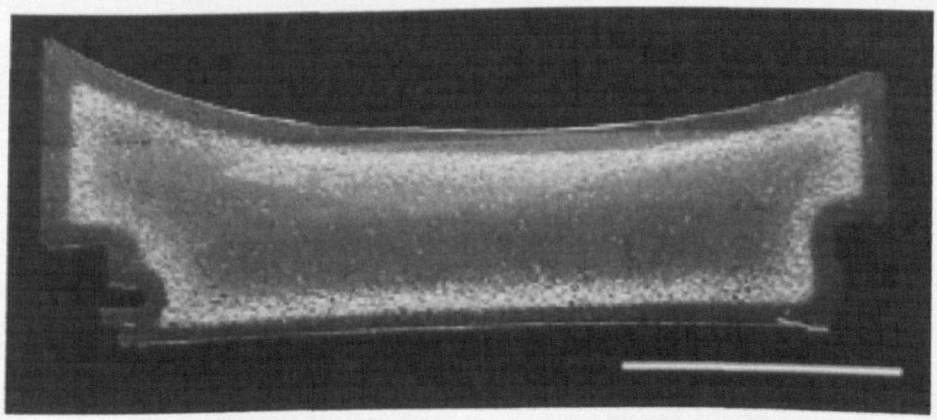

Figure 2-16 Optical micrograph of through thickness section from 7 year shelf aged UHMWPE tibial component after gamma-irradiation (Watanabe et al [64]).

An analysis of sub-surface features of retrieved gamma irradiated UHMWPE acetabular components was carried out by Wentz et al [95]. The researchers generated through thickness samples using a freeze fracture technique that involved immersing sections of UHMWPE cups in liquid nitrogen and then fracturing them with a three-point bend test. The SEM image shown in Figure 2-17A is taken from an oxidized region and shows the radially oriented meshlike structures that appear porous in nature. Figure 2-17B was taken in an un-oxidized homogenous region of well consolidated particles. The image was reported to be representative of previous structural analyses carried out on ram extruded UHMWPE bar stock.

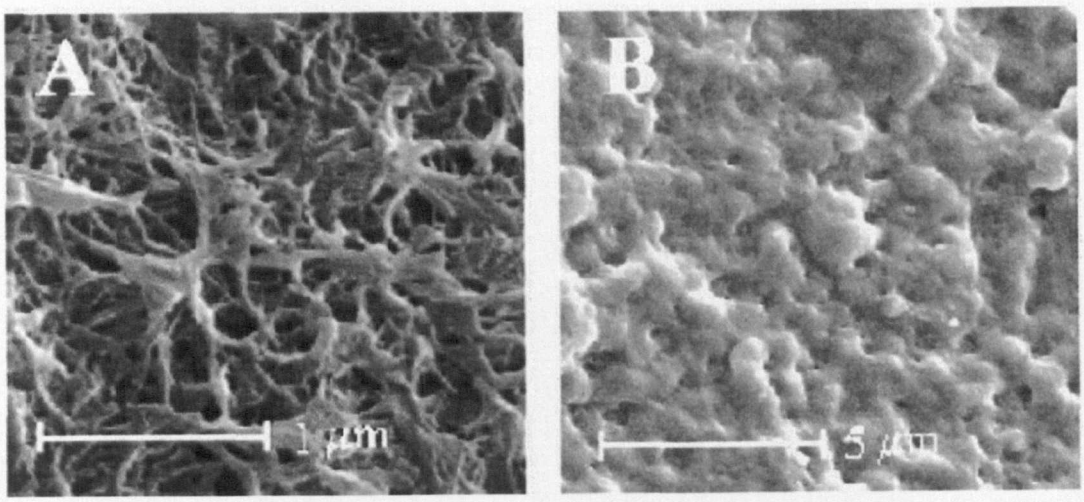

Figure 2-17 SEM images of subsurface regions of a retrieved UHMWPE component

Broadly speaking, post-irradiation aging in air (shelf aging) leads to accelerated ageing, compared to aging in vivo. A number of studies have shown that non-aged UHMWPE irradiated hi air exhibits an accelerated rate of wear in vitro compared with the un-irradiated material [96-98].

2.6.9 Fluid Ingress

Synovial fluid normally contains hyaluronic acid that regulates the viscosity of the synovial fluid and lubricates the surfaces between synovium and cartilage. It also contains lubricin which is secreted by synovial cells and is principally responsible for boundary-layer lubrication between bearing surfaces [99].

The mechanism of diffusion of solids, liquids and gases into polyethylene has been reported previously [100]. The synovial fluid is absorbed on the surface and then moves towards the bulk [101].

Previous researchers have reported that the ingress of synovial fluid into UHMWPE plays a part in the wear process [102, 103]. Diffusion of synovial fluid constituents into the surface of UHMWPE leads to the surface becoming plasticised which results in a reduction in mechanical properties such as tensile strength and ultimate elongation. The reduction in mechanical properties will lead to a reduction in abrasion resistance of the material [104].

Costa et al (2001) [102] identified specific constituents of synovial fluid that had been absorbed by UHMWPE components in-vivo using FT-IR. These included cholesterol, fatty esters of cholesterol and squalene. They also noted that the concentration of these different constituents was dependant on individual patients.

Recently, Costa et al (2002) [105] investigated the chemical properties of 29 retrieved UHMWPE acetabular cups. Each of the cups had been sterilized using ethylene oxide at the time of manufacture as opposed to gamma irradiation. Using FT-IR they found that ingress of fluid had occurred at all of the external surfaces although in worn regions synovial fluid components were observed at greater depths than unworn

regions. They reported that the absorption and diffusion of synovial fluid components would make the wear surface softer than the bulk due to non-homogeneous plasticisation. The presence of synovial fluid components at the surfaces of retrieved UHMWPE components echoed earlier studies by Brach del Prever (1996) [106] and Costa et al (1998) [107] who also used FT-IR to investigate the chemical nature of UHMWPE from retrieved hip joint replacements.

It is probable that the increased absorption of fluid in the worn regions of retrieved components was linked to the mechanical loading in these regions.

Blanchet et al (2002) [108] carried out an in-vitro study into the uptake of serum into un-irradiated and cross-linked UHMWPE under different hip loading conditions. They found that the time-response of fluid absorption was biphasic. Initially, there was a short period (<1 week) of rapid ingress before settling to a steady-state phase of linear absorption with time. Varying the loading between 0.1 and 10MPa resulted in a four fold increase in fluid uptake during the rapid uptake phase and a two fold increase in the steady state uptake of fluid. Another interesting finding was that the steady-state rate of absorption was dependent on temperature, with values at room temperature being two-fold less than at 37°C.

The available surface area will also influence the uptake of fluid into the material. Klapperich et al (2000) [109] investigated this issue by evaluating samples of the same volume but different surface areas. They reported a weight gain of 32mg for samples with 8400mm^2 surface areas and 46mg for samples with 122000mm^2 surface areas. This study inferred that UHMWPE components with larger external surface margins will absorb more fluid than components with small surface areas. The uptake of fluid into

conventional and cross-linked UHMWPE was also reported by Yao et al (2003) [103] who also demonstrated that this absorption of fluid was accompanied by an increase in wear rate.

2.6.10 Crosslinking

Crosslinking of UHMWPE occurs when neighbouring polymer chains form links. This process starts with the scission of a C-H bond leading to the extraction of a mobile H atom. The H atom goes on to extract a second H atom from an adjacent methylene molecule and reacts with it to form Ha along with a trans-vinylene C=C double bond. If there is no available oxygen and two neighbouring secondary alkyl radicals are close enough, they can couple and form a branched or crosslinked chain.

A number of researchers have found that crosslinking UHMWPE can improve the wear resistance of the material. McKellop et al [19] and Wang et al. [20] conducted wear simulator studies on UHMWPE components sterilised by different techniques (ethylene oxide, gas plasma and gamma irradiation). UHMWPE components that had been gamma irradiated with a 25kGy dose demonstrated a 50% drop in wear rate. Despite the promising in-vitro wear testing results, there are concerns over the possible reduction in fatigue resistance of the material following crosslinking. A number of early retrieval studies have now been carried out on components with researchers observing surface damage that had not been predicted by in-vitro studies. [110-112]. Concerns over highly crosslinked UHMWPE are probably heightened by the fact that there have previously been materials such as PTFE, Poly-2 (carbon fibre reinforced UHMWPE) and highly crystalline UHMPWE (Hylamer) that had seemed promising in theory but led to early component failure in-vivo.

2.7 Wear and Degradation of UHMWPE Components

Despite attracting a great deal of attention, the wear mechanisms of UHMWPE acetabular components are still poorly understood.

Investigations into the wear behaviour of UHMWPE components have tended to focus on the macro-scale mechanisms that occur during the wear process and debris generated by wear.

Comparative studies of in-vitro and in-vivo macro-scale wear indicate that wear rates, types of surface damage and wear debris are similar [111]. Improved wear simulation has in part been brought about by an increased understanding of the macro scale wear mechanisms that occur at the bearing surfaces of hip replacements. Wear debris is known to play an important role in the failure of UHMWPE components via aseptic loosening (i.e. loosening in the absence of bacterial or other microbiological infections) with irregularly shaped particles in the size range 0.1 to 10μm shown to stimulate greater macrophage activation than other particles [113]. Much research has been carried out to characterise this debris and its interaction with the body and the role of wear debris is discussed later in this Chapter. However, it is only recently that attention has begun to turn towards developing an understanding of the interactions between mechanical loading and the structure of UHMWPE in the process of wear. The importance of researching this area is highlighted by the fact that wear debris is generated on the micron scale and that clinical wear studies have found links between processing variables (i.e. resin, sterilization method, degree of crosslinking etc.) and wear rates.

2.7.1 Biomechanics of the Hip

During normal activities such as walking, rising from a chair and climbing the stairs, large forces and moments are developed within the hip joint. A number of previous researchers have assessed hip joint forces using instrumented hip prostheses for up to three years following implantation. Data from these studies indicated that the peak force developed across the hip during normal gait varied by a multiple of 2.6 to 4.1 times the patient body weight. Torque acting on the hip prosthesis ranged from 74 to 189 in-lb with peak values up to 291 in-lb. Joint forces were found to increase with body weight, stride length and walking speed. During strenuous exercise, the joint forces were found to increase by up to 8 times the patient body weight.

A simplified mechanical model of the hip joint during one-legged stance is shown in Figure 2-18. The diagram is presented from an anterior-posterior viewpoint. Body weight supported by the hip is represented by a single force (W) passing through the centre of gravity of the body. Muscle contraction balances this force that stabilizes the pelvis by counteracting the leverage developed by the weight of the body. The sum of the muscle forces is represented by a net abductor muscle force (FA) which acts in the direction of the glutei muscles. The hip joint supports approximately 5/6 of the total body weight.

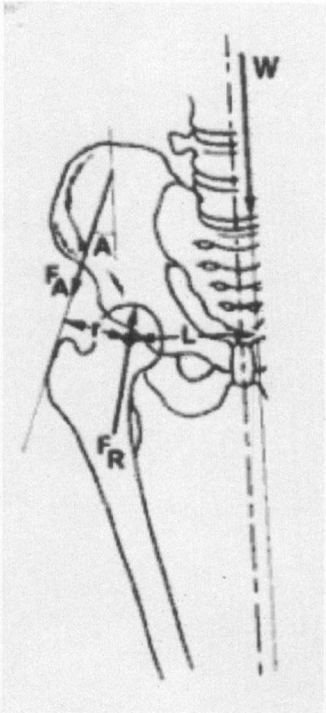

Figure 2-18 Simplified mechanical model of the hip during on-legged stance

Equilibrium of forces is reached when the abducting effect of the forces equals the adducting effect of the body weight acting around the hip joint fulcrum (Equation 2-1)

$$F_A r = \frac{5}{6} WL \qquad \text{Equation 2-1}$$

Where r is the minimum distance from the abductor muscles to the joint centre, W is body weight and L is the horizontal distance from the centre of gravity of the body to the joint centre. Equation 2-1 can be re-arranged in order to assess abductor force as follows (Equation 2-2):

$$F_A = \frac{5}{6} W\left(\frac{L}{r}\right) \qquad \text{Equation 2-2}$$

The re-arranged equation (Equation 2-2) indicates that in order to maintain hip stability, the abductor force required is proportional to the ratio of L and r. Typically, the ratio of L/r is 2.5 which would indicate that the abductor force would need to be 2.1 times body weight. It's also possible to calculate the total force (FR) acting on the hip joint by adding the vertical and horizontal components of the joint reactive force. Taking the L/r ratio of 2.5 again, this gives (Equation 2-3):

$$F_R = \frac{5}{6} W (725 + 5\cos A)^{\frac{1}{2}} \qquad \text{Equation 2-3}$$

Where A is the angle of the abduction force which is typically equal to 20°. For this angle, the value of FR is 2.88 times body weight.

The primary factor in determining the magnitude of the joint reaction force is magnitude of the muscle forces controlling the joint motion. Muscle forces need to be several times larger than the weight of the body in order to balance the forces causing joint motion. When undertaking activities that require greater joint motion, the centre of gravity of the body moves even further from the joint and therefore requires greatly increased muscle and joint reaction forces to balance the joint motion forces.

2.7.2 Wear of Retrieved UHMWPE Acetabular Components.

Wear of UHMWPE components is influenced by design and orientation of prostheses. Several key factors that have received attention previously are cup thickness, femoral head size, radial clearance and acetabular component inclination angle in-vivo.

In the previous section regarding the simplified biomechanics of the hip, the joint reaction force was discussed. The assessment of radiographs of acetabular retrieved components in-vivo reveals a disparity between the direction of peak joint reaction force and the direction of maximum linear wear. This disparity is due to the increased sliding distance of the femoral head at point A compared to point B (Figure 2-19).

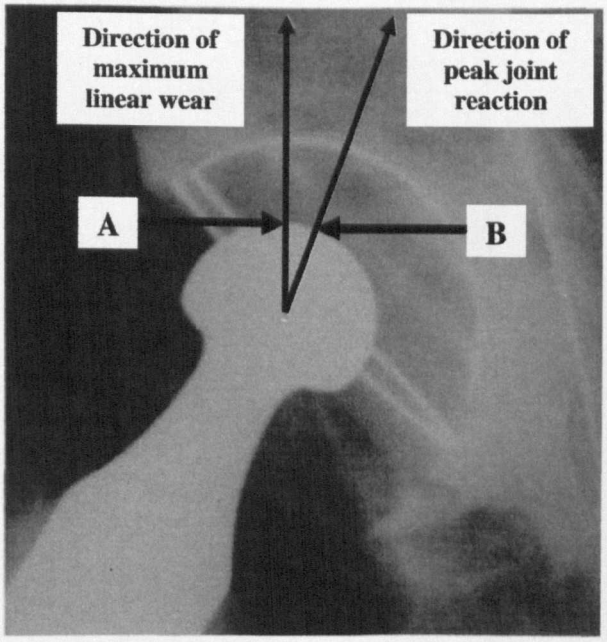

Figure 2-19 Radiograph showing directions of peak joint reaction force and maximum linear wear

The sliding distance in the region of highest wear is inextricably linked to the diameter of the femoral head and it relationship with wear has been reported previously [114-118]. Pietrabissa et al [114] produced a parametric mathematical

model of the head-cup wear coupling in total hip arthroplasty and predicted a linear increase of UHMWPE wear rate as a function of femoral head diameter in accord with Charnley's 'low friction' theory (Figure 2-20).

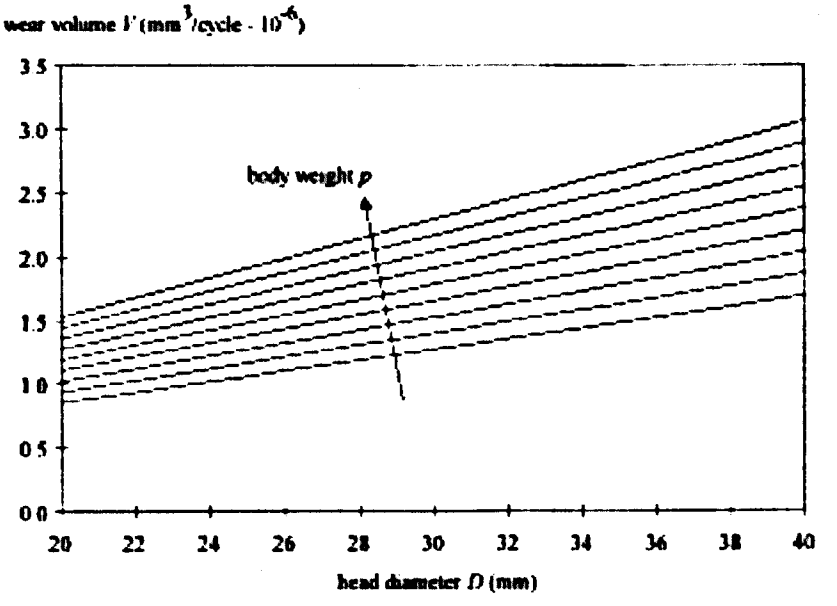

Figure 2-20 Relationship between wear volume and femoral head size

There is however, disagreement over the link between wear rates and femoral head diameter. Certain researchers have found agreement with the linear dependence model [119,120] whilst others have observed that the lowest wear rates are generated by 28mm femoral heads [115-118]. To make matters even more complicated, there is also evidence to suggest that no relationship between femoral head size and wear rates exists. Linear wear rates 0.20mm/year from explanted Charnley acetabular components articulating against 22.25mm femoral have been reported by Hall et al. [121] and Atkinson et al. [122]. Similar linear wear rates have also been reported for acetabular components mated with 28mm and 32mm diameter femoral heads [123].

Aside from sliding distance, the contact stress is also influenced by the size of the femoral head. As the diameter of the head decreases, the contact stress increases

ranging from 8-25MPa in compression [124, 125]. Acetabular cup thickness also increases the contact stress at thicknesses less than 6-8mm [117,126,127].

The inclination angle of acetabular component has been identified as an important factor in the wear of UHMWPE components. Rixrath et al [128] have recently developed and published a mathematical model to calculate the contact stress distribution in total hip replacements between articulating surfaces. The researchers included the clearance between bearing surfaces, inclination of prosthesis and thickness of UHMWPE liner in their model. They found that the magnitude of the maximal contact stress remained constant for inclination values in the range 0-35° but increased significantly with cup clearance and liner thickness for inclination values in the range 35-65° which correspond to physiological implantations. Another point the researchers made was that the cup position generally varied around 45±10° relative to the longitudinal axis but reached extreme values 35-60° in abnormal gait often observed in the elderly population [129]. The impact of inclination angle on wear has also been reported by other researchers who reported similar findings [130].

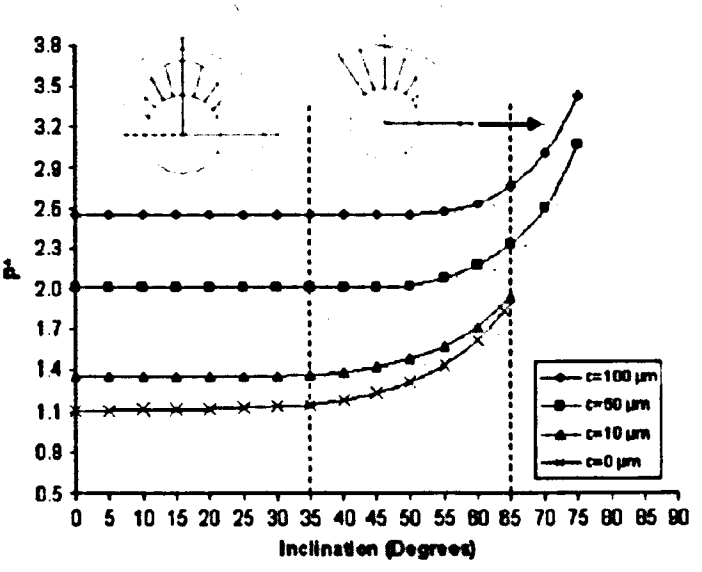

Figure 2-21 Normalized peak contact stress in the gait phase as a function of inclination angle and clearance (taken from Rixrath et al (2008)) [128]

Figure 2-21 shows the normalized peak contact stress in the gait phase as a function of the inclination varying in the range 0-90° for four values of clearance (c=0, 10, 50. 100μm) and where P* is the normalized contact stress. It should be noted that the researchers made several key assumptions including pure radial displacement, no friction between cup and artificial femoral head and static loading conditions and that linear and elastic properties of the UHMWPE and small deformations. The influence of clearance on peak contact stress in the mathematical model is clearly depicted. Contact stress for a clearance of 100μm was constant for inclination angles 0-50° whilst for a clearance value approaching 0μm the peak contact stress increased noticeably at inclination angles greater than 30°.

In a separate study, Patil et al [131] investigated the influence of acetabular component inclination angle in a hip simulator study. They found significantly different wear rates between cups with inclination angles of 45° and 55° (mean wear

rate of 17.2 compared with 21.7 mg/million cycles; $p < 0.01$). They went on to conduct a radiographic analysis of components in-vivo that also showed a significant correlation between inclination angle and the linear polyethylene wear rate. They reported a 40% increase in mean linear polyethylene wear for cups with an inclination angle of 45° or more.

The importance of radial clearance was reported by Rixrath [128] and is depicted in Figure 2-21. Wang [132] also reported the significance of radial clearances demonstrating that as they decreased, the wear factor increased in a linear manner but at clearance values less than 0.5, the wear factor increased markedly in an exponential fashion (wear factor of 3.5 $x10^{-6}$ mm^3/Nm at clearance values approaching 0mm and 1 x $10^{-6}mm^3/Nm$ at clearance of 2mm).

2.7.3 Wear Mechanisms

Wear can be defined as the erosion of material from a solid surface by the action of another solid. In THR, the change in UHMWPE acetabular component dimensions is primarily due to wear but viscoelastic creep also occurs due to compression along the loading axis. The contribution of creep to these dimensional changes is only slight and is generally deemed insignificant [133-135].

Numerous attempts have been made to classify wear in terms of processes involved in producing debris. Burwell proposed one of the earliest classifications that consisted of four main processes, adhesion, abrasion, fatigue and corrosion (tribological-chemical interactions).

Researchers have identified abrasive and adhesive wear as the predominant mechanisms of wear in hip replacements through visual inspection of retrieved UHMWPE bearing surfaces.

Adhesive wear is characterised by the presence of flakes, lumps and shallow pits generated when localised areas of UHMWPE adhere to the opposing metal bearing surface. Adhesive wear behaviour has been related to the plastic flow of the UHMWPE material at the bearing surface and the subsequent generation of wear debris. Large-deformation plastic strain is thought to accumulate at the bearing surface under multi-axial loading conditions until a critical level of strain is reached and wear debris is released [136-138]. The presence of a plasticity induced damage layer is associated with permanent re-orientation of crystalline lamellae [139, 140].

The significance of surface re-orientation of UHMWPE on wear has been investigated by a number of other researchers [141-144]. The direction(s) of wear have been shown to exert a significant influence on the mechanical properties of surface layers of UHMWPE. Broadly speaking, the situation can be broken down into unidirectional and multidirectional wear. Uni-directional wear leads to the preferential orientation of the UHMWPE surface layer in a particular direction and results in an increase in strength in the oriented direction and weakening of the material in the perpendicular direction leading to increased surface hardness [145]. Meanwhile, multidirectional wear results in the surface being constantly subjected to shear stresses and reoriented at acute angles, leading to shearing of the polyethylene and removal of particles from the surface. This re-orientation leads to a reduction in surface hardness.

The elastic modulus values of polymers have been shown to be highly sensitive to crystallinity and crystallite orientation with modulus values increasing approximately linearly with increasing crystallinity. Increased elastic modulus without proportionate increases in yield strength can increase the probability of plastic wear contact at UHMWPE bearing surfaces and hence may increase wear rates.

Abrasive wear occurs between surfaces of different relative hardness and presents as scratching or embedded particles. Abrasive wear can occur in two main ways: Second-body wear occurs when micro-roughened areas or asperities on the harder metal femoral head locally plough through the softer UHMWPE. Third-body wear occurs when hard particles become embedded in the surface of UHMWPE and can include metallic or bone particles and PMMA bone cement debris. Shipway et al (2003) [146] demonstrated that the surface hardness of polymeric materials is correlated to their ability to resist micro-scale abrasion with harder polymers displaying increased micro-abrasion resistance.

2.7.4 Wear Equations

The ability to predict the progression of wear in a total hip replacement is a topic that has and continues to attract a great deal of attention. The Archard equation (Equation 2-4) [147] is a simple model used to describe sliding wear and is based around the theory of asperity contact:

$$Q = \frac{kL}{H} \qquad \text{Equation 2-4}$$

Where Q is the total volume of wear debris produced per unit distance moved, L is the total normal load, H is the hardness, k is a dimensionless constant that reflects the severity of wear ($k=10^{-8}$ for 'mild' wear and 10^{-2} for 'severe' wear). Archard's equation was adapted by Lancaster (Equation 2-5) [148] and is commonly used in hip prosthesis testing:

$$V = KLx \qquad \text{Equation 2-5}$$

Where V is the wear volume (mm^3), L is the load (N), x is the sliding distance (m) and K is the wear factor (mm^3/Nm). The hardness term in Archard's equation has been incorporated in the wear factor. Archard assumed Hertzian contact theory for a flat non-deformable surface in contact with a nominally flat deformable surface with spherical asperities evenly distributed in depth. Lancaster's equation indicates that wear volume is dependent on the load and sliding distance. However, there is not a term for nominal contact stress across the interface. Real contact area increases with increasing load while the apparent contact area remains constant [149].

The precise dependence of the wear factor on contact stress, load and apparent contact area is disputed in the literature. In an attempt to clarify the situation regarding the exact relationship between the magnitude of the wear factor and load applied to the system, Vassiliou & Unsworth [150] conducted a series of pin-on-plate tests using UHMWPE pins and stainless steel 316L plates and found that pin diameter and load had no significant effect on the wear factor whilst the wear factor decreased with increasing contact stress according to the relation:

$$K = 2x10^{-6}\sigma^{-0.84} \qquad \text{Equation 2-6}$$

They calculated the wear factor to be $2.55x10^{-6}mm^3/Nm$ (assumption that 75kg patient, Charnley joint of 22mm diameter and volumetric loss of $50mm^3$/year. Mean clinical wear factors for explanted Charnley prostheses reported by Hall et al [151] and Atkinson et al [122] were $2.1x10^{-6}$ mm^3/Nm and $1.96x10^{-6}mm^3/Nm$.

Equation 2-3 indicates that the magnitude of the wear factor decreases more as the contact stress increases at low stresses than it does at high stresses. This is consistent with the work of Barbour et al [152]. Actual stresses that occur in the UHMWPE acetabular cup are influenced by the design of the prosthesis and the loads that are applied. Component design can control the femoral head size and amount of conformance between the head and the cup. However, load is dictated by muscle forces, inertia and patient gait and can reach up to four times the patient body weight [152].

When assessing the relationship between clinical wear factor and volume of wear for retrieved acetabular components, Dowson and Wallbridge [153] derived and used the following formula:

$$\Delta V = k_{clinical}(2.376NWr) + C \qquad \text{Equation 2-7}$$

Where N is an estimate of the number of cycles to which the joint has been subjected during its life, r is the radius of the femoral head and W is patient mass. Number of cycles can be predicted using an empirical formula derived by Wallbridge and Dowson [154] relating age to activity:

$$N = 0.5(A_r - A_p)x[6.58 - 0.032(A_r + A_p)]x10^6 \qquad \text{Equation 2-8}$$

2.7.5 Wear Debris

The main problem is not the amount of volumetric or linear wear that has occurred per se but rather the generation of micron and sub-micron sized wear debris and its interaction with surrounding biological tissue [113, 155,156]. The size, shape and composition of the wear debris can influence the manner in which cells interact with the debris.

A quantitative technique for assessing wear UHMWPE debris was described by Besong et al [157]. Using a tri-pin-on-disc tribometer they studied the effect of ageing for ten years after gamma irradiation in air on the volumetric wear, particle size distribution and the number of particles produced by UHMWPE when sliding against a stainless-steel counterface. Wear particles were isolated from the bovine serum lubricant by a multistage digestion method that sequentially filtered the wear debris through preweighed polycarbonate filters of 10μm and 0.1μm. The membranes of the filters were then coated with gold and scanned by SEM. Magnifications of 3000 up to 20000 were used to detect boundaries of very small particles with micrographs taken from at least three distinct regions on each filter membrane. An image analysis system was used to determine the distribution of particle size with an average of 2000 particles counted from each sample. Two-dimensional particle analysis was used to determine the mass and frequency distributions as a function of particle size.

Aged and irradiated material produced six times more volumetric wear and 34 times more wear particles than non-sterilised UHMWPE per unit load per unit sliding distance. However, researchers found no discernable difference in the percentage frequency distribution of particle size of the UHMWPE samples. Using the technique

outlined by Besong et al [157], Tipper et al carried out a wear particle analysis and found that typically, debris sizes ranged from 0.1μm to 100μm with most particles being < 1μm in size with an uniform distribution of volume of wear particles [158]. Increased volumetric concentration produced elevated levels of osteolytic cytokines. [113,159].

Biological interactions can result from this interaction leading to osteolysis or bone resorption and the break down of the bone/component interface. This leads to aseptic loosening of the component with associated pain and instability near the joint. Failure of the UHMWPE component in this context refers to the fact that the joint replacement is no longer functioning satisfactorily in-vivo. The UHMWPE may still be intact having neither broken or worn through after in-vivo service.

It is important to investigate the mechanical properties of UHMWPE on the same scale of size (i.e. micron scale) as the wear debris in order to improve the understanding of the processes involved in its generation.

2.7.6 Wear Measurement

Clinical assessment of wear in-vivo can only be conducted using non-invasive methods. Radiography is routinely used to evaluate wear of implanted and retrieved components [160, 161]. A uni-radiographic wear measurement methods was first used by Charnley and Cupic in 1973 at Wrightington to assess the wear of cups fabricated from RCH-1000. Their technique involved measuring the distance from the prosthetic femoral head contour to the contrast wire of the cup. They reported an average linear wear rate of 0.15mm/yr for the first cohort of patients to receive a UHMWPE

component between November 1962 and December 1963 [162].

Griffiths et al (1978) reported the linear wear rate findings for the second cohort of patients implanted at the same hospital, by the same surgeon and with the same implant was 0.07mm/yr [34]. The second cohort of patients seemingly demonstrated greatly reduced wear rates compared to the first cohort. Charnley and Griffiths were in disagreement as to the explanation for the variation in wear rates. Charnley postulated that variations were due to patient factors whilst Griffiths strongly suggested that it was the manufacturing route that was the issue.

Patient activity and manufacturing route both influenced the amount of wear that occurs however, the variation in results seen in these early trials may well have been strongly influenced by experimental error. The radiographic method used by both researchers has been shown to provide poor intra and inter observer repeatability and is considered unsuitable for measuring wear of less than 0.3 to 0.5mm [163, 164].

Charnley and Halley later introduced a duo-radiographic technique that involved measuring the distance from the edge of the head to the contrast wire and subtracting this from the measured thickness of the same line on an initial radiograph. An accuracy of ±0.5mm [165] was reported for this technique and the method was widely used across Europe for assessing cemented components.

Wear rates of 27 cemented Charnley acetabular components that had been implanted for a mean time of 29.7 years (range 27.6 to 31.6 years) were reported by Callaghan et al (2004) [166]. They compared follow-up radiographs to radiographs taken at

implant using a digital edge detection computer technique that has been shown to be 6.4 times more accurate and 7.1 times more reproducible than manual measurement with conventional circular templates [167]. They reported a mean volumetric wear rate of 26.7mm /year (range 0.75 to 61.6mm^3/year) and mean linear wear rate of 0.10±0.06mm/year (range 0.039 to 0.261 mm/year). Comparable wear rates for UHMWPE Charnley acetabular components have also been reported by Maruyama et al (1995) [168], Semlitsch et al (1997) [169] and James et al (1999) [170].

A comparative assessment of five different manual and two computer assisted radiographic techniques with the direct measurement shadowgraph method was carried out by Barrack et al (2001) [171]. They assessed 21 retrieved liners from cementless metal backed components and found that there were significant differences between the various radiographic measurements and measurements derived via shadowgraph. The strongest significant correlation ($p<0.005$) was between the Dorr radiographic technique and shadowgraph with a correlation coefficient of 0.72. The researchers attributed the poor accuracy of the radiographic measurement techniques to the difficulty in defining the edge of the full hemisphere with a cobalt-chromium alloy component. However, there was considerable variation between direct and radiographic techniques with radiographic techniques overestimating linear wear compared to shadowgraph measurements. In addition, the use of computer digitization didn't enhance the accuracy of the manual radiographic assessment methods. Researchers stated that radiographic wear measurement methods should be treated as qualitative rather than quantitative.

A separate study into the accuracy of manual radiographic wear measurement techniques was carried out by Pollock et al [172]. They assessed seventeen UHMWPE acetabular liners using the Dorr, Livermore and a wear template method comparing the results to direct measurements taken on the explanted components. The Dorr method was found to consistently overestimate the true measurement whilst the other two techniques didn't consistently over or underestimate the true measurement. All three techniques demonstrated large standard deviations suggesting that the ranges in error were wide.

In contrast to the previous studies that reported large discrepancies between radiographic and direct wear measurement techniques, Ohlin et al (1993) found significant correlations between wear values obtained via radiographic and direct measurement using a co-ordinate measuring machine. A key point they raised was that *"a prerequisite for a reliable estimation of socket wear rate is that it be based on observations of radiographically intact sockets "*.

Direct measurement of wear for retrieved components is an attractive approach to wear measurement as it eliminates certain key sources of error e.g. not influenced by different operator interpretations of radiographs. Traditionally, direct linear wear measurements have been carried out using a shadowgraph technique [173, 174]. A cast of the acetabular cup is prepared using a high-definition silicone-based moulding agent or dental resin. The replica is then projected, on to the screen of the shadowgraph apparatus using appropriate magnification (i.e. x10). Measurements are taken from the projected image in order to determine both the angle of penetration and the amount of linear wear. Shadowgraph wear assessment is an accurate and

established technique for assessing linear wear rates but volumetric wear rates can only be inferred indirectly from linear wear data. The precision of the shadowgraph technique in measuring wear of retrieved UHMWPE acetabular components was investigated by Cunningham et al [175]. They evaluated 34 explanted components and assessed the influence of different observers, multiple moulds and measurement precision. Three moulds were made of each cup using RTV 2039 (Ambersil Ltd) using a technique previously described by Hall et al [151]. Each mould was examined five tunes by two observers using a shadowgraph (Starrett Sigma HC400) with worn and unworn regions evaluated using a semi-circular template. Results from the study revealed that the observer had a significant influence over the measured values of linear wear with a reported average error of 0.086mm between the two observers. In addition, the researchers found that the moulding process itself introduced significant variations in linear wear measurements but that these errors were only slight ±0.077mm. Finally, repeated measurements by observers were found to be a significant source of error and this error was far greater than the two other sources. Linear wear measurements varied by ±0.299mm and the researchers stated that this figure gave an indication of the precision of the shadowgraph technique for measuring linear wear.

There are only two measurement techniques that can be used to directly determine volumetric wear rates, fluid displacement method (FDM) and coordinate measuring machine.

The fluid displacement method (FDM) of measuring volumetric wear involves injecting a liquid dropwise into the gap between the UHMWPE liner and femoral

head in a controlled manner using pipettes [176]. Biggs et al demonstrated that the accuracy and consistency of this volumetric wear measurement method for wear volumes >300mm^3 was within 3%. Fluid displacement wear assessment was used in a study by James et al [170] who investigated the clinical wear of 63 UHMWPE acetabular components. They injected pure vegetable oil (because it wets UHMWPE) into the wear gap using controlled pipettes with a drop volume of 0.033cm^3. The wear volume was determined from the average of five measurements with the components being cleaned ultrasonically using hexane between measurements. Calculation of wear volume was based on the assumption that the cups were perfectly hemispherical at beginning of their service lives. The mean volumetric wear of components was 0.99 ± 0.52 cm^3 with a mean volumetric wear rate of 0.14 ± 0.09cm^3/yr.

Co-ordinate measuring machines (CMMs) are able to sample the digital pattern of co-ordinates of the bearing surface of acetabular components [177]. These coordinates are then used to generate 3D maps of the worn component that can be compared to a model of an unworn component of the same design in order to calculate linear and volumetric wear. Orthopaedic component manufacturers use CMMs to analyse the accuracy of their manufactured devices to ensure tolerances are being observed. The accuracy of CMM measurements is influenced by the condition of the retrieved components and the availability of comparative reference points on the cup surface. CMMs have been shown to be accurate at measuring linear and volumetric wear [5, 178]. Raimondi et al [5] assessed 65 worn components measuring each component ten times to check the repeatability of the process. They reported a mean volumetric wear value of 121 ± 21.4mm^3. Despite its accuracy and utilisation in the orthopaedic industry, researchers rarely use coordinate measuring machines for assessing the wear

of retrieved components. This is possibly due to a lack of availability of the necessary metrology test equipment. This technique is not suitable for the measurement of wear volumes <100mm^3 as it is unable to distinguish between wear and deformation due to creep [179].

2.8 Micromechanical Testing of UHMWPE

At present, there is not a clear understanding of how in-vivo wear mechanisms influence surface mechanical properties of UHMWPE. In order to develop a better understanding of the wear processes, it is important to investigate the mechanical properties of UHMWPE of the surface and in sub-surface regions of retrieved components.

Previous researchers have used a small punch test technique to investigate the mechanical properties of localized regions of UHMWPE. The technique was adapted from the nuclear industry specifically for testing UHMWPE. ASTM F2183-02 "Small Punch Testing of Ultra-High Molecular Weight Polyethylene Used in Surgical Implants" was first published in June 2002 and details the test method [180].

The technique has been shown to be sensitive to changes in the mechanical properties of UHMWPE due to different sterilisation techniques [181, 182], accelerated aging [182, 183] and cross-linking [184, 185]. Edidin et al (2001) used the technique to investigate the properties of nine retrieved UHMWPE components and found a significant correlation between patient weight and the toughness (work to failure) of components. The heaviest patient was also the one with the shortest longevity in-situ. However, the authors themselves stressed that further testing was required due to the

low number of components evaluated [186].

Kurtz et al. (2003) also used the technique in a retrieval study and found that the peak load, ultimate load and work to failure were all significantly lower at the worn and unworn surfaces (< 25μm from articulating surface) compared to values obtained at subsurface locations (1.5-2mm from the articulating surface) [187].

Small punch testing is a valuable tool for investigating the influence of different factors on the mechanical properties of UHMWPE but the need to fabricate 0.5mm thick and 6.4mm diameter test specimens means it cannot be used to assess variations in mechanical properties on a microscopic scale.

The ability to assess the mechanical properties of retrieved UHMWPE components on the same scale of size as UHMWPE wear debris is important in developing an understanding of the wear process in-vivo. One such technique is instrumented indentation testing (also referred to as depth sensing indentation). This technique is able to determine several micromechanical properties that are inextricably linked to wear behaviour on the micron scale of size comparable to the size of wear debris. It has excellent spatial resolution and allows accurate mapping of hardness and elastic modulus. The technique has only attracted limited amount of attention for the assessment of UHMWPE to date.

Gilbert et al (2002) [188] used instrumented indentation test equipment fitted with a spherical Al_2O_3 indenter with a 38μm radius tip, to investigate the properties of Hylamer™, Marathon™, and GUR 1020 (all of the materials were unsterilised). They

demonstrated that the technique was sensitive to surface mechanical properties of UHMPWE and could consistently be used to distinguish between the materials. Surface modulus values were independent of indentation depth and found to be 651MPa for Marathon, 738MPa for GUR and 1015MPa for Hylamer whilst bulk values were 540MPa for Marathon, 620MPa for GUR and 1380MPa for Hylamer. Microhardness values varied with depth linearly with smaller indents generating smaller hardness values e.g. 0.12GPa at 40μm but 0.079GPa for a 12μm indent. When 12μm indents were formed the microhardness values were 0.079GPa for Marathon, 0.094GPa for GUR and 0.107GPa for Hylamer.

In a separate study [189], they used the same equipment to assess a UHMWPE tibial component that had been gamma irradiated in air and shelf aged for 15 years. The component displayed the classic white band appearance when sectioned and the test was sensitive to the degree of oxidation that had occurred, with increased levels of UHMWPE oxidation resulting in increased modulus and hardness values. At a distance of 100μm from the free surface the microhardness value was 0.75GPa whilst at 1000μm the value was 0.94GPa (values were taken from a graph and are approximate). Microhardness values remained relatively constant up to 3500um before gradually decreasing to ~0.80GPa at 5000μm. Elastic modulus values varied in a similar manner to microhardness with values rising from 0.60GPa 100μm from the free surface to 1.5GPa at a depth of 2000μm before gradually decreasing in a linear fashion to 0.6GPa 5000μm from the free surface.

Researchers have also used instrumented indentation testing to investigate the effect of ion implantation surface modification on the mechanical properties of UHMWPE

[190-194]. Up to three-fold reductions in wear have been reported following ion implantation of UHMWPE bearing surfaces.

The assessment of retrieved UHMWPE orthopaedic components has also been carried out using the technique. A number of studies have investigated the through thickness property distributions of retrieved tibial inserts [93, 94, 195, 196].

Kipping et al (2005) [94] analyzed nine retrieved St. George sled (LINK) uni-compartmental UHMWPE components. Through thickness hardness profiling, in worn regions, showed an increase in hardness values in the subsurface region to a depth of 3mm with a peak at 1.5mm from the bearing surface. Increased hardness values corresponded to increased oxidation absorption values and micro-structural changes previously described as 'white band'. Other researchers found similar correlations between hardness and oxidation in retrieved tibial components [93, 195].

Two studies have attempted to assess the depth dependent properties of retrieved acetabular components. Bruni et al (2002) [197] assessed through thickness sections of new and retrieved acetabular components using a conventional Vickers micro-hardness tester. A hardness peak at 1mm from the 'internal and external component surfaces' was observed for retrieved components whilst no hardness variations were observed for new components. Unfortunately, no component, UHMWPE material, or hardness testing information was reported [197].

The second study utilised instrumented indentation testing to investigate two retrieved acetabular components and a non-implanted control [198]. Variations in hardness

profiles were reported for both retrieved components with peak values at a depth of 1-2mm from the bearing surface. Increased hardness values corresponded to micro-structural observations of incipient cracking and increased crystallinity. The researchers didn't outline the specific regions of the retrieved cups that they evaluated, meaning that the hardness profiles could have corresponded to either worn or unworn regions.

3 PRINCIPLES OF EXPERIMENTAL TECHNIQUES

3.1 Introduction

The initial step in the assessment of retrieved components was to accurately assess the component wear. This was carried out using a co-ordinate measuring machine in order to identify the region of highest wear. Through thickness samples taken from worn and unworn regions and were then investigated using a range of experimental techniques. Each of these techniques was able to analyse variations in properties on the micron scale as a function of distance from the bearing surface. Instrumented indentation testing was used to map the variation in micro-mechanical properties, variations in the chemical properties were then mapped using an FT-IR imaging suite and changes in material morphology were evaluated using ESEM and optical microscopy.

This chapter discusses the theoretical and practical principles of each of the experimental techniques used in this study.

3.2 Co-ordinate Measuring Machine (CMM)

Co-ordinate measuring machines are used to obtain precise dimensional information from objects. CMM's are routinely used by orthopaedic component manufacturers to ensure that products are fabricated in accordance with design tolerances. In this study, a Mitutoyo Euro Apex coordinate measuring machine (CMM) (Figure 3-1) was used to evaluate the linear and volumetric wear of retrieved acetabular components.

Figure 3-1 Mitutoyo Euro Apex co-ordinate measuring machine (CMM)

The system consisted of a computer controlled measuring probe attached to an air cushioned movable gantry. Initially, the measuring probe was oriented using a reference datum on the object. It then gradually traversed across the object recording three-dimensional Cartesian co-ordinates in a measurement pattern defined by the user. The CMM had a scanning accuracy of 2μm and a probing accuracy of 0.7μm whilst the equipment had been recently calibrated. The CMM was controlled by an Engineering Technician who controlled the CMM assessment of the retrieved components on my behalf but under the instruction of the researcher. The key reason for this was that the equipment is used by numerous researchers and the testing had to be scheduled to meet the demands of different people.

3.3 Instrumented Indentation Testing

Assessment of the mechanical properties of small components or samples is difficult because standard bulk testing techniques generally require the use of large test specimens. Instrumented indentation testing was well suited to the assessment of retrieved UHMWPE components as it was sensitive to structural changes in UHMWPE and can accurately map properties of a surface on the micron scale. The fact that it is able to assess the micromechanical properties is particularly important to the development of an understanding of the generation of wear debris.

3.3.1 IIT Test Equipment

Instrumented micro-hardness indentation testing was carried out using a PLINT TE 76 Scanning microhardness tester (Figure 3-2) developed by NPL and manufactured under license by PLINT and Partners.

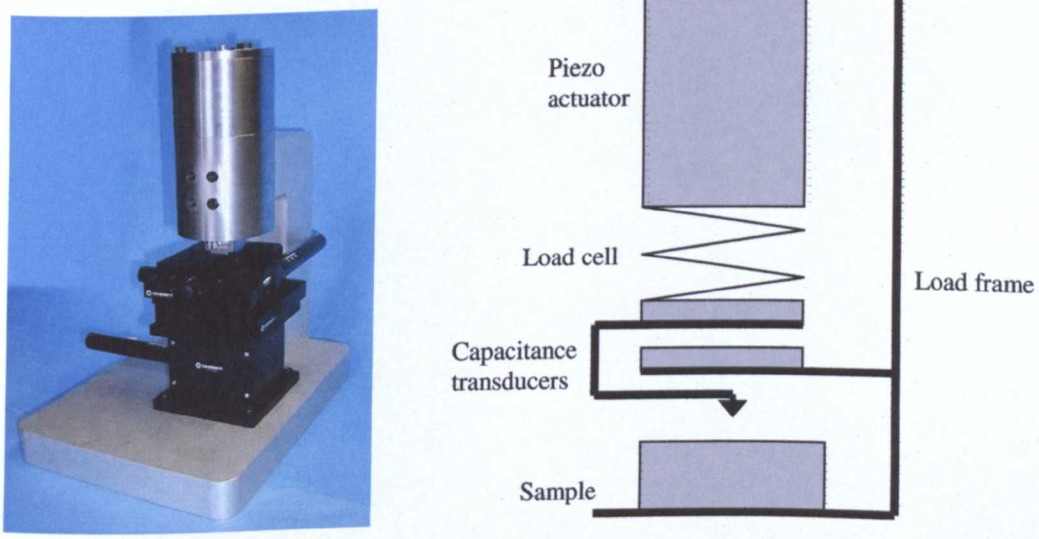

Figure 3-2 Instrumented indentation test equipment

The diamond Vickers indenter was mounted on the underside of a small rigid cage that contained a nano-range non-contacting capacitive displacement sensor. The indenter cage was rigidly fixed to a strain-gauge transducer that in turn was attached to the base of the piezo-actuator. The mechanical arrangement used ensures that the displacement sensor was as close to the indenter as possible and wouldn't register the force transducer deflection.

Test samples were mounted in a sample holder on the surface of an X-Y-Z staging system. The stage had a high vertical stiffness so that the equipment didn't deflect during testing and each axis was connected to a high-resolution dc motor/drive system, which could be controlled independently. The staging system had a positioning resolution of 0.1 um and a maximum deviation from a straight line of 2μm.

The piezo-actuator had a range of motion of 90nm, which was sufficient to accommodate the deflection of the force transducer and the indentation itself. Since the machine operation was fully automated, the Z-stage could be used intelligently both to accommodate a range of sample thicknesses (up to 25mm, the full traverse range of the stage) and to account for any unevenness of the sample surface. Thus, during a mapping routine, the COMPEND 2000 v1.48 software automatically checked to see if the surface was approaching or receding from the indenter and moved the Z-stage automatically to compensate variation.

The user may remove and relocate the sample-mounting fixture accurately. This facilitated the accurate placement of samples in order to ensure that indentation tests

were commenced at specific points.

A diamond Vickers indenter (Figure 3-3) was used for all indentation testing. Vickers indenters are pyramidal in shape with the four faces having angles between opposite faces of the vertex of 136°.

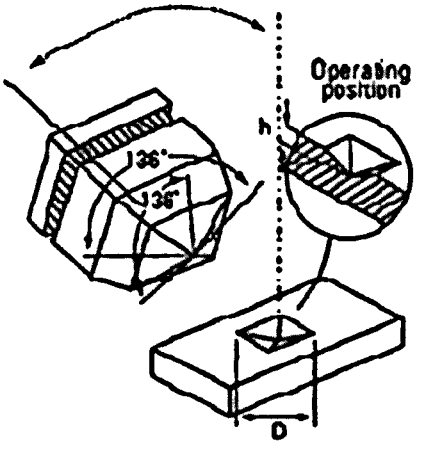

Figure 3-3 Vickers indenter

The test equipment included a motorized stage for mounting samples on. It had a positional accuracy of 0.01μm that facilitated accurate positioning of samples and also accurate arrays of indents.

3.3.2 Indentation Process

This section outlines the generic manner in which the indentation process works whilst the following chapter section contains specific information on indentation testing carried out in this study.

The initial step in a generic indentation process was the detection of the surface of the sample by the test equipment. The indenter advanced towards the test surface in

0.2μm steps until a load equal to or greater than the force threshold was detected, or until the indenter had moved by 10μm. The latter case meant that no surface had been found therefore the indenter moved back to its starting position and the Z stage was moved up by 10μm and the process repeated until the surface was detected. The test equipment used in this study addressed the issue of sample surface detection by advancing the indenter towards the test surface in 0.2μm steps until a load equal to or greater than the force threshold was detected, or until the indenter had moved by 10μm. It was essential to select an appropriate force threshold that is as low as possible so to minimize penetration of the indenter into the surface of the material but high enough to be unaffected by systematic load detection error.

Once the surface was detected, the indentation cycle began. Indentation cycles consisted of the indenter being pressed into the surface of the UHMWPE at a constant ramp rate of 1μm/sec until a maximum indentation depth had been reached. The indenter remained at maximum depth for 0.1sec before the indenter was removed from the surface and the stage re-positioned for a subsequent indent or returned to its home position if all indents had been completed.

Data was recorded during the entire process and initial processing of the data by the software involved the deletion of data that corresponds to the indenter not being in contact with the surface of the material under test. Following this, the test software detected when the indenter was in contact with the test piece so that the total indentation depth could be calculated. The software scanned through the data until it found a force greater than 80% of the force threshold and checked that the next force value was greater than the force threshold (to eliminate possible noisy values - values

significantly affected by experimental error). These two values (force and displacement) were saved as the initial values. A potential problem with this procedure was that the tool moved down in 0.2μm steps until the force threshold was detected before an indentation took place. If a force only 1% smaller than the force threshold was detected, the test sequence then proceeded to ramp the tool one more time. The next time the test sequence was initiated a force could be significantly bigger than the force threshold meaning that the indentation produced by this little step would be substantial. The test software addressed this potential issue by calculating load displacement curves by subtracting the load and displacement values from their corresponding initial values (data was recorded during the whole process). Initial processing of the data by the software involved the deletion of data that corresponded to the indenter not being in contact with the surface of the material under test. Following this, the test software detected when the indenter was in contact with the test piece so that the total indentation depth could be calculated. The software scanned through the data until it found a force greater than 80% of the force threshold and checked that the next force value was greater than the force threshold (to eliminate possible noisy values). These two values (force and displacement) were saved as the initial values. The different test parameters were then calculated from these load displacement indentation curves.

3.3.3 Experimental Data

3.3.3.1 Load-displacement data

Load displacement graphs obtained from instrumented indentation testing are used to calculate a number of different parameters, Martens hardness (H_M), indentation

modulus (E_{IT}), elastic part of indentation work. Figure 3-4 is an example of a load-displacement graph for GUR 1020.

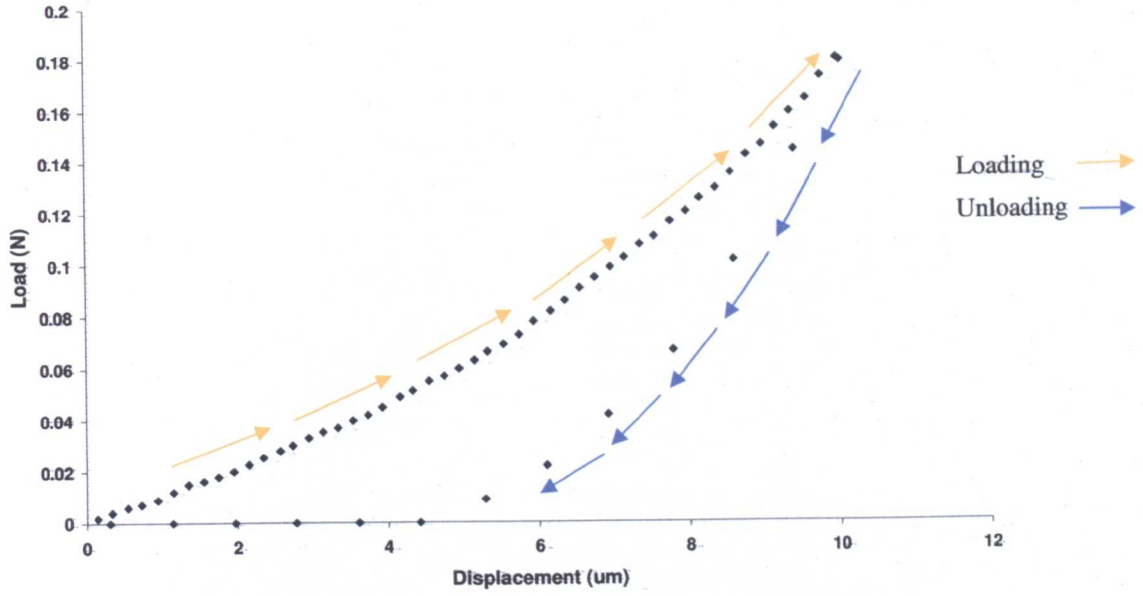

Figure 3-4 Load-displacement graph for virgin GUR 1020 UHMWPE

3.3.3.2 Martens Hardness (H_M)

Martens hardness values are calculated from the test force F, divided by the surface contact area of the indentation As (h) and are expressed in N/mm^2 (h refers to depth of indenter into the surface of the material). For a Vickers indenter, the Martens hardness is defined as (Equation 3-1):

$$H_M = \frac{F}{A_S(h)} \qquad \text{Equation 3-1}$$

Where for a Vickers indenter,

$$A_S(h) = \frac{4\sin\left(\frac{\alpha}{2}\right)}{\cos^2\left(\frac{\alpha}{2}\right)} h^2 \qquad \text{Equation 3-2}$$

As the angle (a) of the Vickers diamond pyramid is 136° Equation 3-2 reduces to:

$$A_S(h) = 26.43.h^2 \qquad \text{Equation 3-3}$$

Therefore Equation 3-1 becomes:

$$H_M = \frac{F}{26.43h^2} \qquad \text{Equation 3-4}$$

As the Martens hardness is calculated at maximum indentation depth and force Equation 3-4 can be re-written as:

$$H_M = \frac{F_{max}}{26.43h_{max}^2} \qquad \text{Equation 3-5}$$

Maximum force and depth are obtained by the software, which searches the data for the maximum force recorded and its corresponding displacement.

3.3.3.3 Indentation Modulus (E_{IT})

The elastic modulus (E) is calculated using the following formula (Equation 3-6) where σ is stress and ε is strain:

$$E = \frac{\sigma}{\varepsilon} \qquad \text{Equation 3-6}$$

Stress is calculated by dividing the applied force F, by the area the force was applied to A (Equation 3-7):

$$\sigma = \frac{F}{A} \qquad \text{Equation 3-7}$$

Strain meanwhile is determined by dividing the change in length of a material by its original length and is therefore unitless (Equation 3-8):

$$\sigma = \frac{\delta l}{l_o} \qquad \text{Equation 3-8}$$

Calculation of the elastic modulus of materials from indentation test data can be carried out using the following formula (Equation 3-9):

$$\frac{1}{E_r} = \frac{1-\upsilon_1^2}{E_1} + \frac{1-\upsilon_2^2}{E_2} \qquad \text{Equation 3-9}$$

where E_i and υ_i (i=l or 2) are the Young's modulus and Poisson ratio of the material under test and indenter material respectively. Equation 3-9 can be rewritten as (Equation 3-10):

$$E_1 = E_r(1-\upsilon_1^2) - \frac{E_2(1-\upsilon_1^2}{(1-\upsilon_2^2)} \qquad \text{Equation 3-10}$$

The reduced elastic modulus (E_r) can be calculated using Equation 3-11 where β is a constant based on the indenter geometry and A is the projected contact area [199].

$$E_r = \frac{\sqrt{\pi}}{2\beta}\frac{S}{\sqrt{A}} \qquad \text{Equation 3-11}$$

S is the contact stiffness and calculated from the gradient (Equation 3-12) of the linear unloading portion of the load-displacement curve (Figure 3-5).

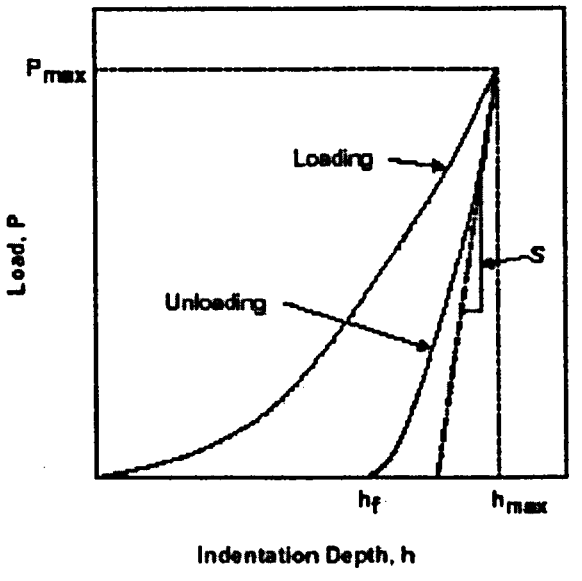

Figure 3-5 Instrumented indentation curve depicting contact stiffness (S)

$$S = \frac{dP}{dh}$$ Equation 3-12

For a Vickers indenter, the constant P = 1.012. The projected area is calculated using

$$A = 24.504 d^2$$ Equation 3-13

Re-arranging Equation 3-10 to take into account Equation 3-11 gives:

$$E_1 = \frac{S\sqrt{\pi}(1-\upsilon_1^2)}{2\beta\sqrt{A}} - \frac{E_2(1-\upsilon_1^2)}{(1-\upsilon_2^2)}$$ Equation 3-14

3.4 Fourier Transform Infra-Red (FT-IR) Imaging

Fourier Transform Infra Red spectroscopy (FT-IR) has been used for many years to assess the chemical structure of organic compounds. The technique utilises the infrared section of the electromagnetic spectrum that consists of wavelengths ranging from roughly 300 GHz (1 mm) to 400 THz (750 nm) (Figure 3-6).

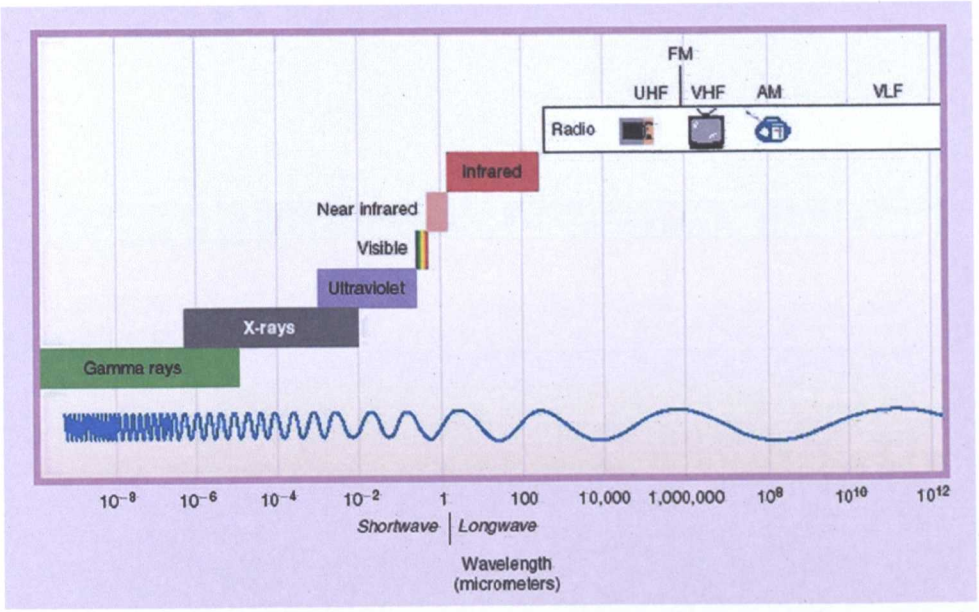

Figure 3-6 Diagramatic representation of the electromagnetic spectrum

The vibrational spectrum of a molecule is considered to be a unique physical property and is characteristic of the molecule. As such, the infrared spectrum can be used as a fingerprint for identification by comparison of the spectrum from an unknown with previously recorded reference spectra. The origin of the sample, its prehistory and the manner in which the sample is handled all have an impact on the final result. When the infra-red beam interacts with a sample during a test, different chemical groups absorb energy at different wavelengths.

3.4.1 FT-IR Imaging Equipment

Conventional Fourier Transform Infra Red spectroscopy (FT-IR) test equipment allows the user to investigate the chemical properties of a single point of a sample. It is a well established technique that has commonly been used to investigate chemical changes in UHMWPE [87, 96, 97, 105, 200]. FT-IR imaging differs from conventional equipment in a number of ways but the key one is that it is fitted with a precise sample positioning stage. This enables the user to accurately map the chemical properties of a sample at high (6.25μm) resolution.

A Perkin Elmer Spotlight 200 system was used to carry out FTIR imaging on specimens from retrieved UHMWPE components. The equipment consists of an infrared microscope, a Spectrum One interferometer and a linear array detector. Specimens were held in sample holder slides that slotted into a sample holder on the machine. Light from the interferometer passes into the microscope, which processes the light using optics based on the Cassigrainian Mirror type rather than lenses. The light collected then passes through a Z-fold x 4 magnifier and then to the detector. The detector contains two elements, a single point detector and a linear array. There is also a conventional visible light path to enable precise selection of sample area.

The detectors are arranged side by side within an area of about 1 sq. mm, each one being hardwired to the outside of the evacuated and cooled detector enclosure. Operation of the microscope can either be by point by point or strip by strip, the switch from one to another being carried out using motorised aperture blades in the optical path. After each scan interferograms are recorded, the stage

is moved, and the next set recorded. Movement of the stage occurs at the ends of the interferometer scan where no useful data is being recorded. A small path extending system is incorporated into the optical path. In one orientation, light goes straight through but if the tubular assembly is rotated about its axis, the optical path is diverted through a combination of mirrors increasing the microscope's magnification by four times. The effect is that each pixel views a patch ~6.25μm square at the sample instead of the normal ~25μm square. So, the user can have high spatial resolution or look at lower resolution over a wider area.

3.4.2 FTIR Experimental Data

A FT-IR spectrometer measures the intensity of transmitted infrared radiation (I) as a function of wave number (v, inverse of wavelength). From this, a transmittance (T) or absorbance (A_v) spectrum can be produced. In this study, absorbance spectra are quoted as this has been the convention in previous studies into the chemical properties of UHMWPE [102, 105, 107, 201]. Absorbance (A_v) is calculated using the ratio of the intensity of the incident radiation (I_0) to that of the transmitted radiation as a function of wave number as follows (Equation 3-15) [202]:

$$A_V = \log\left(\frac{I_0}{I}\right) \qquad \text{Equation 3-15}$$

Crystallinity is measured by calculating the ratio of absorbance at wavelengths corresponding to crystalline and amorphous phases. In UHMWPE, absorption at the 1896cm^{-1} band results from the crystalline phase, whilst the band at 1305cm^{-1}

results from the amorphous phase. The percentage crystallinity can be calculated using the following equation (Equation 3-16) [203].

$$Crystallinity(\%) = \frac{A_{1896} / A_{1305}}{(A_{1896} / A_{1305}) + 0.25} x100 \qquad \text{Equation 3-16}$$

Analysis of the intensity of the carbonyl peak at 1718cm^{-1} has been shown to give a good indication of the post-irradiation oxidation of UHMWPE [87, 105, 200, 204].

The intensity of the 1740cm^{-1} band was used to gauge the level of fluid sorption into the bearing surface of UHMWPE as this band has previously been shown to relate to esters that are a component of synovial fluid [102].

3.5 Environmental Scanning Electron Microscopy (ESEM)

The morphology of microtomed and freeze fractured through thickness surfaces was carried out using ESEM and optical microscopy. Only the technique of ESEM is discussed in this section as optical microscopy is a commonly used standard analytical technique.

Environmental Scanning Electron Microscopy carries out the same function as conventional Scanning Electron Microscopy (SEM) apparatus. However, SEM uses high vacuums and test samples need to be conductive making it more problematic to analyse certain materials such as polymers or biological structures

in their natural state. ESEMs don't use high sample chamber vacuums but operate a system of differential pumping instead that ensures that the electron gun is maintained at high vacuum while the sample chamber can be kept at constant pressures up to 10 torr. A Phillips XL30 ESEM was used in this study and had a wet imaging facility and a low voltage mode (0.2 – 1.0kV) that minimised surface charge effects and meant that UHMWPE samples could be viewed in their natural state without first coating them with a conductive layer. The resolution of the equipment was 2nm and accelerating voltages between 0.2 and 30kV could be used. The ESEM had the ability to magnify samples by between 15 and 500000 times.

3.6 Statistical Analysis

3.6.1 Parametric Versus Non-parametric Tests

There are two families of statistical tests namely parametric and non-parametric with the difference being that parametric tests use an assumption that the data are sampled from a Gaussian distribution. Tests that don't make assumptions about the population distribution are referred to as non-parametric tests. The most commonly used parametric tests include the t-test, analysis of variance (ANOVA) and Pearson correlation. The most commonly used non-parametric tests rank the outcome variable from low to high and then analyze the ranks. These tests include the Wilcoxon, Mann-Whitney test, and Kruskal-Wallis tests.

In order to decide whether to use a parametric or non-parametric statistical test, the distribution of the data has to be assessed to determine whether it follows a

Gaussian distribution. For large data sets (>100 data points) the data can be plotted as a histogram and it should be fairly obvious whether the distribution is approximately bell shaped. An alternative approach is to use a formal statistical test such as the Kolmogorov-Smirnoff test to assess whether the distribution of the data differs significantly from a Gaussian distribution. With few data points, it is difficult to tell whether the data are Gaussian by inspection, and the formal test has little power to discriminate between Gaussian and non-Gaussian distributions.

A key concept in statistics is the central limit theorem that states that the sum of a large number of independent and identically-distributed random variables will approximately follow a Gaussian distribution if the random variables have a finite variance. In practice, the central limit theorem allows researchers to calculate sample mean values from non-Gaussian data distributions and apply parametric statistical tests.

3.6.2 t-test

The t-test is used to assess whether the means of two normally distributed data sets are statistically different from each other. There are a number of different types oft-test that can be employed depending on whether the two samples are independent of each other or paired (data points from one sample have a unique relationship to data points from the second sample).

The t-test employs the statistic (t) to test a given statistical hypothesis about the mean of a population (or about the means of two populations). This statistic is a measure on a random sample (or pair of samples) in which a mean (or pair of

means) appears in the numerator and an estimate of the numerator's standard deviation appears in the denominator. The later estimate is based on the calculated s square or s squares of the samples. If these calculations yield a value (t) that is sufficiently different from zero, the test is considered to be statistically significant.

In practice, the t-statistic will be positive if the first mean is larger than the second and negative if it is smaller. A table of significance should be consulted to determine whether the t-statistic obtained is large enough to say that the difference between the groups is not likely to have been a chance finding. The significance of a test is presented as a p-value and generally p values <0.05 are considered significant. Statistical software packages currently available, automatically determine whether a t-test is significant.

3.6.3 Analysis of Variance (ANOVA)

Analysis of variance is a general technique that can be used to test the hypothesis that the means among two or more groups are equal. There are two hypotheses for the test. The first is the null hypothesis where there is not a significant nonzero relationship between the two variables. Then there is the alternative hypothesis where there is a significant non-zero relationship between the two variables.

ANOVA utilises the central limit theorem to calculate two estimates of a population variance and then calculate an F-statistic (in honour of the statistician Sir Ronald Fisher) and significance value ($p < 0.05$ for significance). Before calculating the F-statistic, a 'critical value' is calculated that is the value that the F-statistic has to be greater than in order for the test to be significant. The critical

value is calculated by dividing the degrees of freedom "between rows" by degrees of freedom "within groups" and the resulting number is identified in the F-table (at the .05 level of confidence) to generate the critical value (automatically determined in statistical software programs such as SPSS)

The F-statistic is generated by dividing the variance of group means by the mean of the within group variances. If this ratio is larger than a critical value, the observed differences among the obtained means are described as being statistically significant.

An assumption of the test is that the variances of the groups of data are equal so as the F-ratio becomes increasingly large, the inference is that this is due to the increasing variance between the groups of data in question.

3.6.4 Pearson Correlation

Correlation is a measure of the strength of the (usually linear) relationship between two variables. The Pearson correlation coefficient ranges from -1 to 1 where a value of +1 corresponds to two variables being related perfectly by an increasing relationship. A value of-1 corresponds to a perfect, but decreasing relationship.

3.6.5 Graphical Representation of Data

Data was graphically displayed where appropriate e.g. where correlations between data sets were present, using scatterplots or boxplots. Scatterplots were utilized when the variables being presented were made up of continuous data. Boxplots

were used to present data about specific subgroups e.g. implantation as a function of gender. An example of boxplot illustrating the key elements of how it is constructed is given below (Figure 3-7).

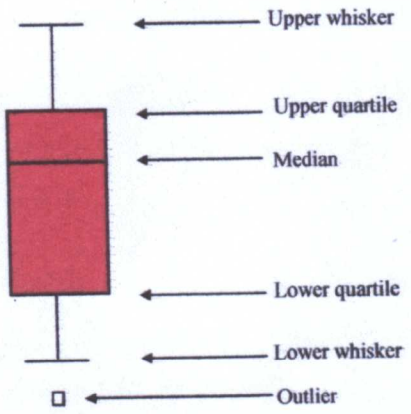

Figure 3-7 Example of a boxplot

The box represents the data spread between the 25% lower quartile to the 75% upper quartile of the data set. Upper and lower whiskers represent the minimum and maximum data values. However these whiskers are a maximum of 1.5 times the length of the box away. Any data points that fall outside this range are depicted as outliers.

4 EXPERIMENTAL METHODOLOGY

This Chapter outlines the specific experimental methodology and protocols used in the assessment of retrieved UHMWPE acetabular components.

4.1 Retrieved UHMWPE Components

4.1.1 Ethical Approval

The nature of the study and requirement to collect retrieved UHMWPE acetabular components meant that ethical approval had to be sought at the start of the study. This process was complicated by the fact that the two hospitals that assisted in the study, Nottingham City Hospital (NCH) and Queens Medical Centre (QMC), were part of different Primary Care Trusts. Therefore, two separate ethical approval applications had to be made to the respective local research ethics committees (LREC). Documents outlining the purpose, methodology, validity and ethical implications of the study were reviewed by Clinical Directors at both sites. The research proposal was accepted without alteration by both LRECs. Finally, the applications were put before a research ethics committee (REC) who gave a favourable decision raising no objections to the research. Approval for the study was granted in mid 2004 and the ethical approval code for the project was 04/Q2403-12. The process of obtaining ethical approval took a great deal longer than had initially been envisaged due to bureaucratic issues rather than concerns over the validity of the work. This meant that retrieved components only began to be collected towards the end of the second year of study, which had a direct impact on the number of components obtained.

4.1.2 Component Collection

Prior to undergoing revision hip surgery, patients were approached in order to ask whether they wished to participate in this study and to gain their consent. The researcher explained the study to patients and gave them an information sheet to keep for future reference. If they were willing to participate, patients signed a consent form to acknowledge that they had understood the nature of the study and that they were willing to allow researchers to collect certain pieces of personal information along with their failed hip replacement component. Following this, various pieces of information were collected such as patient details (age, weight etc), pathology for primary and revision hip surgery, component information and physical activity [40].

If consent was obtained, the retrieved components were kept by the theatre staff following the revision hip surgery. Components were washed (not sterilized) by the theatre staff and were then placed in sealed bags for collection by researchers. Where possible, components were collected from operating theatres on the day of surgery and transferred to a laboratory for anti-microbial processing.

Thirty four patients were approached to take part in the study, one patient declined to take part and the component from another patient was severely damaged during retrieval (Figure 4-1). These patients were not included in the study leaving a total patient population of 32.

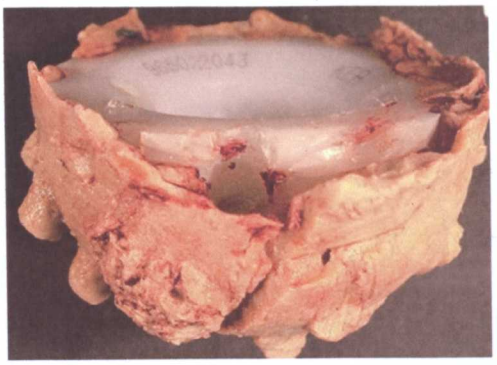

Figure 4-1 UHMWPE component damage during retrieval process

4.1.3 Anti-microbial Processing

Anti-microbial processing of retrieved components was carried out using Gigasept® FF (Schulte & Mayr). Gigasept® FF was used because of its broad microbicidal spectrum of effect and excellent material compatibility. It is commonly used to process heat sensitive polymeric devices and components such as flexible endoscopes that utilise rubber materials in their construction (reference). In addition, Schulke & Mayr use high-density polyethylene (HDPE) containers to package the liquid disinfectant. This is reassuring because HDPE is of a lower molecular weight to UHMWPE and would be more susceptible to chemical attack than UHWMPE. Gigasept FF is effective against bacteria (inc. TB bacilli), fungi, HBV, HIV, adeno viruses, polio viruses, bacterial spores, helicobacter pylori. In order to produce the disinfectant solution, tap water was used to dilute the Gigasept® FF to the recommended 10% solution. Components were immersed in the solution and their surfaces brushed with a soft bristle brush for approx. 2 minutes. After this time, components were left for a further 5 hours immersed in the disinfectant solution as recommended by Schulke & Mayr [205]. Components were then taken out of the solution and thoroughly washed with tap water to remove any residual disinfectant before being left to air dry. Disinfected

acetabular components were sealed in labelled plastic bags.

4.1.4 Preservation of UHMWPE Components

Based on the work by Kurtz et al [206], the kinetics of oxidation in UHMWPE after gamma irradiation in air should decrease by a factor of 3 or 4 for every 10°C the temperature is lowered. Therefore once components had been disinfected, they were stored at -18°C in an upright freezer in order to inhibit further chemical reactions and minimize ex-vivo oxidation of the UHMWPE.

When a component required investigation, it was left at room temperature for 24 hours in its bag to acclimatize.

4.2 Wear Assessment

An assessment of component wear was carried out in order to accurately assess the linear and volumetric wear and identify the regions of highest and lowest wear to be investigated in subsequent testing. In addition, the presence of relationships between patient variables and wear was investigated using correlation testing.

As there was no pre-wear data taken due to components being explanted, scans were carried out on new 22.25 and 28mm cups of the same design as retrieved components, to use as baseline comparators. This approach differs to that of Raimondi et al [5] in that they developed a mathematical model for approximating the original dimensions of the acetabular component possibly due to the wide range of cups they assessed where as in this study, dimensional data

was physically taken from new cups of the same design and used as baseline comparators.

A co-ordinate measuring machine was used to record dimensional information from the entire bearing surface of components using a 500μm x 500μm surface grid typically resulting in 15800 individual data points for a component. Component bearing surfaces were mapped with reference datum taken on unworn sections. Each component data set was processed using AutoCAD R14 to produce a set of curves for the component. The sets of curves were imported into Rhinocerous 3.0 3D modelling software (Robert McNeel & Associates) and the 'loft' command used to produce a surface from the various curves. The modelling software was then used to calculate the linear and volumetric wear by subtracting the worn model from a model of a new unworn component. The volumetric wear rate was calculated by dividing the total wear volume by the amount of time the component was in-vivo. In addition, the maximum linear reduction in component thickness was also measured and used to calculate the linear wear rate by dividing the value by the amount of time the component spent in-vivo.

The acetabular component linear wear (β-angle) and inclination angles (ω-angle) of the 32 components were calculated from CMM models. This was done using AutoCAD R14 software by taking a section through the regions of highest and lowest wear on the CMM model and using the angle measurement facility in the software. The section through the model was oriented so that the most superior point was that of maximum linear as indicated in Figure 4-2. Linear wear angles (β-angle) were calculated by drawing a line through the most superior point

vertically through the centre of the cup. A second line was drawn through the poles of the cup with the angle between the two being the β-angle. Acetabular component inclination angles were calculated by measuring the angle between the line through the poles of the cup and a line drawn in the lateral direction.

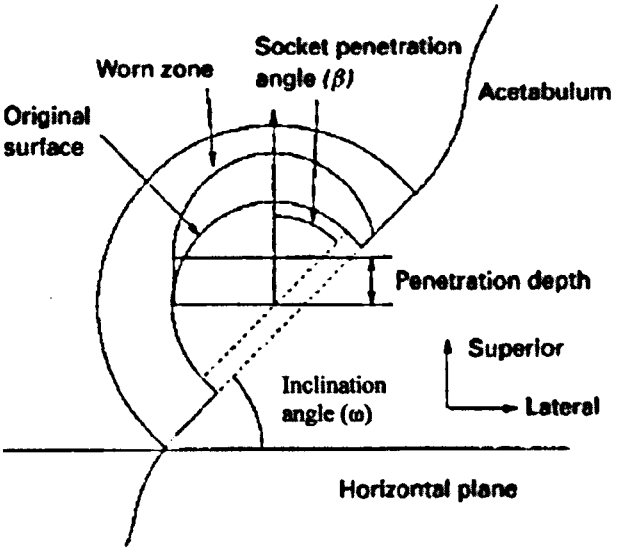

Figure 4-2 Definition of the angles of penetration with respect to both the socket and the body axes, and angle of component inclination. [207]

CMM wear measurements were compared to those obtained by analysing pre-revision hip surgery radiographs. Unfortunately, radiographs taken at implant and at subsequent follow-ups were not present in the notes of patients as the initial procedures had been carried out at different hospitals from the site where the revision surgery was carried out. This meant that radiographic wear measurement techniques such as the Charnley tunneling method and Livermore technique [208] couldn't be used with any confidence as the initial location of the femoral head at implant would have to have been predicted.

4.2.1 Statistical Analysis of Wear Data

Wear data was assessed using a range of mathematical tools. Linear and volumetric wear rates were calculated by dividing the total linear or volumetric wear by the implantation time. The standard deviation of the linear wear rate datasets was calculated to illustrate the spread of the data. Linear wear factors were calculated for the different components using Equation 2-7.

Pearson correlation statistical analysis was carried out on all of the wear and patient variables to investigate possible relationships between different datasets. Where correlations were found, data was presented as scatterplots of boxplots in the manner described previously in the Principles of Experimental Methods chapter.

4.3 Instrumented Indentation Testing (IIT)

Instrumented indentation testing was carried out on the through thickness sections of worn and unworn regions of retrieved UHMWPE components with a total of 260 indents carried out per sample (130 for worn region and 130 for the unworn region of each cup).

Preliminary instrumented indentation validated the sample preparation techniques, sample size and use of parametric statistical tests.

4.3.1 Sample Preparation

Components were sectioned through the regions of highest and lowest wear using a handsaw (Figure 4-4) along line (A-B) (Figure 4-3) in order to prepare through

thickness specimens for further analysis. It was the sectioned surface that had subsequent testing carried out on it.

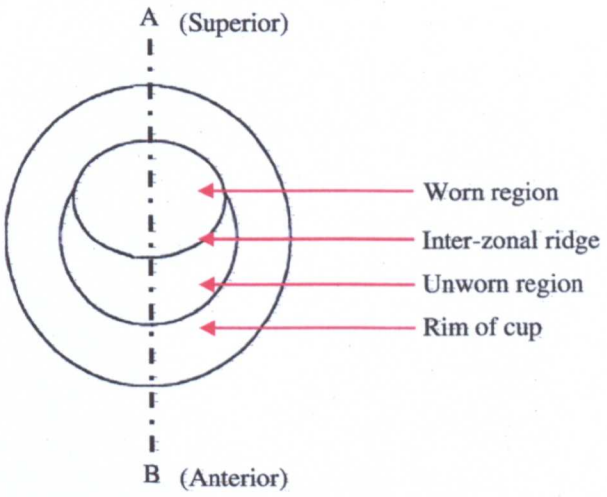

Figure 4-3 Top elevation diagram showing the worn and unworn regions on the bearing surface of a retrieved component.

Figure 4-4 Sectioning of retrieved components

Two smaller sections were then cut from the worn and unworn regions of one half of the retrieved component (Figure 4-5). The red and blue hashed areas in Figure 4-5 relate to the worn and unworn regions of the acetabular cup respectively. The

location of worn and unworn regions is evident from the radiograph in Figure 4-5 where the liner thickness a < b. Line 'a' represents maximum linear wear whilst 'b' is an unworn region of the cup.

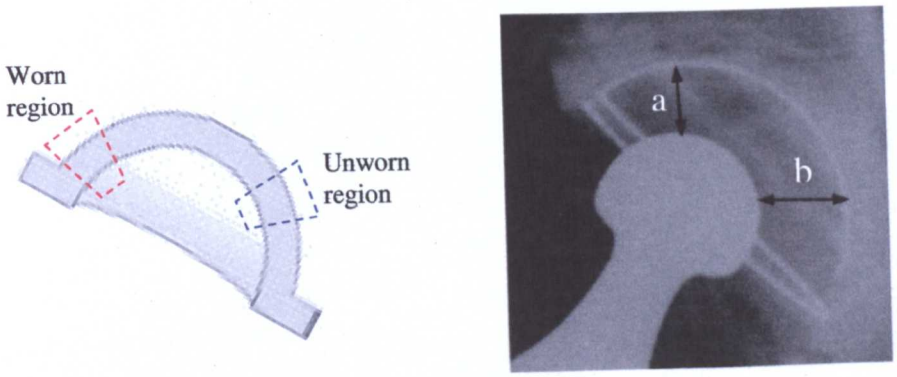

Figure 4-5 UHMWPE component sectioning

The two sections from each component were then mounted in Epofix™ embedding resin with the through thickness sections oriented so that they were parallel to the top surface of the mounted sample. In order to ensure that the top and bottom surfaces of the mounted samples were parallel, they were sectioned using a Struers Accutom-5 precision table-top cut-off wheel fitted with a SiC cutting disc. Sectioning was carried out using the following settings: cutting rate of $0.005mms^{-1}$, cutting disc 3000rpm, sample counter-rotation speed of 20rpm. The system has a positional accuracy of 5μm.

Figure 4-6 Struers Accutom-5 cut-off wheel

Test surface preparation was carried out using the Reichert Jung 1050 Supercut rotary microtome fitted with a d-profile tungsten carbide knife. The sample holder had 3-axis of movement that allowed the user to align the surface to be cut with the knife to ensure that the top and bottom surfaces remained parallel during the cutting process. Microtoming was carried out at room temperature (21±3°C) using a knife angle of 0°, cutting speed of 30mm/s and cutting incremental thickness of 20μm.

4.3.2 Instrumented Indentation Test Procedure

The room temperature that the test equipment was situated in was monitored and testing was only carried out in the range 23 ± 3°C. Test pieces were left for 24 hours to acclimatize to room temperature before testing.

Instrumented indentation testing was carried out using a PLINT TE-76 instrumented indentation test machine. An indentation depth of 10μm (z direction) and indentation spacing (x and y directions) of 200μm were used for all

tests. The system software automatically determined the surface of the sample in the manner described in section 3.3.2.

The load detection error was found to be ±0.007N and a force threshold of 0.015N was used as it provided the best compromise between surface detection sensitivity and dissociation from instrumental error.

UHMWPE test samples (see section 4.3.1) were placed in a metal jig that was then attached to the stage of the instrumented indentation tester. This ensured accurate and reproducible placement of samples on the stage. Accurate and reproducible placement of samples was essential in generating indent arrays that were consistently produced at the required distances from the bearing surface.

Indent arrays were produced that emanated from the bearing surface and moved perpendicular to this surface into the bulk of the sample. Five 10μm deep indents were carried out starting at a depth of 100 ± 10μm and repeated at 200μm intervals from the bearing surface to an ultimate distance of 5.1mm resulting in a total number of 130 indents per sample. The manner in which the indentation process functioned was described in section 3.3.2.

Manipulation of the load-displacement test data was carried out automatically by the COMPEND software in order to calculate HM and BIT values (section 3.3.3).

4.3.3 Instrumented Indentation Test Data

Mean hardness values were plotted as a function of distance from the bearing surface, with a distance of 0 relating to the bearing surface itself. Graphs of hardness and elastic modulus variations with depth were generated for worn and unworn regions of each component.

An important issue relating to worn regions was whether to take into account the linear wear that had occurred. For example, if the surface of a worn region had reduced in thickness by 2000μm should the surface of the worn region be treated as zero depth (unadjusted) or a depth of 2000μm (adjusted)?

A decision was made to investigate through thickness properties of worn regions using both adjusted and unadjusted depth configurations. The reason for this decision lay in the fact that the wear process was thought to influence the properties of the UHMWPE at the surface so assuming that d=0μm at the surface would be valid. However, when assessing long-term changes in the properties of the material caused by oxidation, it is also valid to use d=2170μm for the surface of the worn region.

4.3.4 Statistical Analysis of Hardness and Elastic Modulus Data

Statistical analysis of the hardness and elastic modulus data was carried out in order to evaluate the relationships between hardness and modulus data within individual components and between components.

Initially, the Kolmogorov-Smirnoff test was used to ensure that the distributions of hardness and elastic modulus data were investigated to determine were normally

distributed. The confirmation that the data was normally distributed meant that both the dependent t-test and ANOVA statistical tests could be used to evaluate hardness and elastic modulus data.

In order to assess whether hardness and indentation modulus values in the worn and unworn regions of individual samples varied significantly, the dependent means t-tests were carried out. The five readings at each depth for worn and unworn regions were compared using the test. The hypothesis used for all dependent t-tests (also known as the matched pairs or paired samples t-test) was that there was no variation in the through thickness values of HM and EU of worn and unworn regions of the same sample.

ANOVA was used to investigate the relationship of property profiles in worn and unworn regions between components.

Scatterplots were used to present the relationships between the distance from the bearing surface and hardness of elastic modulus.

4.4 FT-IR Imaging

FT-IR imaging was used to assess the through thickness variations in chemical properties of unworn and worn regions of 5 retrieved UHMPWE components. Originally, it had been intended to evaluate the entire cohort of 32 components. However, the imaging system used during the successful initial trials carried out in November 2004 was on loan from another academic institution and had to be returned to its owner. No other imaging system was available to the researcher within the University and conventional FT-IR equipment was unable to assess the

chemical properties of samples with the spatial resolution required for this study. An alternative imaging system was eventually located at Anglia Ruskin University in Cambridge. Funding was obtained to use the equipment at this Academic Institution that enabled the system to be used for five days. Due to the time constraint, it was not possible to assess all of the components. Instead five components were chosen that had been implanted for a range of time.

Components 27, 2, 14, 15 and 22 were selected for this assessment as they had been implanted for 2.2, 8.3, 12.2, 15.4 and 24 years respectively. In addition, the results from instrumented indentation testing had indicated that significant differences in the through thickness properties existed between the components.

4.4.1 Sample Preparation

FT-IR was carried out in transmission mode and through thickness samples were microtomed from the surface of instrumented indentation test samples that had been stored at -18°C following preparation. A 1000μm surface layer of UHMWPE was removed from samples to eliminate the possibility of erroneous results due to surface oxidation. Sectioning was carried out using the microtome parameters listed previously and generated 20μm thick specimens. The UHMWPE slices were moved using tweezers in order to prevent contamination. They were then placed in individual labelled bags for storage.

4.4.1 FT-IR Imaging Procedure

Each microtomed test specimen was placed in the sample holder and then placed on the FT-IR imaging stage (Perkin Elmer Spotlight 300). Before conducting each test, an assessment of background absorption was carried out. A section from each sample was identified using the optical microscope attached to the system. FT-IR testing was then carried out on this section. Spectra were obtained at intervals of 25μm and 6.25μm across the surface of the sample and each point was scanned 8 times.

Following the completion of the test, the FTIR data was presented to the user using the Perkin Elmer Spotlight software. Background IR data was deducted from the spectra obtained from the sample and the resulting spectra were normalised to the methylene band at 2010cm^{-1} in order to standardise against thickness variations [87].

Every FTIR absorbance data point for specific bands of interest; 1305cm^{-1}, 1718cm^{-1}, 1740cm^{-1} and 1896cm^{-1}, was exported to MS Excel in order to calculate crystallinity values and hence generate graphs of the variation in properties with depth (see section 3.4.2 for further details). This enabled the relationship between instrumented indentation test data and FT-IR data to be directly compared quantitatively.

4.5 Microscopy

The bearing surfaces of retrieved acetabular components and microtomed through thickness sections were visually inspected using optical microscopy.

Specific bearing surface features of components and through thickness UHMWPE samples were then inspected using ESEM. Through thickness samples were prepared using a freeze fracture preparation technique to generate surfaces representative of the underlying structure of the material. Freeze fracture of retrieved UHMWPE acetabular components was carried out using a similar technique to that previously described by Jacob et al [209]. Through thickness samples, 10mm thick, were prepared from worn and unworn regions of the opposing hemisphere of the acetabular cup that the instrumented indentation test samples were generated from. A 1mm deep notch was created in the through thickness surface of samples using a cut-off wheel (Struers Accutom-5) using a SiC cutting disc and cutting rate of $0.005 mms^{-1}$, cutting disc 3000rpm. Samples were then immersed in liquid nitrogen for 30 minutes following which they were removed from the nitrogen and immediately fractured using a pendulum impact tester. Fracture was initiated on the through thickness surface rather than the bearing surface in order to evaluate the morphology of samples through their thickness.

5 RESULTS

5.1 Patient Assessment

Thirty-four patients were approached for their consent before they underwent revision hip surgery. One individual declined to take part for personal reasons and one component was seriously damaged during surgery and could not be used. Having obtained their consent to take part in the study, patients were assessed using a study specific information collection form. Their medical notes were also consulted to identify certain pieces of information such as the reason for primary hip replacement, indication for revision etc. A full summary of patient information is contained in Table 3.

Thirty-two patients took part in this study with male patients constituting 59% (n=19) of the study population. All of the patients were Caucasian British nationals and were undergoing revision of their primary total hip replacement.

The primary diagnosis for primary total hip replacement was Osteoarthritis (n=28). There were also patients who had suffered trauma to the hip (n=2) and Rheumatoid Arthritis (n=2). No statistical links were found between the diagnosis for primary total hip replacement (osteoarthritis, trauma, rheumatoid arthritis) and other patient variables.

The age of patients at revision surgery ranged from 45 to 89 years of age but 95% of patients were aged between 69.2 and 75.7 years. The mean patient age for the whole population was 72.5 ± 1.6 years, 70.7 ± 2 years for male patients and 74.9 ± 2.4 years for female patients.

The age of patients at primary implant was calculated by subtracting the implant time in-vivo from the patient's age. The mean age of patients at primary implant was 56.8 ± 6.6 years with the mean ages of men and women being 56.5 ± 6.2 and 57.0 ± 6.5 respectively.

The weights of different patients differed greatly with the lightest patient being a lady weighing 54kg (patient 16) and the heaviest being a man weighing 110kg (patient 28). All of the patients (n=8) weighing >80kg were male (see Appendix section 0). The average weight of male patients was 77.1 ± 5.9kg and the average for female patients was 61.6 ± 13.8kg.

The BMI of patients ranged from 19.2kgm^{-2} to 30.5kgm^{-2}. The majority of patients (n=26) had BMI ratios in the normal range between 18.5kgm^{-2} and 24.9kgm^{-2}. Seven male patients were classed as overweight (25kgm^{-2} to 29.9kgm^{-2}) and one male patient was obese.

Patient BMI and patient age were also correlated (-0.36, p=0.040). Patients with the highest BMI values tended to also be the youngest (Figure 5-1).

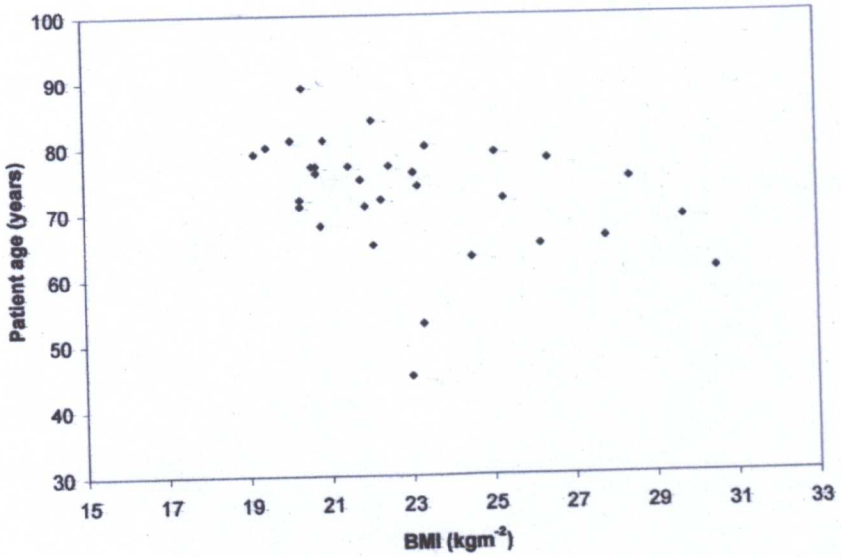

Figure 5-1 Scatterplot of BMI versus patient age

Gender and BMI were also correlated (-0.55, p=0.000) with women having significantly lower BMI values than men (Figure 5-2).

Figure 5-2 Boxplot showing BMI as a function of gender

The assessment of physical activity using the modified Baecke physical activity questionnaire gave three outcome measures. The first was the amount of physical

activity that the patient engaged in, in the home. Secondly, there was a physical activity score that reflected the level of sports & leisure activity that a patient participated in. Finally, there was a total physical activity score that combined the household and sports & leisure activity scores. The household activity scores for different patients displayed little variation and there was a range of scores from 0.7 to 2.7. This is in contrast to the sports & leisure activity scores that varied greatly ranging from 0 to 19.7. Total physical activity scores ranged from 0.7 to 22.4. The various physical activity scores are depicted in the Appendix.

Physical activity values for females were all slightly lower than for males. The mean household activity level for women was 1.45 ± 0.48 whilst for men, the figure was 1.51 ± 0.59. Standard deviations for men and women were similar and represented variations of 33% and 39% respectively. Average sport & leisure physical activity scores for men and women were 3.17 ± 3.96 and 4.05 ± 6.12. Total physical activity scores were 4.63 ± 4.24 for women and 5.56 ± 6.61 for men. Standard deviations for average sport & leisure and total activity scores were extremely high (>91%).

As might be expected, the age of the patient and their level of physical activity were negatively correlated (-0.52, p=0.002) indicating a decrease in total activity scores with increasing age (Figure 5-3).

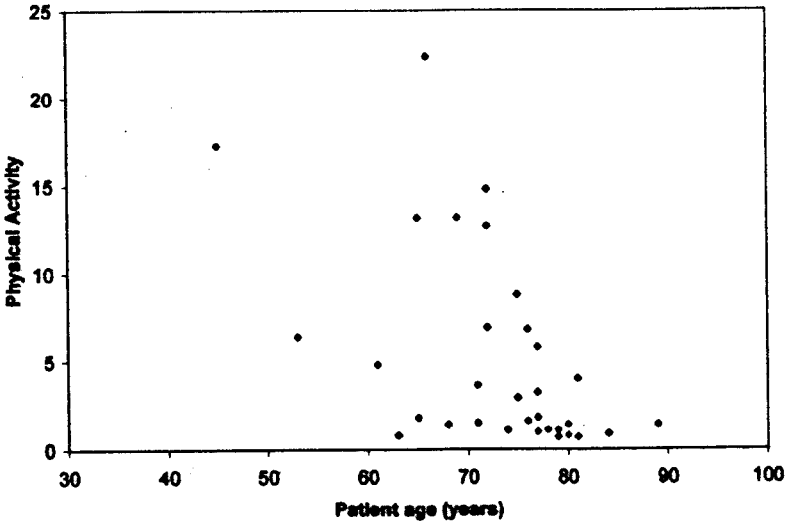

Figure 5-3 Scatterplot of patient age versus physical activity

The BMI of patients was correlated (0.41, p = 0.020) with higher BMI values correlated with increased total activity scores (Figure 5-4).

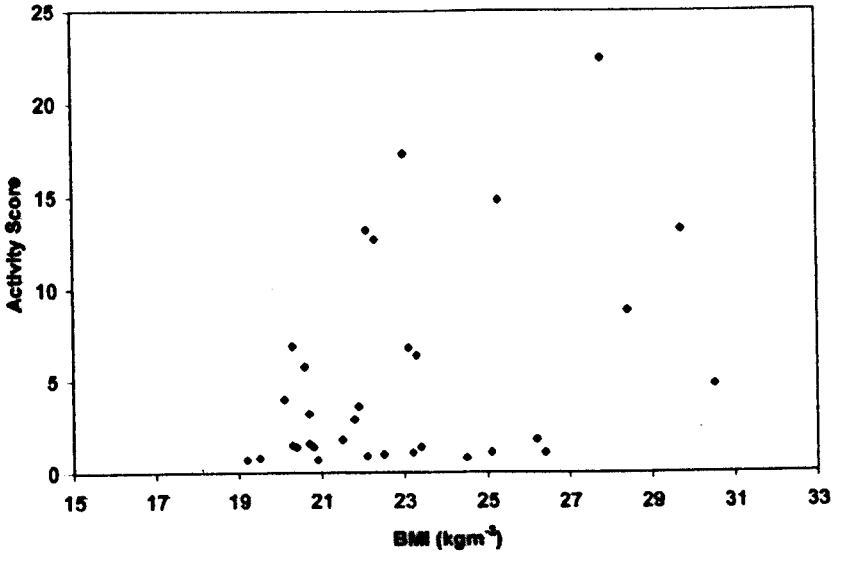

Figure 5-4 Scatterplot of BMI versus patient activity

ID #	Age (yrs)	M/F	Weight (kg)	Height (m)	BMI (kg/m2)	Diagnosis for primary THR	Physical activity score
1	69	M	91	1.75	29.71*	OA	13.2
2	53	F	73	1.77	23.30	OA	6.4
3	80	M	70	1.73	23.39	OA	1.4
4	72	M	58.4	1.52	25.28*	OA	14.8
5	66	M	92	1.82	27.77*	OA	22.4
6	75	M	92	1.80	28.40*	OA	8.8
7	77	F	66	1.79	20.60	OA	5.8
8	74	M	70	1.74	23.19	OA	1.1
9	68	M	65	1.77	20.80	OA	1.4
10	89	F	65.5	1.79	20.44	FR	1.4
11	63	M	81	1.82	24.45	OA	0.8
12	76	M	74	1.79	23.10	OA	6.8
13	71	F	57	1.68	20.28	OA	1.5
14	72	F	65	1.71	22.31	OA	12.7
15	71	M	66	1.74	21.87	OA	3.6
16	77	F	54	1.62	20.69	RA	3.2
17	80	F	63	1.80	19.48	OA	0.8
18	77	F	55	1.60	21.48	OA	1.8
19	81	M	61	1.71	20.94	OA	0.7
20	75	M	67	1.75	21.81	OA	2.9
21	76	F	56	1.65	20.67	OA	1.6
22	79	M	64	1.83	19.20	OA	0.7
23	65	F	69	1.77	22.08	OA	13.2
24	72	F	60	1.72	20.28	OA	6.9
25	77	M	68	1.74	22.53	OA	1.0
26	45	M	74.6	1.80	23.02	OA	17.3
27	65	M	82	1.77	26.17*	OA	1.8
28	61	M	110	1.90	30.47**	OA	4.8
29	78	M	93.2	1.88	26.37*	RA	1.1
30	79	M	86	1.85	25.13*	OA	1.1
31	81	F	55.4	1.66	20.10	OA	4.0
32	84	F	62	1.68	22.06	FR	0.9

OA = Osteoarthritis FR = Fracture RA = Rheumatoid Arthritis * = Overweight ** = Obese

Table 3 Summary of patient information

5.2 Retrieval Analysis

5.2.1 Retrieved Components

Thirty-two UHMWPE components were obtained during this study of which 5 had been implanted with a metal backing and the rest (27 components) were implanted with only PMMA cement. All UHMWPE components had been manufactured by DePuy and were either flanged Ogee (n=9) or LFA Classic (n=22) designs (Figure 5-5). The flanged rim of the Ogee cup was designed to pressurize the cement by restricting its extrusion from the acetabulum during cup insertion.

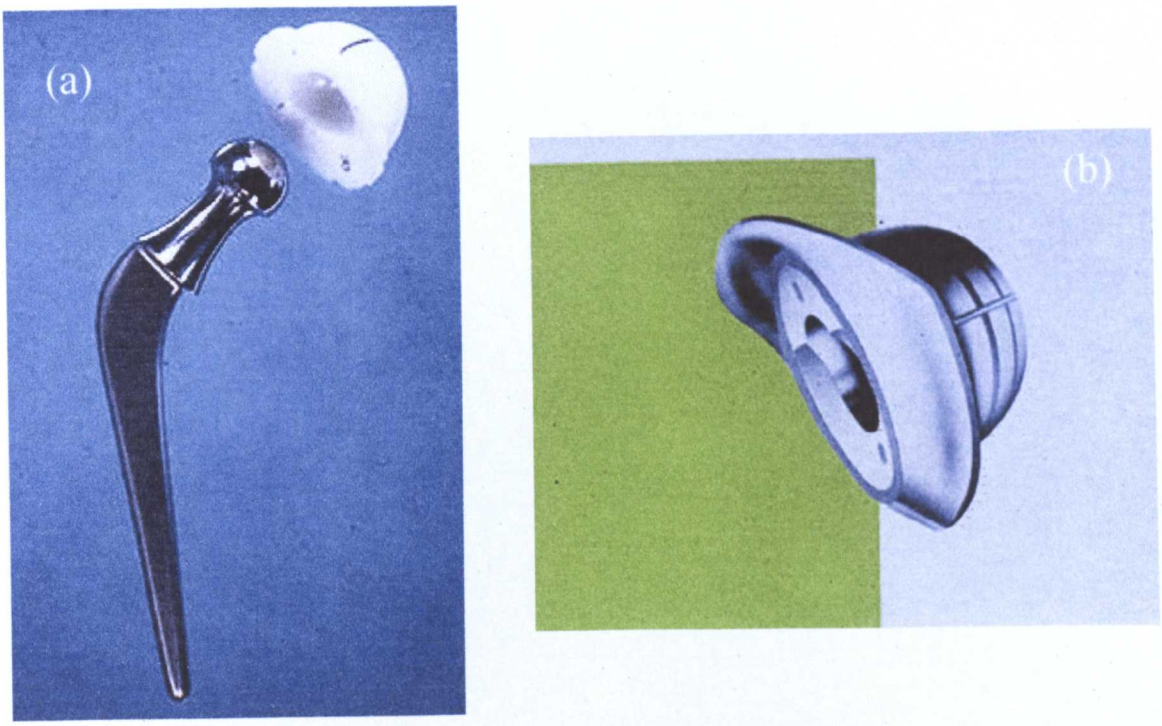

Figure 5-5 (a) LFA Classic and (b) flanged Ogee UHMWPE acetabular component designs

UHMWPE acetabular components had all been mated with metal (stainless steel 316L or cobalt-chrome) femoral heads, none of which required revision.

Four of the components had a metal backing (component 2, 12, 27, 28). A summary of component information is listed in Table 4. The company confirmed that

the acetabular components evaluated in this study were manufactured from GUR1020 (or historical equivalent) and sterilised using gamma irradiation 2.5Mrad. However, specific information on individual components such as date of manufacture and sterilisation details (date, atmosphere) had not been forthcoming at the time of publication of this thesis. The lack of component specific information, in particular the sterilisation details (atmospheric conditions used, date of sterilisation), is a limitation of the study.

Despite the lack of information regarding specific components, it is known that the use of calcium stearate declined significantly by 1998 due to improved processing techniques and Ticona stopped using it in 2002.

The manner in which the components were sterilized (gamma irradiation in air or reduced/inert atmosphere) is important but unknown. However, orthopaedic companies ceased gamma irradiating UHMWPE components in air in 1998 at the latest [62]. Analysis of the time components have been implanted for indicates that there are only 3 acetabular components (12, 27, 28) in this study that may have been gamma irradiated in a reduced/inert atmosphere. Of these components the amount of time that they were stored on the shelf prior to implant is unknown. UHMWPE acetabular components generally have a five year shelf life following sterilization. Based on the amount of time components 12, 27 and 28 had been implanted for (4.3, 2.2 and 3.7 years respectively) and the shelf life of components, an assumption was made that all components had been sterilized using gamma irradiation in air.

For the population as a whole, implantation times varied from 2.2 to 25.2 years with 78.1% components (n=25) surviving >10 years, 62.5% (n=20) >15 years and

37.5% (n=12) of components survived for > 20years. Components implanted in female patients survived longer than those in male patients. At 10 years, there was a 92.0% survival rate for females as opposed to 70.0% rate in males. At 15 years 76.9% components in females had survived against 52.6% in males. Only 26.3% of components hi male patients survived for > 20 years whilst 53.8% survived in female patients. The mean implantation time for acetabular components is longer for female patients (18.39 ± 0.03 years) than male patients (14.20 ± 0.04 years) (Figure 5-6).

Figure 5-6 Boxplot of implantation time as a function of gender

There was a negative correlation between patient weight and in-vivo period of acetabular component. (-0.51, p=0.002). There were eight patients who weighed >80kg at the time of revision and they had a mean acetabular component implant time of 12.1 ± 7.4 years compared to 17.2 ± 6.1 years for patients who weighed < 80 kg.

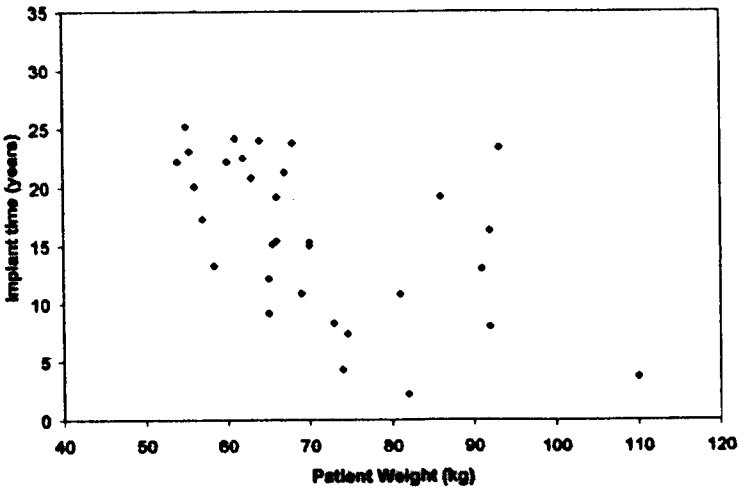

Figure 5-7 Scatterplot of patient weight and implant time

The scatterplot shown in Figure 5-8 depicts the negative correlation between patient BMI and acetabular component implant time in-vivo (-0.51, p=0.002).

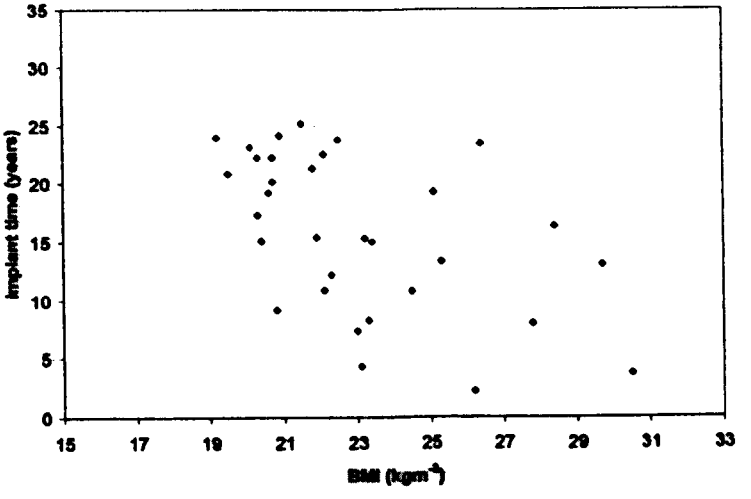

Figure 5-8 Scatterplot of BMI versus implant time

Interestingly, the activity of patients was correlated with component in-vivo time (Figure 5-9) (-0.59, p<0.001) with a trend of increased activity linked to a reduction in acetabular component time in-vivo.

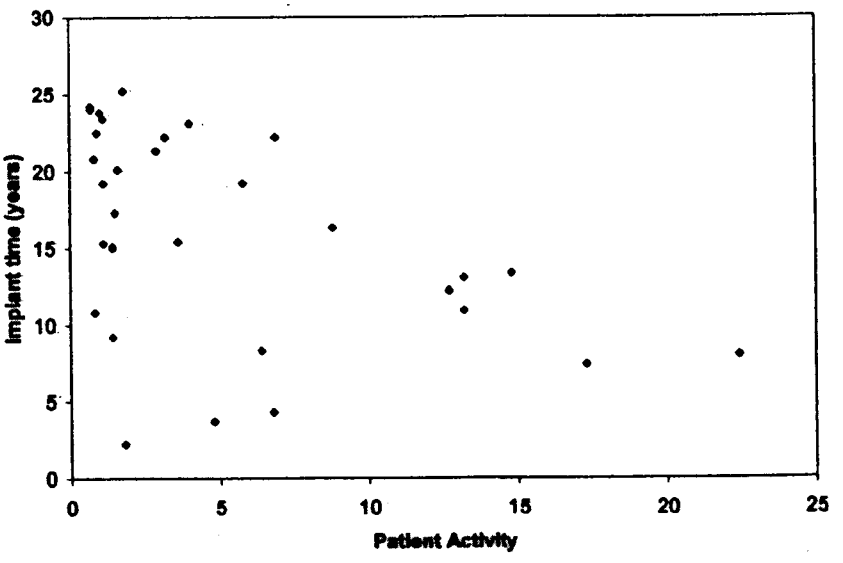

Figure 5-9 Scatterplot of patient activity and implant time

Surgery to revise the acetabular component of the primary THR was carried out for a number of reasons but aseptic loosening was the predominant cause (n=29). The other two surgical procedures were carried out for recurrent dislocation of the joint replacement (n=2) and trauma to the hip following a fall (n=l).

ID #	Acetabular component design	Metal backing	In-vivo (years)	Patient age at primary implant* (years)	Diagnosis for revision surgery	Femoral head diameter (mm)
1	LFA classic	N	13.0	44.7	Loosening	28
2	Ogee	Y	8.3	57.8	Loosening	22.25
3	LFA classic	N	15.0	73.9	Loosening	28
4	LFA classic	N	13.3	53.7	Loosening	22.25
5	Ogee	N	8.0	59.2	Loosening	22.25
6	LFA classic	N	16.3	55.9	Loosening	22.25
7	LFA classic	N	19.2	54.1	Loosening	22.25
8	LFA classic	N	15.3	49.8	Loosening	22.25
9	Ogee	N	9.2	61.5	Loosening	22.25
10	LFA classic	N	15.1	58.7	Loosening	22.25
11	Ogee	N	10.8	58	Loosening	28
12	Ogee	Y	4.3	58.7	Trauma	22.25
13	LFA classic	N	17.3	58.7	Loosening	22.25
14	LFA classic	N	12.2	58.8	Loosening	28
15	LFA classic	N	15.4	71.7	Loosening	22.25
16	LFA classic	N	22.2	55.6	Loosening	28
17	LFA classic	N	20.8	55	Loosening	22.25
18	LFA classic	N	25.2	53.2	Loosening	28
19	LFA classic	N	24.2	37.6	Loosening	28
20	LFA classic	N	21.3	62.8	Loosening	28
21	LFA classic	N	20.1	57.3	Loosening	22.25
22	LFA classic	N	24.0	54.6	Loosening	22.25
23	Ogee	N	10.9	59.8	Loosening	22.25
24	LFA classic	N	22.2	54.8	Loosening	22.25
25	LFA classic	N	23.8	51.8	Loosening	22.25
26	Ogee	N	7.4	57.9	Loosening	22.25
27	Ogee	Y	2.2	56	Dislocation	22.25
28	Ogee	Y	3.7	65	Dislocation	22.25
29	LFA classic	N	23.4	52.2	Loosening	22.25
30	LFA classic	N	19.2	56.8	Loosening	32
31	LFA classic	N	23.1	53.7	Loosening	28
32	LFA classic	N	22.5	59.8	Loosening	22.25

* calculated as patient age minus implant time in-vivo.

Table 4 Summary of component information

5.2.2 Visual Inspection of Retrieved Acetabular Components.

The retrieved components were visually inspected in order to identify any clear defects. All components that were revised due to asceptic loosening displayed clear signs of wear. Fracture of UHMWPE components has been reported in the literature but none of the retrieved components in this study displayed signs of it. There were a number of components (n=8) that displayed delamination of the UHMWPE confined to the rim of the component. The position of maximum wear on the retrieved components was found to be in agreement with previously published data in the literature [134, 135]. Highly worn components displayed a distinct ridge between worn and unworn regions.

Figure 5-10 is a photograph of component 5 with the worn region outlined with a yellow dotted line.

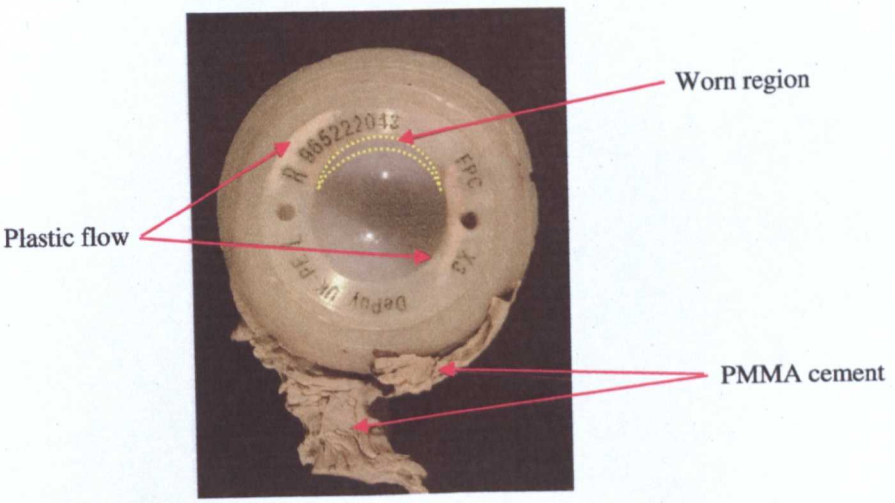

Figure 5-10 Photograph of component 5 displaying delamination of rim

Plastic flow of the surface of UHMWPE has occurred in two opposing areas outside the worn region. The PMMA cement used to fix the component to the pelvic bone is clearly visible.

Severe damage to the rim of component 11 immediately outside the worn region can be seen in Figure 5-11. The damage was probably caused by interference between the acetabular cup and the neck of the femoral component due to misalignment in-vivo. Misalignment may have resulted during the initial implant or because of impingement damage following the loosening of the cup due to osteolysis with the resulting movement of the cup causing the misalignment. The result of this is that the femoral neck can interfere with the acetabular component removing pieces of material (UHMWPE or PMMA cement). Third-body wear can result from this debris if it migrates to the bearing surface where it can cause third-body wear.

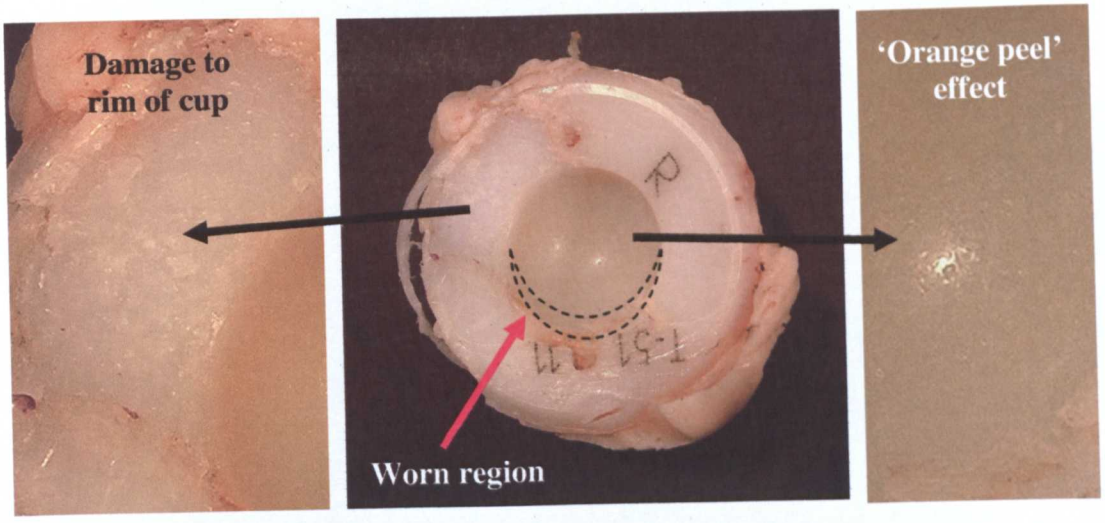

Figure 5-11 Photograph of component 11 showing damage to rim of cup

The 'orange peel effect' referred to in Figure 5-11 is a term used to describe the plastic flow of the UHMWPE that normally occurs just outside the area of high contact stress on the bearing. Plastic flow of this nature results in a roughening of the surface that has the appearance of orange peel. Plastic flow results when the material become sufficiently softened and extruded from the area of high contact

stress. Figure 5-12 is a photograph of component 26. On first inspection the bearing surface appeared to have debris deposited on it but on closer examination it was evident that the surface layer of material had been removed in an oval or 'butterfly' pattern. The likely cause of this wear was adhesion (fretting) as described by previous researchers [210, 211]. Sheared off debris from the fretting wear was flattened by the femoral head and was evident on the bearing surface as a white deposit. Non-uniform brown discoloration of the periphery of the worn surface is also evident. The cause of the discoloration has previously been reported by Schneider et al [212] as in-vivo absorption of proteins from the synovial fluid.

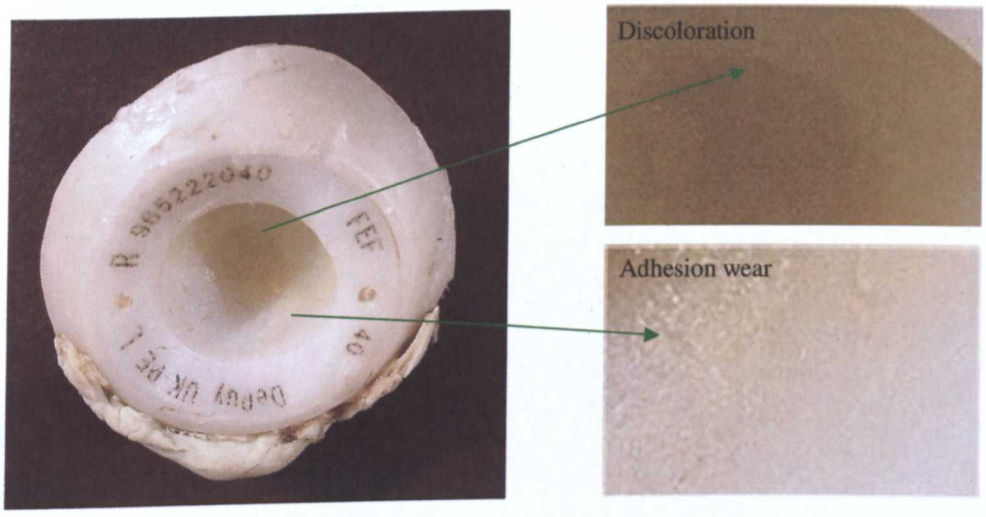

Figure 5-12 Photographs of component 26 displaying adhesion wear and discoloration

Figure 5-13 shows the inter-zonal ridge at the interface between worn and unworn regions of component 25. This ridge was present for all highly worn components.

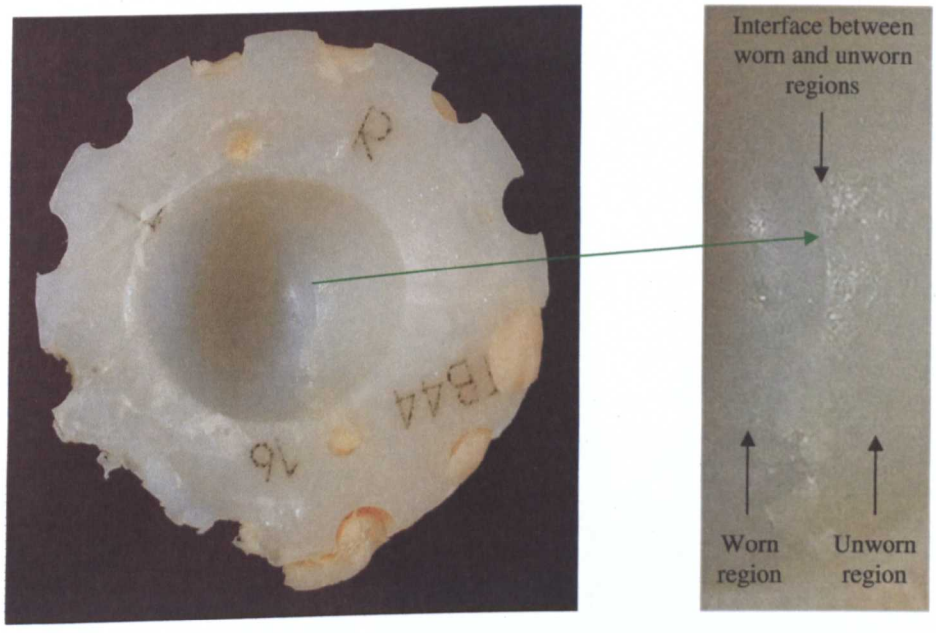

Figure 5-13 Photograph showing inter-zonal ridge between worn and unworn regions (component 25)

5.2.3 Microscopy - Bearing Surface

Specific features from unworn, inter-zonal and worn regions were investigated in further detail using an environmental scanning electron microscope.

The presence of machining marks in unworn regions was common to all components. Machining marks from the unworn surface of component 2 are shown in Figure 5-14. Typically, the surface finish specified for manufacturing of cups is of the order $R_a = 1\mu m$.

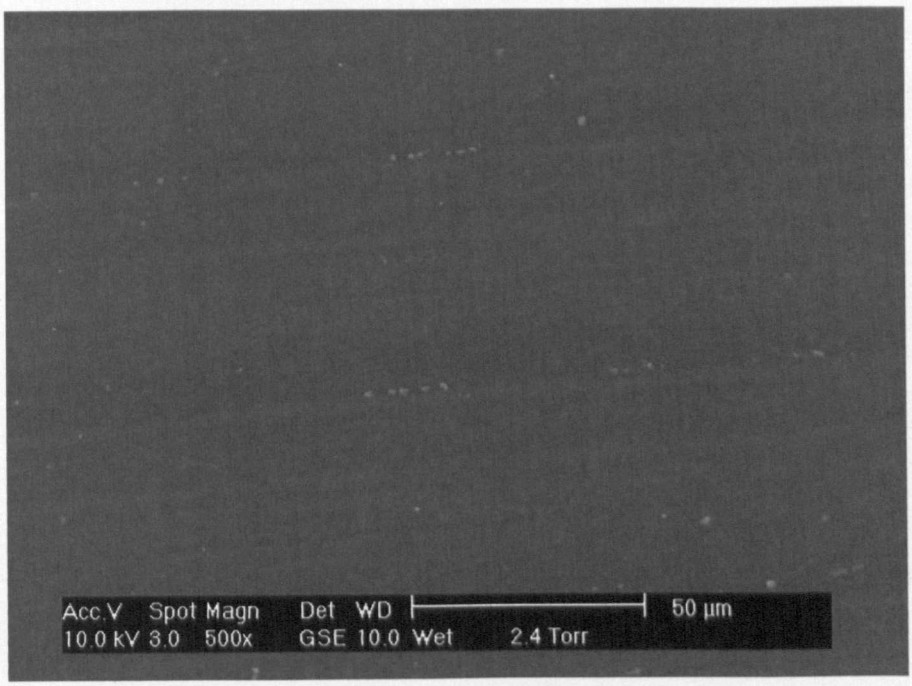

Figure 5-14 ESEM image showing machining marks on the unworn surface of component 2.

All of the examined cups displayed fibril formation in worn regions. The wear features of component 20 are displayed in Figure 5-15 and were indicative of the wear surfaces found on other components. Fibril formation can be seen on the worn surface of component 20.

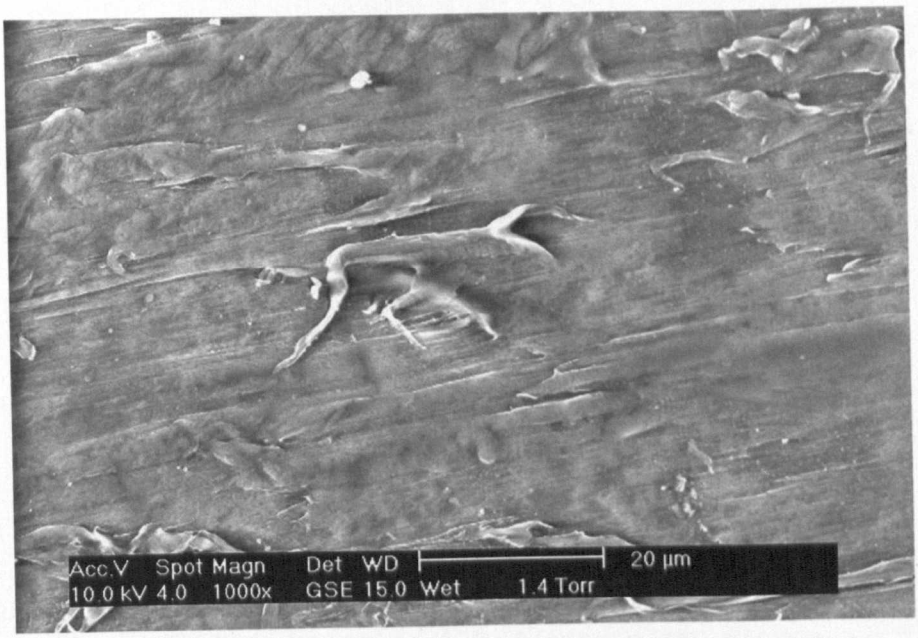

Figure 5-15 ESEM image of the worn surface of component 20 showing fibrils formed during the wear process.

Figure 5-16 is a magnified image of the fibril shown in Figure 5-15.

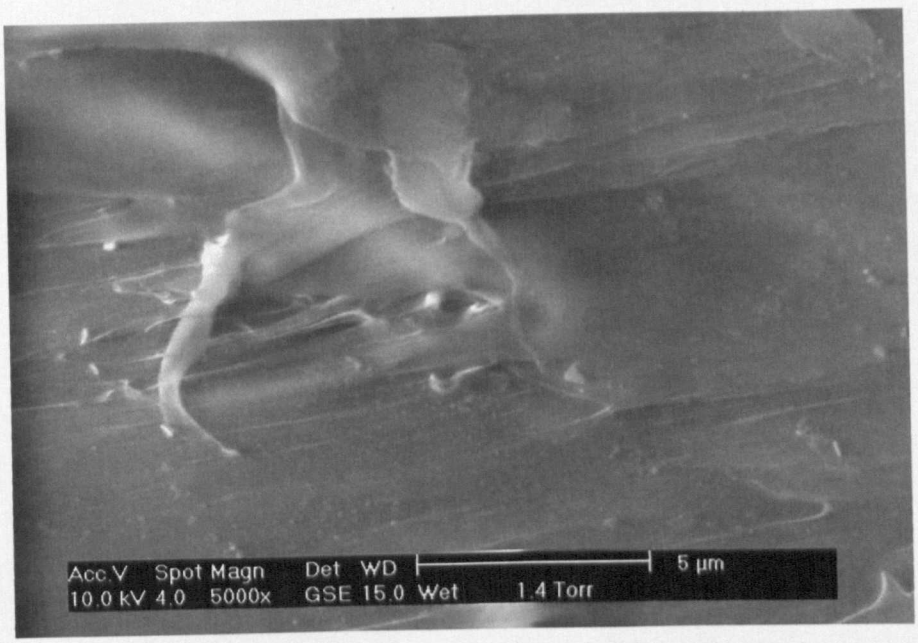

Figure 5-16 ESEM image of a fibril formed on the worn surface of component

Fibril formation on the worn surface of component 31 can also be seen in Figure 5-17.

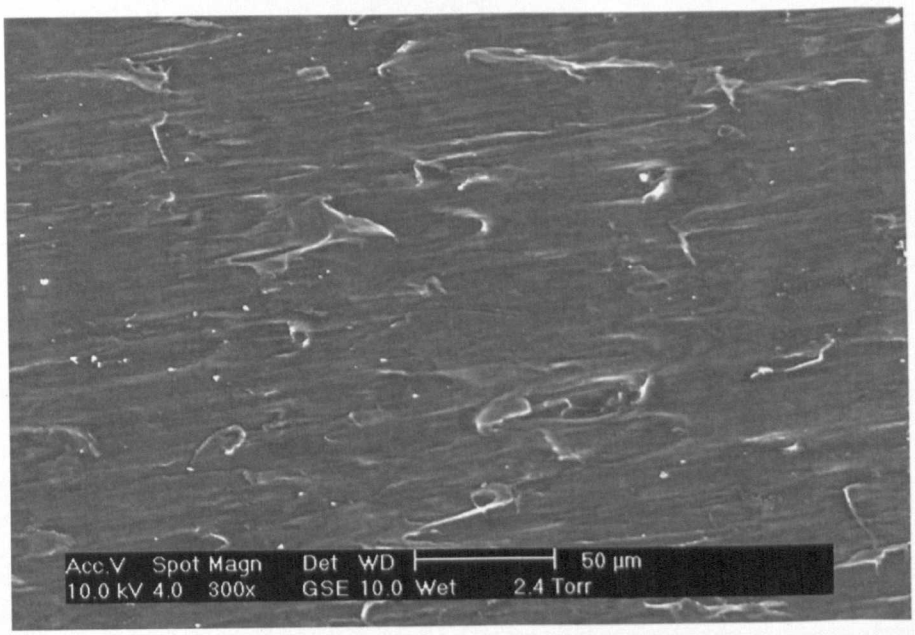

Figure 5-17 ESEM image of fibril formation on highly worn surface of component 31

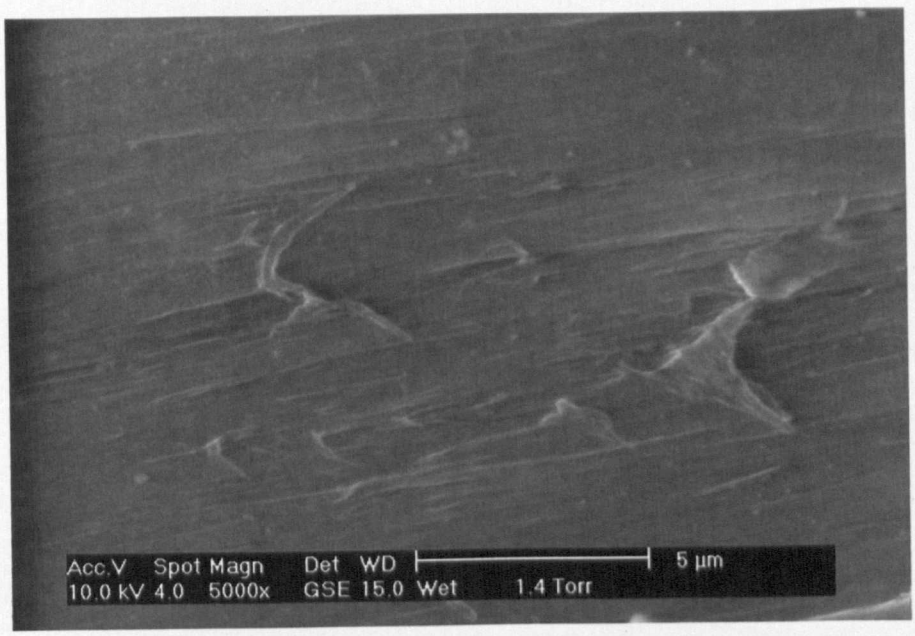

Figure 5-18 ESEM of fibrils on the worn surface of component 31.

The generation and release of fibrillar wear debris from the worn surface can contribute to abrasive wear. A wear particle that has been pressed into the worn surface of component 15 is shown in Figure 5-19 and circled in red.

Figure 5-19 ESEM image of wear debris pressed into the bearing surface of component 15

The presence of wear debris, pressed into the bearing surface of cups was found for all examined cups. Debris tended to be found outside of the pole of the worn region and extending to the interzonal interface surface. Subsequent removal of wear debris that had been pressed into the UHMWPE surface resulted in the formation of craters/pitting as indicated in Figure 5-20. The crater formed on the surface of component 15 has cracks extending from it. These cracks may have formed in response to the removal of load from the bearing surface with the opening of cracks perpendicular to the tensile stress as previously described by Jordan et al [213]. Wear debris is also visible in Figure 5-20 and is circled in red for ease of identification. The presence of craters was noted for 5 components.

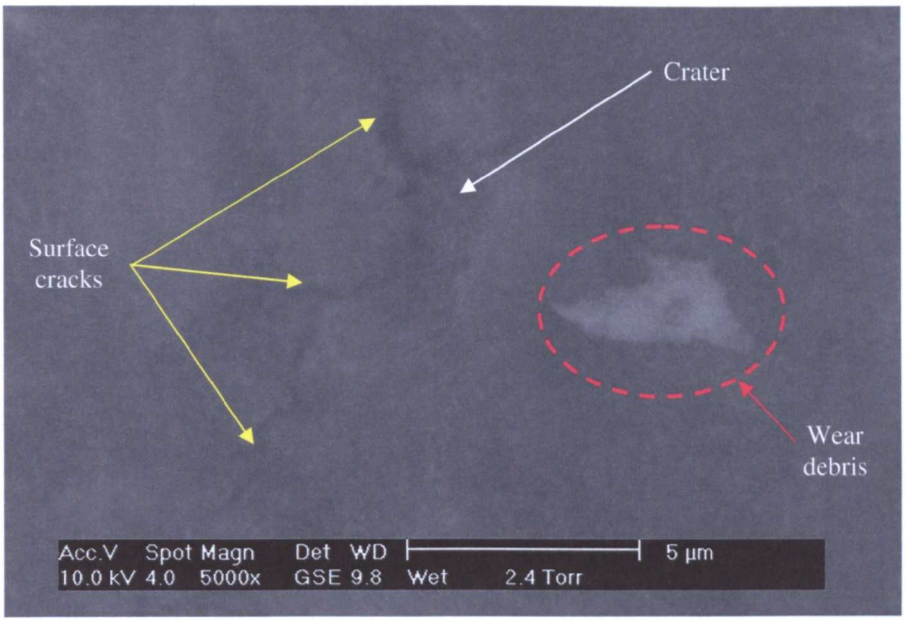

Figure 5-20 ESEM image showing crater, surface cracks and wear debris on the worn surface of component 15.

Adhesion wear was found on component 26 (Figure 5-12) and was investigated further using ESEM. The large crater at the top of the image clearly shows that a localised layer of UHMWPE was ripped of by adhesion to the femoral head exposing the inner surface of the UHMWPE.

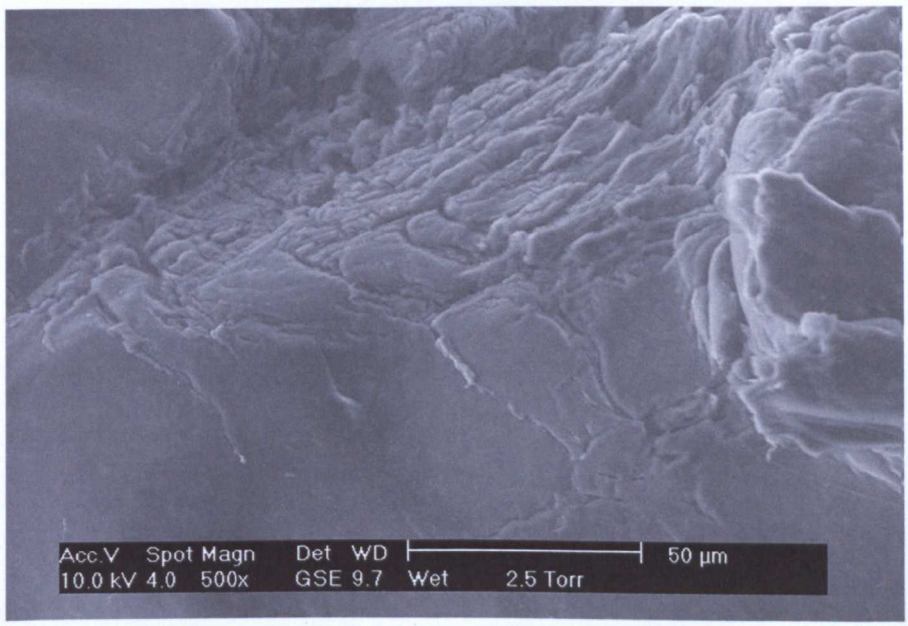

Figure 5-21ESEM image of adhesion wear on the worn surface of component 26

Scratches on the bearing surface were commonly observed and Figure 5-22 shows scratching on the bearing surface of component 2 in the inter-zonal region. The scratch at the bottom left hand side of the ESEM image clearly shows the initiation point of the scratch and the final position and resting place of the third-body particle.

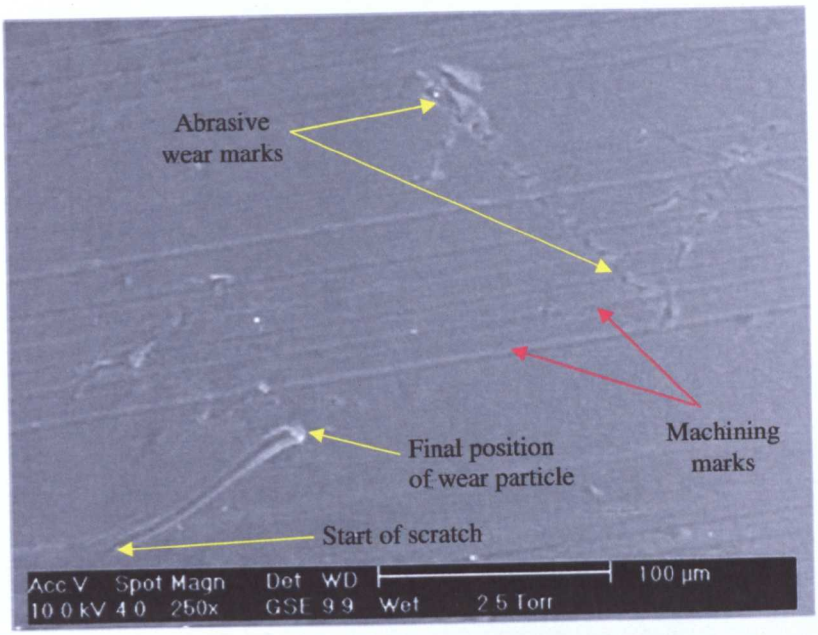

Figure 5-22 ESEM image showing scratches near the inter-zonal interface of component 2.

5.2.4 Microscopy - Through Thickness

Oxidation of UHMWPE in subsurface unworn regions of component 15 is visible in Figure 5-23 as a darker region 1000μm from the bearing surface. There is a definite boundary between the surface layer of the material and the heavily oxidized subsurface layer (white band). There is a gradient of oxidation that then extends from the oxidized region into the bulk. The degree of oxidation shown in the micrograph is an extreme and in general other components displayed the same distribution of subsurface oxidation but not to the same extent as component 15. ESEM images taken at points comparable to A, B and C are presented later in this section. On the left hand side of the image is a diagrammatic representation of the direction and spacing of indents starting 100μm from the bearing surface and moving into the bulk at 200μm intervals.

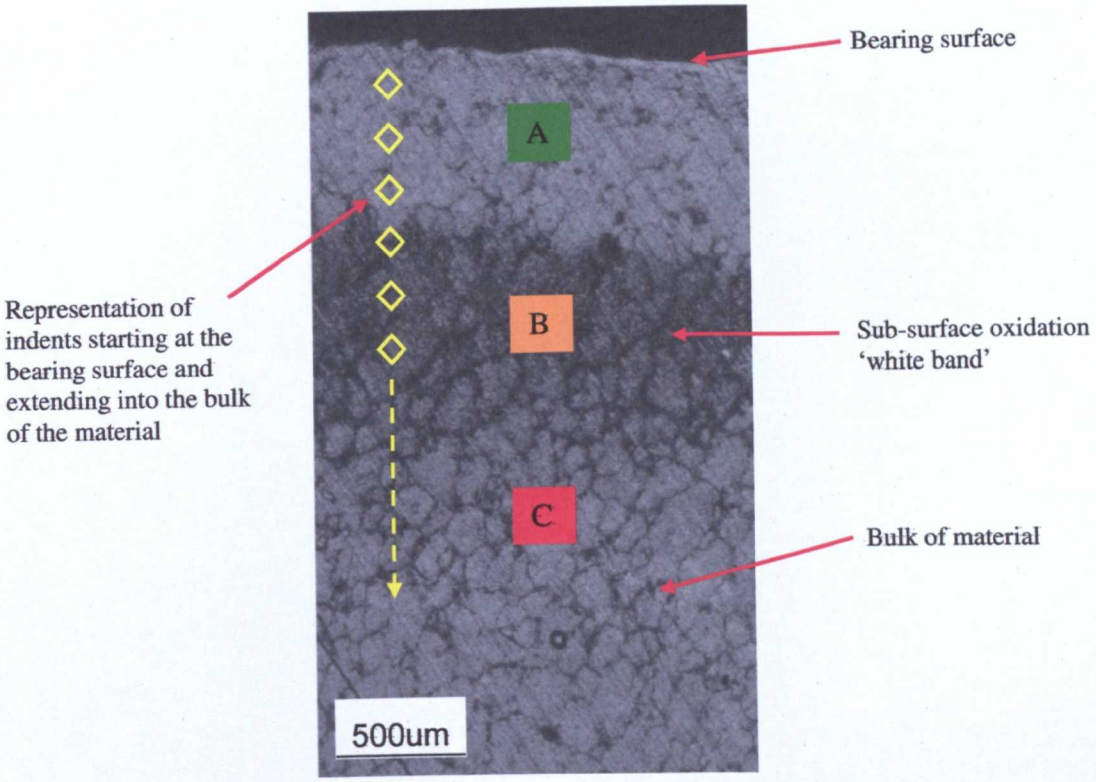

Figure 5-23 Through-thickness micrograph showing subsurface oxidation known as 'white band' (component 15)

In contrast, the worn region of component 15 does not display the 'white band' phenomena (Figure 5-24). Surface, subsurface and bulk microstructures were similar and this was representative of through thickness sections of retrieved UHMWPE components. ESEM images taken at a point comparable to D are presented later in this section. Comparable points from component 15 are used because the micrographs shown in Figure 5-23 and Figure 5-24 were prepared using a microtome whilst the ESEM images were taken of through thickness sections that had been freeze fractured.

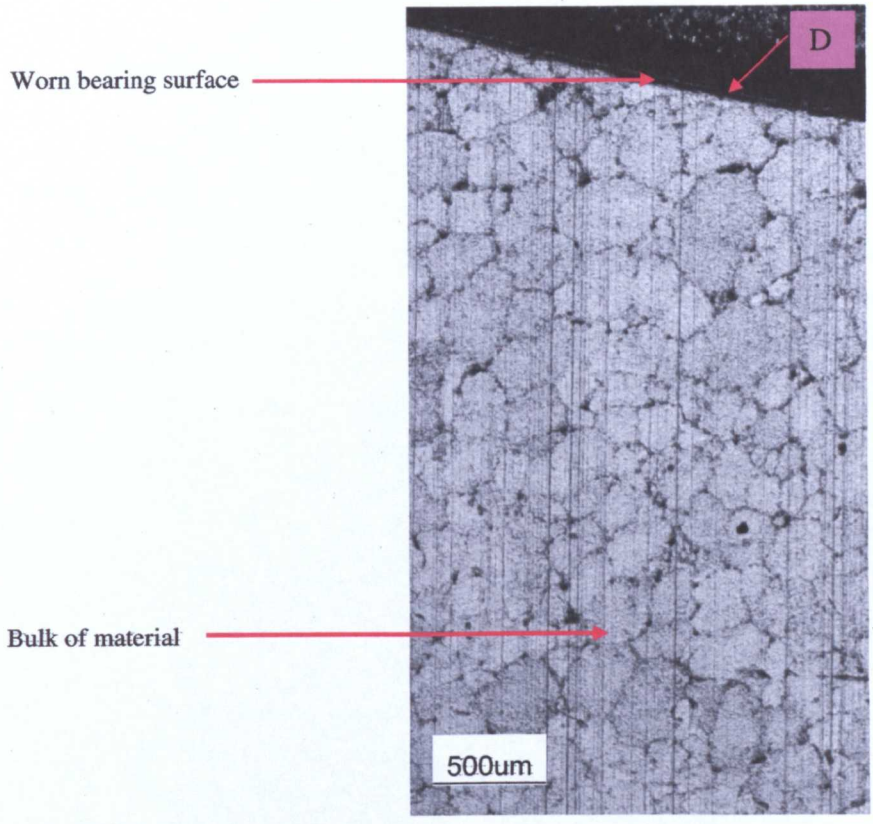

Figure 5-24 Through-thickness micrograph of worn region (component 15)

Figure 5-25 (a) and (b) are ESEM images from point 'A'. The morphology of UHMWPE in surface unworn regions was globular in appearance and showed well consolidated UHMWPE material. Material in the bulk also had this morphology.

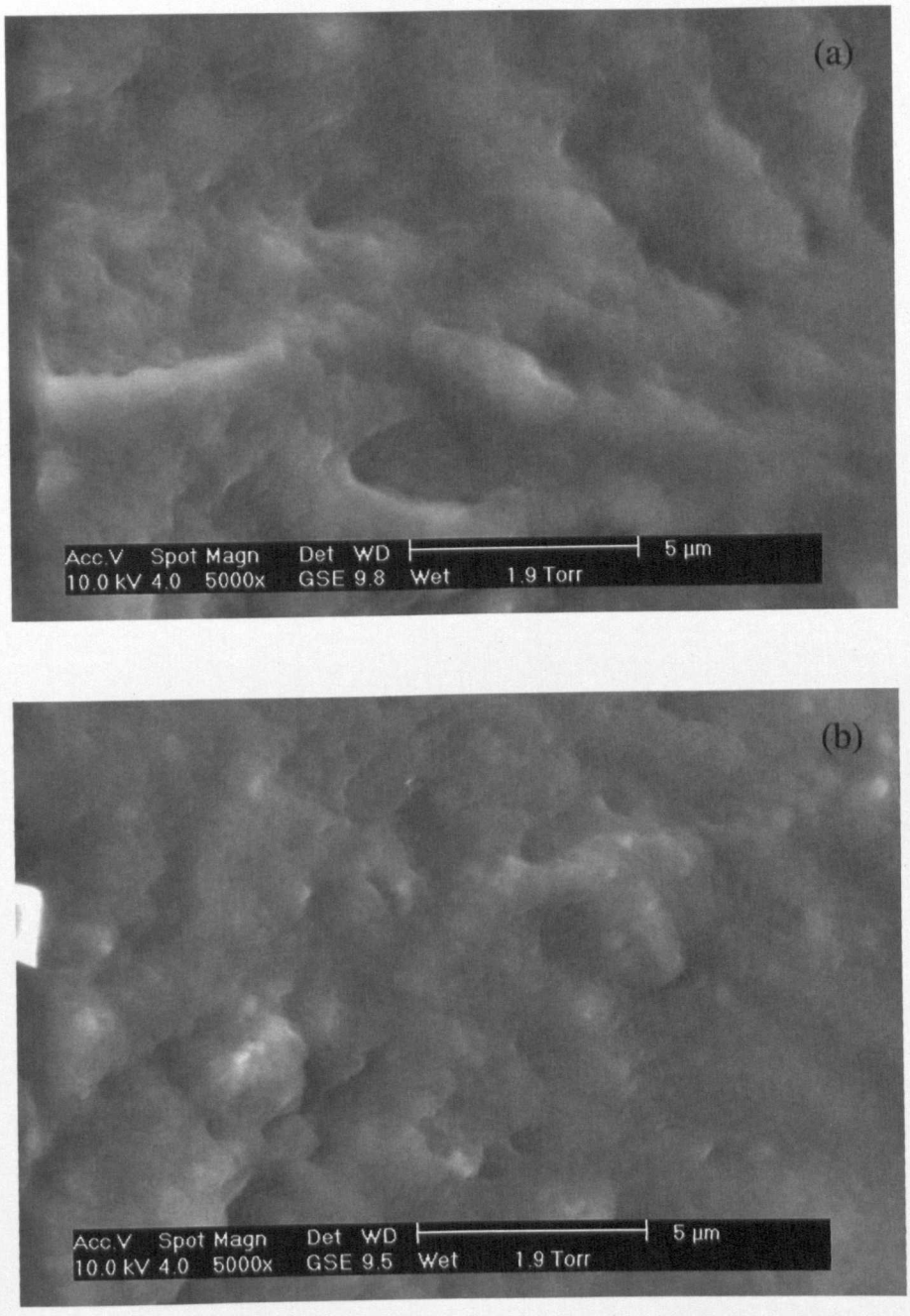

Figure 5-25 Freeze fractured ESEM images from unworn near surface region (A) (component 15)

The morphology of the UHMWPE in highly oxidized unworn region 'B' was completely different to region 'A'. The microstructure appears meshlike and porous in nature (Figure 5-26 (c) and (d)).

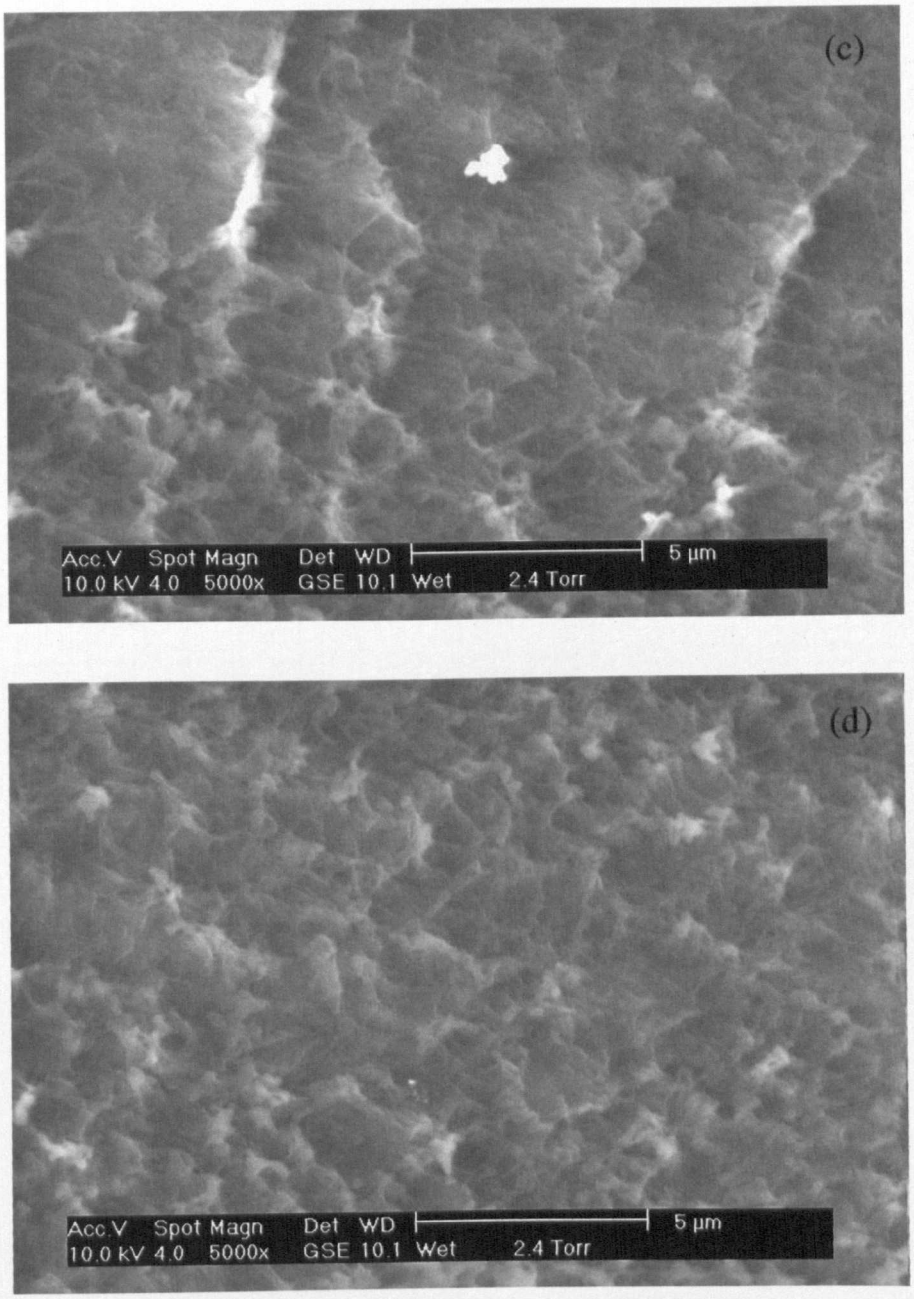

Figure 5-26 Through thickness freeze fractured ESEM images from oxidized region (B) (component 15).

Point 'C' in Figure 5-23 is a transition zone between the highly oxidized subsurface region and the bulk of the material. The microstructure displays

features from both the surface/bulk and oxidized regions and indicates the transition from a well consolidated globular appearance to porous meshlike structure.

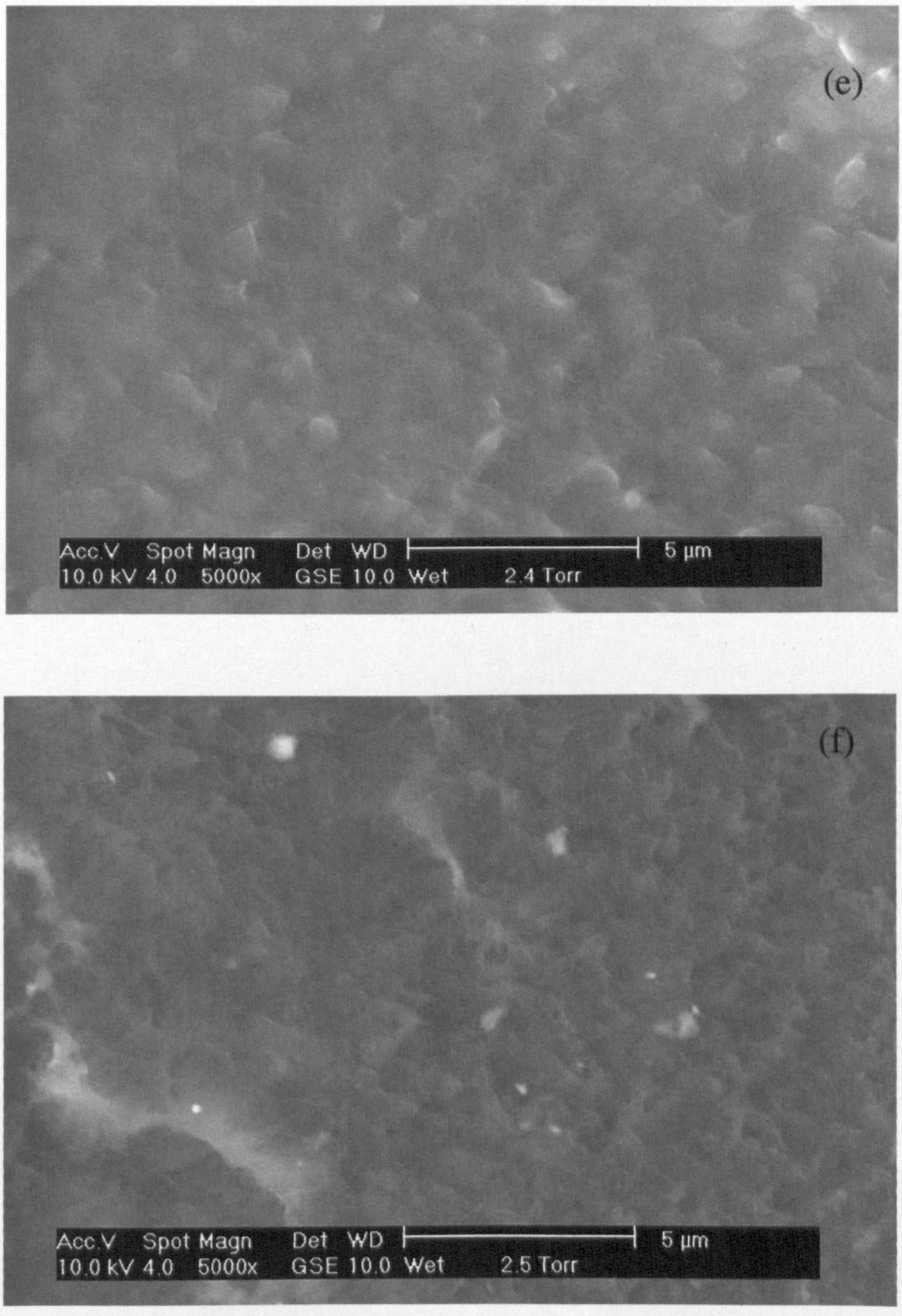

Figure 5-27 Through-thickness freeze fractured ESEM images from transitional zone between subsurface and bulk regions (C) (component 15).

Figure 5-28 is a through thickness freeze fracture ESEM image taken at the bearing surface of the worn region of component 15. Figure 5-29 is an image taken at higher resolution of the region outlined by the red hashed line. A crack can be seen emanating from the bearing surface at 90° to the direction of wear. Delamination is initiated by sub-surface cracks, which can propagate to the articulating surface, leading to the removal of relatively large (>0.5 mm) flake-like debris.

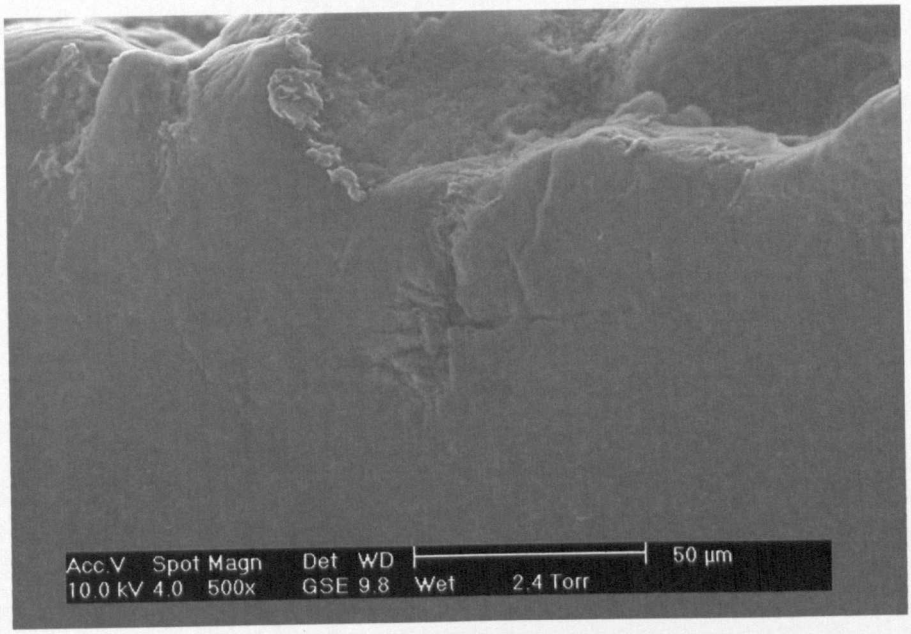

Figure 5-28 Through-thickness freeze fractured ESEM image from bearing surface of worn region (D) (component 15).

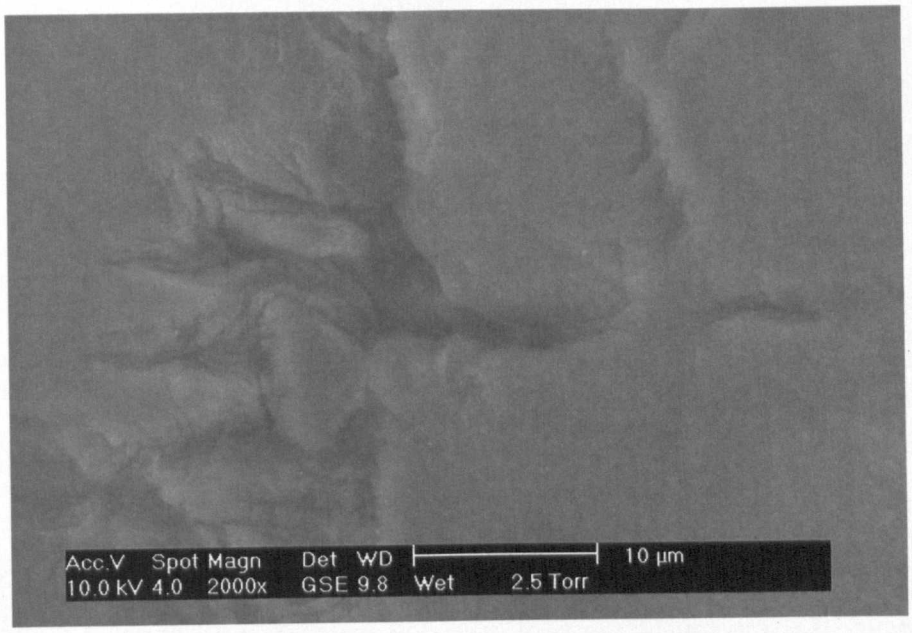

Figure 5-29 Through-thickness freeze fractured ESEM image from bearing surface of worn region (D) (component 15).

Figure 5-30 is an ESEM image of an unconsolidated UHMWPE particle.

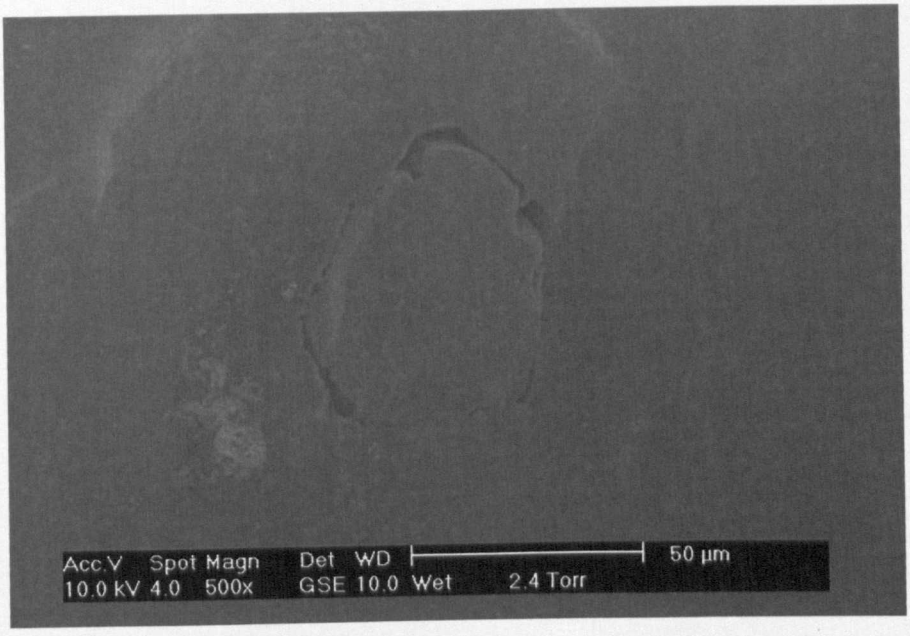

Figure 5-30 ESEM image showing an unconsolidated UHMWPE particle.

5.3 Wear Assessment

The linear and volumetric wear data obtained from the CMM assessment of retrieved components is listed in Table 5 along with the associated wear rates and beta-angles. Volumetric and linear wear rates were calculated by dividing the amount of linear or volumetric wear by time. There was an assumption that the wear process had been linear over time because no wear rate information had been taken at intermediate time periods in the life of the hip replacement.

5.3.1 Component Wear Angles

Linear wear angles (β-angle) and acetabular component inclination angles (ω-angle) for the 32 acetabular components are listed in Table 5. Linear wear angles varied between 24 ± 1° (component 27) and 61 ± 1° (component 4) which corresponded to acetabular cup inclination angles of 66 ± 1° and 29 ± 1° respectively. The mean β-angle was 43 ± 8° (mean ω-angle 47 ± 8°). The CMM models of the five acetabular components that displayed the smallest β-angles are shown in Figure 5-31 whilst Figure 5-32 shows the CMM models of the five acetabular components with the largest β-angles. CMM models are not to scale and are for indication purposes as linear and inclination angles were calculated by analysing sections of CMM models in AutoCAD.

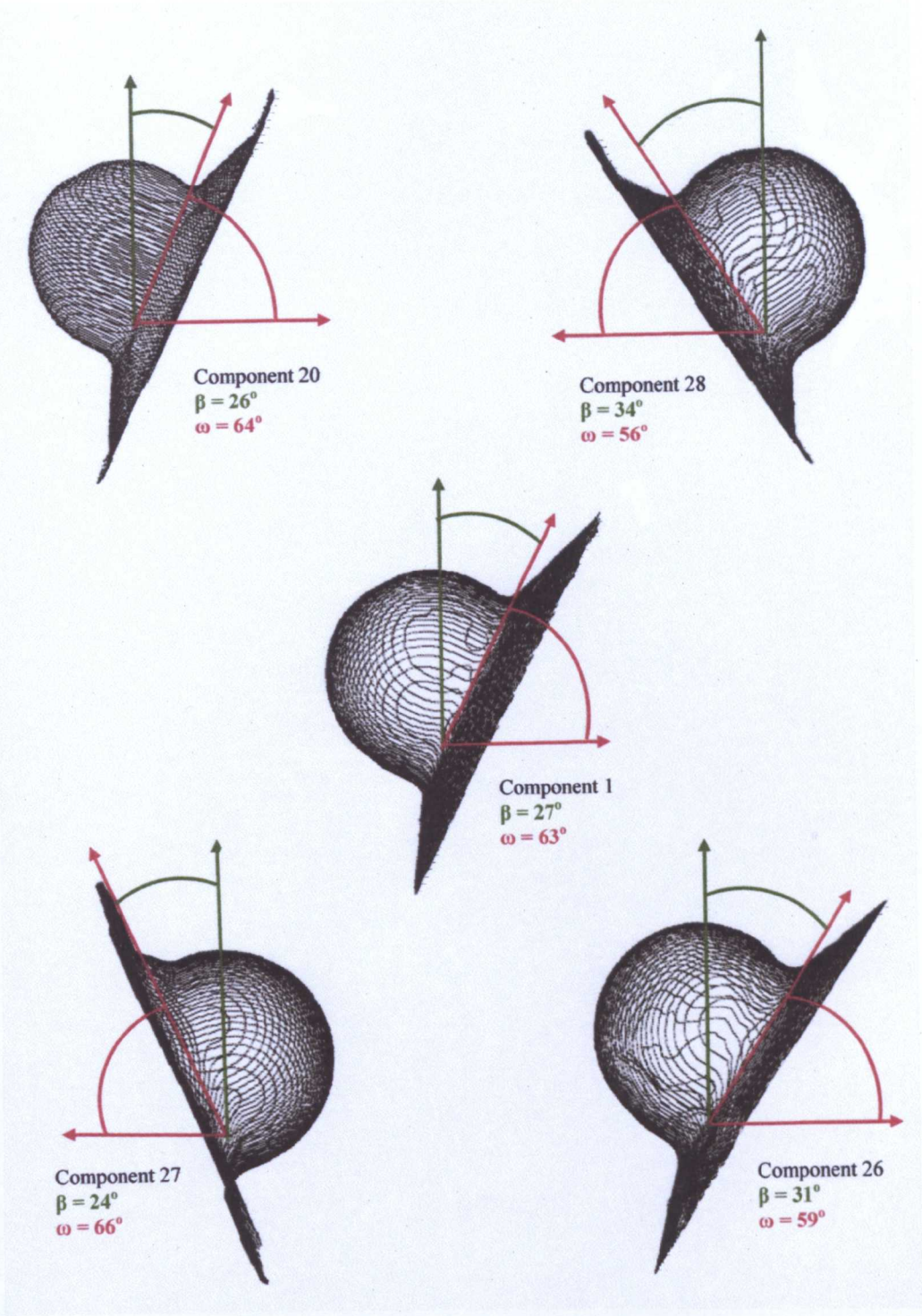

Figure 5-31 CMM models of five components (1, 20, 26, 27, 28) with the smallest β-angles

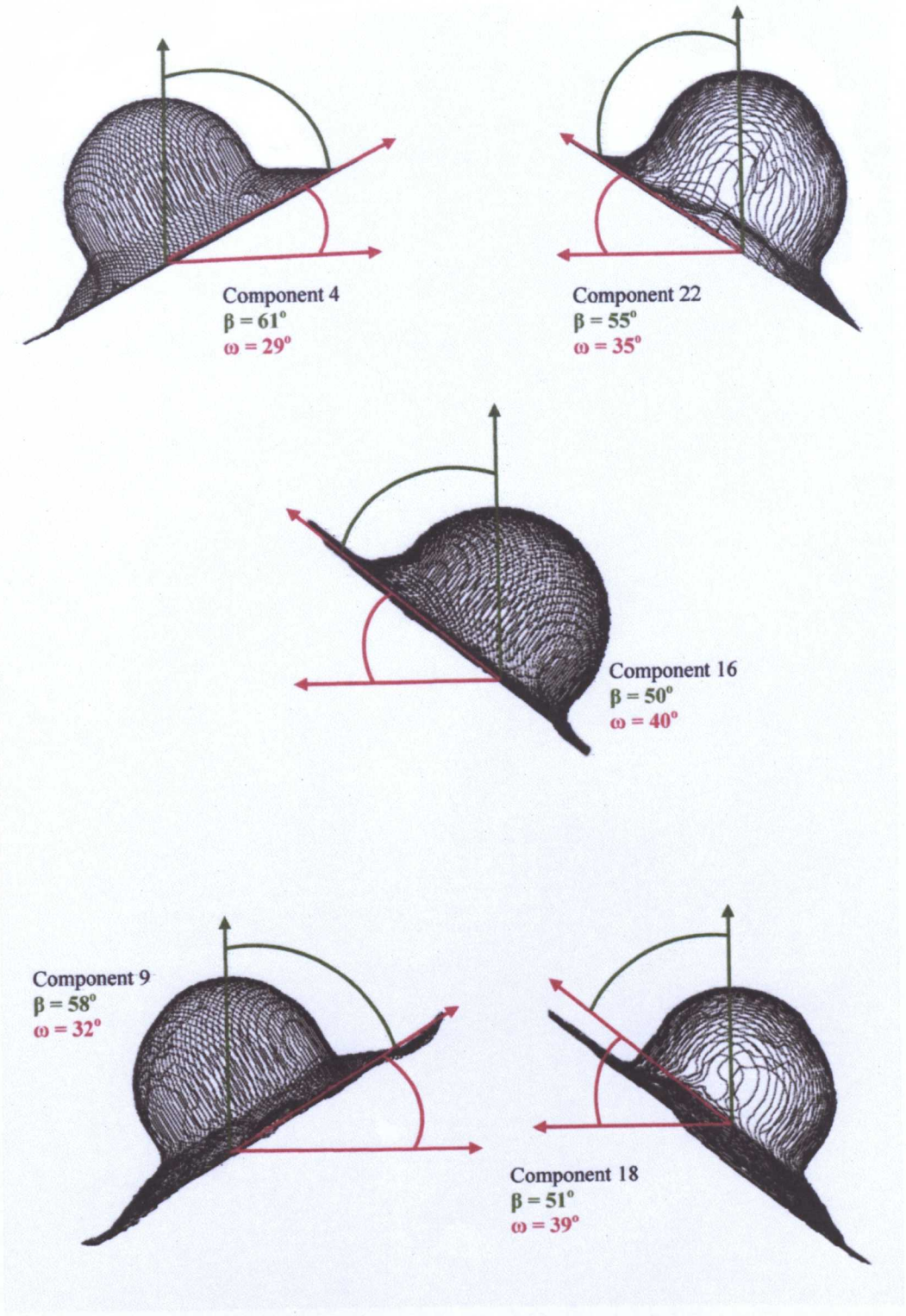

Figure 5-32 CMM models of the five components (4, 9, 16, 18, 22) with the largest β-angles

5.3.2 Linear Wear

The mean linear wear was found to be 2.08 ± 1.04mm with only a marginal difference between the mean values for components from male (2.17 ± 1.26mm) and female (1.97 ± 0.66mm) patients. However, the data for the male group was more varied than the female group as indicated by the two-fold increase in the standard deviation. The mean linear wear rate mean linear wear rate was 0.13 ± 0.04mm/yr.

Linear wear rate was correlated to patient age at the time revision (-0.41, p=0.018) (Figure 5-33). Interestingly, there was no correlation between the patient's age at the time of the primary implant (patient age - implant tune in-vivo).

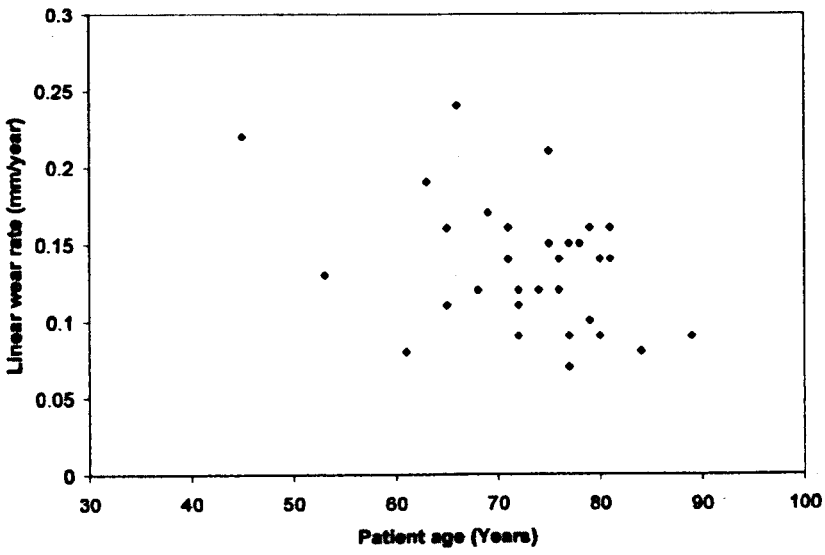

Figure 5-33 Scatterplot of patient age versus linear wear rate

Along with a link between patient age and linear wear rate, there was also a correlation between gender and linear wear rate. Mean linear wear rates for women were 0.109 ± 0.027 mm/year whilst for men they were 0.151 ± 0.043 mm/year. Figure 5-34 graphically shows the distribution of linear wear data as a function of gender.

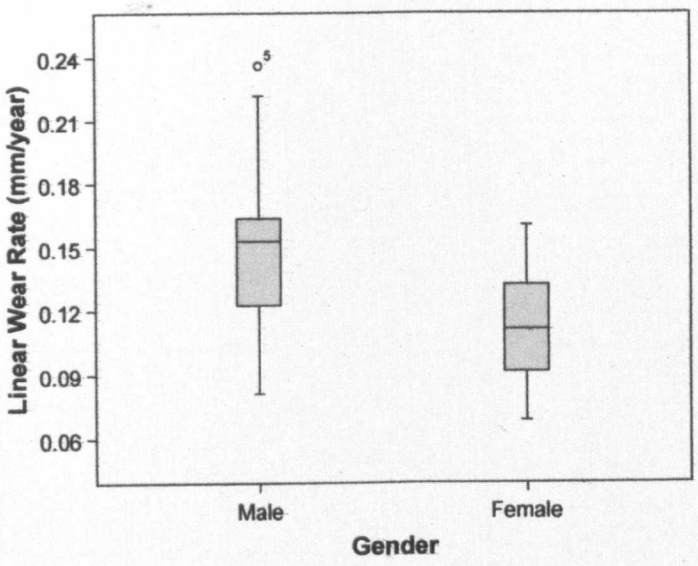

Figure 5-34 Boxplots of linear wear rate as a function of gender

Linear and volumetric wear were correlated (0.81, $p<0.001$) with increased linear wear rates linked to increased volumetric wear rates (Figure 5-35).

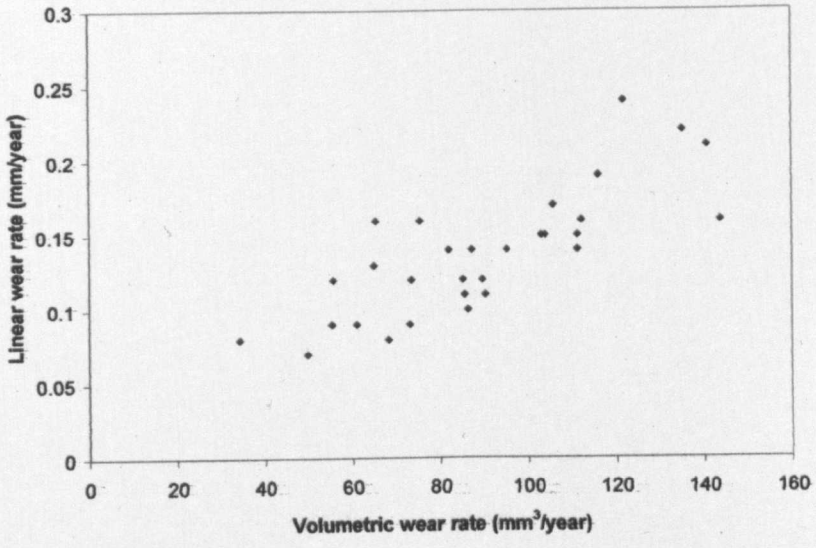

Figure 5-35 Scatterplot of volumetric wear rates versus linear wear rates

The mean volumetric wear rate for 22.25mm cups was 83.6 ± 27.9mm^3/year and 95.9 ± 28.8mm^3/year for 28mm cups. The mean linear wear rate for 22.25mm cups was 0.12 ± 0.04mm/year and 0.16 ± 0.04mm/year for the 28mm cups. It wasn't possible to investigate the link between 32mm heads and wear rates as there was only one component of that size.

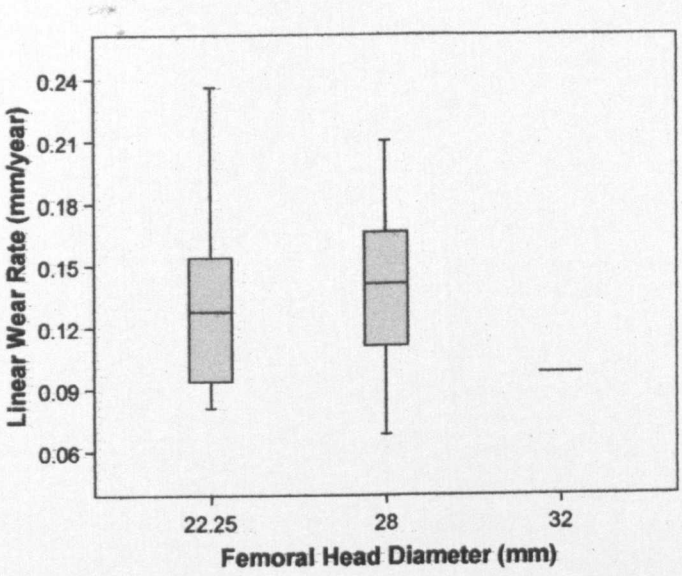

Figure 5-36 Boxplots showing linear wear rate as a function of femoral head diameter

Finally, linear wear was also correlated to β-angles (-0.37, p=0.034) with increased β-angles linked with reduced linear wear rates as depicted in Figure 5-37.

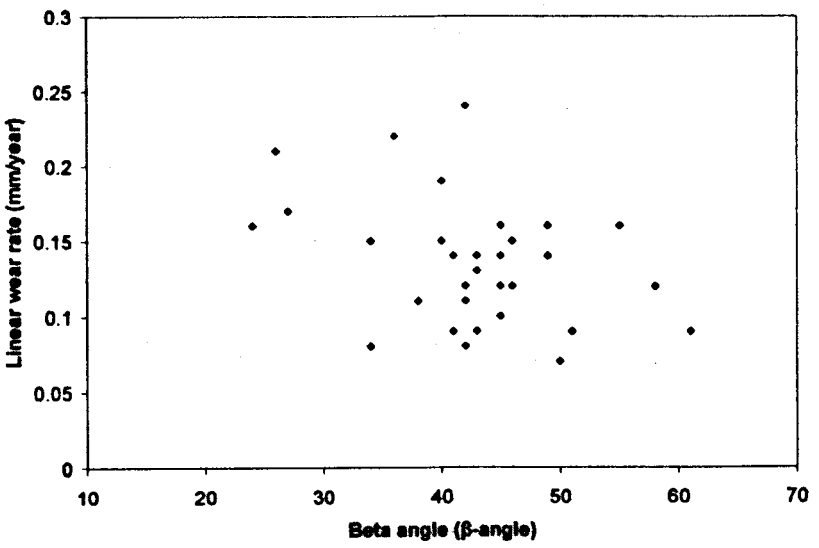

Figure 5-37 Scatterplot of β-angle versus linear wear rate

5.3.3 Volumetric Wear

The mean volumetric wear for the population as a whole was 1429 ± 824mm^3. For the components obtained from male patients, the mean volumetric wear was 1484 ± 994 mm^3 which was ~9% higher than the value for the female group, 1354 ± 537mm^3. Maximum and minimum volumetric wear values for whole population were 3453mm^3 and 126mm^3 respectively. Volumetric wear rates ranged from 34 to 143mm^3/year with a mean value of 87 ± 28mm^3/year. There was a marked difference in the volumetric wear rates for components retrieved from male and female patients. Components implanted in male patients displayed a mean volumetric wear rate of 97±30mm^3/year whilst the rate for female patients was 73±18mm^3/year.

Unlike linear wear rate, volumetric wear rate was not correlated to patient age (-0.13, p=0.447) or β-angle (-0.22, p=0.206). However, volumetric wear rate was correlated to patient age (-0.40, p=0.021) (Figure 5-38) with increased patient age linked to decreased volumetric wear rate.

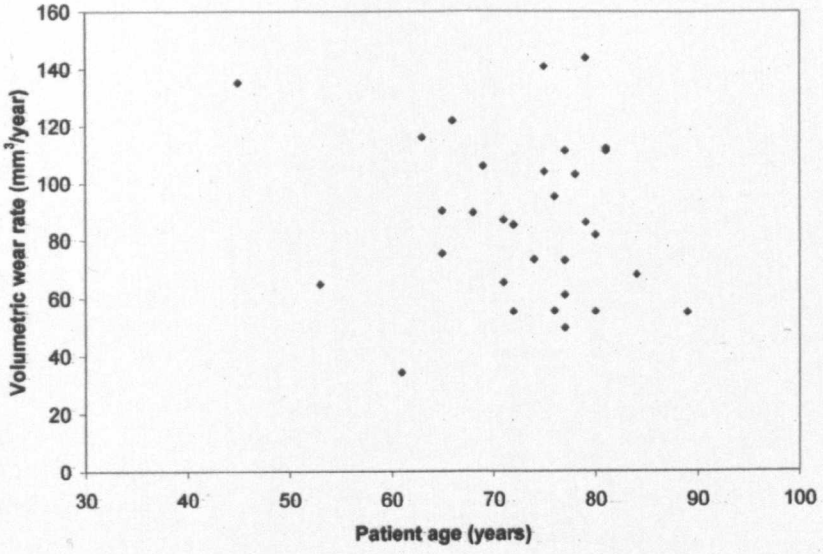

Figure 5-38 Scatterplot of patient age versus volumetric wear

Volumetric wear rate was also correlated to the reason for revision (loosening, dislocation, trauma) (-0.35, p=0.041) (Figure 5-39). The mean volumetric wear rate for patients with asceptic loosening was 90 ± 26mm^3/year whilst for the two patients with recurrent dislocation it was 54 ± 28mm^3/year and 55mm^3/year for the patient who underwent revision surgery for trauma.

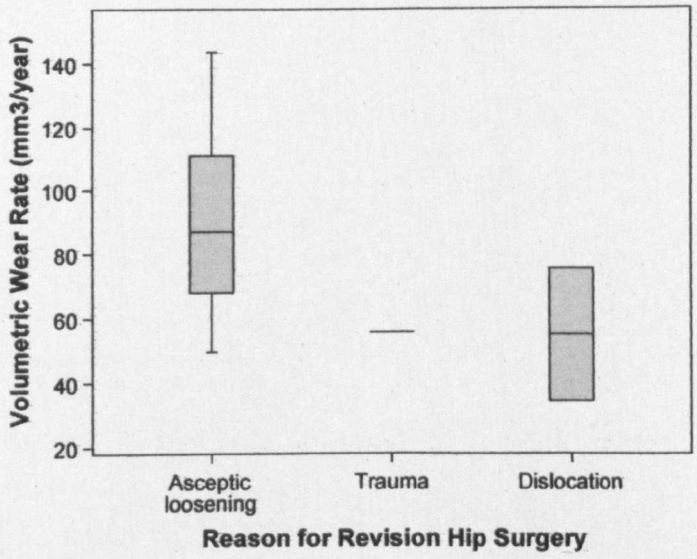

Figure 5-39 Boxplots showing VWR as a function of the reason for revision hip surgery

The mean volumetric wear rate for 22.25mm femoral components was 83 ± 27mm^3/year and 95 ± 28mm^3/year for 28mm diameter femoral components. There was only one 32mm diameter component so statistical analysis of 32mm components wasn't feasible (volumetric wear rate of 86mm^3/year).

The calculated wear factor (K) for components ranged from 0.8x$10^{-6}$$mm^3$/Nm (component 28) to 2.3x$10^{-6}$$mm^3$/Nm (component 16) with a mean value of 1.5 ± 0.4x$10^{-6}$$mm^3$/Nm.

Wear factor for women was higher than men being 1.6 ± 0.4x$10^{-6}$$mm^3$/Nm as opposed to 1.3 ± 0.4x$10^{-6}$$mm^3$/Nm for men. Surprisingly, there were no correlations between calculated wear factors for individual components and any other parameters.

ID #	Cup diameter (mm)	LW (mm)	LWR (mm/yr)	VW (mm^3)	VWR (mm^3/yr)	K ($x10^{-6} mm^3/Nm$)	β-angle (°)	ω-angle (°)
1	28	2.17	0.166	1376	105.8	1.2	27	63
2	22.25	1.1	0.132	540	64.8	1.4	43	47
3	28	2.12	0.141	1228	81.8	2.2	49	41
4	22.25	1.25	0.093	737	55.2	1.5	61	29
5	22.25	1.89	0.236	974	121.7	1.3	42	48
6	22.25	2.53	0.154	1698	103.9	2.3	34	56
7	22.25	1.81	0.094	1400	73.0	1.5	43	47
8	22.25	1.88	0.122	1124	73.3	1.3	45	45
9	22.25	1.13	0.123	821	89.5	2.2	58	32
10	22.25	1.43	0.094	832	55.1	1.4	41	49
11	28	2.04	0.189	1247	116.0	1.9	40	50
12	22.25	0.52	0.122	236	55.5	1.4	46	44
13	22.25	2.78	0.160	1131	65.2	1.3	49	41
14	28	1.35	0.111	1039	85.4	1.2	42	48
15	22.25	2.10	0.136	1342	87.0	1.6	41	49
16	28	1.88	0.068	1101	49.6	1.3	50	40
17	22.25	1.89	0.091	1148	55.3	1.9	43	47
18	28	2.22	0.088	1536	61.0	1.0	51	39
19	28	3.87	0.160	2710	112.1	1.3	45	45
20	28	3.61	0.210	2410	140.7	1.3	26	35
21	22.25	2.8	0.139	1911	95.1	1.5	45	52
22	22.25	3.87	0.161	3453	143.8	2.0	55	35
23	22.25	1.23	0.112	985	90.2	0.8	38	52
24	22.25	2.55	0.115	1886	85.0	1.0	42	48
25	22.25	3.66	0.153	2651	111.2	1.4	40	50
26	22.25	1.65	0.222	1003	135.2	1.0	36	54
27	22.25	0.35	0.161	163	75.2	1.2	24	66
28	22.25	0.3	0.081	126	34.3	1.3	34	56
29	22.25	3.51	0.149	2412	103.0	1.9	46	44
30	32	1.89	0.098	1653	86.2	1.1	45	45
31	28	3.12	0.135	2569	111.2	1.8	43	47
32	22.25	1.87	0.083	1533	68.1	1.2	42	48

Table 5 Summary of wear assessment data

5.4 Analysis of Radiographs

The initial intention regarding radiographs was to collect post-implant, follow-up and pre-revision radiographs in order to carry out a comparison with data obtained via direct measurement with the CMM. Unfortunately, only pre-revision radiographs were available for analysis. All radiographs were taken in the anterior-posterior orientation.

The pre-revision radiograph of component 2 is shown in Figure 5-40. Osteolysis has occurred around the exterior of the metal liner hi a hemispherical region superior to the component. Analysis of the radiograph reveals that the lateral margin of the metal liner is not in contact with the outer margin of the pelvic bone. At retrieval the component was reported to have been mechanically loose. Bone resorption of the femur due to stress shielding is also visible on the radiograph.

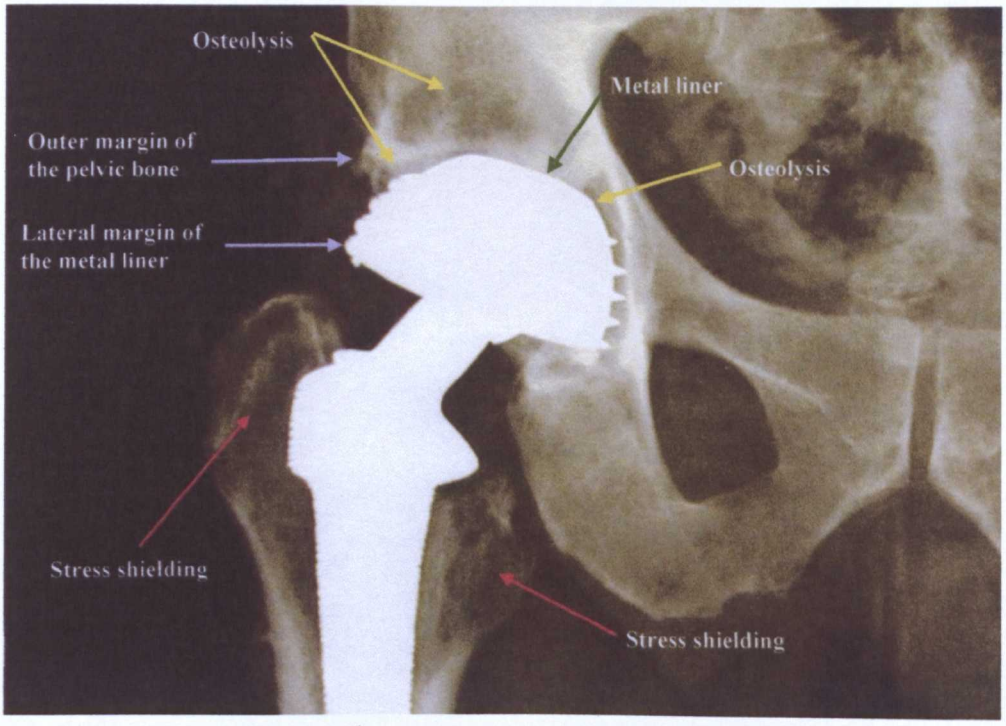

Figure 5-40 Pre-operative radiograph of a loose acetabular component (component 2)

Stress shielding or bone resorption is a common phenomenon that occurs in areas that are relatively unstressed. This is because loading forces are transmitted through the stiff femoral stem rather than the bone of the femur resulting in remodelling and resorption of the femur. The radiographic features evident in Figure 5-40 have been reported previously and a collection of notable radiographic features was reported by Ostlere et al [214].

Stress shielding is also evident in Figure 5-41 where significant resorption of the calcar has occurred medially to the femoral stem. Osteolysis is also evident at the interface of the lateral side of the femoral stem in the form of a wide lucency. Wide areas of lucency can be seen at the PMMA cement interface of the acetabular component as a result of osteolysis. The acetabular component was loose when it was retrieved.

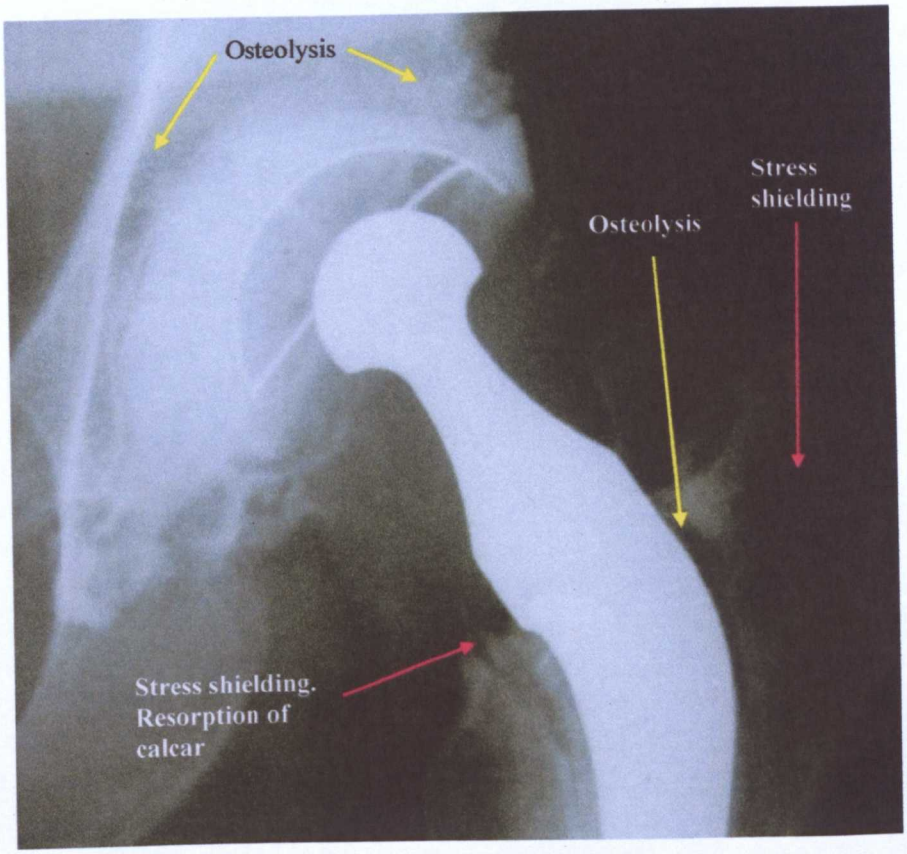

Figure 5-41 Pre-operative radiograph showing severe stress shielding and subsidence of femoral component (component 17)

Wear of the UHMWPE component is depicted in Figure 5-42 (component 29) where the liner thickness (indicated by line A) in the worn region is thinner than in the partially worn region (indicated by line B).

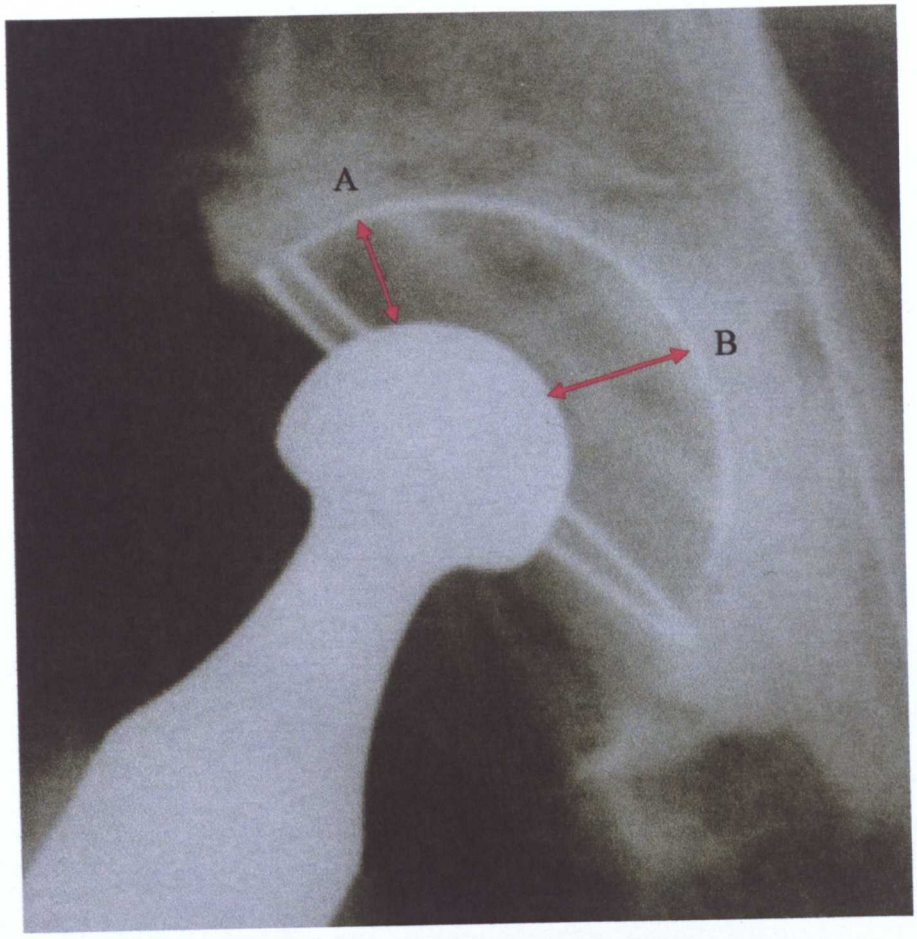

Figure 5-42 Radiograph showing wear of the UHMWPE component (component 29)

Figure 5-43 is the pre-revision radiograph of component 12 and displays Grade II heterotopic ossification. Heterotopic ossification occurs when primitive mesenchymal cells in the surrounding soft tissues are transformed into osteoblastic cells that form mature lamellar bone. It typically occurs around the femoral neck and adjacent to the greater trochanter and the majority of patients with low-grade heterotopic ossification are asymptomatic. If it becomes symptomatic, hip stiffness is the most common complaint. Classification of heterotopic ossification is shown in Figure 5-44.

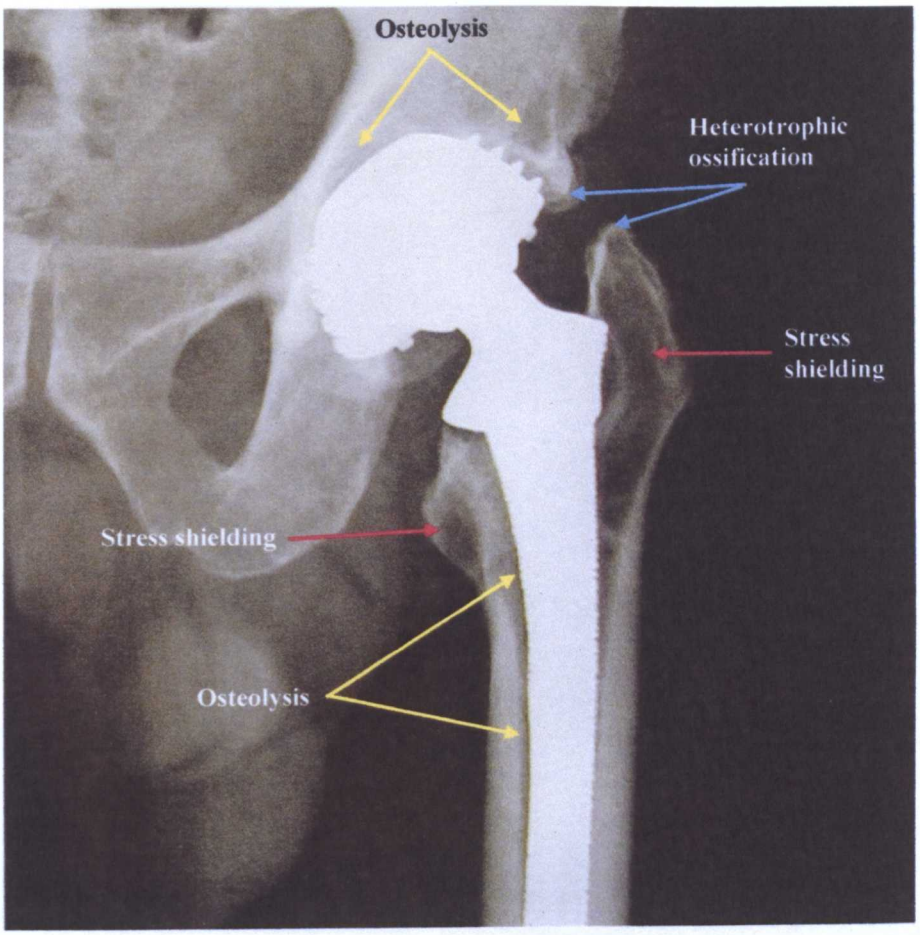

Figure 5-43 Pre-operative radiograph showing heterotrophic ossification (component 12)

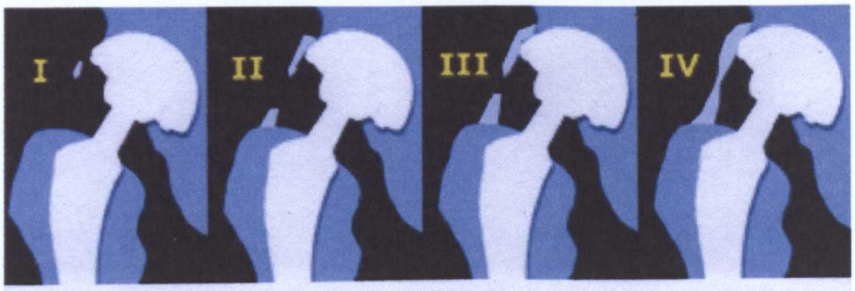

Grade I = Islands of bone within soft tissues.
Grade II = Bone spurs leaving > 1 cm between opposing bone surfaces.
Grade III = Bone spurs leaving < 1 cm between opposing bone surfaces.
Grade IV = Radiographic ankylosis of the hip.

Figure 5-44 Classification of heterotopic ossification

5.5 Instrumented Indentation Testing

The hardness and elastic modulus results from the instrumented indentation testing are presented. Indent arrays were produced that emanated 100μm from the bearing surface and moved perpendicular to this surface into the bulk of the sample. Five 10 μm deep indents were carried out at each distance from the bearing surface to an ultimate distance of 5.1mm resulting in a total number of 130 indents per sample.

5.5.1 Unworn Regions

5.5.1.1 Hardness

Hardness-depth profiles for unworn regions of each of the components are displayed in Figure 5-45.

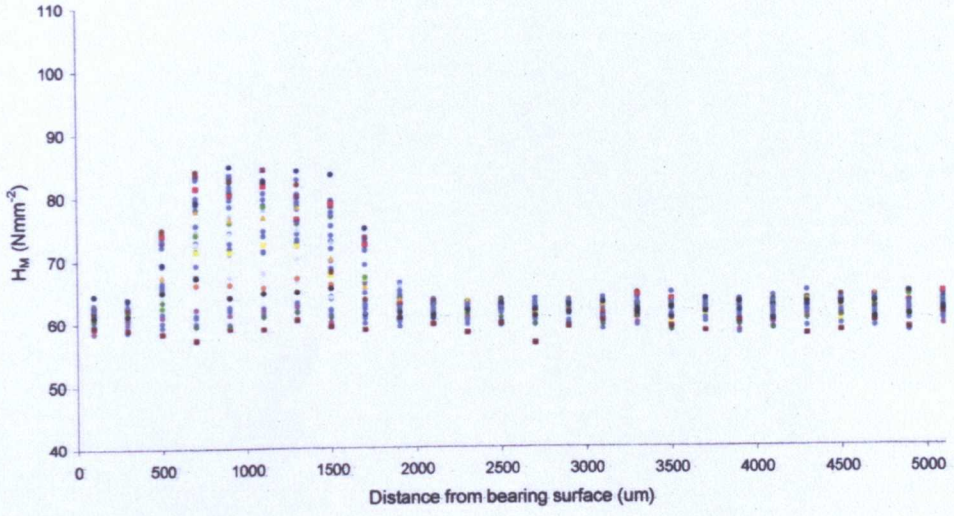

Figure 5-45 H_M depth profiles for unworn regions of all components

Increased values of hardness can be observed between 500μm and 2100μm but there was an apparent variation between components in the amount of hardening that had occurred.

The distribution of F-ratios (see section 3.6.3 for description of ANOVA and F-ratios) for the comparison of unworn regions varied significantly between 500μm and 1700μm whilst remaining within a band of 1.51 to 4.11 at all other distances from the bearing surface (Figure 5-46) distances between 500μm and 1700μm, F-ratios increased sharply to a maximum of 83.07 at 700μm before decreasing back to the standard range at 1900μm. The distribution and magnitude of F-ratios implied that there were significant differences in hardness values at distances of 500μm to 1700μm between components.

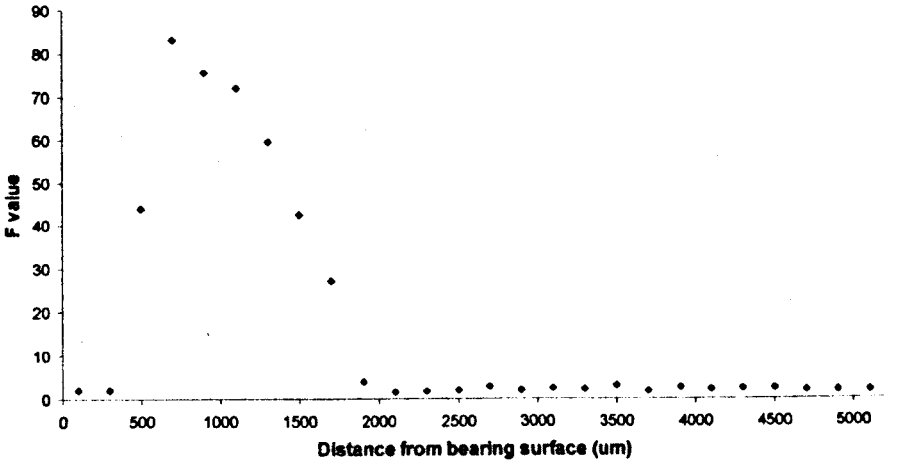

Figure 5-46 F-ratio values unworn H_M data

Figure 5-47 depicts the hardness profiles in unworn regions for the five components that were subsequently analysed using FT-IR imaging. The components represented a range of implantation periods and sub-surface variations in hardness.

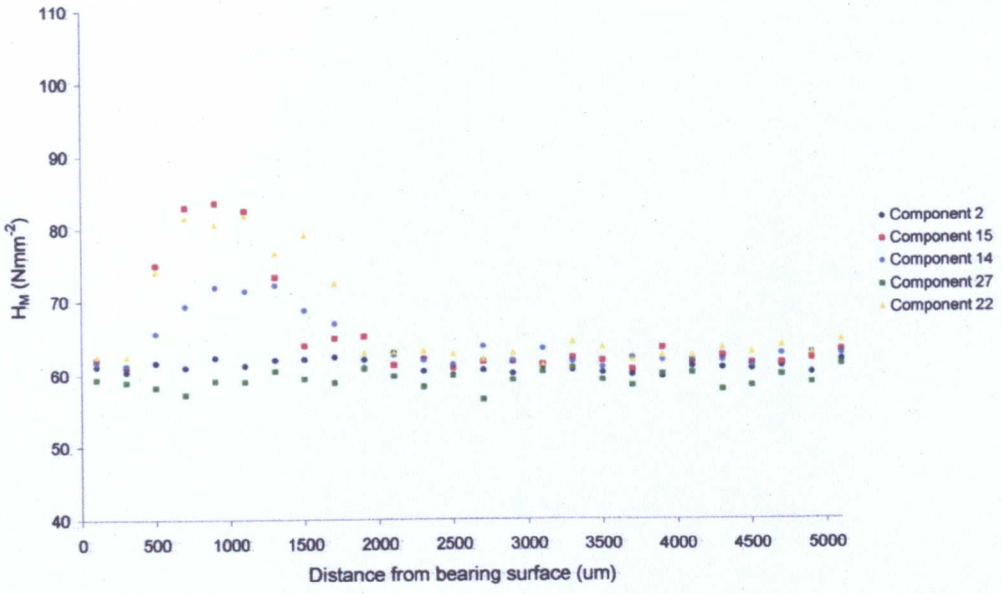

Figure 5-47 H_M depth profiles for the unworn regions of components 2, 14, 15, 22 and 27

The key hardness values for the unworn regions of the live components were:

- Component 2: maximum 62.9Nmm^{-2} (2100μm), bulk 60.3±0.6Nmm^{-2}
- Component 14: maximum 72.2Nmm^{-2} (1300μm), bulk 61.9±0.7Nmm^{-2}
- Component 15: maximum 83.50Nmm^{-2} (900μm), bulk 61.7±0.8Nmm^{-2}
- Component 22: maximum 81.78Nmm^{-2} (1100μm), bulk 62.7±0.8Nmm^{-2}
- Component 27: maximum 60.70Nmm^{-2} (1900μm), bulk 59.4±1.1Nmm^{-2}

5.5.1.2 Elastic Modulus

Elastic modulus data followed a similar pattern as the hardness data. Figure 5-48 graphically depicts the elastic modulus profiles for the unworn regions of all components.

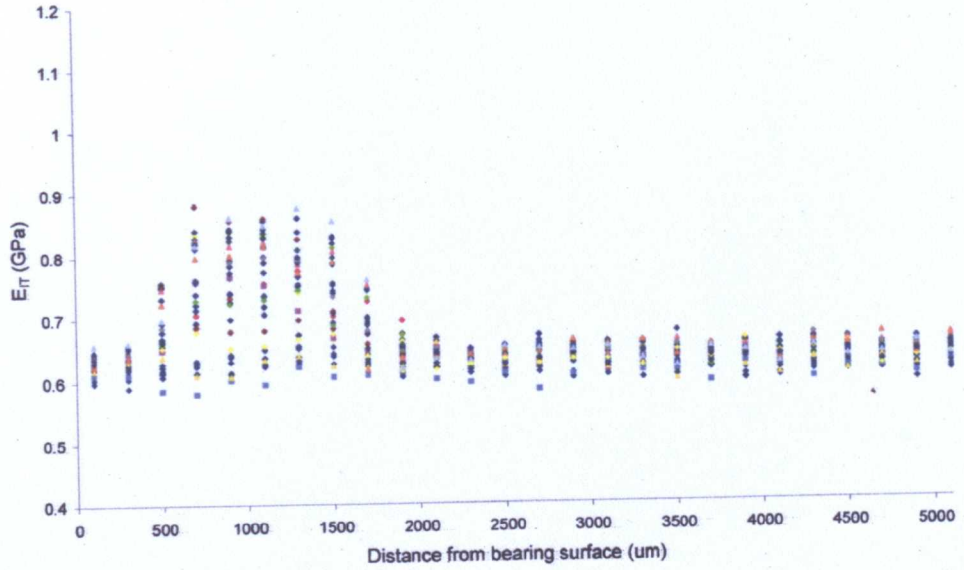

Figure 5-48 E_{IT} depth profiles for unworn regions of all components

There were significant ($p<0.01$) differences in E_{IT} profiles between components at depths ranging from 500μm to 1700μm. All F-ratio values were in excess of 18 with the highest value of 1047.21 recorded at 900μm.

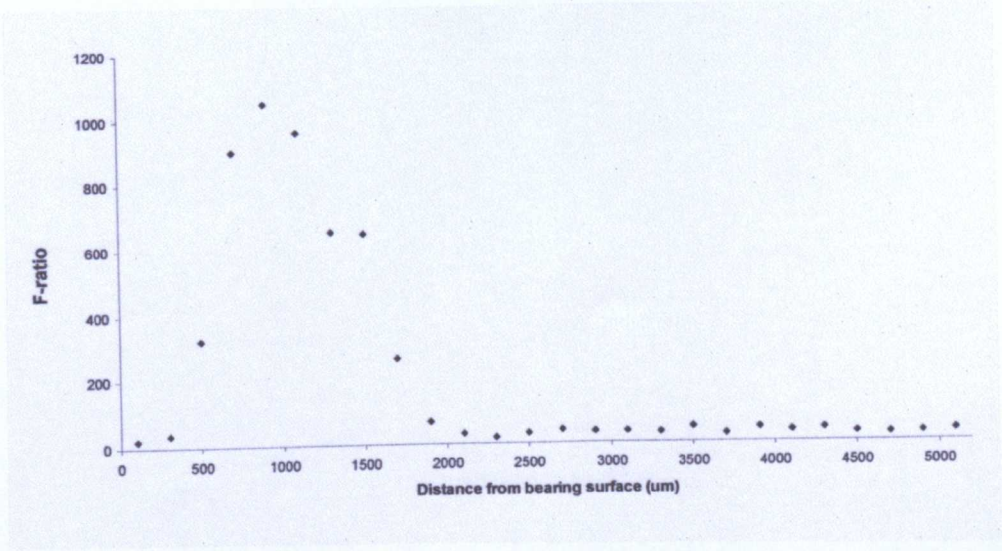

Figure 5-49 F-ratio values – unworn E_{IT} data

Figure 5-50 depicts the elastic modulus profiles for unworn regions for the five

components that were subsequently analysed using FT-IR imaging.

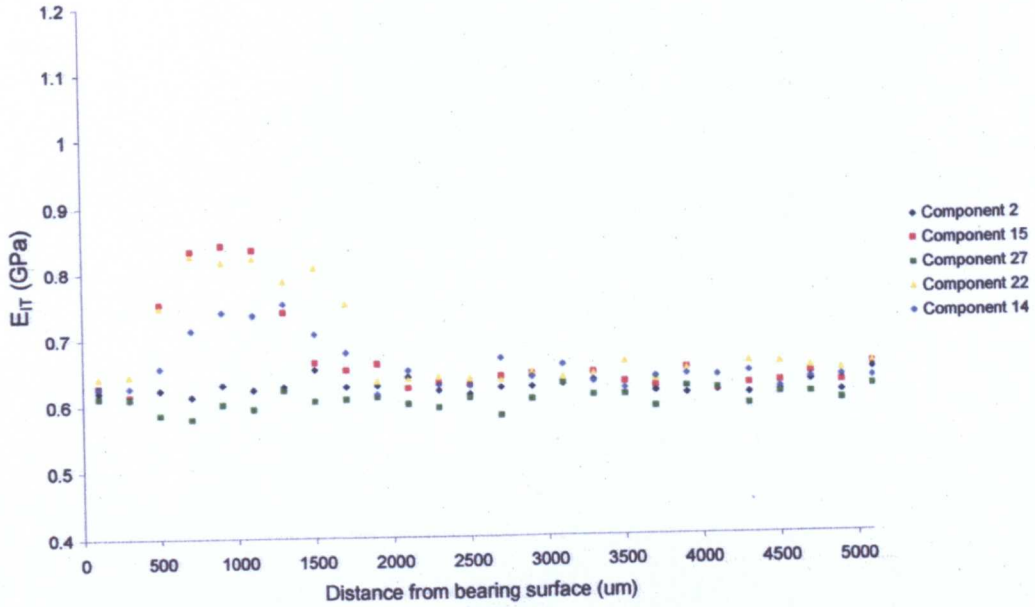

Figure 5-50 E_{IT} depth profiles for the unworn regions of components 2, 14, 22 and 27

The key elastic modulus values for the unworn regions of the five components were:

- Component 2: maximum 0.65GPa (1500μm), bulk 0.60±0.01GPa
- Component 14: maximum 0.75GPa (1300μm), bulk 0.62±0.02GPa
- Component 15: maximum 0.84GPa (900μm), bulk 0.61±0.01GPa
- Component 22: maximum 0.82GPa (900μm), bulk 0.63±0.01GPa
- Component 27: maximum 0.63GPa (3900μm), bulk 0.59±0.02GPa

5.5.2 Worn Regions

5.5.2.1 Hardness

Unlike the distribution of data for unworn regions, H_M and E_{IT} profiles were very similar for the worn regions. All worn regions displayed a reduction in H_M values from the surface to a depth of 100μm, reduced values were also noted at a depth of 300μm in certain samples. No significant variations in H_M values were seen in any of the worn regions (Figure 5-51).

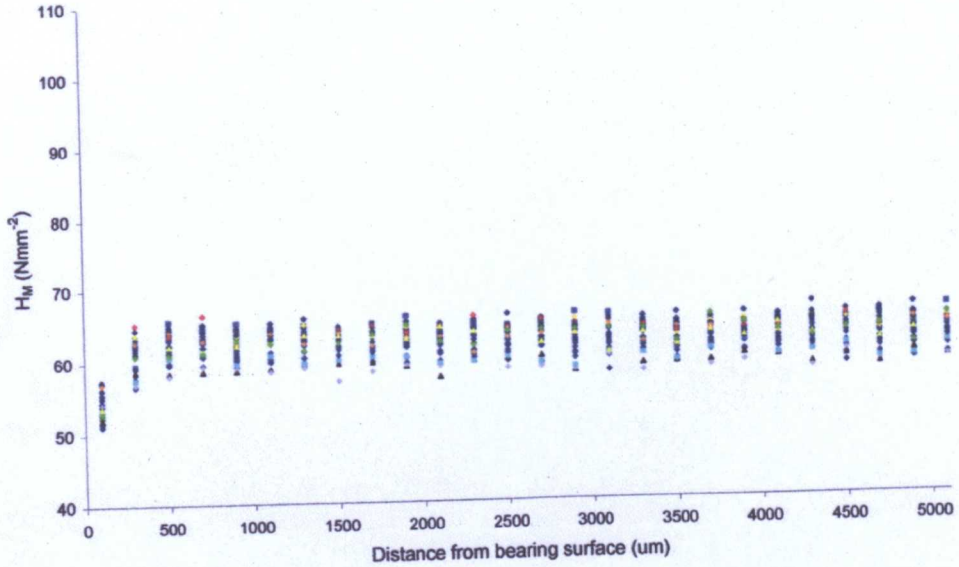

Figure 5-51 H_M depth profiles for worn regions of all components

F-ratio values confirmed that there were statistical differences between the bulk hardness values of components (Figure 5-52) F-ratio values ranged from 3.12 to 5.38 except at 100μm where the value was 9.51 indicating a variation in hardness values between components.

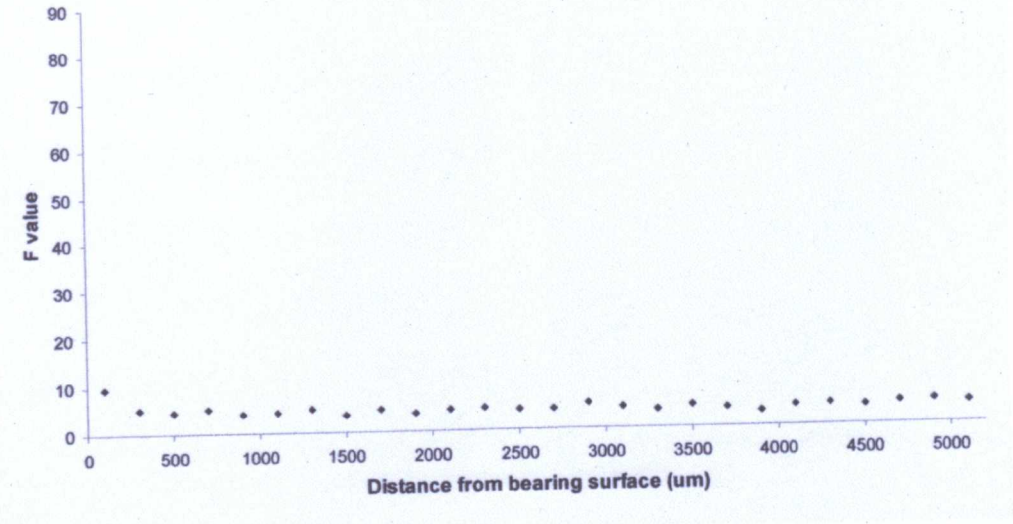

Figure 5-52 F-ratio values - worn H_M data

Using components 2, 14, 15, 22 and 27 again as examples, it can be seen from Figure 5-53 that the H_M depth profiles show reduced hardness values 100μm from the bearing surface. At depths >300um, no variation in individual hardness profiles was seen. There was however, a difference in the bulk hardness values of different components.

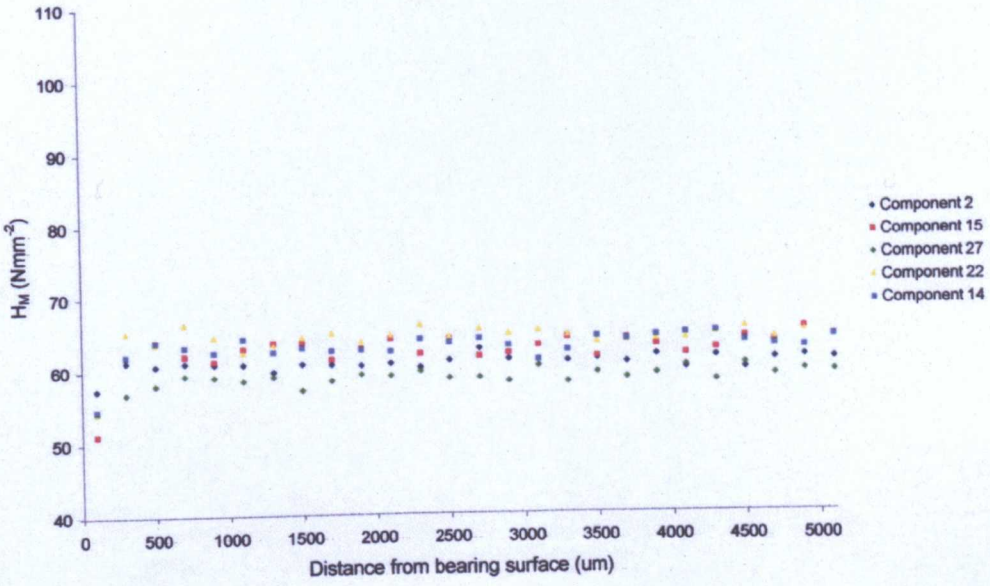

Figure 5-53 H_M depth profiles for the unworn regions of components 2, 14, 15, 22 and 27

The key hardness values for the worn regions of the five components were:

- Component 2: minimum 57.4Nmm^{-2}, bulk 60.6±0.5Nmm^{-2}
- Component 14: minimum 54.5Nmm^{-2}, bulk 63.1±0.7Nmm^{-2}
- Component 15: minimum 51.1Nmm^{-2}, bulk 62.8±0.8Nmm^{-2}
- Component 22: minimum 54.3Nmm^{-2}, bulk 64.3±0.4Nmm^{-2}
- Component 27: minimum 54.2Nmm^{-2}, bulk 58.7±0.6Nmm^{-2}

5.5.2.2 Elastic Modulus

Elastic modulus data followed a similar pattern as the hardness data. Figure 5-54 graphically depicts the elastic modulus profiles for the worn regions of all components.

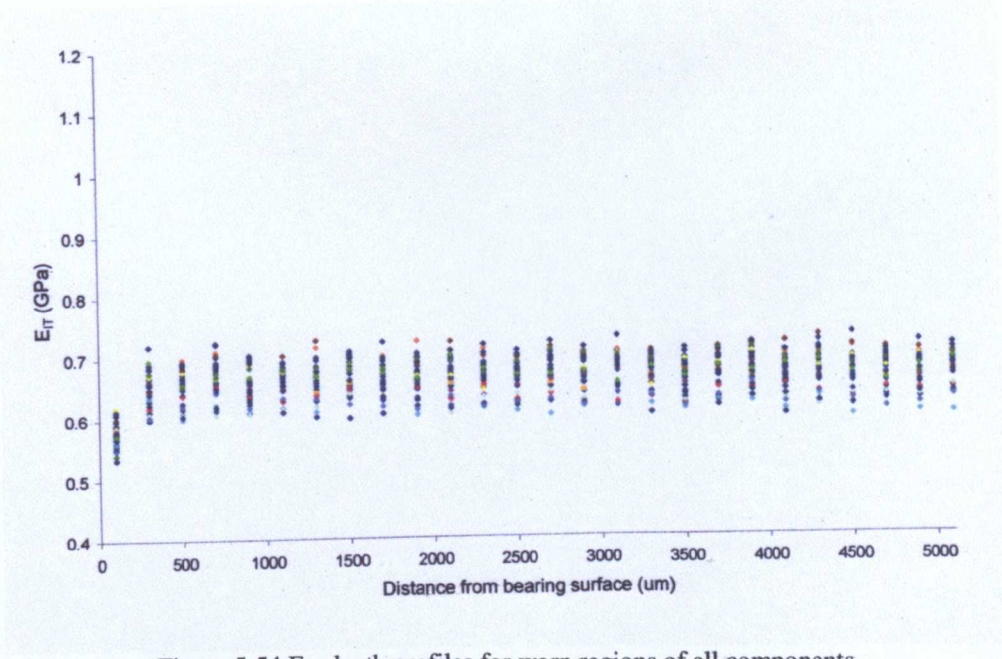

Figure 5-54 E_{IT} depth profiles for worn regions of all components

E_{IT} depth profiles for all components displayed reduced values at 100μm and minimal variation in values at distances ≥500μm.

The F-ratio values shown in Figure 5-55 were in the range 37.7 to 80.7 and support the conclusion that the minor variations in E_{IT} profiles were governed by differences in sampling error rather than variations in properties between different components.

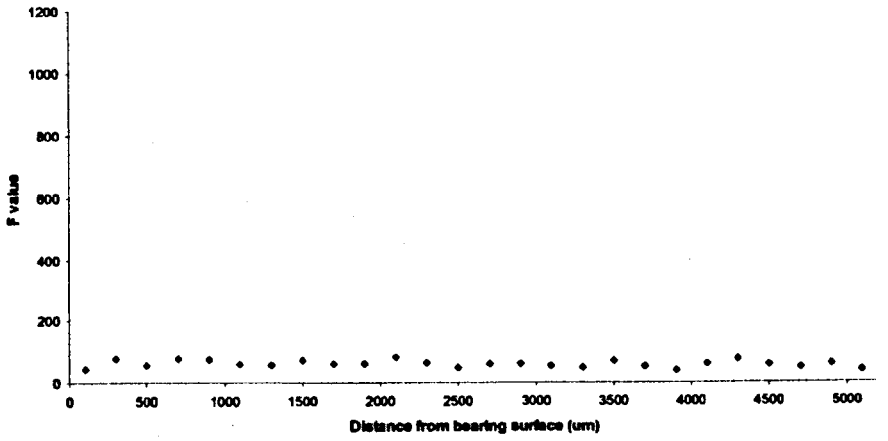

Figure 5-55 F-ratio values – worn E_{IT} data

5.5.3 Worn Regions (Adjusted for Linear Wear)

5.5.3.1 Hardness

The adjustment of hardness profiles for worn regions to account for linear wear meant that it was only at depths ≥4000μm that all of the components contributed data to the statistical analysis. There was insufficient data to carry out a comparison at 100μm because there were fewer than two variables. Figure 5-56 depicts the hardness depth profiles for all components when linear wear was accounted for. It is clear from the graph that depth data was no longer correlated between groups.

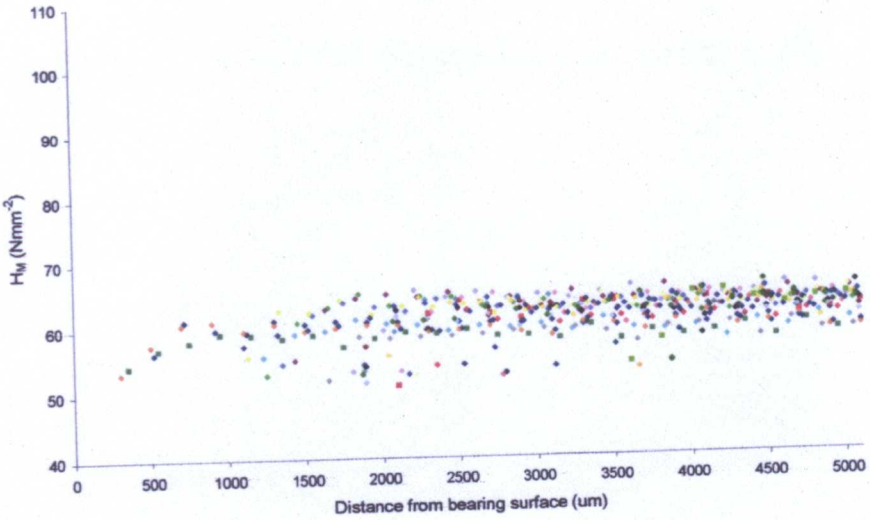

Figure 5-56 H_M depth profiles with linear wear taken into account for worn regions of all components

The F-ratio values for the worn (adjusted depth) comparison are shown in Figure 5-57. The test values serve to highlight the fact that when the linear wear of cups is taken into account, there were significant differences between the depth profiles of different components. This indicates that at the worn surface there was a great deal of scatter in the results with values ranging from 1.58 at 300μm to 24.94 at 1900μm.

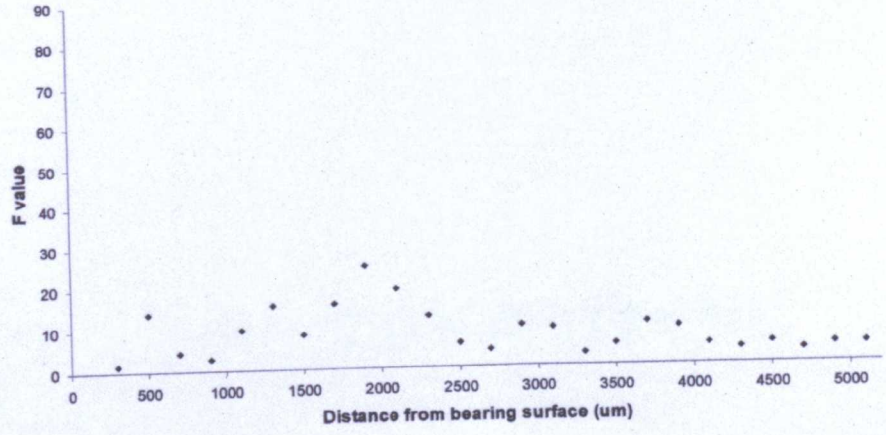

Figure 5-57 F-ratio values worn (adjusted depth) data.

The variation in hardness (with linear wear accounted for) in worn regions of the five components investigated using FT-IR imaging is depicted in Figure 5-58.

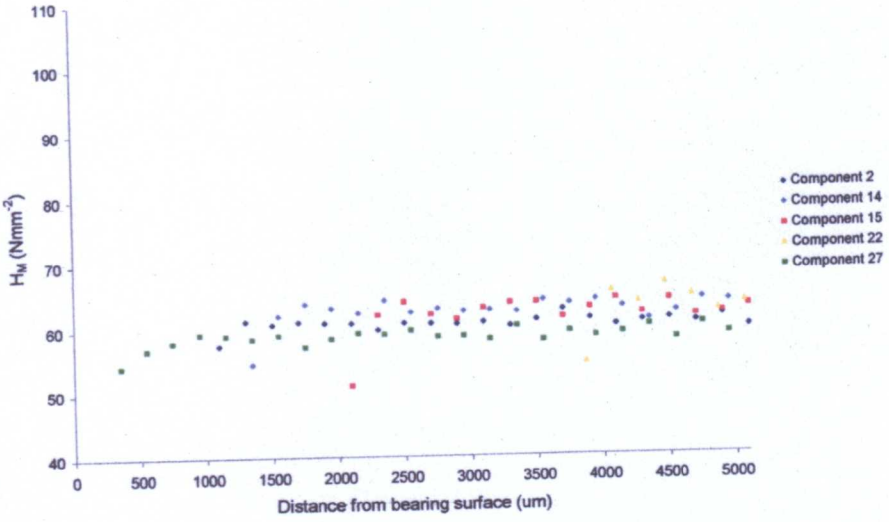

Figure 5-58 H_M depth profiles (with linear wear accounted for) for the unworn regions of components 2, 14, 15, 22 and 27

5.5.3.2 Indentation Modulus

The scatter in the elastic modulus data followed the pattern of hardness data once linear wear had been accounted for (Figure 5-59)

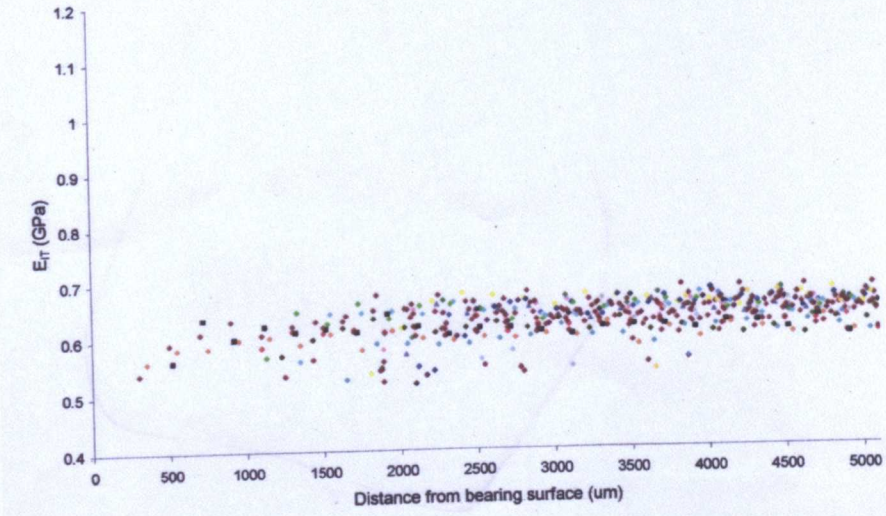

Figure 5-59 E_{IT} depth profiles with linear wear taken into account for worn regions of all components

As was the case with the hardness data for the comparison of worn (adjusted) data, there was insufficient data to carry out a comparison at 100μm as there were fewer than two variables. The plot of F-ratio values (Figure 5-60) served to reinforce the fact that variations between groups were the primary source of variation in E_{IT} values.

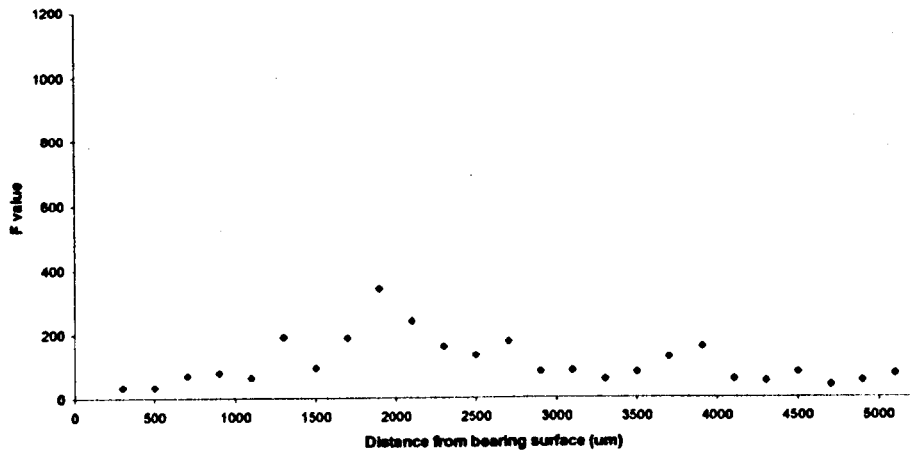

Figure 5-60 F-ratio values worn (adjusted depth) E_{IT} data

Figure 5-61 displays the elastic modulus profiles for the five components. It is clear that there is no correlation between the reduced surface modulus values.

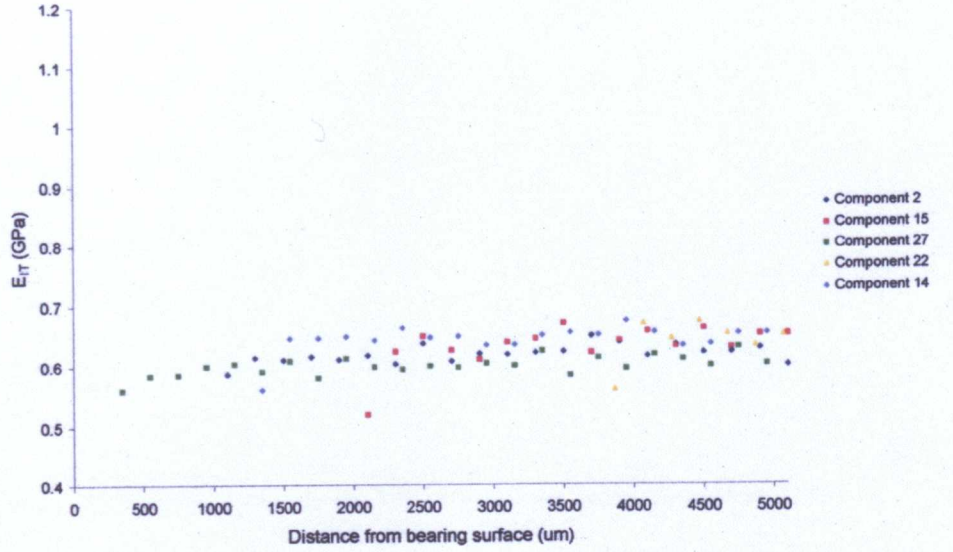

Figure 5-61 E_{IT} depth profiles (with linear wear accounted for) for the unworn regions of components 2, 14, 15, 22 and 27

5.5.4 Variations Between Unworn and Worn Regions of Individual Components

An analysis of variations in hardness and elastic modulus between worn and unworn regions of the same component was carried out. The aim of this being to investigate whether the structure of UHMWPE in different regions of the same acetabular component varied. The statistical analysis of data from worn and unworn regions of the same component was carried out using t-tests (see section 3.6.1). The results from the individual t-tests for the 32 components were combined in one graph for hardness and one for elastic modulus. Graphs of t-ratio values are used to illustrate whether hardness and elastic modulus values were higher in worn or unworn regions. The dashed line on graphs indicates a t-ratio of zero indicating that there was no difference between the two regions.

Any positive values that are above the dashed line (green zone) indicate higher values

for unworn regions than worn regions (pink zone) and vice versa.

5.5.4.1 Hardness

Individual t-tests were carried out on the hardness data from worn and unworn regions of individual cups. The combined H_M t-test data components are depicted in Figure 5-62. The graph shows significant t-test results ($p \leq 0.05$). Each symbol on the graph represents a different sample.

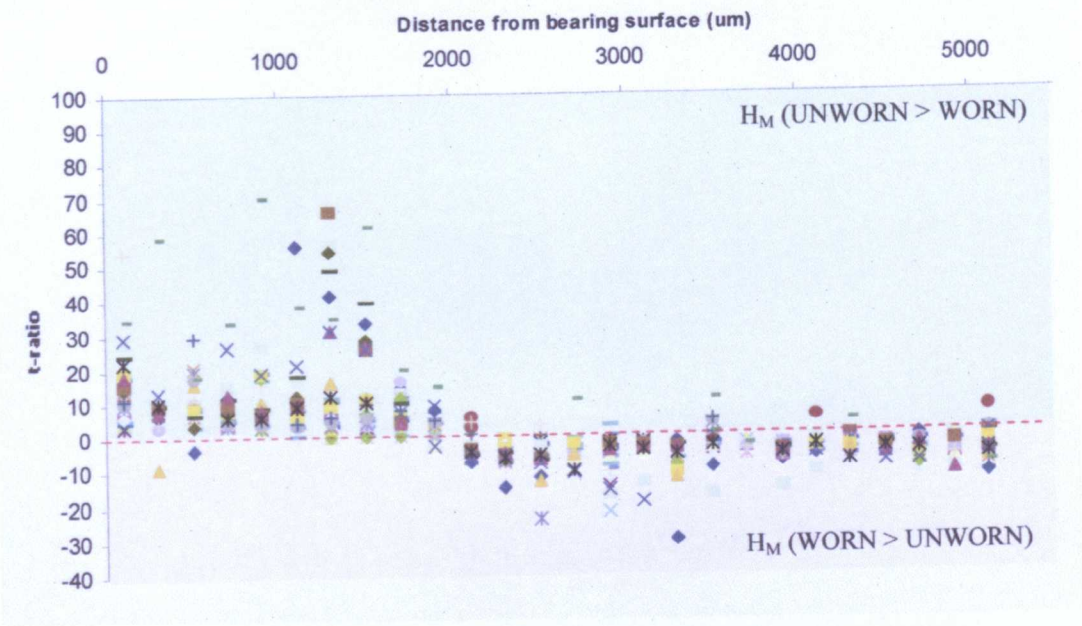

Figure 5-62 Dependent t-test results for intra-sample variation in H_M between worn and unworn regions

Results from the t-test indicate that from 100μm to 2100μm. H_M values for unworn regions were higher than those in worn regions with the largest differences being between 700μm and 1100μm. From 2100μm onwards, t-ratio values indicated that H_M data for unworn regions were lower than worn regions.

5.5.4.2 Elastic Modulus

Figure 5-63 displays the E_{IT} t-ratio values for the comparison of unworn and worn regions of components. The trend in data is similar to the H_M t-ratio data presented in Figure 5-62.

From 100μm to 1700μm, t-ratio values for unworn regions were higher than those in worn regions. Between 1900μm and 2100μm, t-ratio values changed from being controlled by E_{IT} values in unworn regions to those in worn regions. There was little variation in the data ≥2300μm.

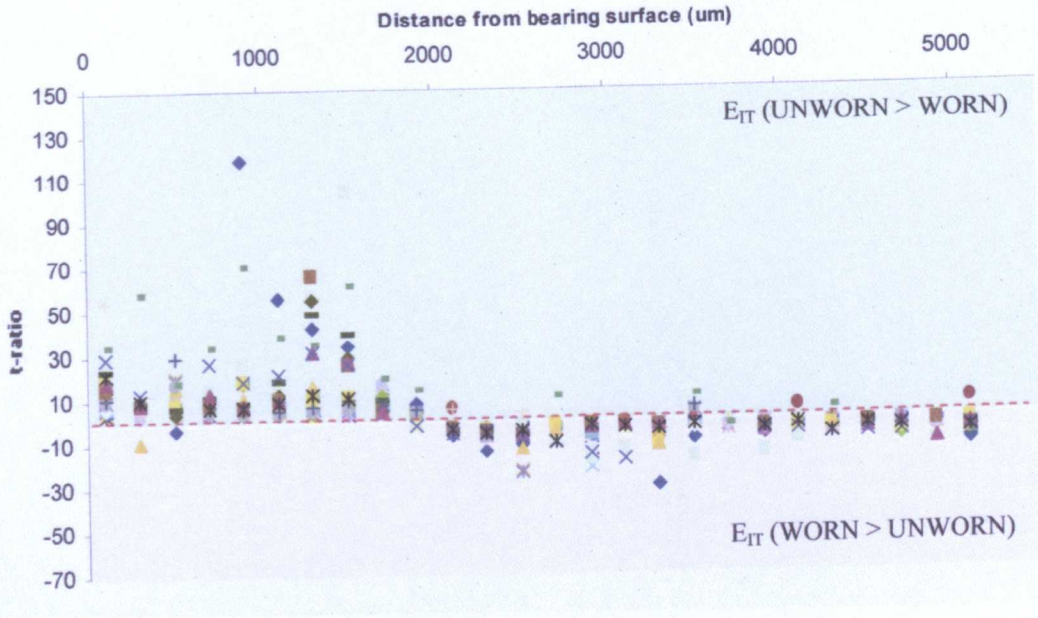

Figure 5-63 Dependent t-test results for intra-sample variation E_{IT} between worn and unworn regions

5.5.5 Unworn and Worn Regions (linear wear accounted for)

5.5.5.1 Hardness

The t-test results for the comparison of unworn and worn (adjusted depths) regions are presented in Figure 5-64. There were only significant t-ratio values from 1100μm onwards because there was insufficient worn data at adjusted near surface depths. At distances ≥2100μm t-ratio values showed little bias towards either worn or unworn region. Between 1100μm and 1900μm however, increased positive t-ratio values were noted. The increased values indicated that hardness values in unworn regions of certain components were significantly higher than corresponding worn regions.

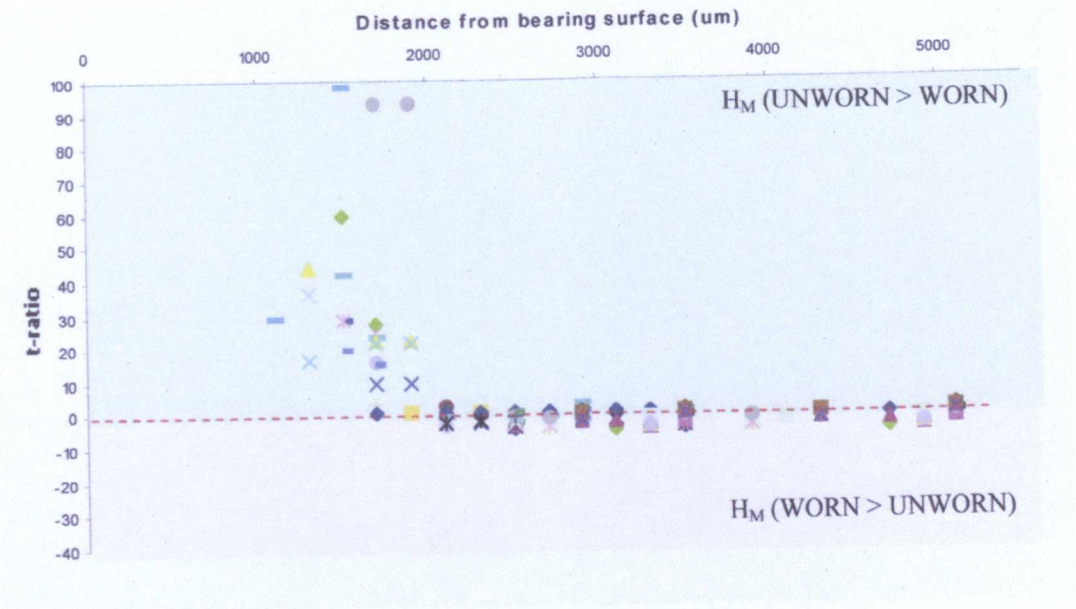

Figure 5-64 Dependent t-test results for intra-sample variation in H_M between worn and unworn regions

5.5.5.2 Elastic Modulus

The elastic modulus t-ratio data for the comparison of unworn and worn regions (adjusted depth) is shown in Figure 5-65.

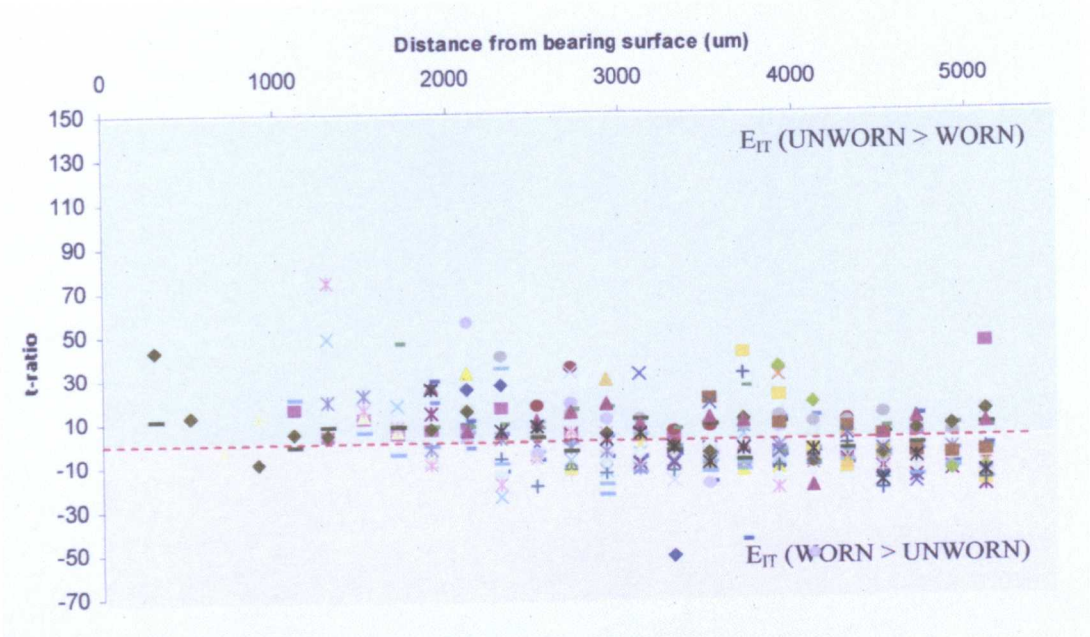

Figure 5-65 Dependent t-test results for intra-sample variation E_{IT} between worn and unworn regions

There was limited t-ratio data ≤1100μm. A decreasing trend in values was noted between 1300μm and 3300μm with the figures at 1300μm being dominated by E_{IT} values in unworn regions whilst values at 3300μm were controlled by values from worn regions. There was an increase in values between 3300μm and 3700μm before decreasing again up to 4100μm. Values then remained within a narrow range up to 5100μm.

5.5.6 Correlation Between Hardness and Implantation Time

Figure 5-66 displays the correlation between the maximum hardness values in unworn and worn regions and time in-vivo. These values were plotted as a function of time in order to investigate the influence of time-dependant oxidation on the hardness of UHWMPE. There was no correlation between H_M values at worn surfaces and implantation time whilst increased H_M values in unworn regions were clearly related to implantation time. This indicates that the variations in hardness values in unworn regions was related to implantation time and in all probability were due to post-irradiation oxidation. In contrast no significant increase in hardness was noted for worn regions and probably due to the consistent removal of UHWMPE from the surface at a rate greater than or equal to the rate of oxidative degradation of the material.

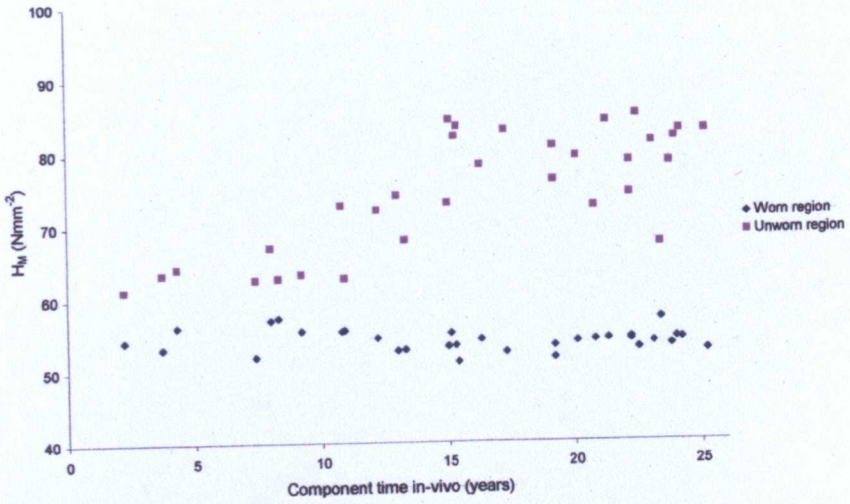

Figure 5-66 Graph of maximum H_M values for worn and unworn regions as a function of component time in-vivo.

The rate of change in hardness values for unworn regions was calculated by subtracting the bulk hardness values from the maximum values of the same components and then dividing by the component implantation time. A rate of

$0.8\pm0.3 Nmm^{-2}$ per year was found. This value is only indicative as the influence of pre-implantation ageing was unknown and the rate of oxidation in different regions of material was inhomogeneous.

The same relationship between implantation time and maximum elastic modulus in unworn and worn regions was observed (Figure 5-67). A rate of change of elastic modulus was calculated in the same manner as the hardness value. It was found to be 0.010±0.004GPa per year.

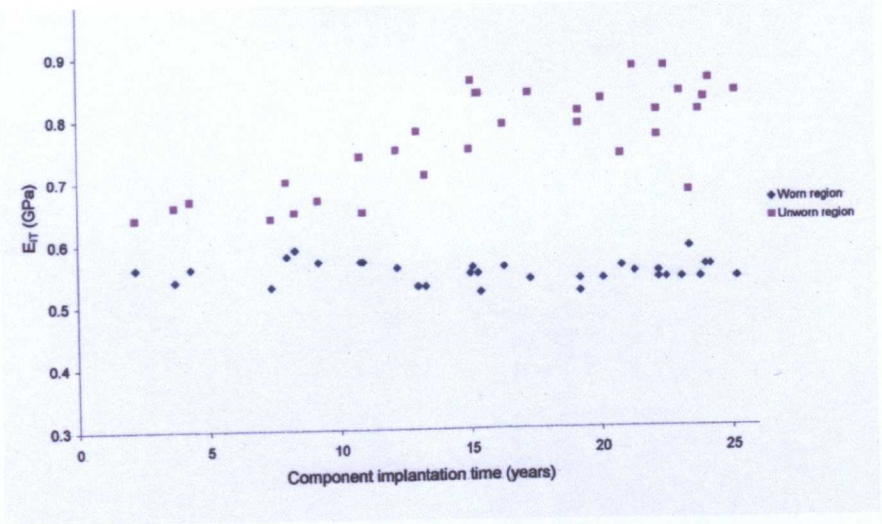

Figure 5-67 Graph of maximum E_{IT} values in unworn and worn regions

Despite the lack of variation in bulk hardness values for individual components, minor variations were observed between components. The relationship between bulk hardness values in worn and unworn regions and implantation time is shown in Figure 5-68.

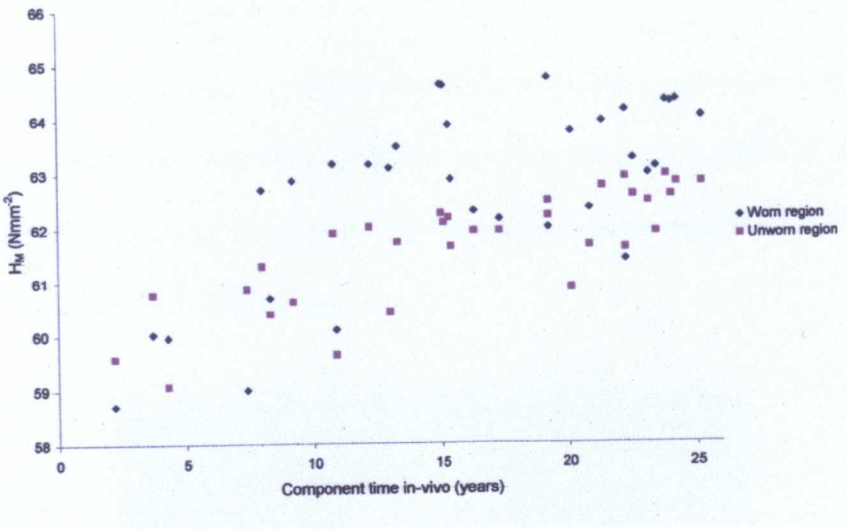

Figure 5-68 Graph of mean bulk H_M values for worn and unworn regions as a function of implantation time

Unsurprisingly, there was also a correlation between bulk E_{IT} values and component implantation time.

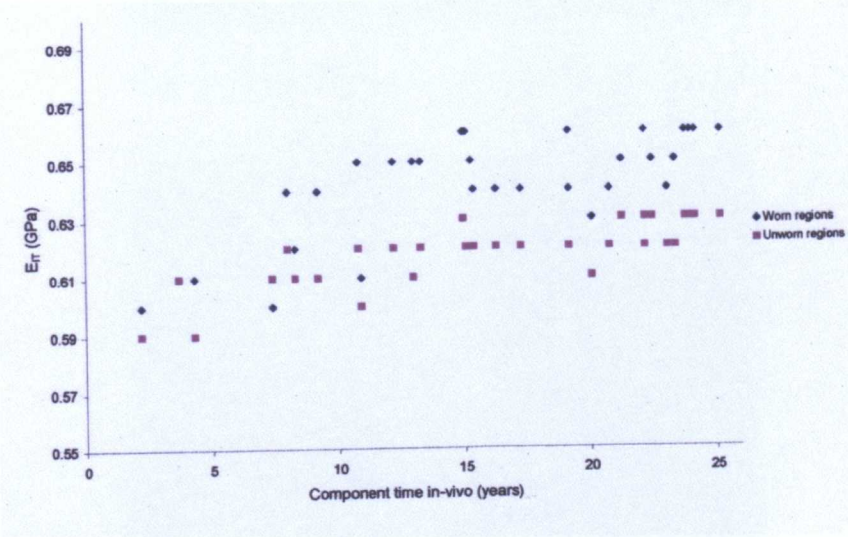

Figure 5-69 Graph of mean bulk E_{IT} values in worn and unworn regions

It is possible that some of the variation in H_M and E_{IT} values could be attributed to variations in the properties of the UHMWPE used to fabricate the components.

5.5.7 Microscopy of Indents

Figure 5-70 is a 10μm deep indent in the oxidized subsurface region of component 14. The margins of the indent are clearly visible and there was no evidence of piling up or sinking in at the edges of the indent. An indent produced in the surface of virgin GUR1020 is shown as a comparison.

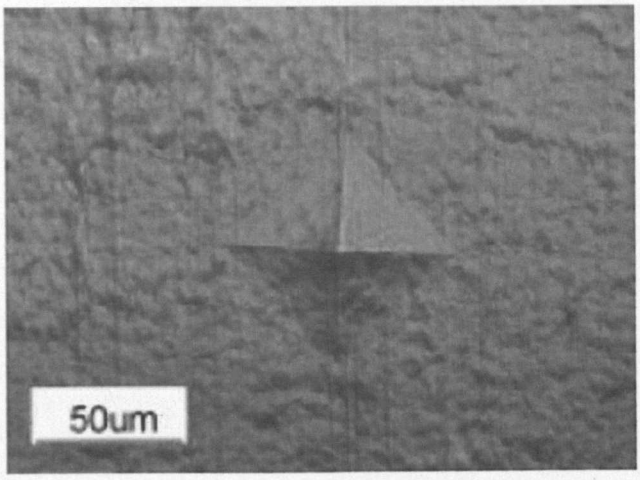

Figure 5-70 10μm indent from sub-surface oxidized region

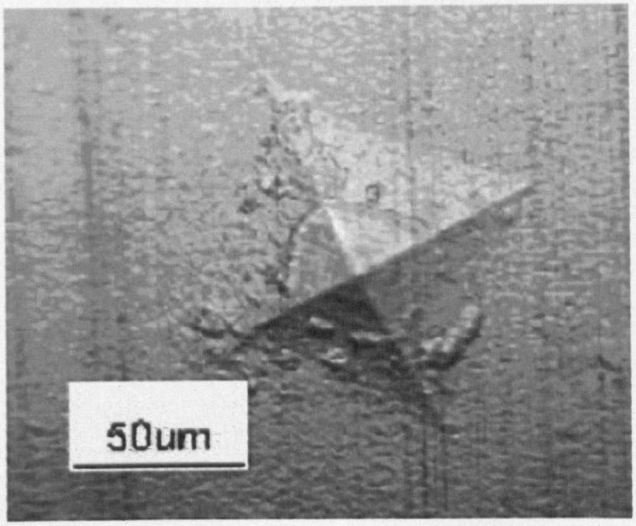

Figure 5-71 10μm indent in the surface of virgin GUR1020

The machining marks can be seen on the micrographs and the influence of surface preparation technique was assessed during preliminary testing. For microtomed

surfaces prepared using a newly sharpened blade, the surface preparation technique did not significantly influence the hardness test if 10μm deep indents were used.

Figure 5-72 shows the worn region of component 2 and an array of indents that were produced to assess the hardness and elastic modulus of the UHMWPE. The indents are precisely positioned from the surface of the sample.

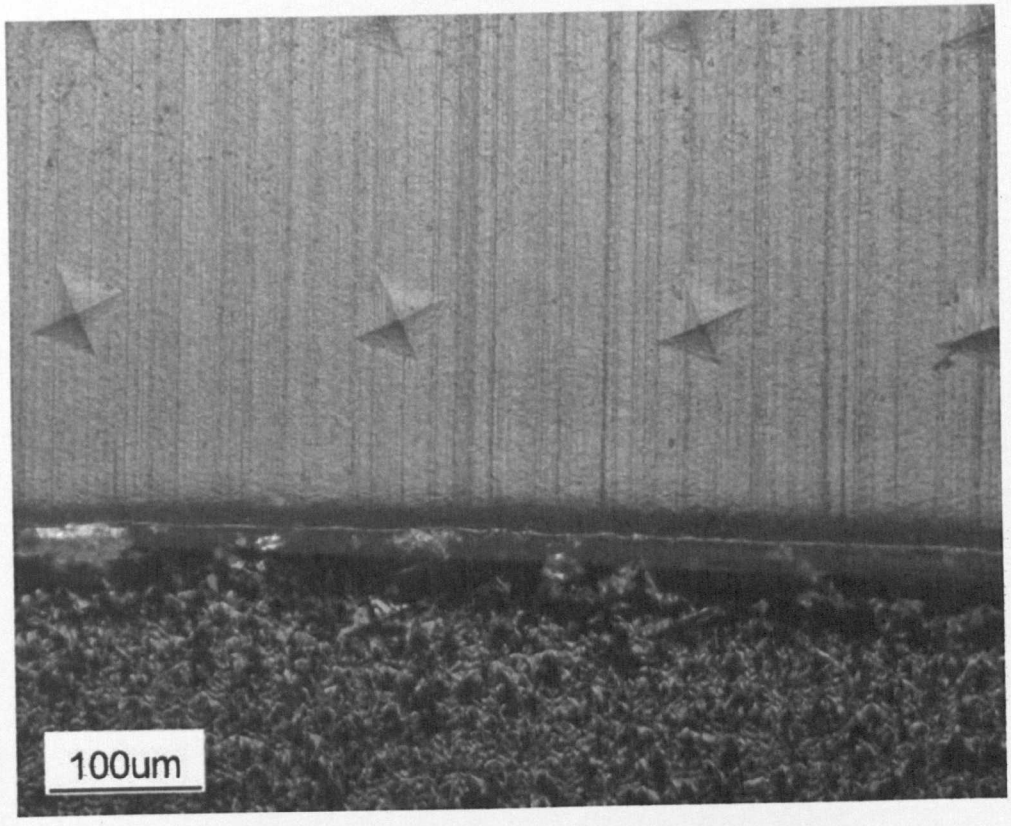

Figure 5-72 Indents at bearing surface of retrieved component sample

5.6 FT-TR Imaging Results

FT-IR imaging was carried out on five components (14, 15, 22 and 22) that had been implanted for varying amounts of time. Sections of worn and unworn regions of each component were analyzed using the technique in order to evaluate the depth profiles of oxidation crystallinity and also to determine whether there had been fluid ingress into the material. Typically, the results of each test consisted of >1500 different spectra recorded at 25μm intervals. The data was exported into MS Excel in order to plot the data for oxidation, crystallinity and fluid ingress as a function of distance from the bearing surface. The data for worn and unworn regions is presented separately.

Figure 5-29 and Figure 5-80 are FTIR spectra taken from the bulk and near surface regions of component 15 and the absorbance bands of interest are shown. Note the absence of 1718cm^{-1} and 1740cm^{-1} absorbance bands in Figure 5-79.

5.6.1 Unworn Regions

5.6.1.1 Crystallinity

The through thickness variations in crystallinity values for the unworn regions of components 2, 14, 15, 22 and 27 are displayed in Figure 5-73.

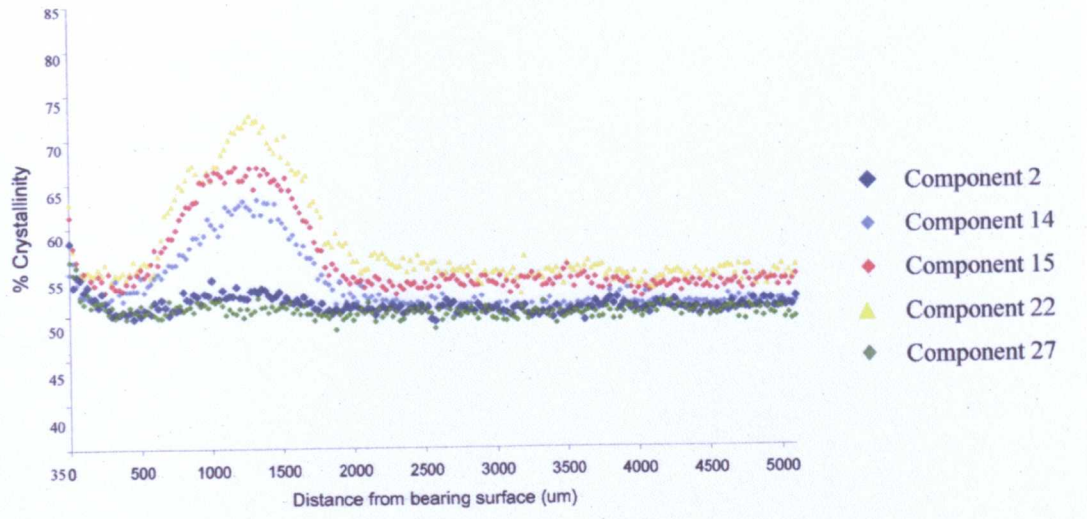

Figure 5-73 Graph showing variation of crystallinity with distance from unworn surfaces of components 2, 14, 15, 22 and 27

An increase in crystallinity values was observed at the bearing surface of unworn regions. The respective crystallinity values for the different components were: 58.7% for component 2, 57.2% for component 14, 62.0% for component 15, 63.9% for component 22 and 56.1% for component 27.

Increased crystallinity values were observed in the sub-surface regions of three components ranging from 500μm to 2000μm. Component 14 had a maximum crystallinity value of 63.6% at a depth of 1275μm, component 15 displayed a peak of 66.2% at a depth of 1175μm and component 22 had a peak of 73.6% at a depth of 1350μm.

There were no significant variations in bulk crystallinity in individual components but there were differences in values between components with components 22 and 15 exhibiting slightly higher crystallinities than the other three components.

5.6.1.2 Oxidation

The oxidation profiles (as a function of the absorption at the 1718cm^{-1} peak) in the unworn regions of different components roughly followed the same pattern as crystallinity (Figure 5-74). An approximate two fold increase in oxidation values was observed at the bearing surface in all components. A distinct subsurface band of oxidation was observed in components 14, 15 and 22 at depths ranging from 300μm to 2000μm. No significant variations in the bulk oxidation values were observed for the components.

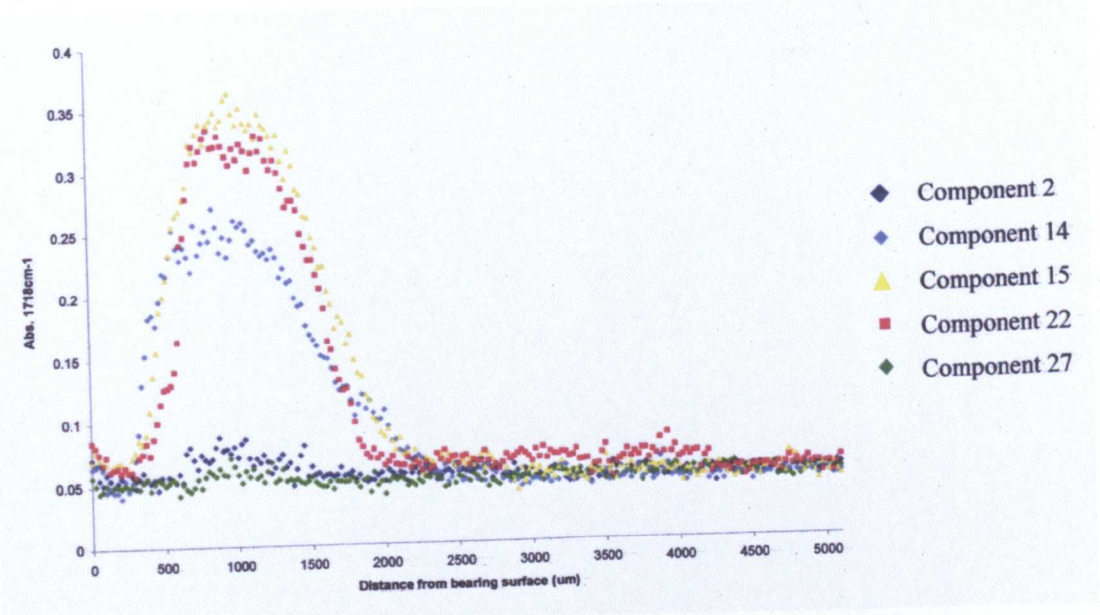

Figure 5-74 Graph showing variation of normalized abs. at 1718cm^{-1} with distance from unworn surfaces of components 2, 14, 15, 22 and 27.

5.6.1.3 Fluid Ingress

Fluid ingress was assessed as a function of the absorption at the 1740cm^{-1} wavelength.

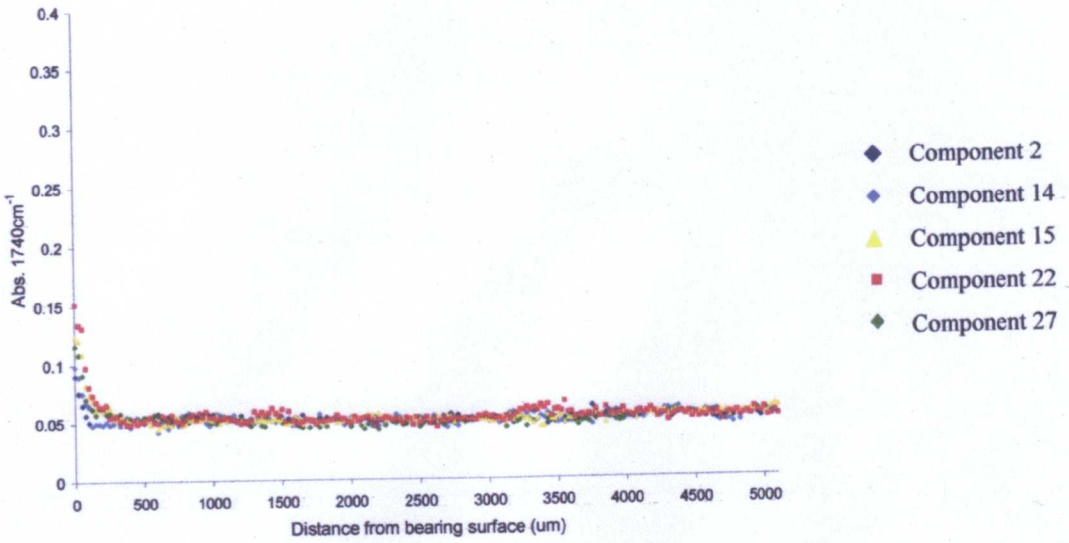

Figure 5-75 Graph showing variation of normalized abs. at 1740cm^{-1} with distance from unworn surfaces of components 2, 15, 22 and 27.

Increased absorbances at 1740cm^{-1} were observed at the surface of unworn bearing surfaces. The level of absorption at this band was directly related to the penetration of synovial fluid constituents into the surface of the material. There was a variation in the penetration of fluid at the surfaces of different components. Fluid penetrated to a depth of 400μm in component 22 whilst the depth of penetration in component 2 was 100μm. There were no increased absorbances in the bulk of any of the components.

5.6.2 Worn regions

5.6.2.1 Crystallinity

Increased crystallinity values were observed at the surface of worn regions in all components. Component 2 exhibited the largest increase in surface crystallinity when compared to the bulk value (62.3% at the surface and 52.3±1.7% in the bulk).

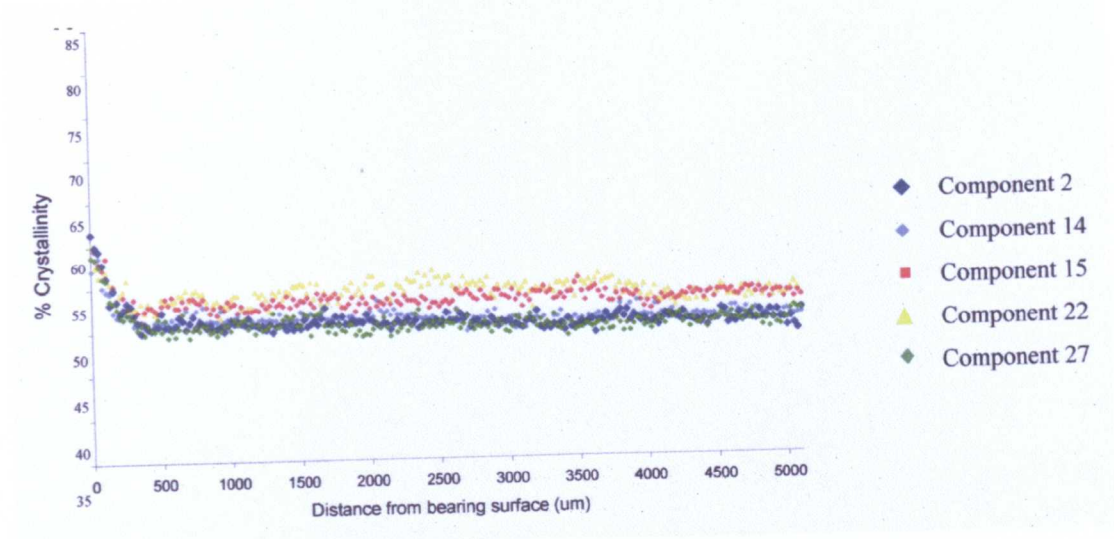

Figure 5-76 Graph showing variation of crystallinity with distance from worn surfaces of components 2, 14, 15, 22 and 27

5.6.2.2 Oxidation

Increased absorbance at 1718cm^{-1} was observed at the surface of all worn components. Component 22 exhibited a threefold increase in oxidation at the worn surface. No variations in oxidation were observed at depths greater than 225μm.

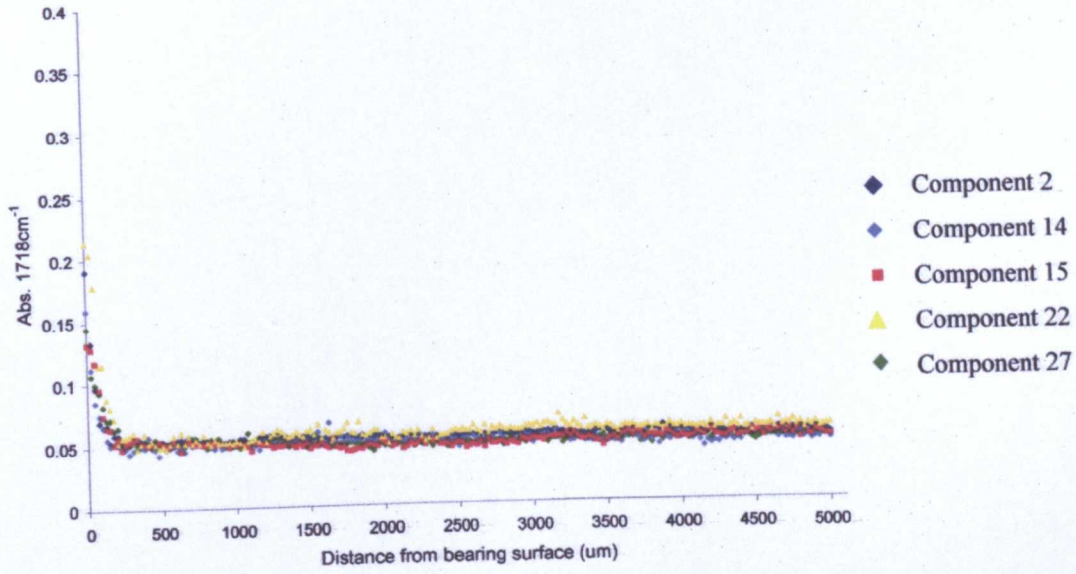

Figure 5-77 Graph showing variation of normalized abs. at 1718cm^{-1} with distance from worn surfaces of components 2, 14, 15, 22 and 27.

5.6.2.3 Fluid ingress

Increased absorbance of the 1740cm^{-1} band indicative of esters in the synovial fluid were noted at the surfaces of worn regions in a similar manner to ingress of fluid at unworn surfaces.

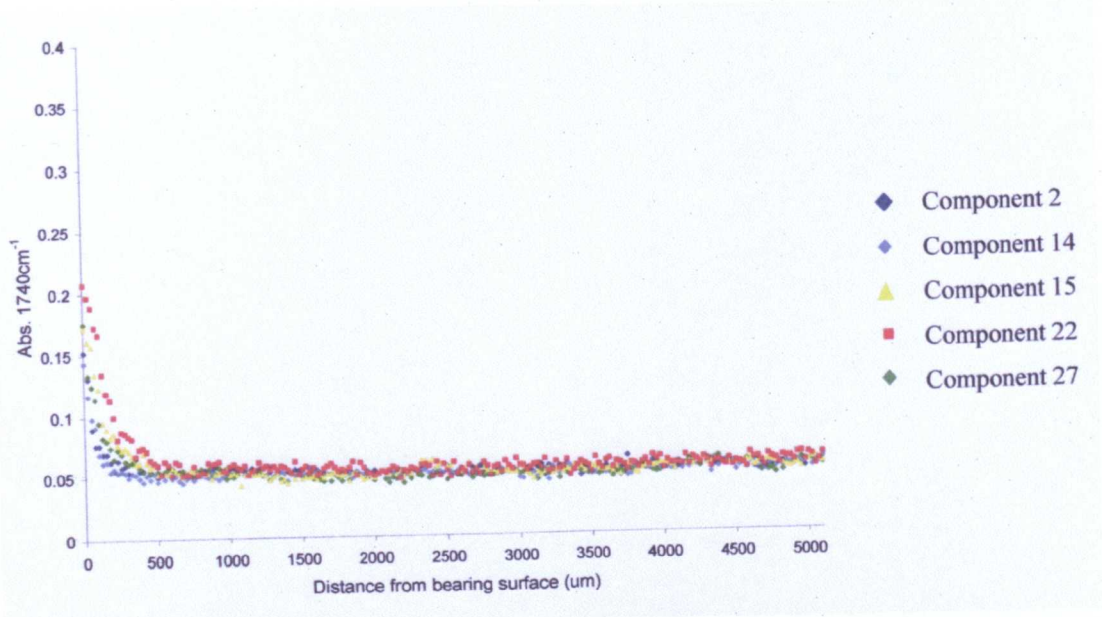

Figure 5-78 Graph showing variation of normalized abs. at 1740cm^{-1} with distance from worn surfaces of components 2, 14, 15, 22 and 27

The magnitude of absorbances at 1740cm^{-1} in worn regions were greater than the values observed in unworn regions with the exception of absorbance values for component 22 where they were 0.1 lower than in unworn regions. The observed reduction in fluid absorption for component 22 is not readily clear but may have been due to removal of surface synovial fluid constituents from the worn surface during the component anti-microbial processing procedure.

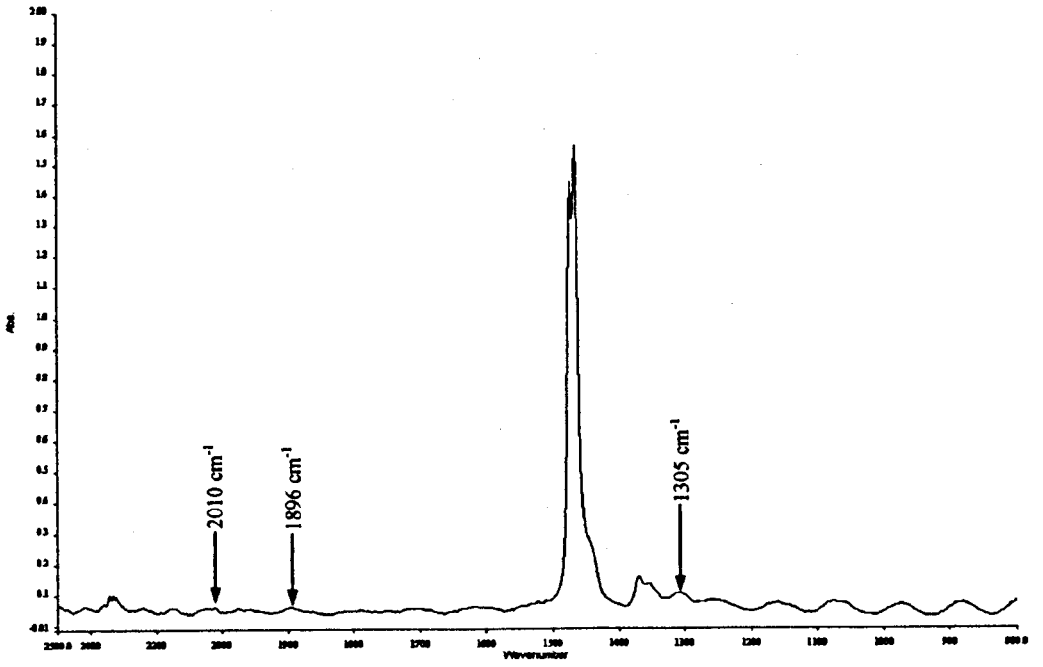

Figure 5-79 FTIR spectra taken in the bulk (d=5000μm) of the unworn region of component 15

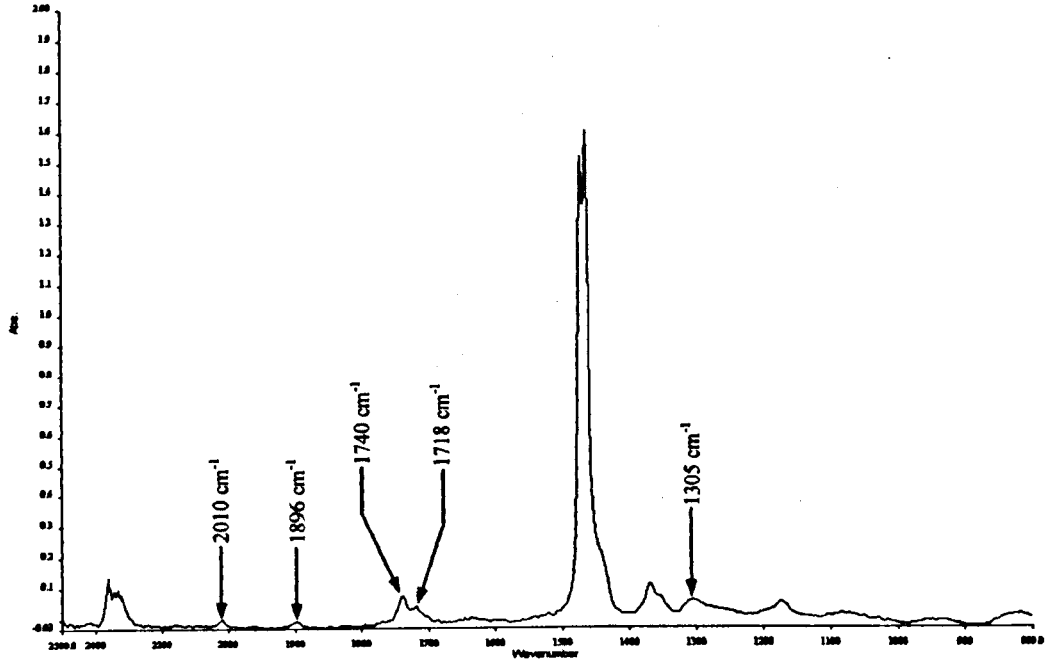

Figure 5-80 FTIR spectra taken d=300μm from the unworn bearing surface of component

6 DISCUSSION

This thesis presents a clear and thorough investigation into the wear and evolution of depth dependant properties in 32 retrieved UHMWPE acetabular components.

Long term years) failure of UHMWPE components in-vivo is predominantly caused by the biological response to sub-micron sized UHMWPE wear debris leading to osteolysis and eventually, asceptic loosening. The generation of UHMWPE wear debris primarily occurs via adhesive and abrasive mechanisms and is thought to be the dominant wear processes in total hip replacement UHMWPE acetabular components [65, 215, 216]

The results from the different analyses undertaken in this study are discussed in turn.

6.1 Patient Information

The patients that took part in the study underwent revision hip surgery at either Queen's Medical Centre or Nottingham City Hospital. There wasn't a selection criterion for inclusion of patients in this study.

Thirty-two patients participated in this study of which thirteen were female and nineteen were male. Patients were all Caucasian British nationals with ages ranging from 45 to 89 years. The average ages for men and women participating in the study were 70.7 ± 2.0 years and 74.9 ± 2.4 years respectively. The average age of patients is typical for people undergoing revision hip surgery. Primary hip replacement is

generally performed on patients aged 60 or over and the average service life of components is variable but typically around 15 years.

Osteoarthritis was the main pathological indication for primary total hip replacement and accounted for 82.8% of patients with hip trauma and rheumatoid arthritis counting for the remaining patient population. The prevalence of osteoarthritis as the reason for primary hip replacement was expected as it is similar to the figure published in an audit of orthopaedic procedures carried out at QMC by Brigden et al (2004). They reported that 94% patients admitted for hip replacement surgery had osteoarthritis.

Patient weight varied from 54kg to 110kg with a mean value of 70.4 ± 13.8kg. There was a negative correlation between patient weight and in-vivo period of acetabular component (-0.51, p=0.002) with increased weight linked to reduced implant time in-vivo. The association between patient weight and acetabular component survival was a theme that Surin et al [32] investigated. They found that patients weighing more than 80kg were at significantly greater risk of prosthetic failure requiring revision. In this study, there were eight patients who weighed >80kg at the time of revision and they had a mean acetabular component implant time of 12.1 ± 7.4 years compared to 17.2 ± 6.1 years for patients who weighed <80kg.

The body mass index (BMI) ratios of patients in this study were predominantly in the 'normal' range of 18.5kgm^{-2} and 24.9kgm^{-2}. There were however, seven male patients who fell into the 'overweight' bracket of 25kgm^{-2} to 29.9kgm^{-2} and one male patient was obese (>29.9kgm^{-2}). There was a correlation between the length of component

service life and BMI indicating that increased BMI led to decreased longevity. BMI was not correlated to any of the wear parameters.

UHMWPE component survival times varied greatly from 2.2 to 25.2 years. A large proportion (78.1%) survived for ≥10 years but this figure was reduced to 62.5% survivorship at 15 years and 37.5% at 20 years. Mean implant survivorship 15.9 ± 6.7 years and 17.2 ± 5.6years if components that have been revised due to reasons other than wear are discounted.

The survival rates reported in this study were much lower than those reported in the Swedish hip registry of 4,124 patients who had a survival rate at 18 years of 83% [15]. However, alternative survival studies reported similar survival rates to those presented in this study of between 76% and 90% at 10 years [15, 17, 166, 218, 219] but significantly higher rates for twenty year survivorship. For instance, Joshi et al [17] found that probability of the UHMWPE acetabular component surviving 20 years was 84% whilst Malchau et al [15] reported a survival rate of 81% at 20 years. Interestingly, there was a marked difference in the survivorship of UHMWPE acetabular components implanted in female patients compared to male patients. At 10 years, the survivorship of components in women was 92.0% compared to a survival rate of 70.0% in men. This trend continued with a 24.3% higher survival rate in women at 15 years and a 27.5% higher survival rate in women at 20 years. This result echoed previous studies that reported higher survival rates for females than males [24-27].

There were three patients with components 12, 28 and 28 that failed (5 years and is all were implanted in men. Seven components failed at implant times (10 years of which six were implanted in men and one implanted in a woman. The first component implanted in a female patient that failed was component 2 after 8.3 years. Fender et al [24] reported that men had a much higher risk of component failure at <5 years compared to woman. The fact that the components in this study that failed <5 years were all implanted in men and that 6 out of 7 implants that failed <10 years were implanted in men seems to reinforce the fact that men are more susceptible to early failure of acetabular components.

Joshi et al (1993) [17] found that the pathological diagnosis significantly influenced implant survival with rheumatoid arthritis patients having a survival probability of 96% at 20 years compared to 81% for osteoarthritis patients. The two patients who underwent primary total hip replacement for rheumatoid arthritis in the current study had survival rates of 23.4 and 22.2 years compared to the average survival rate of 15.2 years for patients with osteoarthritis.

In this study, two patients had received primary THR for trauma to the hip and their implant survival times were 15.1 years (component 10) and 22.5 years (component 32). Torchia et al [23] stated that people who had had previous trauma to the hip had a higher risk of failure than the wider population. The inclusion of only two patients who had received primary total hip replacement for trauma to the hip does not provide a sufficiently large population for comparison. It is interesting to note that the two patients in this study had implant times of 15.1 years (component 10) and 22.5 years (component 32) which were inline with, and in excess of the average.

Aseptic loosening of the UHMWPE component was the predominant reason given for joint failure and occurred in 30 cases. Wear debris has an important role in the process of aseptic loosening and the dominance of this failure mechanism reinforces the fact that research into the generation of wear debris is important.

Total physical activity scores varied greatly between patients with some being highly active whilst others engaged in only minimal physical activity. All patients engaged in some sort of household physical activity. However, only 50% of patients took part in sporting leisure activities with this figure being equally split between men and women. Kahan et al (2005) found the same trend of men participating in more sports leisure activity following their assessment of 406 adults [220]. Physical activity scores were correlated with length of time that components were implanted for, with increased activity leading to reduced component longevity.

6.2 Wear Assessment

Identification of the region of highest wear was an important step prior to subsequent analysis of through thickness properties. This was because the assessment of surface and sub-surface properties in this region are most in indicative of the materials response to in-vivo wear. This study represents the first time that an assessment of wear has been carried out on retrieved components in order to select specific regions for through thickness testing. This is an important point because in previous studies of through thickness properties, it wasn't apparent where samples had been taken from making it difficult to interpret the results. In addition, all of the previous studies have reported the indentation test results from a single through thickness sample.

The component wear data obtained via a co-ordinate measuring machine (CMM) presented in this study represents a contribution to the literature as the technique has only been used on a limited scale by previous researchers.

A CMM was chosen, in preference to other wear measurement techniques, as it was the only available technique that enabled the direct measurement of dimensional data from components. The technique has been shown to be a highly accurate method of obtaining dimensional, and hence wear data. Orthopaedic companies routinely use CMMs to assess newly fabricated components to check that they are within manufacturing tolerances. However, the use of CMMs in research has been extremely limited to date. Previous studies into the wear of acetabular components have primarily utilized radiographic techniques that are prone to measurement error. The use of a CMM to assess the wear of components in this study enabled accurate measurements of wear to be carried out. Accurate data relating to the wear of components in-vivo is important in the development of in-vitro wear simulation tests.

Microscopy and environmental scanning electron microscopy (ESEM) was carried out on the bearing surfaces of retrieved components to gain an insight into the wear mechanisms present.

6.2.1 Bearing Surface Features

Generally, retrieved cups displayed two distinct regions of wear, one region displayed a high degree of wear (worn region) and the second region displayed only slight wear (unworn region). The position of maximum wear on the retrieved components was found to be in agreement with previously published data in the literature (Sychterz

1996, Jasty 1997, Schmalzried 1999). Highly worn components displayed a distinct ridge between worn and unworn regions. Subsequent testing assessed the through thickness properties of test specimens from these regions. The differentiation between worn and unworn regions in components where only slight wear had occurred (i.e. component 28 displayed 0.3 mm linear wear) was possible through analysis of the CMM data but identifying these areas by visual inspection was extremely difficult. The ability to accurately detect small dimensional changes serves to highlight the importance in the assessment of wear in retrieved UHMWPE components. This is especially true for the analysis of components fabricated from highly-crosslinked materials where only very low wear rates are expected to occur.

The features observed on the bearing surfaces of components have all been reported previously by other researchers [64, 213, 221, 222] and are described in sections 5.2.2 and 5.2.3. A summary of the key features is as follows:

- Plastic flow of the surface of UHMWPE occurred on the rim of components in two opposing areas outside the worn region.
- Severe damage to the rim of component 11 immediately outside the worn region caused by interference between the acetabular cup and the neck of the femoral component due to misalignment in-vivo.
- Adhesion (fretting) wear in the worn region presented as an oval crater.
- Non-uniform brown discoloration of the periphery of the worn surface is also evident [212].
- Inter-zonal ridge at the interface between worn and unworn regions.
- Machining marks in unworn regions were common to all components with marks also visible in worn regions of the components that were retrieved due

to dislocation.

- Fibril formation in worn regions of all components.
- The presence of wear debris, pressed into the bearing surface of cups.
- Formation of craters/pitting caused by micro-contact fatigue damage with surface cracks extending from them (n=5 components).
- Scratches on the bearing surface caused by third-body particles.
- Sub-surface cracking.

Optical microscopy of through thickness sections prepared using a microtome highlighted the fact that the microstructure of UHMWPE in worn and unworn regions varied greatly. The appearance and location of a highly oxidized subsurface region is in agreement with the observations of previous researchers [64].

The inspection of through thickness freeze fractured unworn regions using ESEM revealed the true extent of the change in microstructure due to oxidation. Surface and bulk areas of UHMWPE from unworn regions displayed a well consolidated, nodular appearance whilst oxidized regions displayed a meshlike porous structure. The microstructures of oxidized and un-oxidized regions are similar to those reported by Wentz et al [95].

6.2.2 Wear Measurement

The mean linear wear rate for the 32 acetabular components in this study was 0.13±0.04mm/year (0.12±0.04mm/year for 22.25rnm cups). This is in the range of previously reported linear wear rates for Charnley prostheses 0.15mm/year [162], 0.07mm/year [34] and 0.10±0.06mm/year.

The mean volumetric wear rate for the 32 components was 87.2±27.8mm^3/year which was very similar to the value of 85±111mm^3/year reported by Essner et al [223] who used a radiographic method to measure wear for 28mm air irradiated cups. However, the volumetric wear rate reported in this study was much higher than the 26.7mm^3/year reported by Callaghan et al [166] who also used a radiographic wear measurement technique with digital edge detection enhancement [167].

The relationship between linear and volumetric wear rates and acetabular component size has been investigated on numerous occasions. In this study, the mean volumetric wear for 22.25rnm cups was 83.6±27.9mm^3/year and 95.9±28.8 mm^3/year for 28mm cups. The mean linear wear rate for 22.25rnm cups was 0.12±0.04mm/year, 0.16±0.04mm/year for the 28mm cups. This association between lower wear rates and smaller diameter cups reinforces the results of previous researchers who also reported this association.

It should be noted that there was only one acetabular component mated with a 32rnm cup and therefore it wasn't possible to statistically evaluate the relationship between 32mm diameter cups and wear rates.

The correlation between linear wear rate and patient age was an interesting phenomenon and led to the possibility that the patients age at the time of the primary implant (patient age - implant time in-vivo) may have influenced the wear rate in some way. However, there were no correlations between the patient ages at the time of the primary implant and linear or volumetric wear rates. Therefore the correlation of patient age at revision and linear wear rate can perhaps be viewed as being spurious.

There were correlations between gender and both linear and volumetric wear rates that indicated that men had higher wear rates than women. When considered in isolation, it is difficult to interpret the inference of the role of gender in the wear of UHMWPE. However, when other factors related to gender are also taken into account, the link with wear rates becomes more the meaningful. For instance, the total physical activity scores were lower for women 4.63±4.24 than men 5.56±6.61 and women had statistically lower BMI values (correlation of -0.55, p=0.000) than men. Age at primary implant was not a factor though, as the average ages of men and women were 56.5 and 57.0 respectively.

There was no correlation between any of the wear variables and physical activity which is the result that Goldsmith et al [33] also found what they assessed the influence of activity level on linear wear rate. One might expect that the wear of acetabular components in people who were physically active to be greater than in those who were less active. The lack of correlation with wear variables but presence of a correlation with implant longevity indicates that it has a role in the failure of components but via a different mechanism than wear.

The assessment of patient physical activity and its relationship with the in-vivo wear of UHMWPE acetabular components has attracted limited attention from researchers. Therefore the findings from this study represent a significant contribution to the literature.

Wear factors were calculated using the equation developed by Vassiliou and Unsworth [150]. The wear factor for components ranged from $0.8x10^{-6}mm^3/Nm$ (component 28) to $2.3x10^{-6}mm^3/Nm$ (component 16) with a mean value of $1.5\pm0.4x10^{-6}mm^3/Nm$. The mean value of $1.5\pm0.4x10^{-6}mm^3/Nm$ was lower than the figure reported by Vassiliou and Unsworth who calculated the wear factor of a 22.25mm Charnley acetabular component to be $2.55x10^{-6}mm^3/Nm$ on the assumption that patients weighed 75kg. The wear factor in this study is also lower than the mean clinical wear factors for explanted Charnley prostheses $2.1x10^{-6}mm^3/Nm$ [151] and $1.96x10^{-6}mm^3/Nm$ [122]. However, the mean wear factor was very similar to the findings of Saikko et al [224] who carried out simulator testing and reported wear factors ranging from 1.0 to $1.8x10^{-6}mm^3/Nm$. It was interesting that the wear factor for women $1.6\pm0.4x10^{-6}mm^3/Nm$ was higher than the figure for men $1.4\pm0.4x10^{-6}mm^3/Nm$.

Surprisingly, there were no correlations between calculated wear factors for individual components and any other parameters.

6.3 Radiographs

The pre-revision radiograph of component 2 is shown in Figure 5-40. Osteolysis has occurred around the exterior of the metal liner in a hemispherical region superior to the component. Analysis of the radiograph reveals that the lateral margin of the metal liner is not in contact with the outer margin of the pelvic bone. At retrieval the component was reported to have been mechanically loose. Bone resorption of the femur due to stress shielding is also visible on the radiograph.

Stress shielding or bone resorption is a common phenomenon that occurs in areas that are relatively unstressed. This is because loading forces are transmitted through the stiff femoral stem rather than the bone of the femur resulting in remodelling and resorption of the femur. The radiographic features evident in Figure 5-40 have been reported previously and a collection of notable radiographic features was reported by Ostlere et al [214].

Stress shielding is also evident in Figure 5-41 where significant resorption of the calcar has occurred medially to the femoral stem. Osteolysis is also evident at the interface of the lateral side of the femoral stem in the form of a wide lucency. Wide areas of lucency can be seen at the PMMA cement interface of the acetabular component as a result of osteolysis. The acetabular component was loose when it was retrieved.

Wear of the UHMWPE component is depicted in Figure 5-42 (component 29) where the liner thickness (indicated by line A) in the worn region is thinner than in the partially worn region (indicated by line B).

Figure 5-43 is the pre-revision radiograph of component 12 and displays Grade II heterotopic ossification. Heterotopic ossification occurs when primitive mesenchymal cells in the surrounding soft tissues are transformed into osteoblastic cells that form mature lamellar bone. It typically occurs around the femoral neck and adjacent to the greater trochanter and the majority of patients with low-grade heterotopic ossification are asymptomatic. If it becomes symptomatic, hip stiffness is the most common complaint. Classification of heterotopic ossification is shown in Figure 5-44.

6.4 Instrumented Indentation Testing

Abrasive and adhesive wear resistance of polymeric bearing surfaces are influenced by the hardness and elastic modulus of the polymer [225]. Therefore, the hardness and elastic modulus of UHMWPE bearing surfaces influence the generation of sub-micron wear debris. Variations in the hardness and elastic modulus of UHMWPE bearing surfaces may also be responsible for the large variations in in-vivo wear rates that are commonly reported by researchers.

Previous researchers have demonstrated that the mechanical properties of UHMWPE components that gamma irradiated in air have been shown to degrade as a function of time and oxidation [98, 226]. However, despite attracting a great deal of attention, there remains uncertainty over the manner in which the mechanical properties degrade following component implantation.

This study represents the first time that the through thickness properties of worn and unworn regions of retrieved UHMWPE components (irrespective of joint type) have

been investigated. The results from this study clearly indicated significant differences in through thickness properties of worn and unworn regions and the dominance of different underlying mechanisms involved in the modification of the material. The results also demonstrated the sensitivity of the indentation test method to variations in the structure of UHMWPE.

Micro-mechanical properties of UHMWPE in surface and sub-surface regions of acetabular components play a key role in process of wear and hence the longevity of the joint replacement. An instrumented indentation test technique was used to evaluate the hardness and elastic modulus of through thickness surface and sub-surface regions in worn and unworn regions. This test method was chosen for a number of reasons; the technique was highly sensitive to variations in UHMWPE properties, had a high spatial resolution for mapping properties and was able to assess the material on the same scale of size as UHMWPE wear debris. The final reason for using this technique was that the dominant wear mechanisms in hip replacements are sensitive to hardness and elastic modulus.

Distinct differences were found in the hardness and elastic modulus depth profiles of worn and unworn regions within individual components and also between components.

Worn regions were characterized by a significant decrease in hardness and elastic modulus of the UHMWPE at the bearing surface. When linear wear was ignored, the reduction in surface properties was found to be common across all 32 components at a depth of 100μm. When linear wear was taken into account the reduction in surface

properties was noted at different depths and the property profiles of different components weren't correlated. At depths greater than 300μm, there were no statistically significant variations in hardness or elastic modulus values within individual components.

The primary cause of this degradation at the surface of worn regions is thought to be the multi-directional re-orientation of surface layers of worn regions. The presence of multi-directional wear was confirmed by observations of the wear surface where re-orientation of the UHMWPE had resulted in fibril formation. A number of previous researchers have described the significance of molecular re-orientation of UHMWPE on wear [141-144]. In essence, multidirectional wear results in the surface being constantly subjected to shear stresses and re-oriented at acute angles, leading to shearing of the polyethylene and removal of particles from the surface. This persistent re-orientation leads to a reduction in surface hardness. This is in contrast to uni-directional wear where orientation of the UHMWPE surface layer leads to an increase in strength in the oriented direction and weakening of the material in the perpendicular direction leading to increased surface hardness [145]. Reduction in hardness of the worn surface may also be linked to the ingress of constituents of synovial fluid into the surface of the material. This is discussed later in the text.

In contrast to worn regions, unworn regions didn't display a decrease in hardness or elastic modulus at the bearing surface. Unworn regions were characterized by increased hardness and elastic modulus values in sub-surface regions (500μm to 2000μm). Increases in hardness and elastic modulus were not uniform across all components but dependant on the duration of time that the implant had spent in- vivo.

Component 27 for example had been implanted for 2.2 years and didn't display any variation in hardness or elastic modulus whilst component 15 had been implanted for 15.4 years and displayed a significant increase in hardness and elastic modulus in the sub-surface region.

When the maximum hardness and elastic modulus values were plotted as a function of time, the properties of worn regions were found to be independent of length of time that the component had been in-vivo. This indicated that the reduction in surface properties was due to the wear process rather time-dependent post-irradiation effects.

At distances greater than 2100μm from the bearing surface, there were no significant variations in properties of individual components.

However, when bulk hardness and elastic modulus values for worn (>300μm) and unworn regions (>2100μm) were plotted as a function of time, there was a correlation between increased time in-vivo and increased property values.

The results from the unworn regions clearly show that variations in properties in the sub-surface and bulk of UHMWPE were a direct result of time-dependant in post-irradiation effects. However, the results also demonstrate the non-uniformity of the oxidation process as peaks in hardness and modulus values were always observed in the sub-surface region whilst in the bulk, the process of oxidation proceeded at much slower rate. The fact that the unworn region, by definition, has a minimal role in the functioning of the joint replacement meant that the implication of increased sub-surface hardness and elastic modulus values in unworn regions plays only a minor

role but could explain why fracture of UHMWPE acetabular rims occurs.

When hardness and elastic modulus values for discrete distances from the worn and unworn bearing surfaces of the same component were analysed (for example comparison of hardness values obtained at a depth of 500μm in worn and unworn regions), key differences between the regions was noted i.e. increased property values in subsurface regions for unworn components and decreased property values at the surface of worn regions.

These assessments also served to demonstrate the fact that hardness and elastic modulus values in the bulk of both regions were comparable indicating that at depths >2100μm, the progression of oxidation was uniform. The uniformity of these values resulted from the fact that oxidation was inhibited by the low levels of available oxygen in the bulk of the material.

The hardness results from this study were similar to certain results from the two previous studies that utilised depth dependent properties of retrieved acetabular components. Bruni et al [197] reported a hardness peak at 1mm from the `internal and external component surfaces' and no hardness variations were observed for new components. Flores et al [198] also reported peak hardness values at a depth of 1-2mm from the bearing surface and these increased hardness values corresponded to micro-structural observations of incipient cracking and increased crystallinity.

Gilbert et al [189] published an instrumented indentation study of the through thickness properties of UHMWPE tibial components that had been gamma irradiated

in air and shelf aged for 15 years. Components displayed the classic white band appearance when sectioned and the test was sensitive to the degree of oxidation that had occurred. The through thickness profile of hardness and elastic modulus reflected the results presented in the current study for unworn regions. Increased levels of oxidation were associated with increased modulus and hardness values. The hardness values were almost identical to those reported in the present study with a value of $75Nmm^{-2}$ at a distance of 100μm and a peak value of $94Nmm^{-2}$ at 1000μm from the bearing surface. Elastic modulus values varied in a similar manner to microhardness with values rising from 0.6GPa 100μm from the free surface to 1.5GPa at a depth of 2000μm before gradually decreasing in a linear fashion to 0.6GPa 5000μm from the free surface.

Moving away from instrumented indentation testing, Edidin et al (2001) used the small punch test to investigate the through thickness properties of nine retrieved UHMWPE components. They found a significant correlation between patient weight and the toughness (work to failure) of components with the heaviest patient also being the one with the shortest longevity in-situ. There was no such link between surface or bulk hardness and patient activity.

Kurtz et al. (2003) also used the technique in a retrieval study to assess the mechanical properties of 4 regions (unworn surface, worn surface, unworn subsurface and worn subsurface) [187]. They found that that mechanical degradation of unworn surface regions increased with implantation time. Peak load, ultimate displacement and work to failure were all correlated with implantation time in this region. There weren't any correlations with implantation time for the three other regions. Another

interesting point they made was that the loaded surface of liners exhibited less degradation than the unloaded surface. They postulated that the degraded material had been removed by wear. Their findings relating to increased degradation in unworn regions with implantation time and degradation of worn surfaces is in agreement with the hardness and elastic modulus findings from the current study.

6.5 FT-IR Imaging

FT~IR imaging was used in this study as it is a powerful tool that is able to accurately map variations in chemical properties across a sample surface. The use of this technique in combination with instrumented indentation testing has not been utilized before in the assessment of orthopaedic components. However, the combination of techniques provides a powerful approach to the assessment of retrieved components in particular because of the ability to accurately map mechanical and chemical properties and investigate the relationship between the sets of data. Direct correlations were found between mechanical and chemical profiles. The results from the FT-IR assessment demonstrated the sensitivity and accuracy of this technique and its usefulness in assessing gradients of chemical properties in retrieved UHMWPE components.

In this study, samples from the unworn and worn regions of five components
14, 15, 22 and 27) were evaluated using FT-IR imaging. It would have been preferable to have analysed all 32 components but equipment and funding limitations precluded this. The five components were selected as they represented a range of implant times and instrumented indentation testing had indicated significant variations between these samples. Despite the small sample size, the results of each test are

significant as each component scan consisted of >1500 different spectra recorded at 25μm intervals. Another point to stress is that other researchers have used similar sample sizes. Costa et al analysed 10 components each of a different design [87], in a separate study [102] they assessed 10 components of the same design.

Initially, spectra were normalised at 2020cm^{-1} to a 0.05 absorbance. Crystallinity values were then calculated by a ratio of absorbance at 1896cm^{-1} band (crystalline phase) to the band at 1305cm^{-1} (amorphous phase). Oxidation of UHMWPE was assessed by analysing the carbonyl peak at 1718cm^{-1} [87, 105, 200 and 204]. Finally, ingress of synovial fluid into the surface of UHMWPE was inferred from the peak at 1740cm^{-1}. Significant variations in chemical property profiles between regions were noted along with variations between components.

A distinct subsurface band of oxidation was observed in components 14, 15 and 22 at depths ranging from 300μm to 2000μm. Peak values at the 1718cm^{-1} band were up to six times higher than levels in the bulk. Increased values of the 1718cm^{-1} band coincided with a change in through thickness morphology and formation of `white band'. At depths >2000μm no significant variations in the 1718cm^{-1} band were observed for the components.

Worn regions exhibited increased surface absorbance values at 1718cm^{-1} band for all five components. The largest increase in oxidation (compared to bulk values) was for component 22 that exhibited a threefold increase in absorbance. No variations in oxidation were observed at depths greater than 225μm.

Oxidation of UHMWPE is commonly measured using the absorbance of 1718cm^{-1} band. Increased subsurface absorbance measurements at 1718cm^{-1} band presented in this study are similar to those reported previously by Goldman et al [200] and Costa et al [105]. The location of the subsurface increase in 1718cm^{-1} band was also similar to the location reported by Costa et al [105] and Yeom et al [92, 227]. The presence of subsurface oxidized areas in unworn regions had been expected prior to commencing the study. What was surprising was the absence of subsurface oxidized areas in worn regions of components. In addition, the increased bearing surface absorbance values at 1718cm^{-1} band for worn regions was unexpected based on the consistent reporting of increased oxidation values by other researchers.

A potential source of this disparity is the process and conditions that the retrieved components are sterilised and stored under. The majority of previous researchers didn't report the anti-microbial processing, storage conditions or storage time following retrieval. A notable exception was Kurtz et al [228] who carefully described their retrieval processes. They used a similar process of anti-microbial processing and component storage at sub-zero temperatures to make the components safe to handle and post-retrieval oxidation. If components are stored in normal atmospheric conditions post-irradiation oxidation of UHMWPE will continue to progress as oxygen would be freely available and oxidation is a time-dependent process.

In this study oxidation of subsurface regions of unworn regions coincided with increased hardness and elastic modulus values indicating that mechanical properties of the subsurface regions had been modified as a result of the oxidation.

Kurtz et al [228] proposed that in-vivo degradation was influenced by a mechanism that utilises molecular oxygen dissolved in body fluids as the primary chemical fuel for in vivo degradation process. They hypothesised that dissolved oxygen diffuses into the UHMWPE component and reacts with residual free radicals from gamma sterilization in a similar manner to shelf aging but at a slower rate.

Costa et al [87] reported that chain scissions that occur during oxidation lead to a significant reduction of molecular weight. They reported that the molecular weight of a sample was 600000 at the surface reducing to 20000 in the highly oxidized sub-surface region. They also stated that for a hypothetical UHMWPE of original molecular weight 4,000,000, five chain scissions (corresponding to 0.0017% of original bond in each chain) depress the molecular weight to 700,000. Molecular weight was not assessed during the course of this study for a number of reasons. The primary reason was that the main aim of the study had in been to investigate the micromechanical and microphysical properties of UHMWPE and molecular weight measurement techniques tend to function on the macroscale. However, assessing the situation retrospectively, it would have been useful to have measured molecular weights of samples and the lack of this information is a limitation of this study.

Increased crystallinity values were observed in the sub-surface unworn regions of components 14, 15 and 22 with maximum values at depths of 1175μm to 1350μm. Maximum crystallinity values were 63.6%, 66.2% and 73.6% for the respective components. No significant variations in bulk crystallinity were observed.

Increased crystallinity values were observed at the surfaces of worn regions in all

components with the largest increase in surface crystallinity recorded for component 2 (62.3% at the surface and 52.3±1.7% in the bulk). Increased crystallinity measurements at the surface of worn regions may have been caused by a decrease in the amount of the amorphous phase rather than an increase in the crystalline phase. The reason for this may have been the selective removal of amorphous material during the wear process.

Increases in crystallinity values were observed at the bearing surface of unworn regions. Crystallinity values ranged from 56.1% (component 27) to 63.9% (component 22). Unlike worn regions, increased crystallinity values could not be attributed to the wear process. Instead, it is likely that components had a modified surface layer that was formed as a result of machining during manufacture. Unidirectional preferential alignment of polymer molecules in the direction of machining and the observation of machining marks on unworn surfaces reinforces this idea. Taking the idea of unidirectional preferential alignment of the surface layer further, it would have been reasonable to have expected to find an increase in resistance to deformation and therefore increased hardness. However, no such increase was detected during this study. In unworn regions the increased crystallinity values were detected at distances to close to the surface to be assessed by the indenter. However, in worn regions, the presence of increased crystallinity values did occur at depths where indentation testing was carried out at and reductions in hardness and elastic modulus were recorded during to multi-directional surface wear (as opposed to unidirectional alignment of unworn surfaces following machining).

Fluid absorption into the surfaces of UHMWPE has been shown to occur in both

simulated and explant analyses [109, 229]. Absorption of esters ($1740cm^{-1}$), a component of synovial fluid, has been used to quantify fluid ingress by Costa et al.

Costa et al [102] carried out an analysis of products that had diffused into the surface of UHMWPE components in-vivo. Mechanism of diffusion of solids, liquids and gases into polyethylene has been reported previously [100]. The synovial fluid is absorbed on the surface and then moves towards the bulk [101].

Diffusion of synovial fluid constituents into the surface of UHMWPE leads to the surface becoming plasticised which results in a reduction in mechanical properties such as tensile strength and ultimate elongation. The reduction in mechanical properties will lead to a reduction in abrasion resistance of the material [104].

Increased absorbances at $1740cm^{-1}$ were observed at the surface of unworn bearing surfaces. The level of absorption at this band was directly related to the penetration of synovial fluid constituents into the surface of the material. There was a variation in the penetration of fluid at the surfaces of different components. Fluid penetrated to a depth of 400μm in component 22 whilst the depth of penetration in component 2 was 100μm. There were no increased absorbances in the bulk of any of the components.

Fluid ingress occurred at the surfaces of worn regions in a similar manner to ingress of fluid at unworn surfaces.

The magnitude of the absorbances at $1740cm^{-1}$ in worn regions was greater than the values observed in unworn regions with the exception of absorbance values for

component 22 where they were 0.1 lower than in unworn regions. The observed reduction in fluid absorption for component 22 is not readily clear but may have been due to removal of surface synovial fluid constituents from the worn surface during the component anti-microbial processing procedure.

The ingress of synovial fluid constituents into the external surfaces of UHMWPE components in-vivo has been reported by Costa et al [105] and Blanchet et al [108]. However, the ingress of fluid is non-uniform with increased depth of penetration of fluid in the load bearing region. Yao et al [103, 109] postulated that the ingress of fluid may result in plasticisation of the material leading to a decrease in mechanical properties and hence, wear resistance.

A study by Klapperich et al [109] investigated the absorption of serum into UHMWPE. Fluid absorption was measured by weighing components at different time intervals. Gamma irradiated and unsterilized UHMWPE samples were found to gain fluid in relation to the surface area. When surface area was increased by 50% an equivalent increase in fluid absorption was found. Another interesting point was that there was a lower weight gain for UHMWPE samples sterilized using EtO. The researchers made the point that different sterilization processes influence fluid absorption into the material. They also hypothesised that EtO may have a beneficial surface chemistry that resists serum sorption.

Fluid ingress had occurred at the surfaces of worn and unworn regions across all components. The ingress of fluid into the surfaces of worn regions was found to be at a much high level than in worn regions. In addition, the depth of ingress into worn

surface regions was greater than for unworn bearing surfaces. The absorption of synovial fluid constituents into the external surfaces of UHMWPE components has been reported by a number of previous researchers [108, 229, 230]. The increased penetration of synovial fluid may have occurred due to the mechanical loading of the worn surface and increases in fluid pressure between bearing surfaces of the femoral and acetabular components or localised increases in surface area due to microscale roughening of wear surfaces due to abrasive and adhesive wear.

Ingress of fluid may then proceed more easily enabling the penetration of the fluid at increased depths. The ingress of fluid may then act to plasticise the material and reduce its ability to resist deformation.

7 CONCLUSIONS

This thesis presents a clear and thorough evaluation of the variation in through thickness properties of retrieved UHMWPE acetabular components in regions of high and low wear.

The accurate assessment of UHMWPE component wear as a function of in-vivo as service is crucial in validating the use of in-vitro wear test protocols. The ability to accurately measure wear will be especially important in future studies where components fabricated from UHMWPE with improved wear resistance (i.e. highly crosslinked, ion implanted, Vitamin stabilised) will require assessment.

In this study, a co-ordinate measuring machine was used to evaluate the bearing surfaces of 32 retrieved UHMVVPE acetabular components. The wear data obtained from the test allowed the accurate identification of regions of highest and lowest wear. This was an essential step that enabled the fabrication of instrumented indentation test samples whose properties reflected the extremes of in-vivo service within individual components. The accurate direct assessment of component wear was also a valuable contribution to the literature in its own right. This is because the majority of previous wear studies have assessed the wear of components in-vivo using radiographic techniques that can be prone to error.

The assessment of through thickness mechanical properties was carried out using an instrumented indentation tester. The reasons for using this method were that it had previously been shown to be sensitive to variations in the properties of UHMWPE. In

addition, it is also able to assess the properties of a surface without the need to generate standardized test samples as is the case for small punch testing. The key from the indentation test assessment were as follows:

- Decreased hardness and elastic modulus values were detected at the surfaces of every worn region.
- When decreased values were plotted as a function of time, they were found to be independent of the implantation period.
- No significant variations in hardness were observed in samples from worn region at depths >300μm.
- Unworn regions displayed subsurface increases in hardness and elastic modulus but these were non-uniform across all components.
- The magnitude of peak hardness and elastic modulus values in subsurface regions were correlated with implantation time. Increased implantation times resulted in increased property values.
- The values of hardness and elastic modulus in the bulk of components (>2100μm) was seen to increase as a function of time.

FT-IR imaging was used to assess the chemical properties of unworn and worn regions. This study represented the first time that a combination of chemical and mechanical mapping techniques able to assess micron scale properties of materials had been used to assess retrieved UHMWPE components. The key findings were:

- Increased oxidation and crystallinity levels at the surface of both unworn and worn regions. These increased levels are thought to have been the result of the formation of a modified surface layer by in-vivo wear in worn regions and machining in unworn regions.

- Subsurface oxidation and increases in crystallinity in unworn samples were detected and their presence was correlated to increased hardness and elastic modulus values.
- No significant variations in oxidation or crystallinity were detected in subsurface regions of worn samples.
- Fluid ingress occurred at both unworn and worn surfaces but in worn regions penetration of the fluid occurred at greater depths and the levels of esters at the surface of worn samples was also greater than at unworn surfaces. The ingress of fluid combined with the generation of a modified surface layer may have resulted in plasticization of the UHMWPE and reduction in its ability to resist deformation.

ESEM and optical microscopy were used to identify the different morphologies of worn and unworn regions. Severe subsurface oxidation (`white band') was only observed in subsurface regions of unworn components and corresponded to increased hardness/elastic modulus and oxidation levels.

8 FUTURE DIRECTIONS

This study demonstrated, for the first time that the combination of instrumented indentation testing and FT-IR imaging was a powerful technique for assessing variations in the properties of UHMPWE. However, the assessment of mechanical properties on the nano-scale in combination with micron-scale testing would enable researchers to further investigate the effects of in-vivo service on UHMWPE and its ability to resist wear. Future work into the evolution of UHMWPE properties during in-vivo service is essential to the development of our understanding of the wear mechanisms involved in the generation of wear debris which is known to have an important role in the failure of total hip replacements.

APPENDIX

Patient Weights

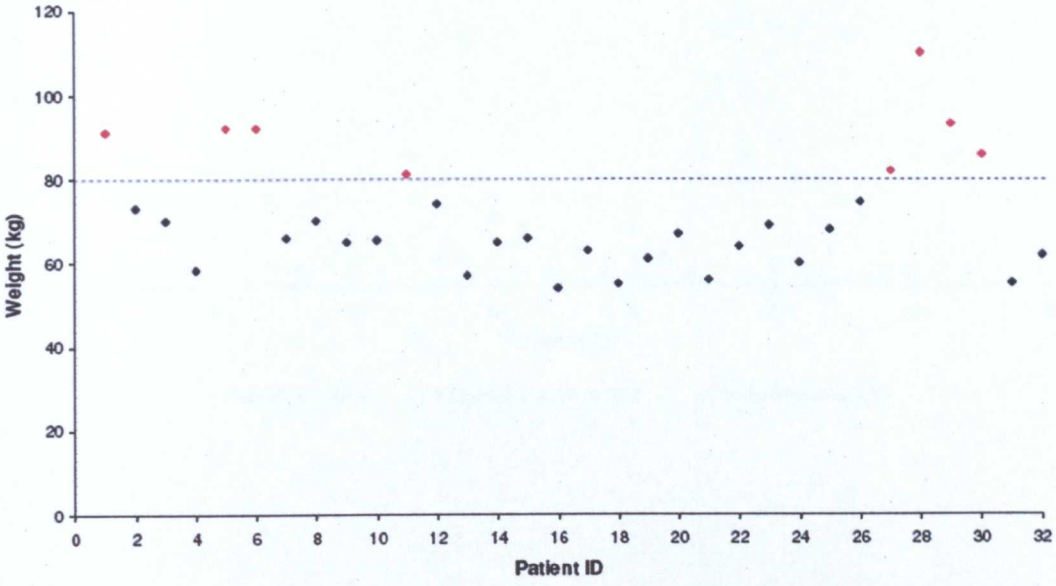

Body Mass Index Scores

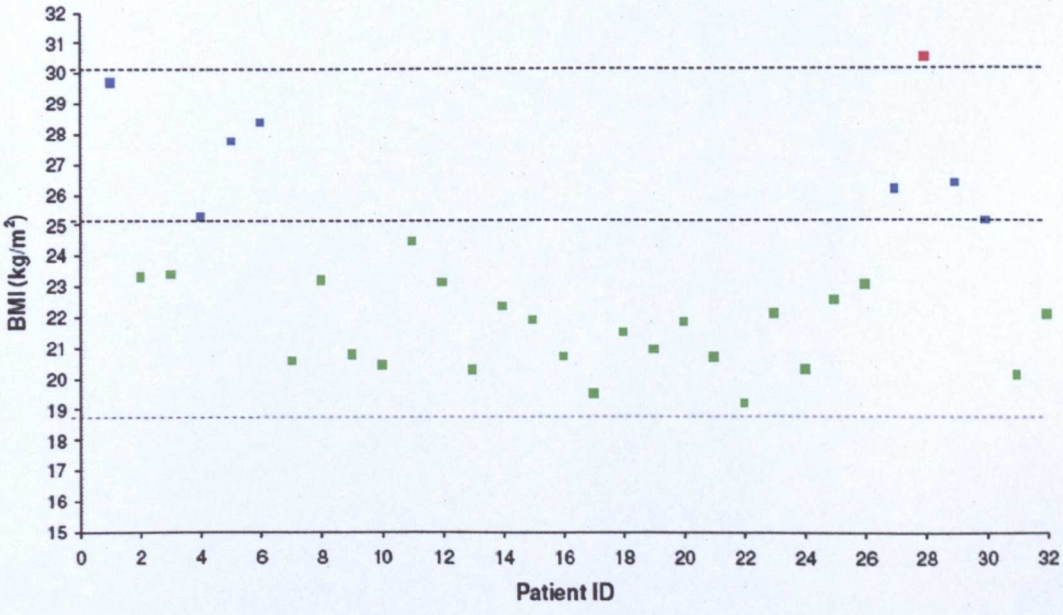

Physical Activity Scores

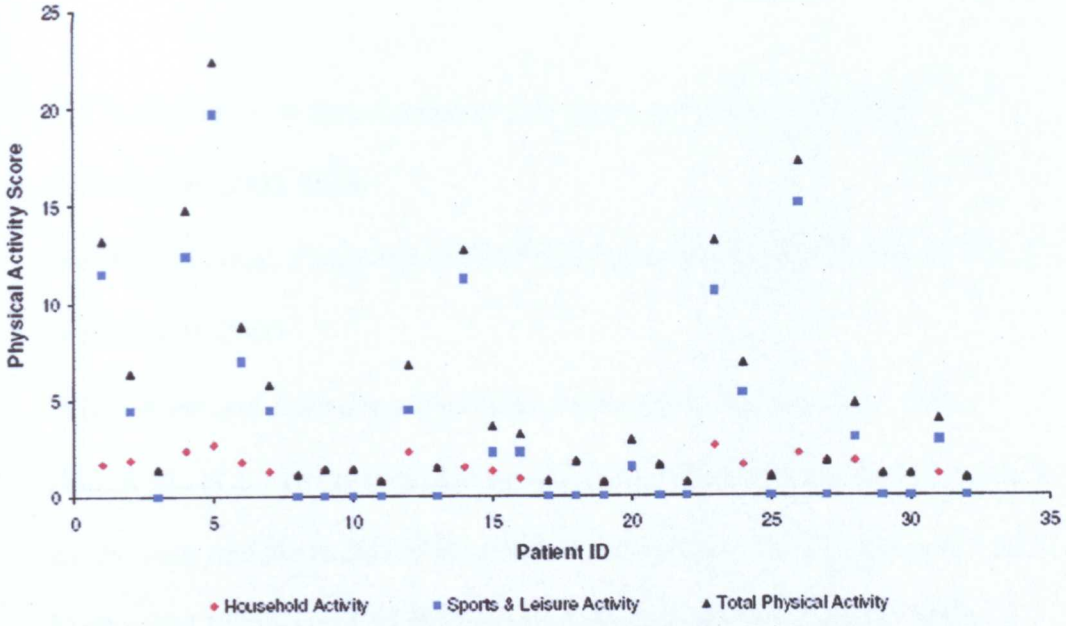

REFERENCES

1. NICE, *Guidance on the selection of prostheses for primary total hip replacement.* 2000, NHS
2. Malchau, H., et al. *Prognosis of Total Hip Replacement. In 67th Annual Meeting of the AAOS.* 2000
3. WHO, *Bone and Joint decade website: frequently asked questions.* 2003.
4. Hall, R.M., et al., *The association between rates of wear in retrieved acetabular components and the radius of the femoral head.* Proceedings of the Institution of Mechanical Engineers, Part H: Journal of Engineering in Medicine, 1998. **212**(5): p321-326.
5. Raimondi, M.T., Sassi, R., and Pietrabissa, R., *A method for the evaluation of the change in volume of retrieved acetabular cups.* Proceedings of the Institution of Mechanical Engineers, 2000. **214**(6): p577-587.
6. Seeley, S., et al., *Anatomy and Physiology,* 4th edition 1998: WCB/McGraw-Hill.
7. Northmore-Ball, M.D., et al., *Clinical challenges in orthopaedics: The hip,* ed. M. Dunitz. 2002.
8. Rona, Z., *Osteoarthritis.* 2002: Alive Books. p64
9. DePuy, *allaboutarthritis.com.* 2003. DePuy.
10. Graves, S., Davidson, D. and Ingerson, L., *National Joint Replacement Registry Annual Report 2003.* 2003, Australian Orthopaedic Association: Adelaide. p1-105
11. Soderman, P., Malchau, P. and Herberts, P., *Outcome of total hip replacement.*

Clinical Orthopaedics and Related Research, 2001. **390**: p163-172

12. NICE, *Guidance on the selection of prostheses for primary total hip replacement.* 2000. NICE. p1-12
13. Klasen, P.A., Parlasca, R.J. and Bianco, A.J., *Total joint arthroplasty. Applications in children and adolescents.* Mayo Clin Proc, 1979. **54**: p579-582
14. Pettine, H.A., Aamlid, B.C. and Cabanela, M.E., *Elective total hip arthroplasty in patients older than 80 years of age.* Clinical Orthopaedics and related Research, 1991. **266**: p127-132
15. Malchau, H. and Herberts, P., *Long term registration has improved the quality of hip replacement,* Acta Orthop Scand, 2000. **71**(2): p111-121
16. Witt, J.D., Swann, M. and Ansell, B.M., *Total hip replacement for juvenile chronic arthritis.* J Bone Joint Surg, 1991. **73B**: p770-773
17. Joshi, A.B., et al., *Long term results of Charnley low friction arthroplasty in young patients.* J Bone Joint Surg, 1993. **75B**: p616-623
18. Lachiewicz, P.F. et al., *Total hip arthroplasty in juvenile rheumatoid arthritis. Two to eleven-year results.* J Bone Joint Surg. **68**(2): p502-508.
19. Roach, J.W. and Paradies, L.H., *Total hip arthroplasty performed during adolescence.* J Pediatr Orthop, 1984. **4**(4): p418-421
20. Chandler, H.P., et al., *Total hip replacement in patients younger than thirty years old.* Journal of Bone and Joint Surgery (Am), 1981, **63**(9): p1426-1434
21. Kobayashi, S., et al., *Comparative study of total hip arthroplasty between younger and older patients.* Clinical Orthopaedics and Related Research 1997. **339**: p140-151
22. Sochart, D.H. and Porter, M.L., *The long-term results of Charnley low-friction arthroplasty in young patients who have congenital dislocation, degenerative*

osteoarthrosis or rheumatoid arthritis. J Bone Joint Surg, 1997. **79**: p1599-1617

23. Torchia, M.E. et al., *Total Hip Arthroplasty with Cement in Patients Less Than Twenty Years Old. Long-Term Results.* J Bone Joint Surg, 1996. **78**: p995-1003
24. Fender, D. et al., *Relationship between outcome and annual surgical experience for the Charnley total hip replacement.* J Bone Joint Surg, 2003. **85-B**: p187-190
25. Furnes, O. et al., *Hip disease and the prognosis of total hip replacements: A review of 53698 primary total hip replacements reported to the Norwegian arthroplasty register* 1987-1999. J Bone Joint Surg, 2001. **83-B**(4): p579-586
26. Schurman, D.J., et al., *Conventional cemented total hip arthroplasty: assessment of clinical factors associated with revision for mechanical failure.* Clinical Orthopaedics and Related Research, 1989. **240**: p173-180
27. Roush, S.E., *Patient-perceived functional outcomes associated with elective hip and knee arthroplasties.* Phys Ther, 1985. **65**(10): p1496-1500
28. Holtzman, J., et al., *Gender differences in Functional Status and Pain in a Medicare Population Undergoing Elective Total Hip Arthroplasty.* Medical Care, 2002. **40**(6): p461-470
29. Flugsrud, G.B., et al., *Risk Factors for total hip replacement due to primary osteoarthritis: a cohort study in 50034 persons.* Arthritis and Rheumatism, 2002. p675-682
30. Flugsrud, G.B., et al., *The impact of body mass index on later total hip arthroplasty for primary osteoarthritis.* Arthritis and Rheumatism, 2006. **54**(3)
31. Olsson, S., et al., *Clinical and radiological long-term results after Charnley-Muller total hip replacement.* Acta Orthop Scand, 1981. **52**(5): p531-542
32. Surin, V.V. and Sundholm, K., *Survival of patients and prostheses after total*

hip arthroplasty. Clinical Orthopaedics and Related Research, 1983. **177**: p148-153

33. Goldsmith, A.A., et al., *The effect of activity levels of total hip arthroplasty.* J Arthroplasty, 2001. **16**(5): p620-627
34. Griffith, M.J., et al., *Socket wear in Charnley low friction arthroplasty of the hip.* Clinical Orthopaedics and Related Research, 1978. **137**: p37
35. Wroblewski, B.M. and Siney, P.D., *Charnley low-friction arthroplasty of the hip: long term results.* Clinical Orthopaedics and Related Research, 1983. **292**: p191
36. Baecke, J.A.H., et al., *A short questionnaire for the measurement of habitual physical activity in epidemiological studies.* Am J Clin Nutr, 1982. **36**: p936-942
37. Washburn, R.A., et al., *The physical activity scale for the elderly (PASE): development and evaluation.* J Clin Epidemiol, 1993. **46**(2): p153-162
38. Godin, G. and RiJ. Shephard, *A simple method to assess exercise behavior in the community.* Canadian Journal of Applied Sport Sciences, 1985. **10**: p141-146
39. Jacobs Jr, D.R. et al., *A simultaneous evaluation of 10 commonly used physical activity questionnaires.* Medicine & Science in Sports & Exercise, 1993. **25**: p81-91
40. Voorrips, L.E., et al., *Modified Baecke questionnaire for older adults.* Medicine & Science in Sports & Exercise, 1997. **29(Supplement June)**: p117-121
41. Bink, B., et al., *Assessment of the energy expenditure by indirect time and motion study.* In Proceedings of the Bertostolen Symposium. 1966. Oslo University
42. Pols, M.A., et al., *Validity and repeatability of a modified Baecke questionnaire on physical activity.* Int J Epidemiol, 1995. **24**(2): p381-388

43. Pols, M.A., et al., *Repeatability and relative validity of two physical activity questionnaires in elderly women.* Medicine & Science in Sports & Exercise, 1996. **28**(8): p1020-1025

44. Florindo, A.A., et al., *Validation and reliability of the Baecke questionnaire for the evaluation of habitual physical activity in adult men.* Revista Brasileira de Medicina do Esporte, 2003. **9**(3): p129-135

45. Shephard, R.J., *Limits to the measurement of habitual physical activity by questionnaires.* British Journal of Sports Medicine, 2003. **37**: p197-206

46. Klesges, R.C., et al., *The accuracy of self-reports of physical activity.* Medicine & Science in Sports & Exercise, 1990. **22**: p690-697

47. Bannister, G.C., *History and basic science*, in *Clinical challenges in orthopaedics: The hip*, M.Dunitz, Editor. 2002. p59-67

48. Anon., *A century in orthopaedics.* Orthopaedics today, 2000

49. Murphy, J.B., *Arthroplasty.* Annals of surgery, 1913. **5**: p513

50. Smith-Petersen, M.N., *Evolution of the mold arthroplasty of the hip joint.* J Bone Joint Surg, 1948. **30**: p59-75

51. Densply, *Vitallium.* 2003

52. Law, W.A., *Results of virallium mold arthroplasty of the hip.* J Bone Joint Surg (Am), 1962. **44A**: p1497-1517

53. Waugh, W., *John Charnley: The man and the hip,* 1991. 286

54. Waugh, W., *The growth of an idea: 1951-1961.*, in *John Charnley: The man and the hip,* 1990. Springer-Verlag: London

55. Charnley, J., *The lubrication of animal joints.* Institution of Mechanical Engineers: Symposium on Biomechanics, 1959. **17**: p12-22

56. Charnley, J., *Low Friction Principle*, in *Low Friction Arthroplasty of the Hip:*

Theory and Practice. 1979, Springer-Verlag

57. Waugh, W., *The plan fulfilled 1959-1969.*, in *John Charnley: The man and the hip.* 1990
58. Bevill, S.L., et al., *Finite element simulation of early creep and wear in total hip arthroplasty.* Journal of Biomechanics, 2004. **38**(12): p2365-2374
59. Bartz, R.L., et al., *The effect of femoral component head size on posterior dislocation of the artificial hip joint.* J Bone Joint Surg, 2000. **82**: p1300
60. Burns, A. and McCalden, R., *Current techniques and new developments in acetabular revision surgery.* Current Orthopaedics, 2006. **20**: p162-170
61. Peacock, A.J., *Handbook of polyethylene: Structures, properties and applications.* 2000: Marcel Dekker. 534
62. Kurtz, S.M., *The UHMWPE handbook: Ultra-High Molecular Weight Polyethylene in Total Joint Replacement.* Vol. 1. 2004: Academic Press. 379
63. Eyerer, P., et al., Polyethylene, in Concise Encylopaedia of medical and Dental Materials
64. Wantanabe, E., et al., *Oxidation-induced dynamic changes in morphology reflected on freeze-fractured surface of gamma-irradiated ultra-high molecular weight polyethylene components.* Journal of biomedical Materials Research, 2002. **62**(4): p540-549
65. Wang, A., et al., *Lubrication and wear of ultra high molecular weight polyethylene in total joint replacements.* Tribology International, 1998. **31**(1-3): p17-33
66. UHMWPE.org, *UHMWPE*, 2003
67. Bellare, A. and Spector, M., *The polyethylene History*, in *Total Knee Arthroplasty: A guide to better performance*, J. Bellemans, M. Ries and J.

Victor, Editors. 2004. p45-50

68. ASTM F648-00 *Standard specification for ultra high molecular weight polyethylene powder and fabricated form for surgical implants.* 2000

69. Swarts, D., et al., *Aging of calcium stearate-free polyethylene.* In *5th World Biomaterials Conference.* 1996

70. Schmidt, M.B. and Hamilton, J.V., *The effects of calcium stearate on the properties of UHMWPE.* In *42nd Meeting of the Orthopedic Research Society.* 1996

71. Han, K.S., et al., *Powder compaction, sintering and rolling of ultra-high molecular weight polyethylene and its composites.* Journal of Macromolecular Science, 1981. **B19**: p313-349

72. Bellare, A. and Cohen, R.E., *Morphology of rod stock and compression moulded sheets of ultra-high molecular weight polyethylene used in orthopaedic implants.* Biomaterials, 1996. **17**: p2325-2333

73. Kurtz, S.M., *Analysis of contemporary resins and conversion methods.* 2001, ASTM working group for medical grade UHMWPE, p1-3

74. Biomet, *Arcom.* 2002, Biomet

75. NHS-Estates, *Health Technical Memorandum 2010 – Sterilization.* 1994, UK Health Departments – NHS

76. Block, S.S., *Disinfection, sterilization and preservation.* 5th Ed. 2001, Philadelphia: Lippincott, Williams and Wilkins.

77. Dirix, Y., et al., *The influence of steam sterilization on retrieved UHMW-PE parts.* European Cells and Materials, 2004. **7**: p24-25

78. Benson, R.S., *Use of radiation in biomaterials science.* Nuclear Instruments and Methods in Physics Research B, 2002. **191**: p752-757

79. Isotron, *Gamma irradiation.* 2003

80. Trieu, H.H. and Paxon, R.D., *The oxidized surface layer in shelf aged UHMWPE tibial inserts.* Transactions of the 41st Annual Meeting of the Orthopaedic Research Society, 1995: p758

81. Baker, D.A., et al., *Compression and tension fatigue resistance of medical grade ultra high molecular weight polyethylene: the effect of morphology, sterilization, aging and temperature.* Polymer, 2001. **41**: p795-808

82. Edidin, A.A. et al., *Degradation of through thickness mechanical properties over time is more sever than previously estimated using indirect measurement techniques.* In 45th Annual Meeting of the Orthopaedic Research Society. 1999. Anaheim, California

83. Yau, S.S. et al., *Effect of gamma sterilization in air and shelf aging on wear of "enhanced" and conventional UHMWPE acetabular cups.* In *46th Annual Meeting of the Orthopaedic Research Society.* 2000

84. Nusbaum, H.J. and Rose, R.M., *The effects of radiation sterilization on the properties of ultra high molecular weight polyethylene.* Journal of Biomedical Materials Research, 1979. **13**: p557-576

85. McGinniss, V.D., *Cross-linking with radiation,* in *Encyclopedia of Polymer Science and Engineering.* 1986. John Wiley and Sons Inc. p418-449

86. Clough, R., *Radiation Chemistry of Polymers, in Effects of radiation on high technology polymers,* E. Reichmanis and J.H. O'Donnell, Editors. 1988, ACS Symposium Series No. 381: Washington D.C. p1-13

87. Costa, L., et al., *Oxidation in orthopaedic UHMWPE sterilized by gamma radiation and ethylene oxide.* Biomaterials, 1998. **19**: p659-668

88. Schnabel, W., *Polymer Degradation: Principles and Practical Applications.*

1981, New York: Hanser International.

89. Hawkins, W.L., *Polymer Degradation and Stabilization.* 1984, New York: Springer-Verlag

90. Medel, F., et al., *Microstructure changes of extruded ultra high molecular weight polyethylene after gamma irradiation and shelf aging.* Polymer Degradation and Stability, 2005. p1-19

91. Willie, B.M., et al., *Possible explanation for the white band artifact seen in clinically retrieved polyethylene tibial components.* Journal of Biomedical Materials Research, 2000. **52**: p558-566

92. Yeom, B., et al., *Profile of oxidation in irradiated polyethylene.* Journal of Polymer Science Part A: Chemistry, 1998. **36**: p329-339

93. Wernle, J. and J.L. Gilbert, *Micromechanics of shelf aged and retrieved UHMWPE tibial inserts: indentation testing, oxidative profiling and thickness effects.* J Biomed Mater Res B Appl Biomater, 2005. **75**(1): p113-121

94. Kipping, M.G.E. et al., *Microhardness and FTIR testing of retrieved UHMWPE St. Georg Sled knee replacements.* In *19th European Conference on Biomaterials.* 2005. Sorrento, Italy

95. Wentz, M., et al., *Subsurface morphology of retrieved UHMWPE acetabular liners*, in *46th Annual Meeting, Orthopaedic Research Society.* 2000: Orlando. p0553

96. Affatato, S., et al., *Effects of the sterilization method on the wear of UHMWPE acetabular cups tested in a hip joint simulator.* Biomaterials, 2002. **23**: p1439-1446

97. Bell, C.J., et al., *Oxidation and wear resistance of directly moulded UHMWPE.* in *45th Annual Meeting of the Orthopaedic Research Society.* 1999.

98. Edidin, A.A., et al., Degradation of mechanical behavior in UHMWPE after natural and accelerated aging. Biomaterials, 2000. 21: p1451-1460

99. *Chemical Biology & Medical Application Hyaluronan.* Wenner-Gren Volume 72, Ed. T.C. Laurent. 1998

100. Klein, J. and Briscoe, B.J., *The diffusion of long-chain molecules through bulk polyethylene.* Proceedings of the Royal Society of London – A, 1979. **365**: p53-73

101. Billingham, N., *Physical phenomena in the oxidation and stabilization of polymers, in Oxidation inhibition in organic materials*, J. Pospisil and P.P. Lemchuk, Editors. 1989: Boca Raton: p262

102. Costa, L., et al., *Analysis of products diffused in UHMWPE prosthetic components in vivo.* Biomaterials, 2001. **22**: p307-315

103. Yao, J.Q., et al., *Effect of fluid absorption on the wear resistance of UHMWPE orthopaedic bearing surfaces.* Wear, 2003. **255**: p1113-1120

104. Lancaster, J.K., *Encylopedia of polymer science and engineering.* Vol.1. 1985, New York: Wiley.

105. Costa, L., et al., *Oxidation of orthopaedic UHMWPE.* Biomaterials, 2002. **23**: p1613-1624

106. Brach del Prever, E., et al., *Unacceptable biodegradation of polyethylene in vivo.* Biomaterials, 1998. **17**: p873-878

107. Costa, L., et al., *In vivo UHMWPE biodegradation of retrieved prosthesis.* Biomaterials, 1998. **19**: 1371-1385

108. Blanchet, T.A., et al., *Serum lubricant absorption by UHMWPE orthopaedic bearing implants.* Journal of Tribology, 2002. **124**(1): p1-4

109. Klapperich, C., et al., *Fluid sorption of orthopaedic grade ultrahigh molecular*

weight polyethylene in a serum environment is affected by the surface area and sterilization method. Journal of Biomedical Materials Research, 2000. **53**: p73-75

110. Bradford, L., et al., *Wear and surface cracking in early retrieved highly cross-linked polyethylene acetabular liners.* Journal of Bone and Joint Surgery (Am), 2004. **86**: p1271-1282
111. Rieker, C.B., et al., *In-vivo and in-vitro surface changes in a highly cross linked polyethylene.* J Arthroplasty, 2003. **18**: p48-54
112. Fisher, J. et al., *Influences of sterilising techniques on polyethylene wear.* The Knee, 2004. **11**: p173-176
113. Green, T.R., et al., *Polyethylene particles of a 'critical size' are necessary for the induction of cytokines by macrophages in-vitro.* Biomaterials, 1998. **19**: p2297-2302
114. Pietrabissa, R., et al., *Wear of polyethylene cups in total hip arthroplasty: a parametric mathematical model.* Medical Engineering & Physics, 1998. **20**(3): p199-210
115. Cates, H.E., et al., *Polyethylene wear in cemented metal-backed acetabular cups.* Journal of Bone and Joint Surgery (Br), 1993. **75B**: p249-253
116. Seedom, B.B. & Wallbridge, N.C., *Walking activities and wear of prostheses.* Annals of the Rheumatic Diseases, 1985. **44**: p838-843
117. Bartel, D.L., et al., *The effect of conformity, thickness and material on stresses in ultrahigh molecular weight components for total joint replacement.* Journal of Bone and Joint Surgery (Am), 1986. **68A**: p1041-1051
118. Livermore, J., et al., *Effect of femoral head size on wear of the polyethylene acetabular component.* Journal of Bone and Joint Surgery (Am), 1990. **72A**:

p518-528

119. Kabo, J.M., et al., *In-vivo wear of polyethylene acetabular components.* Journal of Bone and Joint Surgery (Br), 1993. **75B:** p254-258

120. Wroblewski, B.M., *15-21 year results of the Charnley low-friction arthroplasty.* Clinical Orthopaedics and Related Research, 1986. **211**: p30-35

121. Hall, R.M., et al., *Wear in retrieved Charnley acetabular sockets.* Proceedings of the Institution of Mechanical Engineers, 1996. **210**: p197

122. Atkinson, J.R., et al., *Laboratory wear tests and clinical observations of the penetration of femoral heads into acetabular cups in total replacement hip joints: 3. the measurement of internal volume changes in explanted Charnley sockets after 2-16 years in-vivo and the determination of wear factors.* Wear, 1985. **104**: p225

123. Elfick, A.P.D., et al., *Wear in retrieved acetabular components.* J Arthroplasty, 1998. **13**(3): p291-295

124. Bartel, D.L., et al., *The effect of metal backing on stresses in polyethylene acetabular components* in *The Hip: Proceedings of the 11th Open Scientific Meeting of the Hip Society.* 1983.

125. Maxian, T.A., et al., *Variability of polyethylene contact stress due to current industrial tolerances for femoral head sizes* in *41st Annual Meeting of the Orthopaedic Research Society.* 1995.

126. Jin, Z.M., et al., *A parametric analysis of the contact stress in ultra high molecular weight polyethylene acetabular cups.* Medical Engineering & Physics, 1994. **16**: p398-405

127. Kurtz, S.M., et al., *The effects of thickness, backside polishing and cup angle on contact stresses in a metal backed acetabular component* in *38th Annual Meeting*

of the Orthopaedic Research Society. 1996

128. Rixrath, E., et al., *Design parameters dependences on contact stress distribution in gait and jogging phases after total hip arthroplasty.* Journal of Biomechanics, 2008. **41**: p1137-1142

129. Lewinnek, G.E., et al., *Dislocations after total hip replacement arthroplasties.* J Bone Joint Surg, 1978. **60**: p217-220

130. Patil, S., et al., *Polyethylene wear and acetabular component orientation.* J Bone Joint Surg, 2003. **85-A Suppl. 4**: p56-63

131. Patil, S., et al., *Polyethylene wear and acetabular component orientation.* J Bone Joint Surg, 2003. **85-A** (Supplement 4): p56-63

132. Wang, A., *A unified theory of wear for ultra high molecular weight polyethylene in multi-directional sliding.* Wear, 2001. **248**: p38-47

133. Bigsby, R.J., et al., *Wear of ultra high molecular weight polyethylene acetabular cups in a physiological hip joint simulator in the anatomical position using bovine serum as a lubricant.* Proceedings of the Institution of Mechanical Engineers Part H, 1997. **211**: p265-269

134. Sychertz, C.J., et al., *Wear of polyethylene cups in total hip arthroplasty. A study of specimens retrieved post mortem.* J Bone Joint Surg, 1996. **78A**(8): p1193-1200

135. Jasty, M., et al., *Wear of polyethylene acetabular components in total hip arthroplasty. An analysis of one hundred and twenty-eight components retrived at autopsy or revision operations.* J Bone Joint Surg, 1997. **79A**(3): p349-358

136. Wang, A., et al., *Role of cyclic plastic deformation in the wear of UHMWPE acetabular cups.* J Biomed Mater Res, 1995. **29**: p619-626

137. Cooper, J.R., et al., *Macroscopic and microscopic wear mechanisms in ultra*

high molecular weight polyethylene. Wear, 1993. **162-164**: p378-384

138. Jasty, M., Goetz, D.D. and Bragdon, C.R., *Wear of polyethylene acetabular components in total hip arthroplasty. An analysis of one hundred and twenty-eight components retrived at autopsy or revision operations.* J Bone Joint Surg, 1997. **79A**: p349-358

139. Lee, K.R. and Kim, S., *Effect of crystalline lamellar orientation on the wear of UHMWPE* in *46th Annual Meeting of the Orthopaedic Research Society,* 2000. Orlando, Florida.

140. Davey, S.M., et al., *Measurement of molecular orientation in retrieved ultra high molecular weight polyethylene (UHMWPE) hip sockets using Fourier-transform infrared spectroscopy.* Strain, 2004. **40**(4): p203

141. Wang, A., et al., *Mechanistic and morphological origins of ultra high molecular weight polyethylene wear debris in total joint replacement prostheses.* Proceedings of the Institution of Mechanical Engineers Part H, 1996. **210**: p141-155

142. Bragdon, C.R., et al., *The importance of multi-directional motion on the wear of polyethylene.* Proceedings of the Institution of Mechanical Engineers, 1996. **210**: p157-154

143. Saikko, V. and Ahlroos, T., *Wear simulation of UHMWPE of total hip replacements with a multidirectional motion pin-on-disk device: effects of counterface material, contact area and lubricant.* Journal of Biomedical Materials Research, 2000. **29**: p147-154

144. Joyce, T.J., et al., *A multi-directional wear screening device and preliminary results of UHMWPE articulating against stainless steel.* Journal of Biomedical Materials Research, 2000. **10**: p241-249

145. Chang, N. et al., *Effect of molecular orientation on the wear of ultra high molecular weight polyethylene*, in *45th Annual Meeting of the Orthopaedic Research Society*, 1999. Anaheim.

146. Shipway, P.H. and Ngao, N.K., *Microscale abrasive wear of polymeric materials.* Wear, 2003. **255**: p742-750

147. Archard, J.F., *Contact and rubbing of flat surfaces.* Journal of Applied Physics, 1953. **24**(8): p981-988

148. Lancaster, J.K., *Dry bearings: a surface of materials and factors affecting their performance.* Tribology, 1973. **6**: p219-251

149. Greenwood, J.A. and Williamson, J.B.P., *Contact of nominally flat surfaces.* Proceedings of the Royal Society of London – A, 1966. **295**: p300-319

150. Vassiliou, K. and Unsworth, A., *Is the wear factor in total joint replacements dependent on the nominal contact stress in ultra-high molecular weight polyethylene contacts?* Proceedings of the Institution of Mechanical Engineers, 2004. **218**(2): p101-107

151. Hall, R.M., et al., *Measurement of wear in retrieved acetabular sockets.* Proceedings of the Institution of Mechanical Engineers Part H, 1995. **209**: p233-242

152. Barbour, P.S.M. et al., *The influence of contact stress on the wear of UHMWPE for total replacement hip prostheses.* Wear, 1995. **181**: p250-257

153. Dowson, D. and Wallbridge, N.C., *Laboratory wear tests and clnical observations of the penetration of femoral heads into acetabular cups in total replacement hip joints I: Charnley prostheses with polytetrafluoroethylene acetabular cups.* Wear, 1985. **104**: p203-215

154. Wallbridge, N.C. and Dowson, D., *The walking activity of patients with*

artificial joints. Eng Med, 1982. **11**: p95

155. Jacobs, J.J., et al., *Osteolysis: a basic science.* Clinical Orthopaedics and Related Reseach, 2001. **393**: p71-77
156. Manley, M.T., et al., *Osteolysis: a disease of access to fixation interfaces.* Clinical Orthopaedics and Related Research, 2002. **405**: p129-137
157. Besong, A.A., et al., *Quantitative comparison of wear debris from UHMWPE that has not been sterilized by gamma irradiation.* J Bone Joint Surg, 1998. **80-B**: p340-344
158. Tipper, L., et al., *Quantitative analysis of polyethylene wear debris, wear rate and head damage in retrieved Charnley hip prostheses.* Journal of Materials Science: Materials in Medicine, 2000. **11**(2): p117-124
159. Matthews, J.B., et al., *Evaluation of the response of primary human peripheral blood mononuclear phagocyted to challenge with in-vitro generated clinically relevant UHMWPE particles of known size and dose.* Journal of Biomedical Materials Research, 2000. **52**: p296-307
160. Isaac, G.H., et al., *An investigation into the origins of time-dependent variation in penetration rates with Charnley acetabular cups – wear, creep or degradation?* Proceedings of the Institution of Mechanical Engineers, 1996. **210**(3): p209-216
161. Isaac, G.H., et al., *A tribological study of retrieved hip prostheses.* Clin Orthop Rel Res, 1992(115-125)
162. Charnley, J. et al., *The nine and ten year results of the low-friction arthroplasty of the hip.* Clin Orthop Rel Res, 1973. **95**: p9-25
163. Dumbleton, J.H., et al., *A literature review of the association between wear rate and osteolysis in total hip replacement.* J Arthroplasty, 2002. **17**(5): p649-661

164. McCalden, R.W., et al., *Radiographic methods for the assessment of polyethylene wear after total hip arthroplasty.* Journal of Bone and Joint Surgery (Am), 2005. **87**(10): p2323-2335

165. Charnley, J., et al., *Rate of wear in total hip replacement.* Clin Orthop Rel Res, 1975. **112**: p170-179

166. Callaghan, J.J. et al., *Results of Charnley total hip arthroplasty at a minimum of thirty years.* Journal of Bone and Joint Surgery (Am), 2004. **86-A**(4): p690-695

167. Shaver, S.M., et al., *Digital edge-detection measurement of polyethylene wear after total hip arthroplasty.* J Bone Joint Surg, 1997. **79**: p693-700

168. Maruyama, M., et al., *Socket wear of Charnley low friction arthroplasty: fifteen year follow-up.* Bull Hosp Jt Dis, 1995. **53**(4): p37-42

169. Semlitsch, M., et al., *Clinical wear behaviour of ultra high molecular weight polyethylene cups paired with metal and ceramic ball heads in comparison to metal-on-metal pairings of hip joint replacements.* Proceedings of the Institution of Mechanical Engineers: H, 1997. **211**(1): p73-88

170. James, S.P., et al., *Clinical wear of 63 ultrahigh molecular weight polyethylene acetabular components: effect of starting resin and forming method.* Journal of Biomedical Materials Research, 1999. **48**: p374-384

171. Barrack, R.L., et al., *Radiographic wear measurements in a cementless metal-backed modular cobalt-chromium acetabular component.* J Arthroplasty, 2001. **16**(7): p820-828

172. Pollock, D., et al., *A clinically practical method of manually assessing polyethylene liner thickness.* J Bone Joint Surg, 2001. **83-A**: p1803-1809

173. Hall, R.M., et al., *Measurement of wear in retrieved acetabular sockets.* Proceedings of the Institution of Mechanical Engineers Part H, 1995. **209**(4):

p233-242

174. Yamaguchi, M., et al., *Three dimensional analysis of multiple wear vectors in retrieved acetabular cups.* The Journal of Bone and Joint Surgery, 1997. **79**: p1539-1544

175. Cunningham, J.L., et al., *Precision of wear measurement using the shadowgraph technique.* Proceedings of the Institution of Mechanical Engineers Part H, 2006. **221**: p899-902

176. Biggs, S., et al., *A new method of volumetric quantification of retrieved polyethylene components* in *42nd Annual Meeting ORS*, 1996. Atlanta.

177. Derbyshire, B., et al., *Assessment of the change in volume of acetabular cups using a coordinate measuring machine.* Proceedings of the Institution of Mechanical Engineers Part H, 1994. **208**: p151-158

178. Bills, P., et al., *A metrology solution for the orthopaedic industry.* Journal of Physics: Conference series, 2005. **13**: p316-319

179. Bigsby, R.J., et al., *Wear of ultra high molecular weight polyethylene cups in a physiological hip joint simulator in the anatomical position using bovine serum as a lubricant.* Proceedings of the Institution of Mechanical Engineers Part H, 1997. **211**: p265-269

180. ASTM, *F2183-02 Small punch testing of ultra high molecular weight polyethylene used in surgical implants*, 2002. ASTM. p1-4

181. Edidin, A.A., et al., *Sterilization of UHMWPE in nitrogen prevents oxidative degradation for more than ten years.* in *46th Annual Meeting, Orthopaedic Research Society*, 2000.

182. Edidin, A.A., et al., *Accelerated aging studies of UHMWPE. I Effect of resin,*

processing and radiation environment on resistance to mechanical degradation. Journal of Biomedical Materials Research – Part A, 2002. **61**(2): p312

183. Edidin, A.A., et al., *Accelerated aging studies of UHMWPE. II. Virgin UHMWPE is not immune to oxidative degradation.* Journal of Biomedical Materials Research – Part A, 2002. **61**(2): p323
184. Kurtz, S.M., et al., *Advances in the processing, sterilization and crosslinking of ultra-high molecular weight polyethylene for total joint arthroplasty.* Biomaterials, 1999. **20**(18): p1659-1688
185. Kurtz, S.M., et al., *Radiation and chemical crosslinking promote strain hardening behavior and molecular alignment in ultra high molecular weight polyethylene during multi-axial loading conditions.* Biomaterials, 1999. **20**(16): p1449-1462
186. Edidin, A.A., et al., *Mechanical behavior, wear surface morphology and clinical performance of UHMWPE acetabular components after 10 years of implantation.* Wear, 2001. **250**(1-12): p152-158
187. Kurtz, S.M., et al., *Degradation of mechanical properties of UHMWPE acetabular liners following long-term implantation.* Journal of Arthroplasty, 2003. **18**(7): p68-78
188. Gilbert, J.L., et al., *Surface micromechanics of ultrahigh molecular weight polyethylene – microindentation testing, crosslinking and material behaviour.* J Biomed Mater Res, 2002. **61**: p270-281
189. Gilbert, J.L. and Merkhan, I., *Rate effects on the microindentation based mechanical properties of oxidized, crosslinked and highly crystalline ultrahigh molecular weight polyethylene.* J Biomed Mater Res, 2004. **71A**: p549-558
190. Boampong, D.K., et al., *N+ ion implantation of Ti6Al4V and UHMWPE for*

total joint replacement application. Journal of Applied Biomaterials and Biomechanics, 2003. **1**: p164-171

191. Shi, W., et al., *Wear performance of ultra high molecular weight polyethylene ion implanted weight.* Surface Engineering, 2003. 19(4): p279-283
192. Turos, A., et al., *Ion beam modification of surface properties of polyethylene.* Vacuum, 2003. **70**: p206-210
193. Ujvari, T., et al., *Nanomechanical property analysis of fast atom beam (FAB) treated ultrahigh molecular weight polyethylene.* Surface and Interface Analysis, 2006. **38**: p894-897
194. Valenza, A., et al., *Characterization of ultra high molecular weight polyethylene (UHMWPE) modified by ion implantation.* Polymer, 2004. **45**: p1707-1715
195. Gilbert, J.L., et al., *Depth sensing microindentation testing of retrieved and shelf aged UHMWPE tibial trays: Mechanical profiling and thickness effects.* in *49th Annual Meeting of the Orthopaedic Research Society*, 2003.
196. Torrisi, L., et al., *Study of hardness and roughness modification in expxlanted joint components.* Biomed Mater Eng., 2004. **14**(3): p251-261
197. Bruni, P., et al., *Damaged polyethylene acetabular cups microscopy FT-IR and mechanical determinations.* Vibrational Spectroscopy, 2002. **29**: p103-107
198. Flores, A., et al., *Mechanical changes linked to embrittlement at the wear surface of polyethylene implants in hip joints.* Polymer, 2000. **41**: p7635-7639
199. Hay, J.L., et al., *Instrumented indentation testing,* in *ASM Handbook Volume 08: Mechanical Testing and Evaluation,* ASM. p231-243
200. Goldman, M., et al., *Oxidation of ultrahigh molecular weight polyethylene characterized by Fourier Transform Infrared Spectroscopy.* Journal of Biomedical Materials Research, 1997. **37**(1): p43-50

201. Costa, L., et al., *Effects of microtomy on the material properties of ultra high molecular weight polyethylene.* Polymer Testing, 2001. **20**: p649-659

202. Nishikida, K., et al., *Selected applications of modern FT-IR techniques.* 1995, Tokyo: Gordon and Breach Science Publishers S.A. 289

203. Rueda, R., et al., *An I.R. study of the "amorphous" phase in melt crystallized polyethylene.* Spectrochim Acta, 1978. **34A**: p475

204. Buchanan, F.J., et al., *The influence of gamma irradiation and aging on degradation mechanicsms of ultra high molecular weight polyethylene.* J Mater Sci Mater Med, 2001. **12**(1): p29-37

205. Eigener, U., et al., *Test of the sporicidal effect of the instrument disinfectant Giagsept FF.* 1985, Schulke & Mayr: Norderstedt. p2

206. Kurtz, S.M., et al., *Evolution of morphology in UHMWPE following accelerated aging: the effect of heating rates.* J Biomed Mater Res, 1999. **46**: p112-120

207. Hall, R.M., et al., *Observations on the direction of wear in Charnley sockets retrieved at revision.* Journal of Bone and Joint Surgery (Br), 1998. **80-B**: p1067-1072

208. Livermore, J., et al., *Effect of femoral head size on wear of the polyethylene acetabular component.* J Bone Joint Surg, 1990. **72**: p518-528

209. Jacob, R.J., et al., *Molecular anatomy of freeze-fractured ultra-high molecular weight polyethylene as determined by low-voltage scanning electron microscopy.* Journal of Biomedical Materials Research, 1997. **37**(4): p489-496

210. Wang, A., et al., *Wear mechanisms and wear testing of ultra high molecular weight polyethylene in total joint replacements.* in *Polyethylene Wear in Orthopaedic Implants Workshop, Society for Biomaterials.* 1997.

211. Bennett, D., et al., *The influence of shape and sliding distance of femoral head*

movement loci on the wear of acetabular cups in total hip arthroplasty. Proceedings of the Institution of Mechanical Engineers Part H, 2002. **216**: p393-402

212. Schneider, W., et al., *O1222 Analysis of early retrieved acetabular cups of highly crosslinked UHMWPE.* in *European Federation of National Associations of Orthopaedics and Traumatology (EFFORT).* 2003. Helsinki
213. Jordan, N.D., et al., *In-depth morphological changes and embrittlement near the wear surface of UHMWPE inserts from uncemented hip systems.* Journal of Biomedical Materials Research, 2001. **55**(2): p158-163
214. Ostlere, S. et al., *Imaging of prosthetic joints.* Imaging, 2003. **15**: p270-285
215. Edidin, A.A. et al., *Mechanical behavior, wear surface morphology and clinical performance of UHMWPE acetabular components after 10 years of implantation.* Wear, 2001. **250**: p152-158
216. Pintaude, G., et al., *Effect of indentation size and microhardness calculation on abrasive wear severity.* Scripta Materialia, 2001. **44**: p659-663
217. Brigden, S., *Hip and knee replacement audit.* 2004, QMC: Nottingham. p1
218. Berry, D.J., et al., *Twenty five year survivorship of two thousand consecutive primary Charnley total hip replacements – factors affecting survivorship of acetabular and femoral components.* Journal of Bone and Joint Surgery (Am), 2002. **84**(17): p1-7
219. Iorio, R., et al., *Cemented revision of failed total hip arthroplasty: survivorship analysis.* Clinical Orthopaedics and Related Research, 1995. **316**: p121-130
220. Kahan, E., et al., *Correlations of work, leisure and sports physical activities and health status with socioeconomic factors: a national study in Israel.* Postgrad Med J, 2005. **81**: p262-265

221. Elfick, A.P.D., et al., *A re-appraisal of wear features of acetabular sockets using atomic force microscopy.* Wear, 2002. **253**: p839-847

222. Wang, F.C., et al., *Microscopic asperity contact and wear mechanism for UHMWPE bearing surfaces.* in *49th Annual Meeting of the Orthopaedic Research Society.* 2003.

223. Essner, A., et al., In-*vitro and in-vivo acetabular cup wear corroboration.* in *47th Annual Meeting of the Orthopaedic Research Society.* 2001. San Francisco

224. Saikko, V., et al., *Effect of slide track shape on the wear of ultra high molecular weight polyethylene in a pin on disk wear simulation of total hip prosthesis.* Journal of Biomedical Materials Research Part B, 2004. **69B**: p141-148

225. Buchanan, F.J. and Shipway, P.H., *Microabrasion – a simple method to assess surface degradation of UHMWPE following sterilization and aging.* Biomaterials, 2002. **23**: p93-100

226. Edidin, A.A., et al., *Mechanical behavior of acetabular components after implantation.* in 47th *Annual Meeting of the Orthopaedic Research Society.* 2001

227. Ely, S., et al., *Determination of through thickness mechanical characteristics on aged and unaged oxygenless packaged UHMWPE.* in *46th Annual Meeting of the Orthopaedic Research Society.* 2000. Orlando.

228. Kurtz, S.M., et al., *Degradation of mechanical properties of UHMWPE acetabular liners following long term implantation.* Journal of Arthroplasty, 2003. **18**(7 supplement 1): p68-78

229. Bragdon, C.R., et al., *New insights into fluid imbibition into highly crosslinked polyethylene acetabular components*, in *46th Annual Meeting of the Orthopaedic Research Society.* 2000

230. Clarke, I., et al., *Fluid-sorption phenomena in sterilized polyethylene acetabular*

prostheses. Biomaterials, 1985. **6**(3): p184-188

231. Ferry, S., *Hardness testing of medical device components.* Medical Device & Diagnostic Industry Magazine, 2001. March: p1-9